LBL-11357 c.2

# Lawrence Berkeley Laboratory
UNIVERSITY OF CALIFORNIA

## Materials & Molecular Research Division

THE APPLICATION OF HIGH RESOLUTION ELECTRON ENERGY LOSS SPECTROSCOPY TO THE CHARACTERIZATION OF SMALL MOLECULES ADSORBED ON RHODIUM SURFACES

Lawrence Henry Dubois
(Ph.D. thesis)

RECEIVED
LAWRENCE
BERKELEY LABORATORY

OCT 1 7 1980

LIBRARY AND
DOCUMENTS SECTION

July 1980

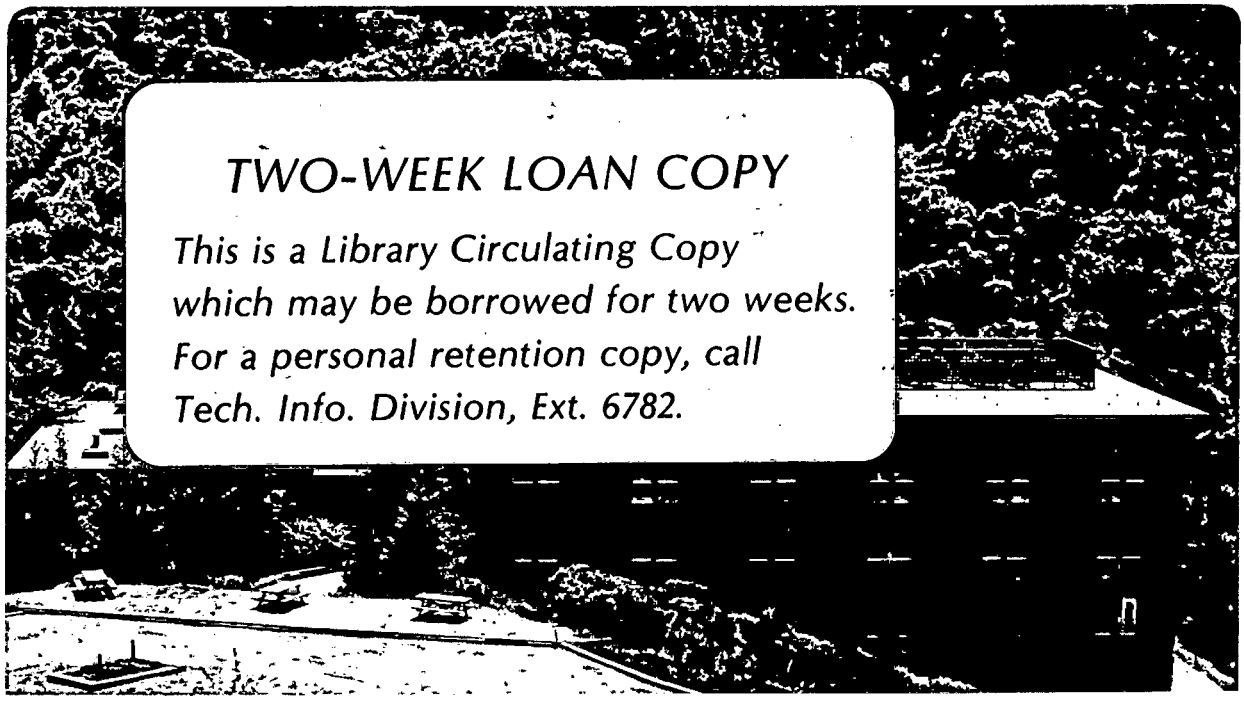

TWO-WEEK LOAN COPY

*This is a Library Circulating Copy which may be borrowed for two weeks. For a personal retention copy, call Tech. Info. Division, Ext. 6782.*

LBL-11357 c.2

Prepared for the U.S. Department of Energy under Contract W-7405-ENG-48

## DISCLAIMER

This document was prepared as an account of work sponsored by the United States Government. While this document is believed to contain correct information, neither the United States Government nor any agency thereof, nor the Regents of the University of California, nor any of their employees, makes any warranty, express or implied, or assumes any legal responsibility for the accuracy, completeness, or usefulness of any information, apparatus, product, or process disclosed, or represents that its use would not infringe privately owned rights. Reference herein to any specific commercial product, process, or service by its trade name, trademark, manufacturer, or otherwise, does not necessarily constitute or imply its endorsement, recommendation, or favoring by the United States Government or any agency thereof, or the Regents of the University of California. The views and opinions of authors expressed herein do not necessarily state or reflect those of the United States Government or any agency thereof or the Regents of the University of California.

# The Application of High Resolution Electron Energy Loss Spectroscopy to the Characterization of Small Molecules Adsorbed on Rhodium Surfaces

Lawrence Henry Dubois
Lawrence Berkeley Laboratory, University of California
Berkeley, California 94720

## Abstract

High resolution electron energy loss spectroscopy (ELS), thermal desorption mass spectrometry (TDS), low-energy electron diffraction (LEED) and Auger electron spectroscopy (AES) are used to study 1) the chemisorption of CO, $CO_2$ and $O_2$ on the Rh(111) single crystal surface; 2) the bonding and chemical transformations of $C_2H_2$ and $C_2H_4$ on Rh(111); 3) the chemisorption and subsequent reactions of NO, $O_2$ and CO on Rh(331) and 4) the chemisorption of CO on model alumina supported rhodium catalysts. The vibrational spectra of carbon monoxide on Rh(111) indicate two distinct binding sites (atop and bridged) whose relative populations and vibrational frequencies are determined by both the substrate temperature and the background pressure. TDS measurements show the bridge bonded CO to have an approximately 4 kcal/mole lower binding energy to the surface than the species located in the atop site. The adsorption of carbon dioxide yields virtually identical TDS and ELS spectra to that of chemisorbed CO, indicating dissociative adsorption. This is confirmed by studying the adsorption of isotopically labelled $^{13}CO_2$. $O_2$ adsorption on Rh(111) is dissociative at all temperatures studied (>250 K) and only a single metal-oxygen vibrational frequency is observed at all coverages. Evidence for "surface oxide" formation on Rh(111) is also presented.

Below 270 K ELS measurements indicate that acetylene chemisorbs on Rh(111) with its C≡C bond oriented parallel to the surface forming an approximately $sp^2$ hybridized species. LEED investigations show that both

$C_2H_2$ and $C_2H_4$ form metastable (2x2) surface structures on Rh(111) below 270 K. An irreversible order-order transformation occurs between 270 and 300 K to a stable c(4x2) hydrocarbon overlayer. The stable species formed from both molecules are identical. Hydrogen addition to chemisorbed acetylene is necessary to complete this conversion. The geometry of the adsorbed ethylene species does not change during this transformation although the overlayer structure does. This stable hydrocarbon fragment is identical to the hydrocarbon species formed from the chemisorption of either $C_2H_4$ or $C_2H_2$ and hydrogen on Pt(111) above 300 K. This species has now been identified as ethylidyne ($\geqslant C-CH_3$). Decomposition of these molecules to CH fragments occurs on the Rh(111) surface above ~420 K.

Evidence for an oxygen intermediate in the reaction of NO and CO to form $N_2$ and $CO_2$ over rhodium surfaces is presented. High resolution ELS measurements indicate that both NO and CO molecules associatively adsorb on the Rh(331) single crystal surface at 300 K. Chemisorbed NO readily dissociates on this surface upon heating to 450 K. At 700 K high resolution ELS and Auger electron spectroscopy both indicate that only oxygen is present on the catalyst surface. $N_2$ desorption below this temperature is easily detected by mass spectroscopy. The addition of CO to this surface oxygen at 700 K results in the formation of gaseous $CO_2$ and the removal of the surface oxygen species. Similar results are obtained when $O_2$ was substituted for NO as a control indicating that surface oxygen is indeed a reaction intermediate under our experimental conditions.

Model supported metal catalysts are fabricated by evaporating a small quantity of rhodium onto an oxidized aluminum substrate. High resolution electron energy loss spectroscopy can be successfully used to obtain the vibrational spectra of carbon monoxide chemisorbed on these model catalysts.

The ELS spectra are compared with vibrational spectra obtained by infrared spectroscopy and inelastic electron tunneling spectroscopy for CO chemisorbed on similar model catalysts.

The theory of inelastic electron scattering from metal surfaces and the advantages of this technique for studying the vibrational spectra of adsorbed molecules are reviewed. The details of the spectrometer design and construction are discussed as well.

# DEDICATION

To my parents

## Acknowledgements

It is very difficult to sit down at this time and thank everyone for all of the help that I have received over the past four years. So many people have contributed so much during my stay here at Berkeley that I can't possibly mention everyone. I would first like to thank Brett Sexton for introducing me to the field of high resolution electron energy loss spectroscopy and without whose help this project would never have been attempted. I would also like to thank Peter Stair, David Castner and Larry Kesmodel for patiently teaching me the fundamentals of modern surface science and technology. Both Emery Kozak and Phil Eggers deserve a special acknowledgement for constructing both the spectrometer and the electronics in record time. The technical help of Bob McCallister and Jack Wodei during the performance of most of these experiments cannot be applauded enough.

The list of people who have contributed not only to my growth as a scientist at Berkeley but to my maturing as an adult is endless. Let me take this opportunity to thank all of my friends throughout the Chemistry Department, MMRD and the Somorjai group (both past and present) for their help and support. Especially Henry Luftman, Steve Oblath, Vera Mainz, Linda Young, Pauline Ho, Greg Girolami and Tempestuous. Three people deserve a very special acknowledgement: First, to my wife Ellen who has made my stay here the best four years of my life. Without her sincere encouragement and early rising times a good portion of this work would not have been completed. I am especially grateful for the friendship of Prof. Paul Hansma. I thank him not only for, his scientific assistance, but for his patience and understanding as well. Finally, I wish to

thank Prof. Gabor Somorjai without whose help this thesis could never have been completed. His guidance throughout my graduate career has been invaluable. The freedom with which he has allowed me to pursue my own interests and experiments has taught me more than I can say.

This work was supported by the Division of Materials Sciences, Office of Basic Energy Sciences, United States Department of Energy under Contract No. W-7405-ENG-48.

TABLE OF CONTENTS


| CHAPTER | | Page |
|---|---|---|
| I | Introduction | 1 |
| | A. Background | 1 |
| | B. The Advantages of High Resolution ELS | 4 |
| | C. Simple Normal Co-ordinate Calculations: CO/Rh | 6 |
| | References | 17 |
| II | Theory of Adsorbate Vibrational Excitation by Inelastic Electron Scattering from Metal Surfaces | 20 |
| | A. Background | 20 |
| | B. The Scattering Process | 21 |
| | C. The Inelastic Scattering Cross-section | 28 |
| | D. Numerical Calculations | 35 |
| | E. Long Range Nature of the Scattering | 36 |
| | F. The Dipole Selection Rule | 42 |
| | References | 54 |
| III | Experimental | 56 |
| | A. Spectrometer Design and Construction | 56 |
| | B. The Tuning Procedure | 68 |
| | C. The Vacuum System | 75 |
| | References | 80 |
| IV | The Chemisorption of Carbon Monoxide on Rh(111) | 81 |
| | A. Background | 81 |
| | B. CO Chemisorption on Clean Rh(111) | 85 |
| | C. CO Chemisorption on Pretreated Rh(111) | 100 |
| | D. Vibrational Analysis of the CO/Rh System | 109 |
| | E. Correlation Between Surface Structure and C≡O Vibrational Frequency | 112 |

TABLE OF CONTENTS (continued)


| CHAPTER | | Page |
|---|---|---|
| IV | F. Summary | 114 |
| | References | 118 |
| V | The Dissociative Chemisorption of Carbon Dioxide on Rhodium Surfaces | 123 |
| | A. Background | 123 |
| | B. Experimental Results | 125 |
| | C. Discussion | 134 |
| | D. "Surface Oxide" Formation on Rh(111) | 135 |
| | References | 142 |
| VI | Evidence for an Oxygen Intermediate in the Catalytic Reduction of NO by CO on Rhodium Surfaces | 144 |
| | A. Introduction | 144 |
| | B. The Molecular Chemisorption of NO on Rh(331) | 145 |
| | C. The Dissociation of NO on Rh(331) | 149 |
| | D. The Chemisorption of CO on Rh(331) | 153 |
| | E. The Interaction of CO with Molecular NO | 160 |
| | F. The Reaction of CO with Dissociated NO | 161 |
| | G. The Reaction Mechanism | 164 |
| | H. Summary | 167 |
| | References | 170 |
| VII | The Application of High Resolution Electron Energy Loss Spectroscopy to the Study of Model Supported Metal Catalysts | 172 |
| | A. Introduction | 172 |
| | B. Sample Preparation | 173 |
| | C. Experimental Results | 177 |

TABLE OF CONTENTS (continued)


| CHAPTER | | Page |
|---|---|---|
| VII | D. Discussion | 183 |
| | E. Summary | 191 |
| | References | 193 |
| VIII | The Chemisorption of Acetylene and Ethylene on Rh(111) | 195 |
| | A. Introduction | 195 |
| | B. LEED Studies of Acetylene and Ethylene Adsorption on Rh(111) | 196 |
| | C. High Resolution ELS Studies of Acetylene Adsorption on Rh(111) | 200 |
| | D. High Resolution ELS Studies of Ethylene Adsorption on Rh(111) | 206 |
| | E. TDS Studies of Acetylene and Ethylene Adsorption on Rh(111) | 213 |
| | F. Correlations with $C_2H_2$ and $C_2H_4$ Chemisorption on Pt(111) | 219 |
| | G. The Chemisorption of Ethylene on Pt(111): Evidence for Ethylidyne Formation | 222 |
| | H. Correlations with $C_2H_2$ and $C_2H_4$ Chemisorption on Ni(111): Evidence for Surface CH Species | 237 |
| | I. Summary | 240 |
| | References | 242 |

# CHAPTER I. Introduction

## A. Background

The scattering of low energy electrons by adsorbate covered metal surfaces has been explored for many years.[1,2] These studies have yielded a wealth of information on the structure, bonding and electronic properties of the outermost layers of atoms. The electrons' ease of generation and detection and high surface sensitivity (low penetration depth) make it an ideal probe for surface scientists.[1,2] An incident electron can interact with the surface in basically two ways: it will either elastically reflect (or diffract) from the surface without losing energy or lose a portion of its incident energy and inelastically scatter. In this thesis we will be concerned with only one of many possible inelastic scattering processes: the loss of the electron's energy to the vibrational modes of atoms and molecules chemisorbed on the surface.

If one considers the scattering of an electron by a rigid crystal lattice, then the incident electron can either specularly reflect or Bragg diffract. Conventional low-energy electron diffraction (LEED) measurements combined with sophisticated scattering theories yield detailed information about the geometry of the surface region.[3,4] Due to the complexity of these calculations, however, only a few surface-adsorbed molecules have been studied to the point of yielding bond lengths and bond angles. To date these are carbon monoxide (CO) adsorbed on Ni(100),[5,6] Cu(100),[5] Pd(100)[7] and Rh(111),[8] and acetylene ($C_2H_2$) and ethylene ($C_2H_4$) adsorbed on Pt(111).[9,10] Extension of these studies to more complex molecules is quite difficult at present.

If the consequences of the small lattice vibrations are considered, two important changes to this simple diffraction model occur. Most significantly, the intensity of the elastically scattered electrons is reduced by a Debye-Waller factor[3,4] (a measure of the mean square displacement of the surface atoms). In addition, when the electrons are near the surface they may either emit or absorb one or more phonons. If the surface is covered by an adsorbed layer of gas, then vibrational excitations of the adsorbate are possible. Hence a study of inelastic electron scattering can yield detailed information on both surface and adsorbate vibrations. Analysis of the vibrational spectra can in turn give us structural information on the adsorbed molecules. Unlike LEED, we have the possibility of studying very complex surface species. Studying this scattering phenomenon has proved to be an extremely difficult experimental problem, however. Since both phonon and adsorbate vibrational energies are in the range of 40-400 meV (320-3200 $cm^{-1}$; 1 meV = 8.065 $cm^{-1}$), the incident electron beam (1-10 eV) must be monochromatic to within 10 meV (80 $cm^{-1}$).

The design of electron optics has improved to the point where inelastic electron scattering by small molecules in the gas phase is a routine method for obtaining vibrational spectra.[11] The first application of this technique, now known as high resolution electron energy loss spectroscopy (ELS), to the study of molecules adsorbed on metal surfaces can be traced to the work of F. M. Propst and T. C. Piper in 1967.[12] Credit for the expansion of this technique, however, must be given to Harold Ibach and his graduate students[2,13] who played a key role in both the advancement of spectrometer design and in the performance of outstanding experiments. At present there are almost a dozen working systems throughout the world and more are being built every month.

Both Evans and Mills[14] and Ibach[15] showed that the photon-surface oscillating dipole and the long range electron-surface oscillating dipole interactions are similar and therefore, to first order, infrared spectroscopy and high resolution ELS provide the same information. Furthermore, due both to the long range nature of this interaction[14,15] and to the large dielectric constant of the substrate, the same selection rules should apply. Specifically, only vibrational modes which contain an oscillating dipole moment with a component perpendicular to the surface can be excited.[14,15] A detailed discussion of the theory of the inelastic scattering of low-energy electrons by surface vibrational modes will be presented in the next chapter.

During the past fifty years infrared (IR) spectroscopy has been a very powerful technique for studying the molecular structure of matter in the solid, liquid and gaseous phases. The pioneering work of Eischens, Pliskin and Francis in 1954 was the first application of vibrational spectroscopy to the study of molecules adsorbed on metal surfaces.[16] They studied the IR spectra of CO adsorbed on silica supported Cu, Pt, Pd and Ni.[17] Due to the small absorption cross-section for infrared photons, most studies have been carried out on high surface area powdered samples.[18,19] Unfortunately, these samples lack a well-defined surface structure and composition. Furthermore, due to light adsorption by the support material below ~1200 $cm^{-1}$ low frequency vibrational modes, which are essential in structural determination, are completely masked.[20-22] More recently, Raman spectroscopy[23] and inelastic electron tunneling spectroscopy (IETS)[24-26] have been used to obtain the vibrational spectra of molecules adsorbed on oxide supported transition metal surfaces. These spectroscopic techniques can extend the spectral range over which

a sample can be studied, but both present problems of their own including substrate fluorescence and sample heating in the case of Raman spectroscopy[23] and uncertainty due to the top metal electrode in the case of tunneling spectroscopy.[27]

The extension of these experiments to well characterized single crystal metal surfaces has met with limited success. Most experiments to date have dealt with the adsorption of carbon monoxide.[28,29] Although the C≡O stretching vibration (1800-2100 $cm^{-1}$) can be observed with very high resolution (<2 $cm^{-1}$) and good signal-to-noise (due to the large dipole derivative of this mode), no metal-carbon stretching or bending vibrations (400-600 $cm^{-1}$) have been reported.[28,29] Neither Raman spectroscopy nor IETS have been successfully applied to the study of molecules adsorbed on single crystal surfaces.

## B. The Advantages of High Resolution ELS

The advantages of high resolution electron energy loss spectroscopy for studying the vibrational spectra of molecules adsorbed on metal surfaces are numerous. Firstly, the entire infrared region of the spectrum (from 300 to 4000 $cm^{-1}$) can be scanned in less than twenty minutes. These studies can also be easily extended to the visible portion of the electromagnetic spectrum.[30] Unlike optical measurements, all of these experiments can be accomplished without changing windows, prisms (gratings) or lenses. Secondly, for strong scatterers ELS is sensitive to less than 0.1% of a monolayer[13] (approximately $10^{11}$ molecules), far more sensitive than most other techniques. Because of both this surface sensitivity and the nature of the inelastic scattering process (see Chapter II), single crystal metal surfaces make ideal targets. Thus,

studies can be carried out on clean, well characterized substrates under ultra-high vacuum (UHV) conditions. Furthermore, a variety of complementary surface sensitive probes (such as LEED, Auger electron spectroscopy (AES), thermal desorption mass spectrometry (TDS) and X-ray and ultraviolet photoelectron spectroscopy (XPS and UPS)) can be applied to the study of a given chemisorption system. Through this combination of techniques located in a single UHV chamber, a complete picture of the structure, bonding and reactivity of adsorbed monolayers can be obtained. Also, because of this surface sensitivity ELS can be used to detect hydrogen both through its vibration against the substrate[31] and against other heavier adsorbed atoms.[13] Thirdly, unlike many other techniques, both disordered[32,33] and optically rough[33] surfaces can be readily studied. Finally, due to the low incident beam energies and beam currents (see Chapter III), high resolution electron energy loss spectroscopy is a non-destructive technique which can be used to probe the structure of weakly adsorbed molecules.

While discussing the advantages of high resolution ELS, mention should be made ot two of it's major disadvantages. First, by optical standards the terms "high resolution" are a misnomer since the resolution is limited, at present, to about 60 $cm^{-1}$ (the full width at half maximum of the elastic scattering peak). Peak assignments can be made much more accurately ($\pm 5$ $cm^{-1}$), however. This limits the use of isotopic substitution and the analysis of closely spaced vibrational modes. The second major drawback is that the maximum pressure under which experiments can be carried out is approximately $5 \times 10^{-5}$ Torr due to electron-gas collisions inside the spectrometer. High pressure catalytic reactions and chemisorption at the solid-liquid interface cannot be readily studied.

Nevertheless, a tremendous number of studies on the adsorption of atoms, diatomic molecules and large hydrocarbons on transition metal surfaces have been performed.

### C. Simple Normal Co-ordinate Calculations: CO/Rh

Since we now have a technique for obtaining the vibrational spectrum of a molecule adsorbed on a metal surface, one might ask the question: What vibrational frequencies should be observed? For the case of carbon monoxide adsorbed on a rhodium surface we can answer this question to a reasonable degree by applying a normal co-ordinate analysis to the stretching and bending modes of model metal cluster carbonyls. In this section we will use a simple valence force model and neglect all stretch-stretch, stretch-bend and bend-bend interactions. Force constants derived from infrared and Raman studies of organometallic compounds will be applied to the study of linear triatomic, linear tetraatomic and bridged tetraatomic rhodium carbonyls. Bond lengths will be taken from appropriate organorhodium compounds. LEED structural studies on the chemisorption of CO on Ni(100),[5,6] Cu(100)[5] and Pd(100)[7] show this to be a reasonable approximation (good to $\pm$ 0.1 Å). Although the degree of sophistication in the present calculations is rather crude, the agreement with experiment is quite good (see Chapter IV).

At the simplest level we consider a linear triatomic species, Rh-C≡O, as a model for carbon monoxide bonded in an atop site on a rhodium surface. A linear triatomic molecule should have 3x(3)-5 or 4 vibrational degrees of freedom. In our case these will be essentially the carbon-oxygen stretch ($\nu_1$), the rhodium-carbon stretch ($\nu_3$) and the doubly degenerate Rh-C≡O bend ($\nu_2$). See Figure 1a. We use the stretching force constants

Figure 1. Approximate vibrational modes observed for a (a) linear triatomic, (b) linear tetraatomic and (c) bridged tetraatomic metal carbonyl.

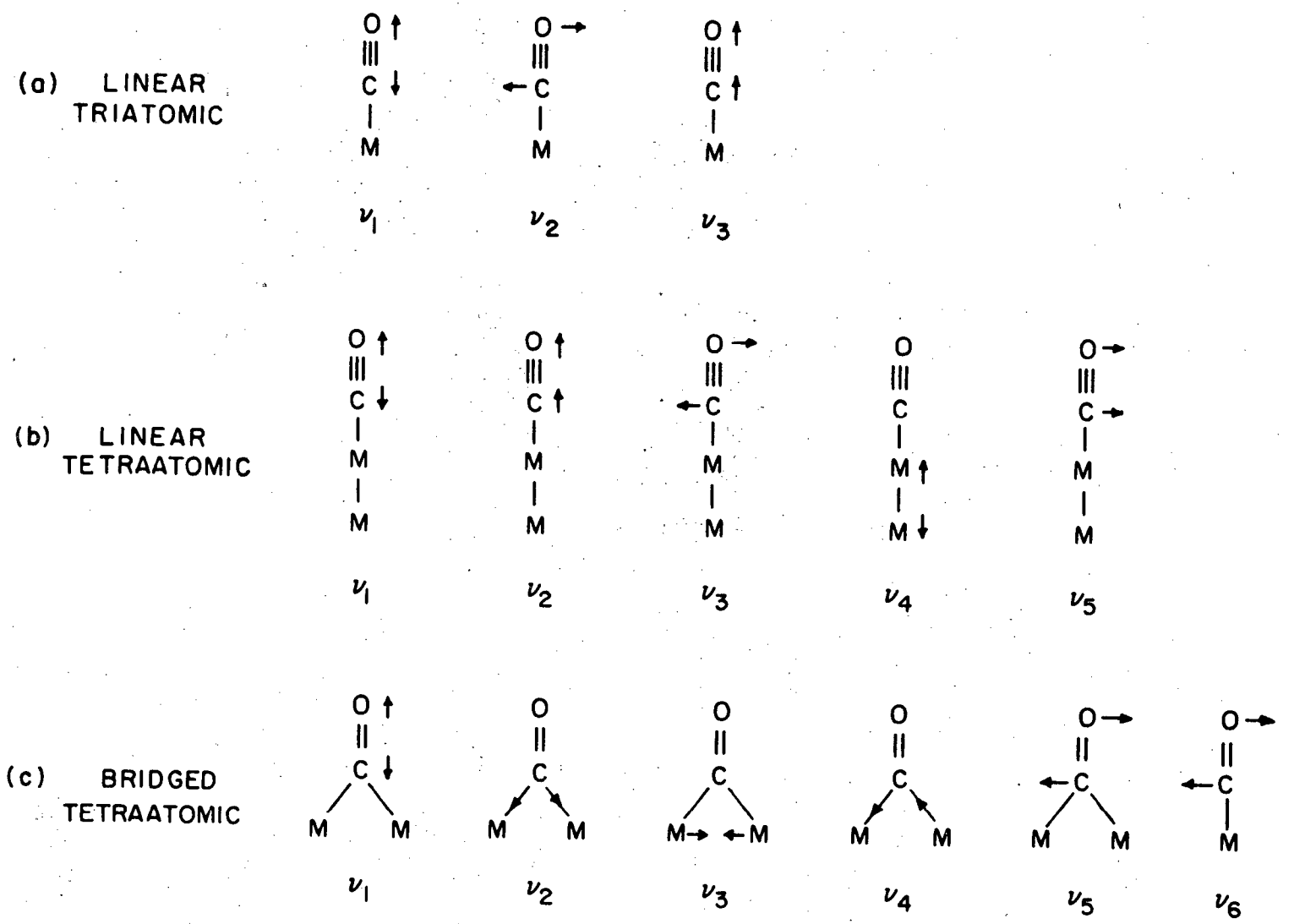
(a) LINEAR TRIATOMIC
$\nu_1$
$\nu_2$
$\nu_3$
(b) LINEAR TETRAATOMIC
$\nu_1$
$\nu_2$
$\nu_3$
$\nu_4$
$\nu_5$
(c) BRIDGED TETRAATOMIC
$\nu_1$
$\nu_2$
$\nu_3$
$\nu_4$
$\nu_5$
$\nu_6$

XBL 806-5320

derived by Richardson and Bradshaw[34] from the chemisorption of CO on Ni(100)[35] ($k_{C\equiv O}$ = 16.8 mdyne/Å, $k_{Rh-CO}$ = 2.6 mdyne/Å) and bending force constants from molybdenum hexacarbonyl ($k_{Rh-C\equiv O}$ = 0.45 mdyne Å/rad$^2$).[36] This should be a reasonable approximation to the bending force constants of the adsorbed molecule since the OC-Mo-CO bonds are all 90° and should approximately model the steric hindrance found in bending a surface Rh-C≡O bond. Bond lengths were taken from $Rh_6(CO)_{16}$ ($r_{C\equiv O}$ = 1.155 Å, $r_{Rh-C}$ = 1.864 Å).[37] Unfortunately no normal co-ordinate calculations on related rhodium carbonyls have been reported. Model compounds were chosen on the basis of similar metal-CO geometry (bond length, bond angle) and similar metal mass. The predicted vibrational frequencies can be computed using the equations presented by Herzberg.[38] These frequencies are listed in Table Ia.

A more reasonable approximation to the vibrational spectra may be obtained by assuming the mass of the rhodium atom is infinite (i.e., the carbon monoxide molecule is vibrating against a rigid crystal lattice). Table Ia indicates that this only seriously affects the metal-carbon stretching vibration ($\nu_3$) and leaves the other two modes relatively unchanged. The true situation should be somewhere between these two limits and with this choice of force constants we expect $\nu_3$ to occur slightly above 400 cm$^{-1}$. All of these modes are within the accessible scanning range of the spectrometer (400-4000 cm$^{-1}$). However, $\nu_2$ is parallel to the surface and because of the normal dipole selection rule (discussed in Chapter II) may not be observed.

A slightly more sophisticated approximation can be obtained by assuming a linear tetraatomic species: $Rh_{(a)}$-$Rh_{(b)}$-C≡O. In this case we have added a new doubly degenerate bending mode ($\nu_5 = \nu_{Rh-Rh-CO}$) and a

Table I. Calculated Frequencies (in $cm^{-1}$) for On-top CO on Rhodium

a) linear Rh-C≡O

| $m_{Rh}$ | $\nu_1$ | $\nu_2$ | $\nu_3$ |
|---|---|---|---|
| 102.9 | 2093 | 404 | 436 |
| ∞ | 2092 | 401 | 387 |

b) linear $Rh_{(a)}$ - $Rh_{(b)}$ - C≡O

| $m_{Rh_{(a)}}$ | $m_{Rh_{(b)}}$ | $\nu_1$ | $\nu_2$ | $\nu_3$ | $\nu_4$ | $\nu_5$ |
|---|---|---|---|---|---|---|
| 102.9 | 102.9 | 2092 | 443 | 418 | 153 | 76 |
| ∞ | 102.9 | 2092 | 441 | 417 | 102 | 71 |
| ∞ | ∞ | 2092 | 387 | 413 | 0 | 51 |

$k_{C\equiv O}$ = 16.8 mdyn/Å $r_{C\equiv O}$ = 1.155 Å

$k_{Rh-C}$ = 2.6 mdyn/Å $r_{Rh-C}$ = 1.864 Å

$k_{Rh-C\equiv O}$ = 0.45 mdyn Å/$rad^2$

$k_{Rh_{(a)}-Rh_{(b)}-C}$ = 0.3 mdyn Å/$rad^2$

metal-metal stretching vibration ($\nu_4 = \nu_{Rh-Rh}$). $\nu_5$ and $\nu_3$, the Rh-C≡O bending modes can be likened to a frustrated surface translation and to a frustrated surface rotation, respectively.[34] This is shown in Figure 1b. The new force constants $k_{Rh-Rh-CO}$ (0.3 mdyne Å/rad$^2$) and $k_{Rh-Rh}$ (0.82 mdyne/Å) were taken from $Ru_3(CO)_{12}$.[39] The rhodium-rhodium bond length is assumed to have the bulk value (2.69 Å).[40] The results of these calculations using the equations of Kohlrausch[41] are shown in Table Ib. As we expect, the computed frequencies are not significantly different than those calculated above since the geometry and the force constants have remained essentially unchanged. If we assume that the mass of $Rh_{(a)}$ is infinite (i.e., the $Rh_{(b)}$-CO unit is vibrating against a rigid lattice), then most of the calculated vibrational frequencies shift only slightly. We expect $\nu_4$ (the rhodium-rhodium stretch) to be significantly affected. Assuming that both rhodium atoms have infinite masses shifts $\nu_4$ to 0 and decreases $\nu_5$ to 51 cm$^{-1}$ (see Table Ib). Unfortunately observation of the low frequency modes (specifically $\nu_4$ and $\nu_5$) are out of the range of our spectrometer. Again, observation of vibrations parallel to the surface will be difficult.

A bridge bonded carbon monoxide molecule can be modeled by the $Rh_2 > C=O$ species shown in Figure 1c. Here we have six possible normal modes of vibration: a C=O stretch ($\nu_1$), a symmetric ($\nu_2$) and an asymmetric ($\nu_4$) $Rh_2 > CO$ stretch, a metal-metal stretch ($\nu_3$) and an in-plane ($\nu_5$) and an out-of-plane ($\nu_6$) $Rh_2 > C=O$ bend. The stretching force constants for these calculations were taken from the work of Richardson and Bradshaw ($k_{C=O}$ = 14.9 mdyne/Å, $k_{Rh_2>CO}$ = 1.1 mdyne/Å).[34] We take $k_\Delta$ (out-of-plane bend) equal to $k_{Rh_2>C=O}$ (in-plane bend) and use the force constant from $Mo(CO)_6$ (0.45 mdyne Å/rad$^2$).[36] Kroeker <u>et al</u>. have shown

this to be a reasonable approximation for the chemisorption of CO on alumina supported iron particles.[42] The Rh-C-Rh bending force constant can be approximated using the metal-metal stretching vibration and the metal-carbon bond length ($k_{Rh-C-Rh} \simeq k_{Rh-Rh}(r_{Rh-CO})^2 = 3.31$ mdyne Å/rad$^2$). Bond lengths for the bridge bonded species were taken from $(C_5H_5)_2Rh_2(CO)_3$ ($r_{C=O} = 1.155$ Å, $r_{Rh-C} = 2.01$ Å).[43] The Rh-C-Rh bond angle can be easily calculated knowing the bulk rhodium-rhodium separation and the rhodium-carbon bond length ($\langle Rh-C-Rh = \sin^{-1}(r_{Rh-Rh}/2r_{Rh-C}) \simeq 84°$).

The calculated values of the vibrational frequencies for the tetra-atomic bridged species are shown in Table II. Even though Figure 1c indicates that each mode is of a distinctive character, for realistic force constants there is a strong mixing of the low frequency stretching and bending vibrations of the same symmetry. However, most of the low frequency modes can become uncoupled when the mass of the two rhodium atoms goes to infinity. As expected, $\nu_3$, the metal-metal stretching vibration is zero in this case (see Table II). $\nu_3$ and $\nu_5$ are out of the range of our spectrometer, but are also essentially parallel to the surface and will therefore not be observed. Again, in these calculations we have neglected all interaction force constants. Inclusion of these force constants would certainly add complexity to the present calculations, but add little new physical insight. Furthermore, values of these force constants are not well-known.

Low frequency vibrational modes do have an effect on the geometry of the adsorbed species and this can be shown by calculating the mean square displacement of the adsorbed species. If we assume that the system can be treated in the harmonic oscillator approximation and that a Boltzmann distribution governs the population of the vibrational levels,

Table II. Calculated Frequencies (in $cm^{-1}$) for Bridged CO on Rhodium ($Rh_2 > C{=}O$)

| $m_{Rh}$ | $\nu_1$ | $\nu_2$ | $\nu_3$ | $\nu_4$ | $\nu_5$ | $\nu_6$ |
|---|---|---|---|---|---|---|
| 102.9 | 1981 | 429 | 150 | 627 | 179 | 433 |
| ∞ | 1981 | 398 | 0 | 621 | 139 | 431 |

$k_{C=O}$ = 14.9 mdyn/Å  $r_{C=O}$ = 1.155 Å

$k_{Rh-C}$ = 1.1 mdyn/Å  $r_{Rh-C}$ = 2.01 Å

$k_{Rh-C\equiv O}$ = $k\Delta$ = 0.45 mdyn Å/rad$^2$  $<_{Rh-C-Rh}$ = 84°

$k_{Rh-C-Rh}$ = 3.31 mdyne Å/rad$^2$

then[34,44]

$$\langle Q_i^2 \rangle = \frac{16.86}{\hbar\Omega_i} \coth(0.719\ \hbar\ \Omega_i/T).$$

Here $\langle Q_i^2 \rangle$ is the mean square amplitude of the vibrational normal coordinate i in $\mathring{A}^2$, $\hbar\,\Omega_i$ is the frequency of the mode involved (in $cm^{-1}$) and T is the temperature in °K. We can approximate the mean inclination $\langle\Theta\rangle$ by knowing the geometry of the adsorbed species ($\langle\Theta\rangle \simeq \tan^{-1}[\langle Q_i^2\rangle/(r_{Rh-C} + r_{C=O} \cos(\langle Rh-C-Rh/2)))]$). For the $\nu_5$ mode at 160 $cm^{-1}$ (its average value in Table II), $\langle\Theta\rangle$ is approximately 6° at 300 K. Thus the molecule is no longer completely perpendicular to the surface. Unfortunately such small changes in bond angle cannot be observed by low-energy electron diffraction.[3,4] However, the effects of these low frequency bending vibrations have been observed in recent electron stimulated desorption, ion angular distribution (ESDIAD) experiments.[45]

The amplitude (angular excursion) of these low frequency modes can become significant at elevated temperatures and may even be important in surface chemical reactions. We can calculate the population of a given vibrational level n using a simple Boltzmann distribution

$$N_n/N_o = e^{-n\hbar\Omega/kT}.$$

At a surface temperature of 570 K the population of high vibrational levels of $\nu_5$ (160 $cm^{-1}$) can be significant (see Table III). We can calculate the angular excursion of this mode ($\Theta_n$) in the harmonic approximation by assuming[45]

$$E_n = (n+\tfrac{1}{2})\,\hbar\,\Omega \simeq \tfrac{1}{2}k_{Rh_2>C=O}\ \Theta_n^2.$$

Table III. Relative Populations and Angles as a Function of Vibrational Level for the $\nu_5$ mode of $Rh_2 > CO$

| n | $N_n/N_o$ | $\Theta_n$ |
|---|---|---|
| 0 | 1 | 4.8° |
| 1 | 0.668 | 8.3 |
| 2 | 0.446 | 10.8 |
| 3 | 0.298 | 12.7 |
| 4 | 0.199 | 14.5 |
| ⋮ | ⋮ | ⋮ |
| 10 | 0.018 | 22.1 |
| 15 | 0.002 | 26.8 |
| 20 | $3.1 \times 10^{-4}$ | 30.8 |

Using the value of $k_{Rh_2>C=O}$ from Table II, we find that $\Theta_n$ is 22° for n=10 (see Table III). These high amplitude vibrational modes can cause a significant interaction between the molecular orbitals of the oxygen atom and of the metal surface. This will become especially important for carbon monoxide molecules adsorbed at step and/or defect sites since the CO bond is no longer perpendicular to the surface, even at low temperatures. Extensive orbital overlap may also lead to carbon-oxygen bond scission.

The application of these relatively simple calculations to more complex surface species is rather difficult at present due to the lack of accurate force constant information. Currently the best way to analyze high resolution electron energy loss spectra is by analogy with the infrared and Raman spectra of model organometallic compounds of known molecular structure.[10] Throughout the remainder of this thesis this approach will be used to discuss the structure of carbon monoxide chemisorbed on Rh(111) (Chapter IV),[46,47] the dissociative chemisorption of carbon dioxide on Rh(111) (Chapter V),[48] the structure and reactions of nitric oxide and carbon monoxide adsorbed on Rh(331) (Chapter VI),[49] the structure of CO chemisorbed on a rhodium on alumina model catalyst (Chapter VII)[33] and finally, the structure of acetylene, ethylene[47,50] and their decomposition fragments[47] chemisorbed on Rh(111) (Chapter VIII). Although at present this is the best way of analyzing the vibrational spectra of surface species, recent studies by Kroeker _et al_. have shown that care must be taken in making the direct comparison between adsorbed molecules and organometallic compounds.[42]

## References


1. G. Ertl and J. Kuppers, Low Energy Electrons and Surface Chemistry (Verlag-Chemie, Germany, 1974).

2. H. Ibach, ed., Electron Spectroscopy for Surface Analysis (Springer-Verlag, Berlin, 1977).

3. J. B. Pendry, Low Energy Electron Diffraction (Academic Press, London, 1974).

4. M. A. Van Hove and S. Y. Tong, Surface Crystallography by LEED (Springer-Verlag, Berlin, 1979).

5. M. Passler, A. Ignatiev, F. Jona, D. W. Jepsen, and P. M. Marcus, Phys. Rev. Lett. 43, 360 (1979).

6. S. Andersson and J. B. Pendry, Phys. Rev. Lett. 43, 363 (1979).

7. R. J. Behm, K. Christmann, G. Ertl, M. A. Van Hove, P. A. Thiel, and W. H. Weinberg, Surface Sci. 88, L59 (1979).

8. M. A. Van Hove, L. H. Dubois, R. J. Koestner, and G. A. Somorjai, Proc. 8th Intern. Vacuum Congress (Cannes, 1980), in press.

9. L. L. Kesmodel, R. C. Baetzhold and G. A. Somorjai, Surface Sci. 66, 299 (1977).

10. L. L. Kesmodel, L. H. Dubois, and G. A. Somorjai, Chem. Phys. Lett. 56, 267 (1978); J. Chem. Phys. 70, 2180 (1979).

11. G. J. Schulz, Principles of Laser Plasmas, G. Beketi, ed. (John Wiley and Sons, New York, 1976) p. 33.

12. F. M. Propst and T. C. Piper, J. Vac. Sci. Technol. 4, 53 (1967).

13. H. Ibach, "Proc. Conference on Vibrations in Adsorbed Layers," (Julich, Germany, 1978) p. 64 and references therein.

14. E. Evans and D. L. Mills, Phys. Rev. B5, 4126 (1972).

15. H. Ibach, Surface Sci. 66, 56 (1977).

16. R. P. Eischens, W. A. Pliskin, and S. A. Francis, J. Chem. Phys. 22, 1786 (1954).

17. R. P. Eischens and W. A. Pliskin, Adv. Catalysis, 10, 1 (1958).

18. L. H. Little, Infrared Spectra of Adsorbed Species (Academic Press, London, 1966).

19. M. L. Hair, Infrared Spectroscopy of Surface Chemistry (Dekker, New York, 1967).

20. W. H. Weinberg, Ann. Rev. Phys. Chem. 29, 115 (1978).

21. P. K. Hansma, Phys. Rep. 30, 145 (1977).

22. J. Kirtley and P. K. Hansma, Acc. Chem. Res. 11, 440 (1978).

23. W. Krasser and A. Renouprez, "Proc. Conference on Vibrations in Adsorbed Overlayers" (Julich, Germany, 1978) p. 175.

24. H. E. Evans, W. M. Bowser, and W. H. Weinberg, Surface Sci. 85, L497 (1979).

25. R. M. Kroeker, W. C. Kaska, and P. K. Hansma, J. Catal. 57, 72 (1979); J. Catal. 61, 87 (1980).

26. H. E. Evans and W. H. Weinberg, J. Am. Chem. Soc. 102, 872 (1980).

27. J. Kirtley and P. K. Hansma, Phys. Rev. B13, 2910 (1976).

28. J. Pritchard, Surface and Defect Properties of Solids, 7, M. W. Roberts and J. M. Thomas, eds. (Specialist Periodical Reports, Chemical Society, London, 1978).

29. N. Sheppard and T. T. Nguyen, Advances in Infrared and Raman Spectroscopy, 5, R. J. H. Clark and R. E. Hester, eds. (Heyden and Son, Ltd., London, 1978) p. 67.

30. H. Froitzheim, H. Ibach, and D. L. Mills, Phys. Rev. B11, 4980 (1975).

31. See for example: S. Andersson, Chem. Phys. Lett. 55, 185 (1978).

32. A. Adnot, "Proc. Conference on Vibrations in Adsorbed Layers," (Julich, Germany, 1978) p. 109.

33. L. H. Dubois, P. K. Hansma, and G. A. Somorjai, Appl. Surface Sci., in press.

34. N. V. Richardson and A. M. Bradshaw, Surface Sci. 88, 255 (1979).

35. S. Andersson, Solid State Commun. 21, 75 (1977).

36. L. H. Jones, R. S. McDowell, and M. Goldblatt, Inorg. Chem. 8, 2349 (1969).

37. E. R. Corey, L. F. Dahl and W. Beck, J. Am. Chem. Soc. 85, 1202 (1963).

38. G. Herzberg, Molecular Spectra and Molecular Structure II Infrared and Raman Spectra of Polyatomic Molecules (Van Nostrand, Princeton, N.J., 1945).

39. C. O. Quicksall and T. G. Spiro, Inorg. Chem. 7, 2365 (1968).

40. C. Kittel, Introduction to Solid State Physics (John Wiley and Sons, New York, 1976) p. 32.

41. K. W. F. Kohlrausch, Der Smekal-Raman-Effekt, Erganzungsband 1931-1937 (J. Springer, Berlin, 1938) p. 64.

42. R. M. Kroeker, P. K. Hansma, and W. C. Kaska, J. Chem. Phys. 72, 4845 (1980).

43. O. S. Mills and E. F. Paulus, J. C. S. Chem. Comm. 815 (1966).

44. S. J. Cyvin, Molecular Vibrations and Mean Square Amplitudes (Elsevier, Amsterdam, 1968).

45. T. E. Madey, Surface Sci. 79, 575 (1979).

46. L. H. Dubois and G. A. Somorjai, Surface Sci. 91, 514 (1980).

47. L. H. Dubois and G. A. Somorjai, ACS Symposium Series, Vol. 000, A. T. Bell and M. L. Hair, eds.(American Chemical Society, Washington, D. C. 1980).

48. L. H. Dubois and G. A. Somorjai, Surface Sci. 88, L13 (1979).

49. L. H. Dubois, P. K. Hansma, and G. A. Somorjai, J. Catal., in press.

50. L. H. Dubois, D. G. Castner and G. A. Somorjai, J. Chem. Phys. 72, 5234 (1980).

# CHAPTER II. Theory of Adsorbate Vibrational Excitation by Inelastic Electron Scattering from Metal Surfaces

## A. Background

The theory of long-wavelength surface optical phonons in ionic crystals was first discussed by Fuchs and Kliewer in 1965.[1] Subsequently, numerous groups have tackled the related problem of the inelastic scattering of low-energy electrons by surface vibrational modes.[2-20] Lucas and Sunjic solved for the differential scattering cross-section using a classical treatment of the electron as a point particle traveling along a single, specific trajectory (specular reflection).[2] They assumed that the electron remained in the vacuum above the crystal at all times and excited surface vibrations by means of its Coulomb field. Their results predicted only single phonon losses. However, their calculated inelastic scattering cross-sections agreed extremely well with those measured in early experiments.[21] An extension of this theory allowed for multiple phonon excitation bands (overtone and combination frequencies) with the intensities of the loss peaks given by a Poisson distribution.[3]

Evans and Mills[5] pointed out several problems with the classical treatment and emphasized that a fully quantum mechanical description of the electron-solid interaction must be used. The experimental conditions on the energy distribution require that $\Delta E_o/E_o$ be no greater than $10^{-2}$ where $E_o$ is the incident electron energy (2-7 eV) and $\Delta E_o$ is the energy width of the beam (8-12 meV). The uncertainty principle tells us that $\Delta r \Delta p \gtrsim 2\pi\hbar$ where $\Delta r$ is the spatial extent of the wavepacket and $\Delta p$ is the spread in the electron momentum. Putting this in terms of the electron energy and rearranging we find that

$$\Delta r \gtrsim \frac{4\pi\hbar}{\sqrt{2mE_o}} \left(\frac{E_o}{\Delta E_o}\right)$$

where m is the rest mass of the electron. If we substitute typical values for $E_o$ and $\Delta E_o$ we find that a minimum uncertainty width wave-packet is on the order of 2000 Å and therefore the electron can no longer be treated as a point particle. However, in the limit of specular reflection from an ideal surface the inelastic scattering cross-sections calculated from either the classical or the quantum mechanical treatment agree exactly.[5]

## B. The Scattering Process

The derivation of the differential inelastic scattering cross-section presented in this chapter will mainly follow that of References 10, 12, 13, 16 and 17. This theory will be a full quantum mechanical treatment. We will only consider the long range electron-dipole interaction, however. The theory of short ranged "impact" scattering has been presented recently by several authors.[18-20]

Consider an array of molecules, M, chemisorbed on a semi-infinite plane metal surface and assume that the interaction between neighboring adsorbed species can be neglected (see Fig. 1a). An electron beam incident on the surface from the vacuum ($z \geq 0$), will set-up an electric field on the surface. If the electrons are a long distance from the surface, then the electron-molecule interaction can be described by an electron-dipole term. This is the lowest order multipole interaction possible since the adsorbed molecules are neutral. Even in the case of chemisorption involving extensive charge transfer to or from the surface,

Figure 1. (a) An incident electron beam interacts with an array of molecules M chemisorbed on a plane metal surface. (b) If we take the Fourier transform of the electric field, $E(\omega)$, we find that all possible vibrational frequencies can be excited simultaneously.

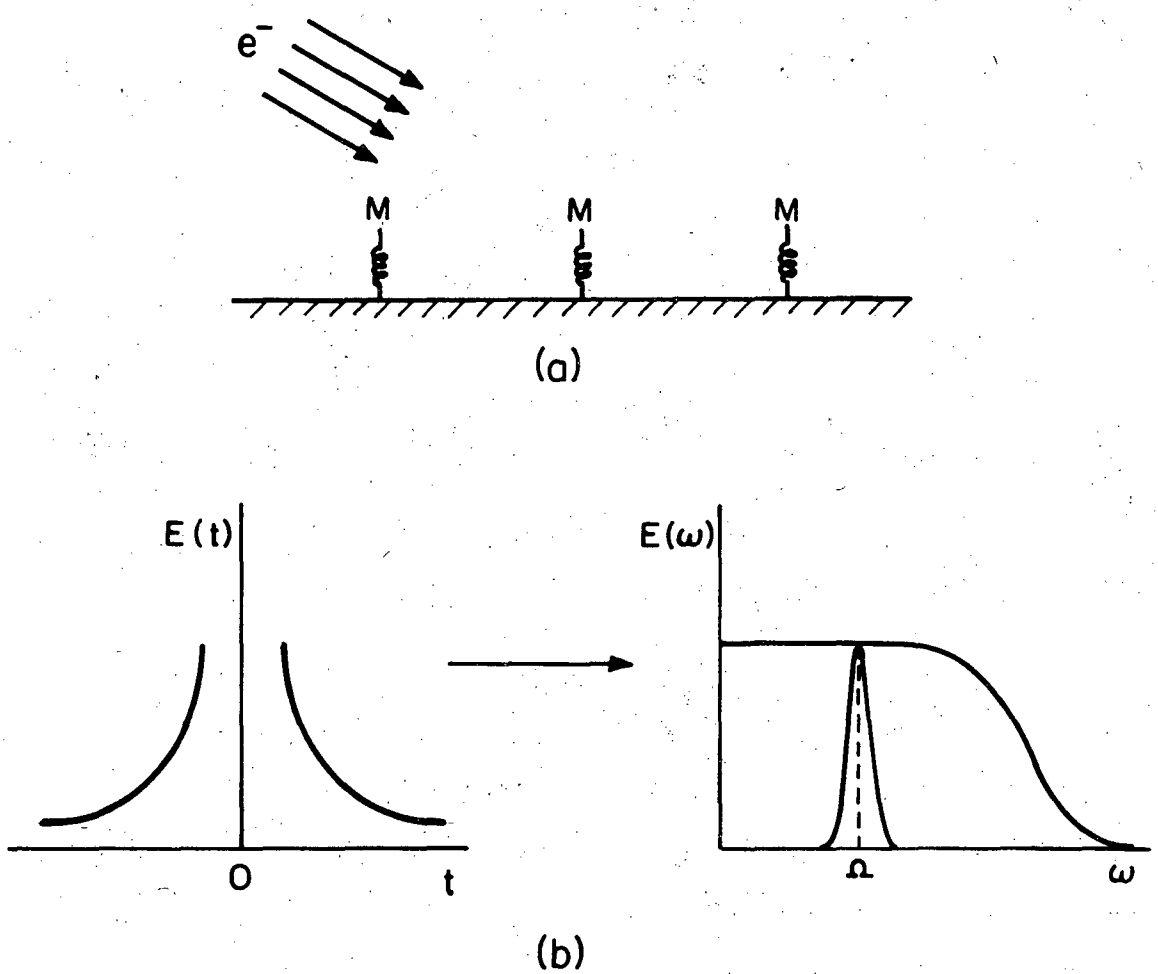


XBL 806-5310

overall neutrality must be retained.[16] Since we are constructing a time dependent electric field, a continuous distribution of vibrational energies will be excited. This can be seen if we take the Fourier transform of the field

$$E(t) = \int d\omega\, E(\omega)\, e^{i\omega t}. \tag{1}$$

Equation (1) is shown schematically in Figure 1b. Thus, unlike infrared spectroscopy, all possible surface vibrational modes can be excited simultaneously.

The interaction Hamiltonian between the incoming electrons and the adsorbed molecules, H', can be written as[10,17]

$$H' = -\vec{\mu}(\vec{R}) \cdot \vec{E}(\vec{r})$$

where $\vec{\mu}(\vec{R})$ is the total dipole moment operator (permanent plus oscillating) for one (arbitrary) molecule and $\vec{E}(\vec{r})$ is the electric field of the incident electrons at the position of the molecule. The scattering geometry is shown in Figure 2a. Expanding $\vec{\mu}(\vec{R})$ about the ground state configuration yields

$$\vec{\mu}(\vec{R}) = \vec{\mu}(\vec{R}_o) + (\vec{\nabla} \cdot \vec{\mu}(\vec{R}_o))\vec{R} + \ldots$$

We will neglect the first term, $\vec{\mu}(\vec{R}_o)$, which is the permanent dipole moment, since it only contributes to elastic electron scattering (see below). Furthermore, we will only assume a single vibrational mode of frequency $\Omega$ can be excited. Thus

$$\vec{\nabla} \cdot \vec{\mu}(\vec{R}_o) = \left.\frac{d\mu(R)}{dR}\right|_{R=R_o} \equiv \mu'.$$

Figure 2. (a) The scattering geometry. The subscripts o and s refer to the incident and scattered electron beams, respectively. The plane of incidence is defined as $\phi_o = 0$. (b) The position of the incident electron ($\vec{r}$) above the metal surface and its image ($\vec{r}'$) below the surface.

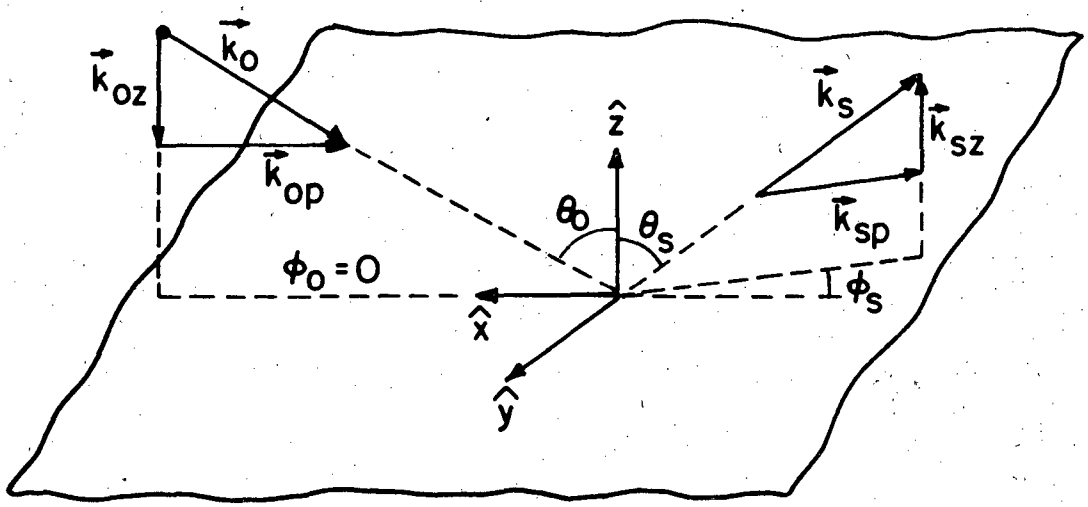


(a)

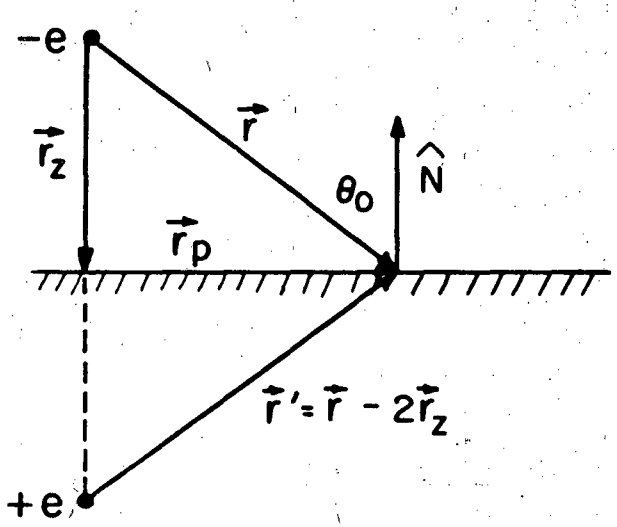


(b)

XBL806-5311

The contribution of different modes to the vibrational spectrum is additive at this level of sophistication in the theory.[16]

The electric field felt by a molecule in free space from a single incident electron is simply

$$\vec{E}(\vec{r}) = \frac{-e\vec{r}}{|\vec{r}|^3} \tag{2}$$

The electron-adsorbed molecule interaction is more complicated since the incident electron will also affect the electrons in the metal. This induced charge density will try to screen the external electric field and therefore add an additional term to Equation (2). Returning to Equation (1) we find that only the term $E(\Omega)\ e^{-i\Omega t}$ can excite a molecular vibration of frequency $\Omega$ (assuming the excited state has an infinite lifetime).[17] Therefore only the response of the electrons in the metal to this component of the electric field need be considered. Since $\Omega$ is much smaller than the plasma frequency $\omega_p$ ($\hbar\Omega \simeq 0.2$ eV, $\hbar\omega_p \simeq 10$ eV), the electrons in the metal can easily follow the slowly (on the scale of $1/\omega_p$) varying external field. Simple electrostatics tells us that we can replace the induced charge density in the metal by an image of the incident electron (see Fig. 2b). This is true regardless of the velocity (and therefore the energy) of the incident beam.[17] If the adsorbate is in the image plane, then Equation (3) gives us the electric field at the molecule from the electron in the vacuum at $\vec{r}$ and its image charge at $\vec{r}' = \vec{r} - 2\vec{r}_z$.[10]

$$\vec{E}(\vec{r}) = \frac{(-e)\vec{r}}{|\vec{r}|^3} + \frac{e(\vec{r}-2\vec{r}_z)}{|\vec{r}'|^3} = \frac{-2e\vec{r}_z}{|\vec{r}|^3} \tag{3}$$

This simplification can be performed since $|\vec{r}| = |\vec{r}'|$ (see Fig. 2b).

Equation (3) requires the electric field to be normal to the surface at all times. Therefore only those molecular vibrations with a nonzero oscillating dipole moment perpendicular to the surface can be excited. This normal dipole selection rule has been shown to be valid for infrared spectroscopy[11-13] as well as for ELS and will be discussed in more detail in Section F.

For a one-dimensional harmonic oscillator oriented perpendicular to the surface, the interaction Hamiltonian can now be written as

$$H' = -(\mu'\vec{R}) \cdot \left(\frac{-2e\vec{r}_z}{|\vec{r}|^3}\right)$$

$$= 2\ e\mu'|\vec{R}|\ \frac{|\vec{r}_z|}{|\vec{r}|^3}\ . \qquad (4)$$

C. The Inelastic Scattering Cross-section

Since the adsorbed molecules are very heavy compared to the incident electrons, we can write the zero-order wavefunction in a seperable form (the adiabatic approximation).

$$\psi_{\vec{k}}(\vec{r},\vec{R}) = \Phi_{\vec{k}}(\vec{r})\ \chi(\vec{R})$$

where $\vec{r}$ refers to the incident electron and $\vec{R}$ is the normal coordinate of the individual atoms in the adsorbed molecule. We can solve for the transition amplitude, T, using first-order time dependent perturbation theory.

$$T = \langle\psi_{\vec{k}_s}(\vec{r},\vec{R})|\ H'\ |\psi_{\vec{k}_o}(\vec{r},\vec{R})\rangle.$$

The subscripts o and s refer to the incident and inelastically scattered electron waves, respectively. T can be readily calculated by substituting

$\psi_{\vec{k}}(\vec{r},\vec{R})$ and H' (Eq. (4)) and separating the integrals

$$T = 2e\mu' < \Phi_{\vec{k}_s}(\vec{r}) | \frac{|\vec{r}_z|}{|\vec{r}|^3} | \Phi_{\vec{k}_o}(\vec{r}) > < \chi_1(\vec{R}) | \; |\vec{R}| \; | \chi_0(\vec{R}) >. \qquad (5)$$

The second integral is the easiest to solve and will be discussed first. We can write the normal mode displacement R of a one-dimensional harmonic oscillator in terms of the second quantized oscillator operators[22]

$$R = \left(\frac{\hbar}{2M\Omega}\right)^{\frac{1}{2}} (a + a^{\dagger})$$

where

$$\left.\begin{matrix} a \\ a^{\dagger} \end{matrix}\right\} = \left(\frac{M\Omega}{2\hbar}\right)^{\frac{1}{2}} R \pm ip(2M\Omega\hbar)^{-\frac{1}{2}}.$$

M and $\Omega$ are the reduced mass and frequency of the mode, respectively. p is the momentum of the oscillator. $\chi_0(\vec{R})$ and $\chi_1(\vec{R})$ are the ground state ($|0>$) and first excited state ($|1> = a^{\dagger}|0>$) wavefunctions of a harmonic oscillator. The vibrational transition matrix element is then

$$<\chi_1(\vec{R}) | \; |\vec{R}| \; | \chi_0(\vec{R}) > = <1| \; R \; |0> = \left(\frac{\hbar}{2M\Omega}\right)^{\frac{1}{2}}. \qquad (6)$$

The scattering transition matrix element (the first integral in Equation (5)) is slightly more difficult to calculate. The wavefunction for a plane wave in free space is

$$\Phi_{\vec{k}}(\vec{r}) = e^{i\vec{k}\cdot\vec{r}}.$$

This must be modified to include a reflected wave after scattering from a surface (see Fig. 2a), however.

$$\Phi_{\vec{k}}(\vec{r}) = e^{i\vec{k}_p\cdot\vec{r}_p}\left[e^{-i\vec{k}_z\cdot\vec{r}_z} + R(\vec{k})\, e^{-2i\delta(\vec{k})}\, e^{i\vec{k}_z\cdot\vec{r}_z}\right]$$

$\vec{k}_p$ and $\vec{k}_z$ are the parallel and perpendicular components of the electron momentum ($\vec{k}$), respectively. $\vec{r}_p$ and $\vec{r}_z$ are defined in Figure 2b. $R(\vec{k})$ is the reflection coefficient which specularly scatters the incident wave $e^{i\vec{k}\cdot\vec{r}}(=e^{i\vec{k}_p\cdot\vec{r}_p}\, e^{-i\vec{k}_z\cdot\vec{r}_z})$. The reflectivity of the surface is given by $|R(\vec{k})|^2$. $\delta(\vec{k})$ is the phase shift experienced by the reflected electron wave. Inserting this modified wavefunction into the first integral of Equation (5) and simplifying we find four contributions to the scattering transition matrix element.

$$S \equiv \langle\Phi_{\vec{k}_s}(\vec{r})|\,\frac{|\vec{r}_z|}{|\vec{r}|^3}\,|\Phi_{\vec{k}_o}(\vec{r})\rangle = \int_{r_z>0} d^3r\,\frac{|\vec{r}_z|}{|\vec{r}|^3}\, e^{i(\vec{k}_{o_p}-\vec{k}_{s_p})\cdot\vec{r}_p}$$

$$\times\left[e^{-i(\vec{k}_{o_z}-\vec{k}_{s_z})\cdot\vec{r}_z} + R^*(\vec{k}_s)\, e^{2i\delta(\vec{k}_s)}\, e^{-i(\vec{k}_{o_z}+\vec{k}_{s_z})\cdot\vec{r}_z}\right.$$

$$+\; R(\vec{k}_o)\, e^{-2i\delta(\vec{k}_o)}\, e^{i(\vec{k}_{o_z}+\vec{k}_{s_z})\cdot\vec{r}_z} + R^*(\vec{k}_s)R(\vec{k}_o)$$

$$\left.\times\; e^{-2i(\delta(\vec{k}_o)-\delta(\vec{k}_s))}\, e^{i(\vec{k}_{o_z}-\vec{k}_{s_z})\cdot\vec{r}_z}\right]. \qquad (7)$$

These four contributions are shown schematically in Figure 3. The first term in Equation (7) (Fig. 3a) is equivalent to the scattering of electrons by molecules in the gas phase. The incident electrons are both inelastically scattered and "reflected" by the adsorbed molecule. The cross-section for this process is extremely small except for certain electron energies where short-range impact (or resonant) scattering occurs. This is discussed in detail in References 18-20. The most probable scattering mechanisms are illustrated in Figures 3b and 3c. Here electron reflection from the surface is either preceded by or followed by small

Figure 3. Four possible contributions to the inelastic electron scattering cross-section: (a) The adsorbed molecule both inelastically scatters and reflects the incident electron. Electron reflection from the surface can also be (b) preceded by or (c) followed by vibrational excitation of the adsorbate. The probability of (d) electron reflection from the surface followed by large angle inelastic scattering and reflection from the surface once again is low.

Inelastic Electron Scattering

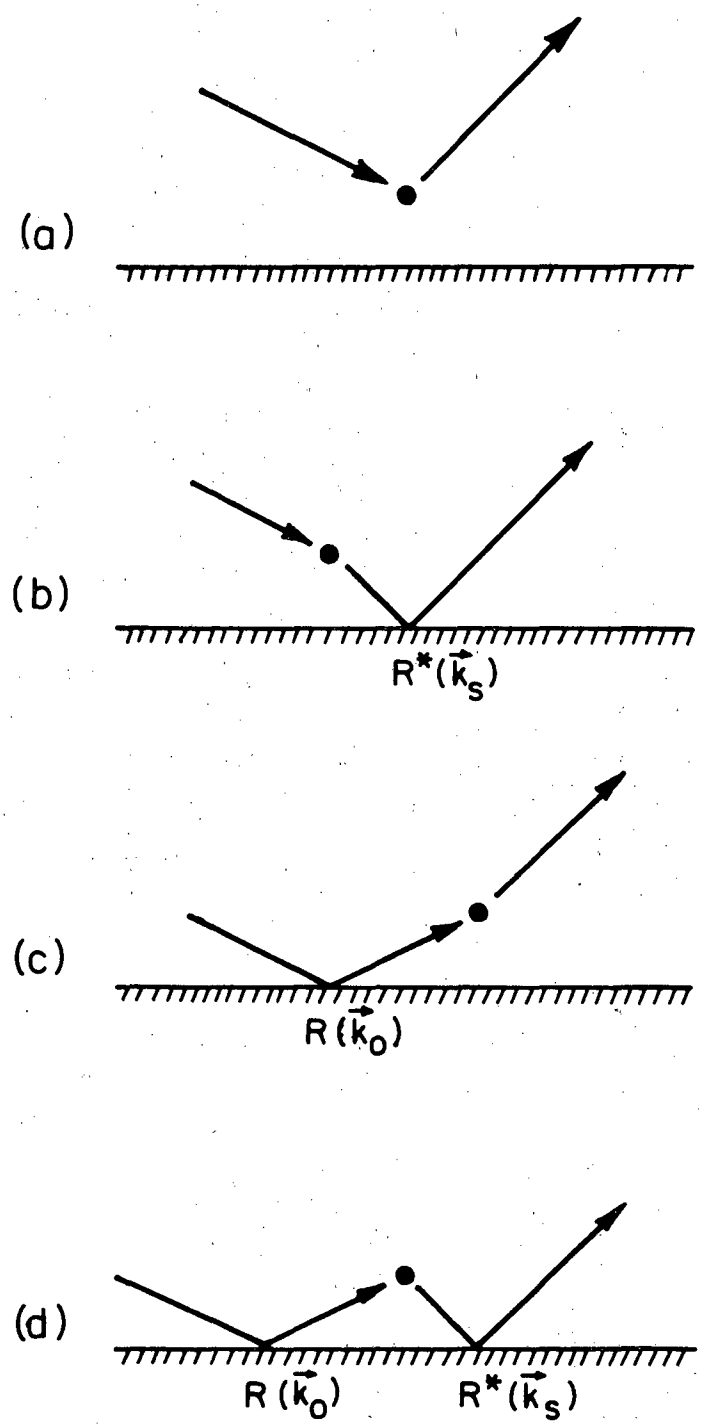


XBL 806-5312

angle inelastic scattering from the molecule. The probability of reflection from the surface followed by large angle inelastic scattering and reflection from the surface (Fig. 3d) will be small.

Analytical solutions to Equation (7) are difficult to obtain since both $R(\vec{k})$ and $\delta(\vec{k})$ cannot be accurately calculated. However, by making several assumptions a reasonable approximation to the solution can be obtained. Since these quantities are only functions of $\vec{k}$ and since the momentum transfer to the surface during excitation of a molecular vibration is small (see Section E), we will assume that $R(\vec{k})$ and $\delta(\vec{k})$ are slowly varying functions of $\vec{k}$ and therefore

$$R(\vec{k}_o) = R(\vec{k}_s) \equiv R \qquad\qquad \delta(\vec{k}_o) = \delta(\vec{k}_s) \equiv \delta.$$

This has been shown experimentally by McRae and Caldwell[23] and Watts[24] for elastic low-energy electron scattering from nickel surfaces. Furthermore, we will define $\Delta_{\vec{p}}$, $\Delta_{\vec{z}}$ and $\Delta_{\vec{z}}$ as follows:

$$\Delta_{\vec{p}} \equiv \vec{k}_{o_p} - \vec{k}_{s_p} \qquad\qquad \Delta_{\vec{z}} \equiv \vec{k}_{o_z} - \vec{k}_{s_z} \qquad\qquad \Sigma_{\vec{z}} \equiv \vec{k}_{o_z} + \vec{k}_{s_z}$$

Equation (7) can now be written in a more compact form.

$$S = \int_{r_z>0} d^3r \, \frac{|\vec{r}_z|}{|\vec{r}|^3} \, e^{i\Delta_{\vec{p}}\cdot\vec{r}} \Big[ e^{-i\Delta_{\vec{z}}\cdot\vec{r}_z} + R^* \, e^{2i\delta} \, e^{-i\Sigma_{\vec{z}}\cdot r_{\vec{z}}} + R \, e^{-2i\delta} \, e^{i\Sigma_{\vec{z}}\cdot\vec{r}_z} + R^* R \, e^{i\Delta_{\vec{z}}\cdot\vec{r}_z} \Big] . \tag{8}$$

Again, the four contributions to the scattering amplitude of Equation (8) are represented schematically in Figure 3a-d.

Sokcevic et al.[12,13,15] have solved the integral in Equation (8).

$$S = \frac{(R^2+1)\Delta_p}{\Delta_p^{\,2}+\Delta_z^{\,2}} + \frac{R}{\Delta_p^{\,2}+\Sigma_z^{\,2}} (\Delta_p \cos 2\delta + \Sigma_z \sin 2\delta) + \frac{i(R^2-1)}{\Delta_p^{\,2}+\Delta_z^{\,2}} \tag{9}$$

We can now combine the results of Equations (6) and (9) to calculate the transition matrix element T.

$$T = 2e\mu' \left(\frac{\hbar}{2M\Omega}\right)^{\frac{1}{2}} \left[ \frac{(R^2+1)\Delta_p}{\Delta_p^{\,2}+\Delta_z^{\,2}} + \frac{R}{\Delta_p^{\,2}+\Sigma_z^{\,2}} (\Delta_p \cos 2\delta + \Sigma_z \sin 2\delta) + \frac{i(R^2-1)}{\Delta_p^{\,2}+\Delta_z^{\,2}} \right] \quad (10)$$

In converting the scattering amplitude (10) to a differential scattering cross-section, we must take into account the flux of incident electrons and the relative velocities of the incoming and outgoing electron beams.[22,25] Electrons are detected in a cone $d\Theta d\phi$ and therefore

$$\frac{d^2\sigma}{d\Theta d\phi} = \frac{m^2}{4\pi^2\hbar^4} \frac{1}{\cos\Theta} \left(\frac{v_s}{v_o}\right) |T|^2 \, \delta(E_o-(E_s+\hbar\Omega)) \quad (11)$$

$v_s$ and $v_o$ are the velocities of the inelastically scattered and incident electrons, respectively. The $\delta$ function is to insure conservation of energy. $E_o$ and $E_s$ refer to the energies of the incident and scattered electrons, respectively. Substituting (10) into (11) and rearranging in terms of known quantities, we find

$$\frac{d^2\sigma}{d\Theta d\phi} = \frac{e^2(\mu')^2}{8\pi^2 E_o \hbar\Omega\cos\Theta} \frac{m}{M} \left(\frac{E_s}{E_o}\right)^{\frac{1}{2}} f^2 \, \delta(E_o - E_s - \hbar\Omega) \quad (12)$$

$f(=2k_oS)$ is a dimensionless scattering amplitude. This quantity (Equation (9)) is determined from the characteristics of the incident ($E_o$, $\Theta_o$) and outgoing electrons ($E_s$, $\Theta_s$) and by the details of the reflection process. f can be more accurately calculated using the wavefunctions and scattering potentials developed for low-energy electron diffraction.[26,27]

## D. Numerical Calculations

Unfortunately, accurate differential scattering cross-sections are difficult to determine experimentally, even when the scattering amplitude is known well. The measurements are further complicated by disordered overlayers and the non-zero angular acceptance of the spectrometer. These potential problems can be alleviated by taking the intensity ratio of the inelastic ($I_s$) to the elastic ($I_o$) scattering peaks. Several authors have calculated approximate values for the case of specular electron reflection from a well ordered surface.[5,11]

$$\frac{I_s}{I_o} = 4\pi\left(\frac{m}{M}\right) \frac{e^2(\mu')^2}{\hbar\Omega E_o} \; n \cos\Theta \; g(E_o, \Theta_o) \tag{13}$$

n is the concentration of surface oscillators ($cm^{-2}$) and $g(E_o, \Theta_o)$ is an angular term

$$g(E_o, \Theta_o) = (\tan^2\Theta - 2)\left(\frac{\alpha^2}{\alpha^2+\beta^2}\right) + (\tan^2\Theta + 2)\ \ln\left(1 + \frac{\alpha^2}{\beta^2}\right).$$

Here we assume the spectrometer accepts electrons in a cone with half angle $\alpha$ (circular aperture) about the specular beam. $\beta$ is a dimensionless beam width parameter given by

$$\beta = \frac{\hbar\Omega}{2E_o} .$$

For one third of a monolayer of carbon monoxide chemisorbed on a clean Rh(111) single crystal surface, Equation (13) gives a value of $I_s/I_o$ of approximately 0.007. The values used in the calculation, including the operating characteristics of the spectrometer to be used in the following experiments (see Chapter III), are listed in Table I.

$\mu'$ was taken from gas phase data,[28] but this agrees quite well with the value calculated from the chemisorption of CO on Pt(111) ($\mu' = 0.90 \times 10^{-19}$ C).[15,29] Using a value of $\mu'$ derived from the inelastic electron tunneling results of Kroeker et al.[30] from the chemisorption of carbon monoxide on alumina supported rhodium particles ($3.6 \times 10^{-19}$ C) increases $I_s/I_o$ to approximately 0.09. We expect the observed inelastic scattering intensities in our experiments to be somewhere between these two values.

Table I. The Chemisorption of CO on Rh(111)

| | |
|---|---|
| $\mu' = 3.1\ \Delta/\mathring{A} = 1.04 \times 10^{-19}$ C | $E_o = 5$ eV |
| $\hbar\Omega = 2100\ cm^{-1} = 0.26$ eV | $\Theta_o = 60°$ |
| $n = 5.3 \times 10^{14}\ cm^{-2}$ | $\alpha = 1.5°$ |

## E. Long Range Nature of the Scattering

Much has been said about the long-range nature of the inelastic scattering process. It is because of this long-range electron surface oscillating dipole interaction that the momentum transfer to the surface during vibrational excitation is small. Therefore, the inelastically scattered electrons should be scattered very close to either the specular beam or to one of the Bragg beams. The normal dipole selection rule (mentioned earlier and discussed in more detail below) is also a consequence of this long-range interaction.

The question arises: Just how far above the surface does this interaction begin to take place? First we consider elastic electron scattering from a semi-infinite rigid lattice of metal atoms.[31] For an incident electron far from the crystal the potential $\phi(\vec{r}) = \phi(\vec{r}_p, \vec{r}_z)$ must satisfy Laplace's equation

$$\nabla^2\phi(\vec{r}_p, \vec{r}_z) = 0. \tag{14}$$

For a periodic crystal, the surface charge density $\rho(\vec{r}_p, \vec{r}_z)$ may be expanded in a power series of reciprocal lattice vectors $\vec{G}_p$.

$$\rho(\vec{r}_p, \vec{r}_z) = \sum_{\vec{G}_p} \rho_{\vec{G}_p}(\vec{r}_p)\, e^{i\vec{G}_p\cdot\vec{r}_p}.$$

This is similar to the series expansion in terms of Bloch functions in three dimensions. The potential felt by the electron must reflect this two dimensional periodicity. Thus

$$\phi(\vec{r}_p, \vec{r}_z) = \sum_{\vec{G}_p} \phi_{\vec{G}_p}(\vec{r}_z)\, e^{i\vec{G}_p\cdot\vec{r}_p}. \tag{15}$$

If we now substitute this potential into Laplace's Equation (14) and recall that $\phi(\vec{r}_p, \vec{r}_z)$ must go to zero as $|\vec{r}|$ goes to infinity,

$$\phi_{\vec{G}_p}(\vec{r}_z) = \begin{cases} 0 & |\vec{G}_p| = 0 \\ \phi_{\vec{G}_p}(0)\, e^{i|\vec{G}_p||\vec{r}_z|} & |\vec{G}_p| \neq 0 \end{cases}$$

$\phi_{\vec{G}_p}(0)$ is found by the boundary conditions at $|\vec{r}_z| = 0$ (on the metal surface).

The important point here is that for elastic electron scattering the potential (Equation (16)) goes to zero rapidly, even at small $|\vec{r}_z|$. If $a_o$ is the lattice constant (~2-3 Å), then the smallest non-zero value of $|\vec{G}_p|$ is $2\pi/a_o$. Thus from (16)

$$\phi_{\vec{G}_p}(a_o) = \phi_{\vec{G}_p}(0)\, e^{-2\pi} \simeq 0.002\, \phi_{\vec{G}_p}(0).$$

Therefore, the electron-rigid crystal lattice interaction is <u>short-ranged</u> for elastic scattering. The incident electrons do not significantly interact with the metal atoms until they penetrate the actual charge distribution of the surface. Thus, we can obtain structural information by analyzing both the angle and intensity of the elastically scattered (diffracted) electrons.[26,27]

If the effects of the small surface (or adsorbate) vibrations are considered, then the incident electrons can lose energy by interacting with one of these modes. Using an analysis similar to the above, we can show that the inelastic electron scattering occurs via a long-range Coulomb potential. Let $\delta\phi_{\vec{k}_p}(\vec{r}_p, \vec{r}_z)$ be the change in $\phi(\vec{r}_p, \vec{r}_z)$ caused by the excitation of a surface vibrational mode of wave vector $\vec{k}_p$.

$$\delta\phi_{\vec{k}_p}(\vec{r}_p, \vec{r}_z) = \delta\phi_{\vec{k}_p}(\vec{r}_z)\, e^{i\vec{k}_p \cdot \vec{r}_p}.$$

This is analogous to Equation (15) above. If we substitute (17) into (14) we find that

$$\delta\phi_{\vec{k}_p}(\vec{r}_z) = \begin{cases} 0 & |\vec{k}_p| = 0 \\ \delta\phi_{\vec{k}_p}(0)\, e^{-|\vec{k}_p||\vec{r}_z|} & |\vec{k}_p| \neq 0. \end{cases} \tag{18}$$

Again the potential must go to zero as $|\vec{r}_z|$ approaches infinity. $\delta\phi_{\vec{k}_p}(0)$ is found from the boundary conditions at $|\vec{r}_z| = 0$. Unlike the case in Equation (16), there is no longer a minimum value of $|\vec{k}_p|$. Thus at $|\vec{r}_z| = 1/|\vec{k}_p|$,

$$\delta\phi_{\vec{k}_p}(1/|\vec{k}_p|) = 1/e\ \delta\phi_{\vec{k}_p}(0)$$

we can easily find the value of $1/|\vec{k}_p|$ at which this happens.

Conservation of monentum parallel to the surface requires that

$$|\vec{k}_p| = |\vec{k}_{op} - \vec{k}_{sp}|$$

$|\vec{k}_p|$ can easily be calculated knowing the characteristics of our spectrometer. Using the data in Table I for carbon monoxide chemisorbed on a rhodium surface we find that $|\vec{k}_p| \approx 10^6$ cm$^{-1}$ and therefore $1/|k_p| \approx 100$ Å. The effect of this potential at 100 Å above the surface is only decreased from its value at $|\vec{r}_z| = 0$ by a factor of 1/e (~0.37).

Because of the long-range nature of the inelastic scattering process, the momentum transferred to the surface by the incident electrons is quite small for vibrational excitation of the adsorbed species. Therefore, the inelastically scattered electrons should be scattered very close to either the specular beam or to one of the Bragg beams. This has been shown experimentally by Ibach.[32] We can use the expression derived in Equation (9) to calculate the angular distribution of the inelastically scattered electrons. This is shown in Figure 4a for the chemisorption of carbon monoxide on rhodium. The two values of $\hbar\Omega$, 2100 and 500 cm$^{-1}$ refer to the carbon-oxygen and metal-CO stretching vibrations, respectively (see Chapter I). The rather arbitrarily chosen values of R(0.2) and $\delta(\pi/2)$ do not significantly affect the results. The intensities of these two modes are normalized to 1. $f_p$ and $f_z$ refer to the scattering amplitude parallel and perpendicular to the surface, respectively. d is the height of the molecule above the surface.

The full width at half maximum in the angular distribution of $|f_z|^2$ for the 2100 cm$^{-1}$ mode is ~2°. This angle depends on both the incident beam energy and the frequency of the vibrational mode involved and its

Figure 4. (a) The angular distribution of inelastically scattered electrons by modes at 2100 and 500 $cm^{-1}$. The two curves are normalized to 1. (b) If a vibrational mode of frequency 500 $cm^{-1}$ is spaced above the surface 2.5 Å, a weak parallel component to the scattering amplitude ($|f_p|^2$) is also observed.

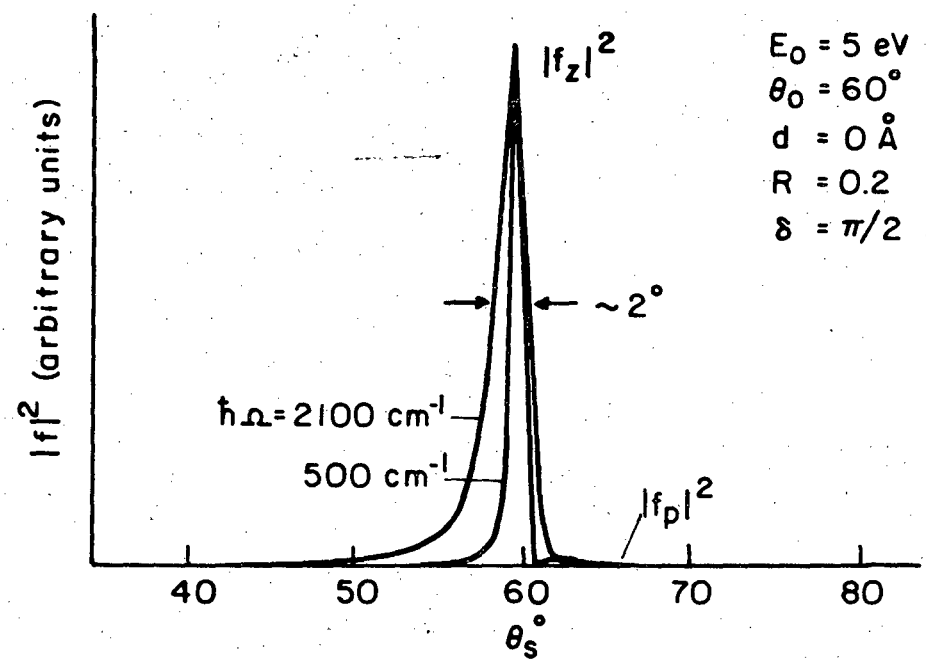


(a)

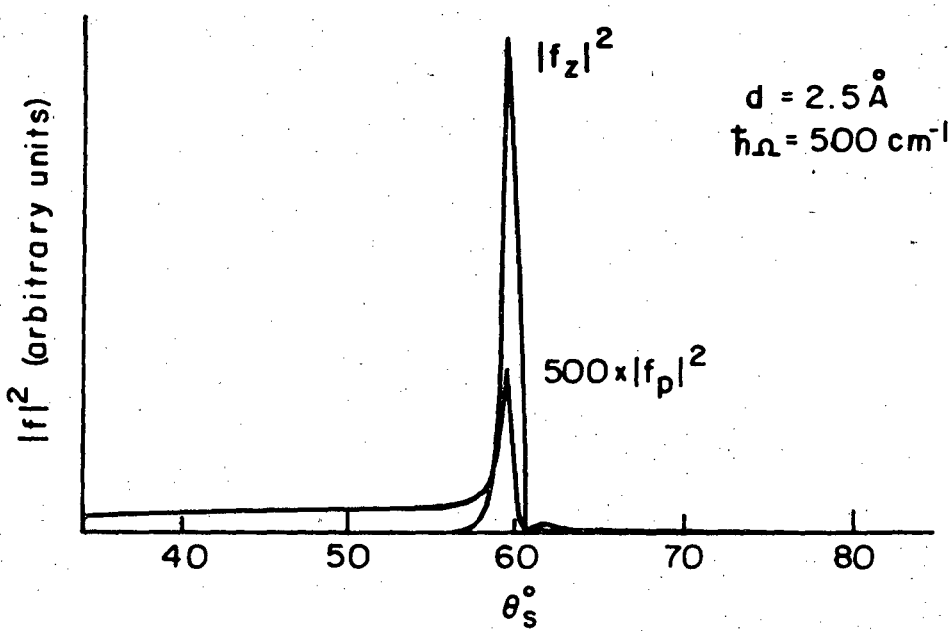


(b)

XBL806-5313

value can be approximated by $\beta$, the beam width parameter ($\hbar\Omega/2E_o$). As the vibrational frequency decreases, both $\beta$ and the angular distribution of $|f_z|^2$ decrease and this is precisely what we see here. As mentioned earlier, the normal dipole selection rule requires $|f_p|^2$ to be zero for an oscillator located at $d = 0$. In the next section we will show how this can breakdown for a molecule located a distance d above the surface.

## F. The Dipole Selection Rule

The normal dipole selection rule has been quoted several times throughout this chapter, but will be repeated here for completeness: Only those vibrations with a changing dipole moment perpendicular to the surface can be excited. There have been several recent reports, however, indicating that this selection rule does not rigorously hold for inelastic electron scattering and vibrational modes parallel to the surface have been observed. For the case of benzene and deuterated benzene parallel bonded to both Ni(111) and Ni(100), Bertolini et al. recorded several modes of $E_{1u}$ symmetry.[33] In the gas phase all of these modes are in the plane of the molecule. Studies on W(001) by Adnot and Carette showed the presence of a W-H bending mode at 632 $cm^{-1}$ for atomically adsorbed hydrogen ($\beta_2$ state).[34] Finally, Backx et al. observed a C-C stretching vibration at 1120 $cm^{-1}$ for acetylene parallel bonded to a W(110) surface.[35,36] They claimed that the coupling of this lateral vibration to the surface (either by a charge redistribution in the metal or by coupling with low-energy phonons) could add a perpendicular component to an otherwise completely parallel mode. There is now evidence that observation of such a mode in specular electron reflection may be caused by non-dipole scattering.[37]

Sokcevic et al.[12,13] have also shown that the "perpendicular dipole selection rule," which should rigorously hold for infrared spectroscopy, does not necessarily apply to high resolution ELS. In the IR the photon wavelengths ($\lambda$) are such that $\lambda >> d$, where d is the height of the oscillating dipole above the surface. Therefore both the molecule and its "image" interact with the radiation together, giving cancellation of all parallel vibrations. However, this is not the case for ELS since the incident electrons have wavelengths on the order of angstroms. There are at least four different causes for a breakdown in the normal dipole selection rule: 1) non-dipole scattering, 2) scattering from insulator surfaces, 3) scattering from molecules located above the surface and 4) scattering from stepped and/or polycrystalline surfaces.

For the case of short-ranged "impact" scattering both theory[18-20] and experiment[38,39] indicate that all possible normal mode vibrations should be observed. The angular distribution of these modes will be quite broad and scattering will not necessarily be observed in the specular direction. The reader is referred to References 18, 20, 38 and 39 for an extensive discussion of this scattering mechanism.

All possible normal mode vibrations should also be observed for molecules adsorbed on insulator surfaces. Due to the relatively low dielectric constant of these surfaces, the incident electrons will not be effectively screened by the image charges and therefore the simple model presented earlier will not work. Thus we might expect the normal dipole selection rule to breakdown in this case as well. To date no experiments have been reported on well characterized insulator surfaces and this postulate remains untested.

Even for the case of a molecule chemisorbed on a perfectly clean, flat and reflective metal surface, parallel vibrations can be observed. This was hinted at in the last section. A molecule located a distance d above a metal surface will feel a parallel component to the electric field. We can show this mathematically by modifying Equation (3) slightly

$$\vec{E}(\vec{r}) = \frac{(-e)(-\vec{r}+\vec{d})}{|-\vec{r}+\vec{d}|} + \frac{(e)(-\vec{r}'+\vec{d})}{|-\vec{r}'+\vec{d}|} . \tag{19}$$

The scattering geometry is shown in the insert to Figure 5a. We can easily resolve Equation (19) into parallel and perpendicular components of $\vec{E}(\vec{r})$.

$$E_p = er \sin\Theta_o[(r^2+d^2-2rd\cos\Theta_o)^{-3/2} - (r^2+d^2+2rd\cos\Theta_o)^{-3/2}]$$

$$E_z = e[(r\cos\Theta_o-d)(r^2+d^2-2rd\cos\Theta_o)^{-3/2} + (2r\cos\Theta_o+d)(r^2+d^2 + 2rd\cos\Theta_o)^{-3/2}].$$

The total field is simply $E = (E_p^{\,2} + E_z^{\,2})^{1/2}$. Representative plots of $E_p$, $E_z$ and E as a function of the incident electron's distance from the surface for d = 0, 1 and 2 Å above the surface are shown in Figure 5.

For a molecule on the surface (d=0) the normal dipole selection rule requires that $E_p$ be 0 and $E = E_z$. This is clearly shown in Figure 5a. However, even when a molecule is only 1 Å above the surface, $E_p$ can be significant when the incident electron is close to the molecule (see Fig. 5b). For d=2 Å, (Fig. 5c) $E_p$ can be larger than $E_z$! This is actually a very realistic situation since atoms or molecules located in atop positions will be spaced above the surface at least the sum of the radii of

Figure 5. The parallel ($E_p$), perpendicular ($E_z$) and total (E) electric fields from a single incident electron felt by a molecule spaced a distance of (a) 0, (b) 1 and (c) 2 Å above a plane metal surface.

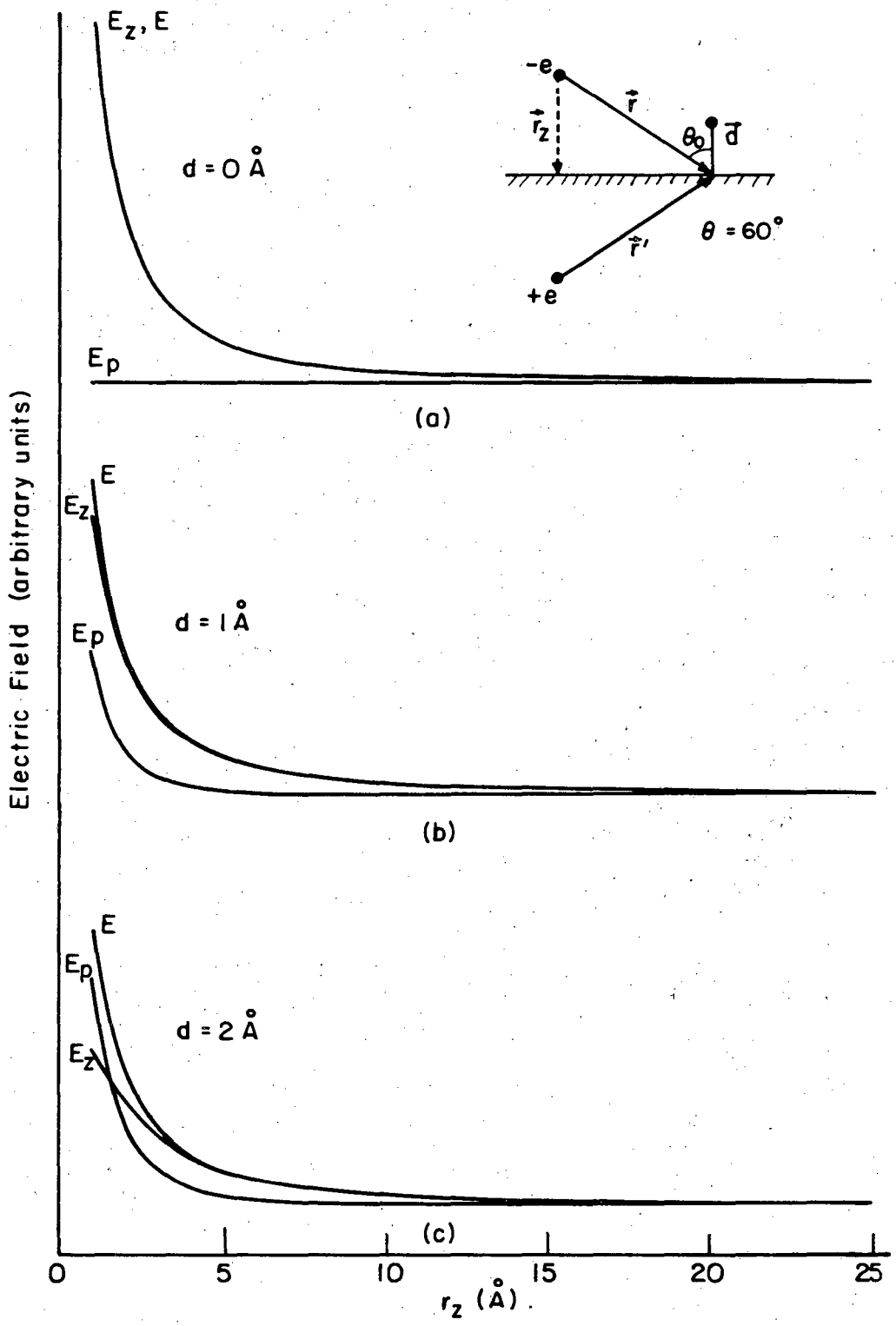
Electric Field (arbitrary units)
$E_z$, E
d = 0 Å
$E_p$
(a)
-e
$\vec{r}$
$\vec{r}_z$
$\theta_0$
$\vec{d}$
$\theta$ = 60°
$\vec{r}'$
+e
E
$E_z$
d = 1 Å
$E_p$
(b)
E
$E_p$
d = 2 Å
$E_z$
(c)
0
5
10
15
20
25
$r_z$ (Å)

XBL 806-5314

the metal and the adsorbate atoms (~2 Å). These calculations are very idealized since we have assumed that the image charges formed inside the metal can exactly screen the incident electrons. Using a more realistic screening potential would both increase the magnitude of $E_p$ and decrease the magnitude of $E_z$. However, a partially compensating effect will be the fact that the 'image' plane and the electron reflection plane will not occur at z=0, but at some small, non-zero value of z. Thus the actual value of d will be smaller than that discussed here. Nevertheless, it is clear that a molecule located above a metal surface will feel a parallel component to the electric field.

Since the electric field is now different, f, the dimensionless scattering amplitude must also be modified. Revised expressions can be derived from the work of Sokcevic et al.[12,13,15]

$$f_z = \frac{k_o(R^2+1)}{\Delta_p^2+\Delta_z^2}[\Delta_p e^{-\Delta_p d} - \Delta_z \sin\Delta_z d] + \frac{2k_o R}{\Delta_p^2+\Sigma_z^2}[\Delta_p e^{-\Delta_p d}\cos 2\delta -$$

$$- \Sigma_z \sin(\Sigma_z d - 2\delta)] + i\frac{k_o(R^2-1)}{\Delta_p^2+\Delta_z^2}\cos\Delta_z d \qquad (20a)$$

$$f_p = \frac{-k_o\Delta_p(R^2-1)}{\Delta_p^2+\Delta_z^2}\sin\Delta_z d + ik_o\Delta_p\left[\frac{R^2+1}{\Delta_p^2+\Delta_z^2}(e^{-\Delta_p d} - \cos\Delta_z d)\right.$$

$$\left. + \frac{2R}{\Delta_p^2+\Delta_z^2}(\cos 2\delta\, e^{-\Delta_p d} - \cos(\Sigma_z d - 2\delta))\right] \qquad (20b)$$

Equations (20a) and (20b) include the effects of the image charges. At d=0 Equation (20a) simplifies to (9) and (20b) goes to zero.

The effects of the parallel component of the electric field become especially important when we consider hydrocarbon vibrations since the

ends of long hydrocarbon chains can be located a significant distance above the surface. Figure 6 shows calculated values of $|f_p|^2$ and $|f_z|^2$ as a function of the distance of the vibrational mode above the surface for $\hbar\Omega = 3000\ cm^{-1}$ (6a). Both the symmetric C-H stretching vibration (normal to the surface) and the asymmetric C-H stretching vibration (parallel to the surface) of a perpendicularly bonded $sp^3$ hybridized species occur at approximately this frequency. Again we choose $E_o = 5$ eV and $\Theta_o = 60°$. The values of R(0.2) and $\delta(\pi/2)$ are somewhat arbitrary. Figure 6a clearly shows that even at distances of only 5 or 6 Å above the surface $|f_p|^2$ can be significant. $|f_p|^2$ goes to zero as d approaches 0 in keeping with the normal dipole selection rule. Unlike previous calculations, $|f_z|^2$ is sensitive to the choice of $\delta$. This is clearly shown in Figure 6b for $\delta = \pi$. $|f_z|^2$ decreases much more rapidly with increasing d in this case.

Consider the stretching and bending vibrations of a carbon monoxide molecule oriented perpendicular to a plane metal surface, but with the center of mass of the vibrational mode located 2.5 Å above the surface. From the simple normal co-ordinate calculations of Chapter I we see that the metal-carbon stretching vibration (normal to the surface) and the M-C≡O bending vibration (parallel to the surface) occur at approximately 500 $cm^{-1}$ (depending on the choice of force constants). The angular distributions of these two modes are shown in Figure 4b. As we expect, the scattering amplitude of a mode oriented parallel to the surface ($|f_p|^2$) is much less than the scattering amplitude of a mode oriented perpendicular to the surface ($|f_z|^2$). Furthermore, the angular distribution of the parallel mode (~1.1°) is broader than the angular distribution of the perpendicular mode. There is also significant tailing of $|f_p|^2$ to lower scattering angles.

Figure 6. Parallel ($|f_p|^2$) and perpendicular ($|f_z|^2$) components of the inelastic scattering amplitude as a function of distance above a metal surface for a vibrational mode at 3000 $cm^{-1}$. In (a) $\delta = \pi/2$ and in (b) $\delta = \pi$.

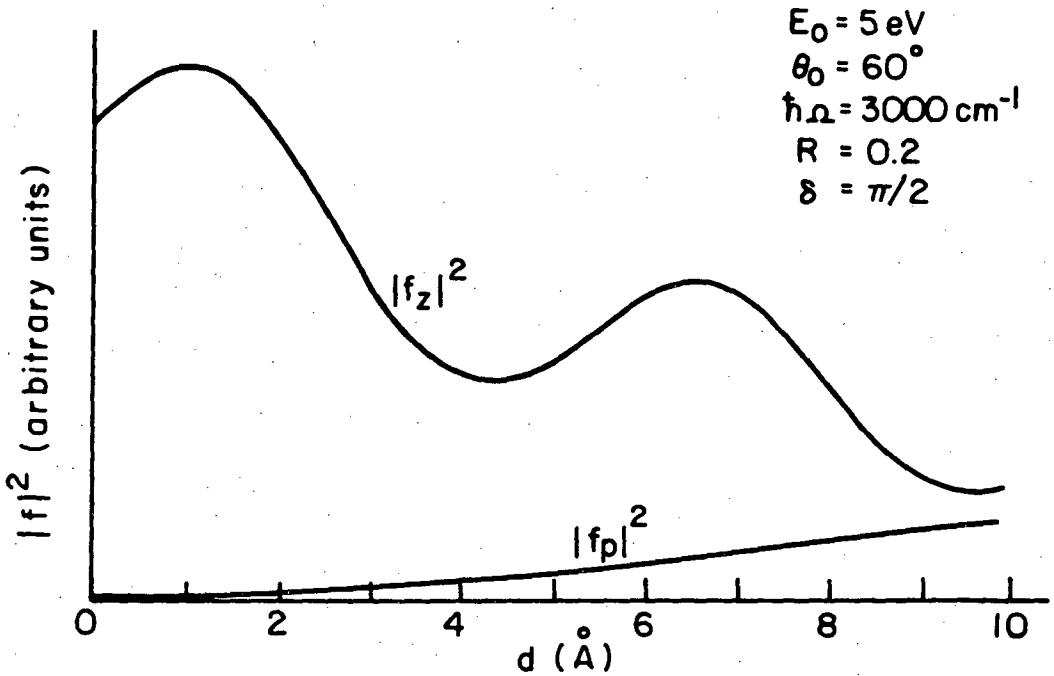


(a)

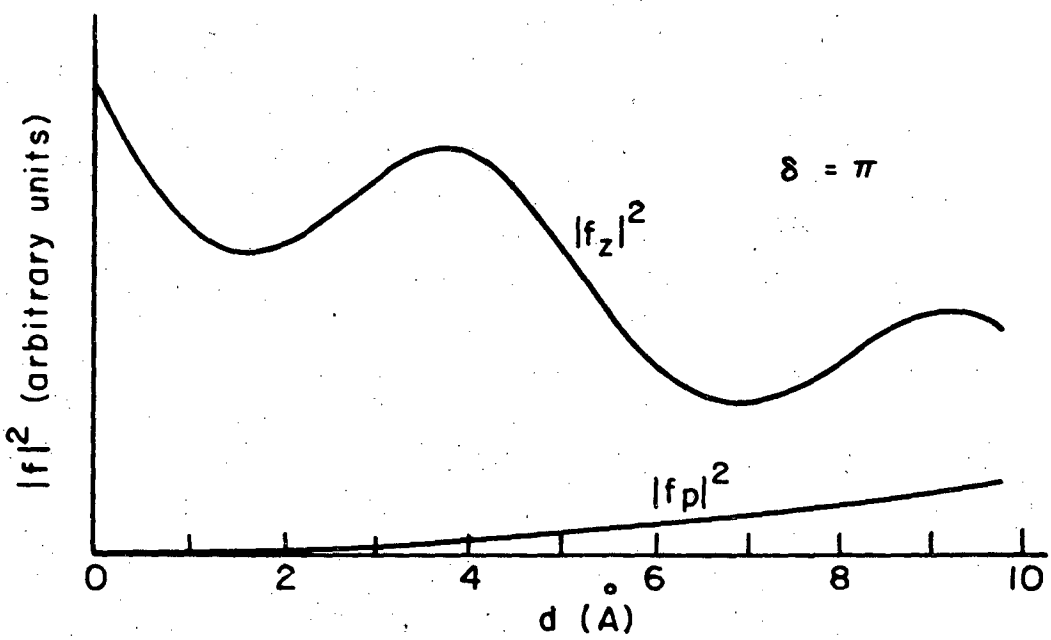


(b)

XBL806-5315

Again one must recall that all of the calculations presented here are highly idealized since only approximate electron-molecule interactions and electron wavefunctions were used. Nevertheless these calculations show significant trends and qualitative agreement with experimental measurements should be expected.

The normal dipole selection rule can also breakdown for molecules chemisorbed on either stepped or polycrystalline metal surfaces. Although we will not demonstrate this mathematically, this is shown schematically in Figure 7b. On a stepped surface the adsorbed molecules are oriented with respect to the microscopic surface normal ($\hat{n}$) while the elastic (specular) beam is scattered with respect to the macroscopic surface normal ($\hat{N}$). The molecules are no longer oriented perpendicular to the image plane and therefore vibrations parallel to the terraces should be excited by the incident electrons. This has not been well tested to date. However, Baro and Ibach[40] recently demonstrated that the asymmetric stretching vibration of hydrogen ($\nu_{Pt-H}$ = 1270 $cm^{-1}$) bridge bonded to a Pt[6(111) x (1$\bar{1}$1)] surface can be observed in the specular direction. The relative intensity of this mode increases for electron scattering out of the specular direction, in agreement with the proposed assignment. Such a vibration has not been observed on the flat Pt(111) surface. In this case $\hat{N}$ and $\hat{n}$ will be parallel (see Fig. 7a). A potentially large amount of information on inelastic electron scattering can be gained by studying the azimuthal angle dependence of the intensity of the energy loss peaks.

Although the normal dipole selection rule is seen to hold in most cases, care must be taken in analyzing any vibrational spectra at present. More experimental and theoretical work needs to be done before the limits of this selection rule are actually known.

Figure 7. Geometry and position of the image charge for electron scattering from (a) a plane metal surface and from (b) a stepped surface.

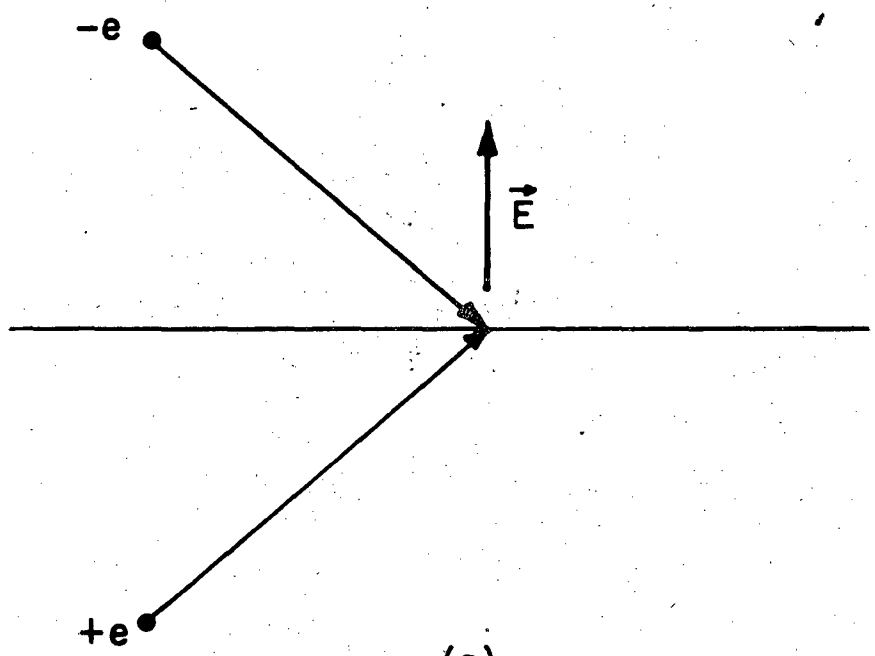


(a)

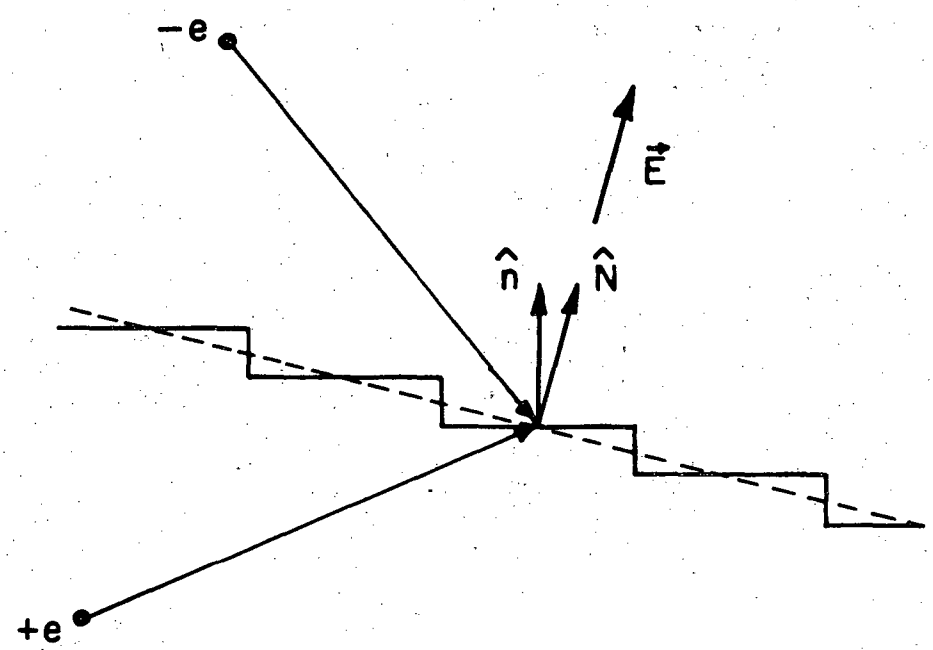


(b)

XBL 806-5316

## References


1. R. Fuchs and K. L. Kliewer, Phys. Rev. 140, A2076 (1965).
2. A. A. Lucas and M. Sunjic, Phys. Rev. Lett. 26, 229 (1971).
3. A. A. Lucas and M. Sunjic, Prog. Surface Sci. 2, 75 (1972).
4. V. Roundy and D. L. Mills, Phys. Rev. B5, 1347 (1972).
5. E. Evans and D. L. Mills, Phys. Rev. B5, 4126 (1972).
6. E. Evans and D. L. Mills, Phys. Rev. B7, 853 (1973).
7. D. L. Mills, Surface Sci. 48, 59 (1975).
8. D. L. Mills, Prog. Surface Sci. 8, 143 (1977).
9. D. M. Newns, Phys. Lett. 60A, 461 (1977).
10. D. N. J. Persson, Solid State Commun. 24, 273 (1977).
11. H. Ibach, Surface Sci. 66, 56 (1977).
12. D. Sokcevic, Z. Lenac, R. Brako, and M. Sunjic, Z. Physik, B28, 273 (1977).
13. M. Sunjic, R. Brako, Z. Lenac, and D. Sokcevic, Intern. J. Quantum Chem. 12, Suppl. 2, 59 (1977).
14. F. Delanaye, A. Lucas and G. D. Mahan, Surface Sci. 70, 629 (1978).
15. Z. Lenac, M. Sunjic, D. Sokcevic, and R. Brako, Surface Sci. 80, 602 (1979).
16. T. N. Rhodin and J. W. Gadzuk, The Nature of the Surface Chemical Bond, T. N. Rhodin and G. Ertl, eds. (North-Holland Publishing Company, Amsterdam, 1979) p. 113.
17. B. N. J. Persson, Surface Sci. 92, 265 (1980).
18. J. W. Davenport, W. Ho, and J. R. Schreiffer, Phys. Rev. B17, 3115 (1978).
19. G. E. Thomas and W. H. Weinberg, J. Chem. Phys. 70, 1000 (1979).
20. S. Y. Tong, C. H. Li, and D. L. Mills, Phys. Rev. Lett. 44, 407 (1980); Phys. Rev. B21, 2057 (1980).
21. H. Ibach, Phys. Rev. Lett. 24, 1416 (1970).

22. G. Baym, Lectures on Quantum Mechanics (The Benjamin/Cummings Publishing Company, Inc., Reading, Massachusetts, 1969).

23. E. G. McRae and C. W. Caldwell, Surface Sci. 57, 766 (1976).

24. C. M. K. Watts, Surface Sci. 23, 453 (1970).

25. M. S. Child, Molecular Collision Theory (Academic Press, London, 1974).

26. J. B. Pendry, Low Energy Electron Diffraction (Academic Press, London, 1974).

27. M. A. Van Hove and S. Y. Tong, Surface Crystallography by LEED, (Springer-Verlag, Berlin, 1979).

28. R. A. Toth, R. H. Hunt, and E. K. Plyer, J. Mol. Spectr. 32, 85 (1969).

29. H. Froitzheim, H. Hopster, H. Ibach, and S. Lehwald, Appl. Phys. 13, 147 (1977).

30. R. M. Kroeker, W. C. Kaska, and P. K. Hansma, J. Catal. 57, 72 (1979).

31. This treatment is similar to that presented in Ref. 8.

32. H. Ibach, J. Vac. Sci. Technol. 9, 713 (1972).

33. J. C. Bertolini, G. Dalmai-Imelik, and J. Rousseau, Surface Sci. 67, 478 (1977).

34. A. Adnot and J.-D. Carette, Phys. Rev. Lett. 39, 209 (1977).

35. C. Backx, R. F. Willis, B. Feuerbacher, and B. Fitton, Surface Sci. 68, 516 (1977).

36. C. Backx and R. F. Willis, Proc. 7$^{th}$ Intern. Vacuum Congress and 3$^{rd}$ Intern. Conference on Solid Surfaces (Vienna, 1977), p. 751.

37. S. Lehwald and H. Ibach, to be published.

38. W. Ho, R. F. Willis, and E. W. Plummer, Phys. Rev. Lett. 40, 22 (1978).

39. R. F. Willis, W. Ho, and E. W. Plummer, Surface Sci. 80, 593 (1979).

40. A. M. Baro and H. Ibach, Surface Sci. 92, 237 (1980).

# CHAPTER III. Experimental

## A. Spectrometer Design and Construction

The high resolution electron energy loss spectrometer used in the present studies is similar in design to that of Froitzheim *et al.*[1] A schematic diagram of the complete system is shown in Figure 1. The principles of operation are quite straightforward: Electrons are emitted by a hot tungsten hairpin filament (JEOL #E-0014) and focused onto the slit of a monochromator by a three element asymmetric electrostatic lens system (A1, A2, A3). The center of the filament is located at the focus of a parabola (repeller) causing an approximately parallel beam of electrons to be emitted from the filament assembly. The repeller is biased negatively with respect to the filament center (cathode). Lenses A1 to A3 were based on the design of Froitzheim[2] and not optimized further. They were formed from 0.15 mm thick tantalum foil for mechanical strength and ease of spot welding. Construction of these lenses is not critical since the electron beam is essentially space charge limited at the monochromator entrance slit[1] (~6 mm from the filament center). With 2.1 amps of current flowing through the filament, a maximum of 25 μamps of current is measured at the monochromator slit. In practice, less than 2 μamps of current pass through the slit and into the monochromator. The use of a low work function thoriated tungsten filament did not appreciably enhance the performance of the spectrometer. Furthermore, we found that the incident beam current measured at the sample position (see Fig. 1) was not very sensitive to the potentials placed on the input lenses. A1, A2 and A3 were all split in a vertical plane to allow deflection of the beam in a horizontal direction. Thus

Figure 1. Schematic diagram of the high resolution electron energy loss spectrometer used in the present experiments. The filament, monochromator and lenses are rotatable so that possible angular effects can be studied. The entire system (including all feedthroughs) is mounted on a 200 mm OD Conflat flange. Typical operating voltages are listed in Table I.

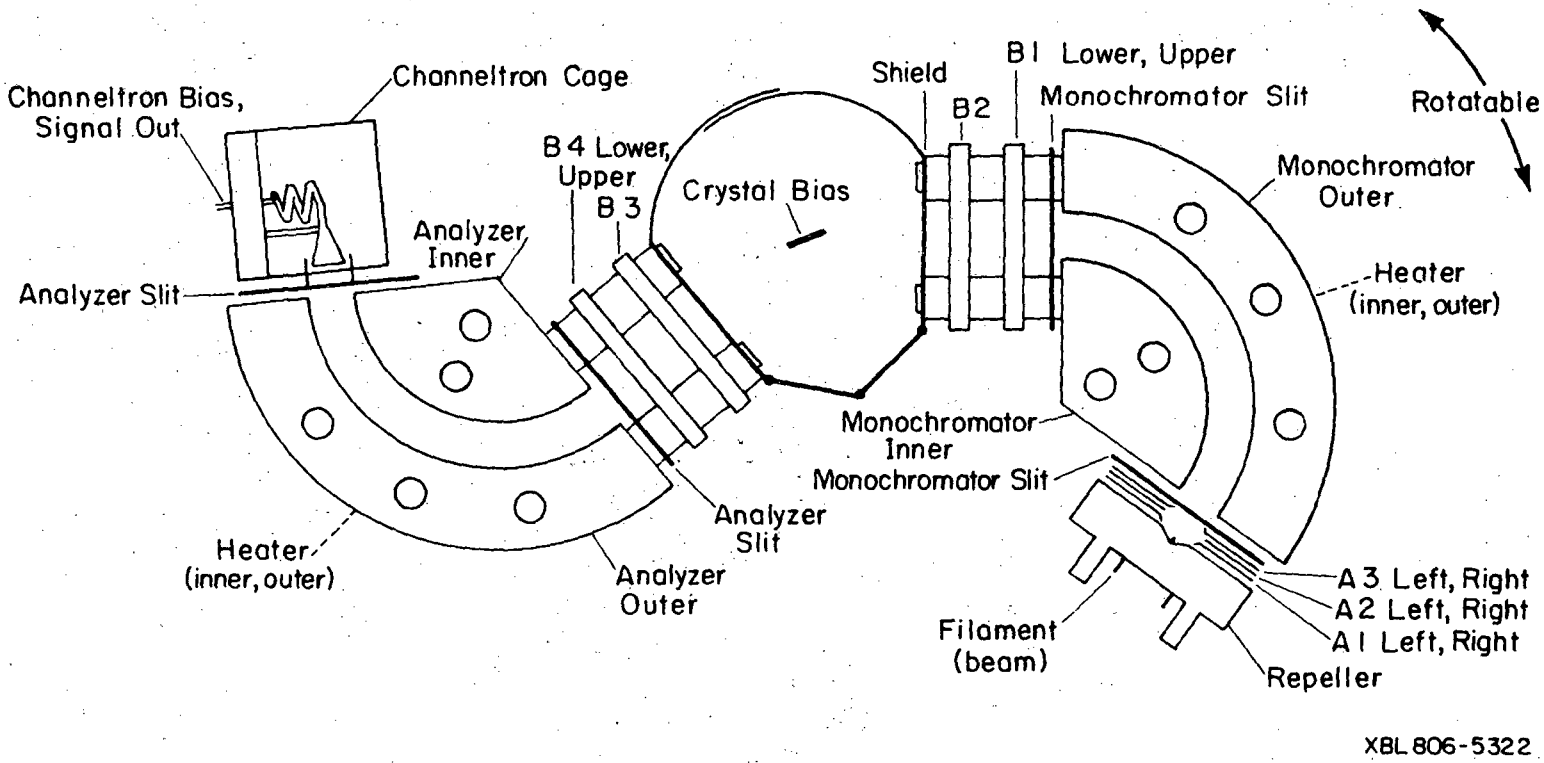
Channeltron Bias,
Signal Out
Channeltron Cage
Analyzer Slit
Analyzer
Inner
B 4 Lower,
Upper
B 3
Crystal Bias
Shield
B2
B1 Lower, Upper
Monochromator Slit
Rotatable
Monochromator
Outer
Heater
(inner, outer)
Monochromator
Inner
Monochromator Slit
Analyzer
Slit
Heater
(inner, outer)
Analyzer
Outer
Filament
(beam)
A 3 Left, Right
A2 Left, Right
A 1 Left, Right
Repeller
XBL 806-5322

the angle of incidence of the electron beam could be easily varied. Deflection of the beam in a vertical direction was thought to be unnecessary.

In our spectrometer the monochromator consists of a 127° cylindrical sector although 180° hemispherical sectors[3,4,5] and cylindrical mirror analyzers[6] have also been successfully used as energy dispersing elements. For an excellent review of the various types of electrostatic energy analyzers and their advantages and disadvantages, see Reference 7. The choice of a 127° cylindrical sector for our system was based on its ease of design, construction, alignment,[7] optimazation and most importantly, its proven performance.[8] Although this type of electrostatic energy analyzer only focusses electrons in a single plane, and in theory is not well suited for electron monochromatization,[9] in practice, cylindrical sectors have out-performed all other types of energy dispersing elements.[8] The design of our sectors was based on the published work of Froitzheim et al.[1] and Roy and Carette.[7,10,11] An expanded drawing of one of the spectrometer sectors is shown in Figure 2.

The differential equation describing the motion of a charged particle in a cylindrical electric field is[9]

$$\frac{d^2u}{d\Theta^2} + u = \frac{E_o}{uE\cos^2\alpha} \qquad (1)$$

where $u \equiv r/R_{mean}$. $(r, \Theta)$ and $E$ are the position and energy of the electron inside the sector, respectively. $R_{mean}$ is the mean radius defined in Figure 2. $E_o$ is the incident energy and $\alpha$ is the angular aberration. A first order solution to Equation (1) was derived by Hughs and Rojansky in 1929.[12]

Figure 2. Expanded view of one of the spectrometer sectors. All dimensions are in mm. The insert shows the details of the "sawtooth" profiling.[1]

Spectrometer Sector

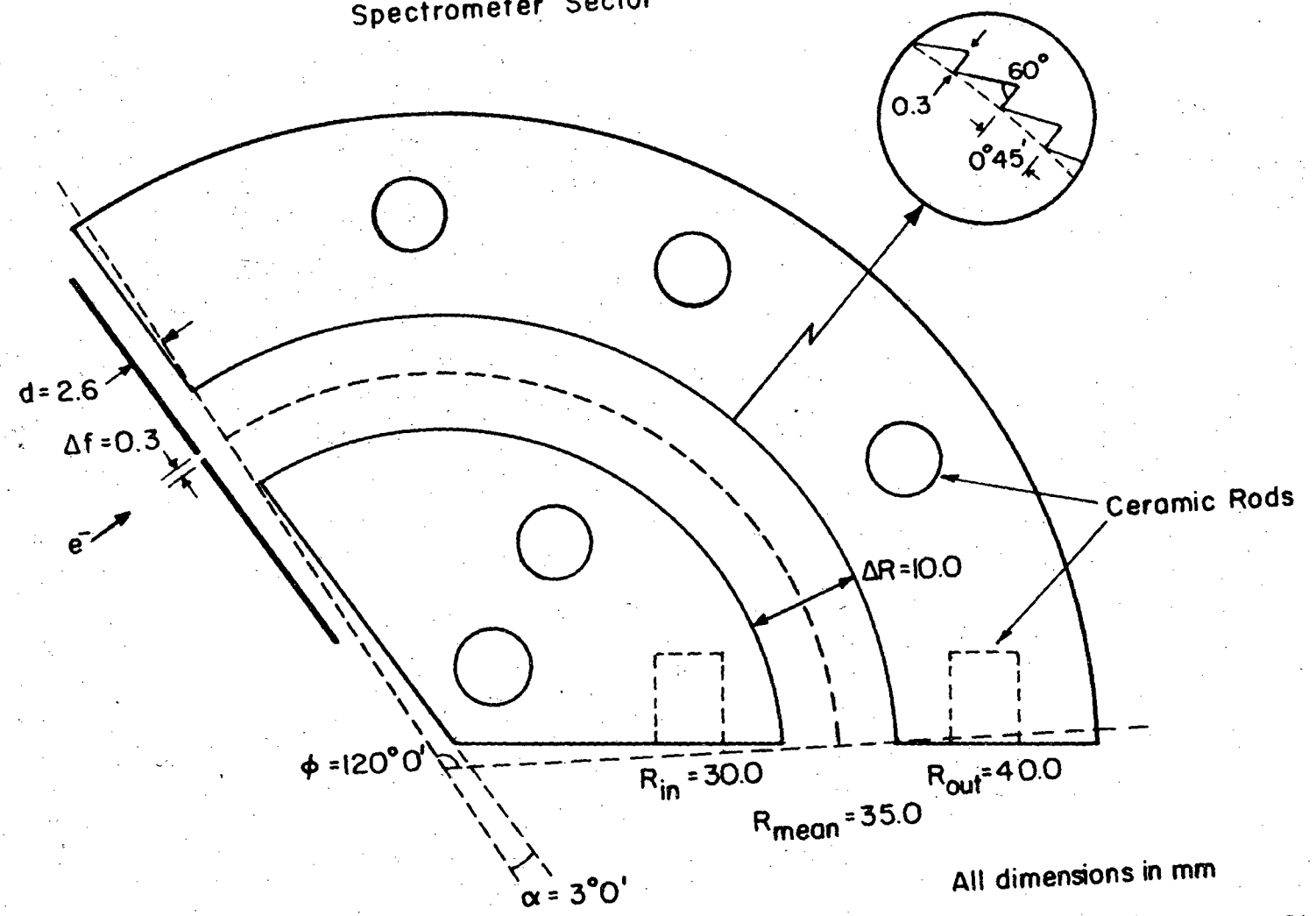


XBL 806-5321

$$\frac{R_{mean}}{r} \simeq \frac{E_o}{E \cos^2\alpha} (1 - \cos\sqrt{2}\,\Theta) + \cos\sqrt{2}\,\Theta - \frac{\tan\alpha}{\sqrt{2}} \sin\sqrt{2}\,\Theta.$$

The last term (which contains the largest aberration term) vanishes for $\Theta = \pi/\sqrt{2} = 127° 17'$. A solution correct to second order in (which also holds at $\Theta = 127° 17'$) can be calculated as well[12]

$$r_o/r_{127} \simeq \frac{2E_o}{E} (1 + \frac{4\alpha^2}{3}) - 1.$$

The design parameters used in the present study are shown in Figure 2. The mean radius is 35.0 mm with a spacing between electrodes of 10.0 mm. The slit dimensions are 0.3 mm wide by 4.0 mm high. The expected energy resolution of the system can now be easily calculated:[9]

$$\frac{\Delta E}{E_o} \simeq \frac{\Delta S}{R_{mean}} + 1/3\ \alpha^2 + 1/4\ \beta^2$$

$\Delta E$ is the full width at half maximum (FWHM) of the energy distribution and $\Delta S$ is the slit width. $\alpha$ and $\beta$ refer to the semiangular apertures in the plane and perpendicular to the plane of deflection, respectively (~3°). Thus the resolving power of each 127° cylindrical sector is only 1% at best.

The sectors were optimized to correct for fringing fields using the calculations of Wollnik and Ewald.[13] The entrance and exit slits were placed 2.6 mm from either end of the sector. To first order, then, the deflection field stays homogeneous until the edges of the sector and then becomes negligible. However, when the object and image distances are zero (i.e., located at the entrance and exit apertures), then the effective deflection angle of the spectrometer is the angle between the apertures.[7]

The optimum deflection angle of an electrostatic cylindrical sector analyzer is in some question at present. According to the simple theory presented earlier, the optimum deflection angle should be 127° 17'. However, extensive Monte Carlo electron trajectory calculations by Roy and Carette[10] indicate that an angle of approximately 135° is optimum. The design of Froitzheim and Ibach is based on a total deflection angle of 120°.[1,14] The theoretical work of Roy and Carette also indicates that the design angle of the sector ($\phi$) is a strong function of the electron's angle of incidence:[10] as the electrons are injected toward the outer half of the sector (positive angle of incidence), the total deflection angle must be decreased. If the incident electron trajectories are all outside of the mean radius ($r < R_{mean}$), then $\phi$ must be reduced to 110°. Conversely, if the electron trajectories are inside the mean radius ($r < R_{mean}$), then $\phi$ must be increased to approximately 145°. In practice neither of these situations can be realized and all trajectories must be considered. The calculations of Roy and Carette also indicate that the spread in electron energies transmitted through the sector field can be minimized by injecting the incident beam toward the outer half of the sector and decreasing the total deflection angle from 135°.[7,10] In our system the electrons are injected and extracted at an angle $\alpha$ of 3° toward the outer half of the sector (suggested by Froitzheim _et al._[1]) and the total deflection angle is fixed at 127°. Using the fringe field corrections discussed earlier for the placement of the entrance and exit slits requires us to cut the sectors at $\phi$ = 120° (see Fig. 2). Roy and Carette have chosen a similar geometry after extensive electron trajectory calculations.[7]

The monochromator, analyzer and filament assembly were fabricated from OFHC copper. Although molybdenum is the recommended material for electron spectrometers[7] (due to its uniform surface potential), OFHC copper is relatively easy to machine, has no residual magnetic fields and is completely UHV compatible. The slits were made from 0.15 mm thick tantalum foil. The height of the sectors is not critical and 40.0 mm was chosen as a convenient value. Top and bottom plates (fixed at the slit potential) are spaced 2.6 mm above and below each sector. Both the inner and outer portions of the sectors were cut with a "sawtooth" profile to minimize stray electron reflection from the walls of the monochromator and analyzer. The dimensions of this corrugation are shown in the insert to Figure 2. Froitzheim et al. have shown that this small modification can reduce background electron scattering by an order of magnitude without affecting resolution.[1] Even with this "sawtooth" profiling however, a small, broad peak centered near 800 $cm^{-1}$ is observed in many vibrational spectra. Simple trajectory calculations by Froitzheim et al. indicate that this apparent loss may be caused by electron reflection from the outer half of the analyzer sector.[1] Further collimation can completely remove this spurious background peak.[15]

The relative energy resolution of each sector is only 1½ - 2% and therefore we work at low pass energies (~0.5 eV) to reach approximately 10 meV (80 $cm^{-1}$) resolution. The electric field at any point inside the monochromator with respect to the mean radius, $R_{mean}$, can be calculated from the design parameters of the sectors.[2,9]

$$E(r) = -\Delta V[\ell n(r/R_{mean})]/[\ell n(R_{out}/R_{in})]$$

$\Delta V$ is the potential difference between the inner and outer halves. Using the sector dimensions shown in Figure 2, the potential on the outer

cylinder ($r = R_{out}$) must be -0.464 $\Delta V$ while the potential on the inner cylinder ($r = R_{in}$) must be 0.536 $\Delta V$. The pass energy of the spectrometer, $E_{pass}$, can also be calculated knowing $\Delta V$.[2,9]

$$E_{pass} = \Delta V/2 \ \ell n(R_{out}/R_{in}).$$

In practice the slit potential, $V_{slit}$, has little to do with the pass energy due to the work function change at the entrance slit, $\Delta\Phi_{slit}$.[9]

$$V_{slit} = E_{pass} + \Delta\Phi_{slit}.$$

In fact, $V_{slit}$ is generally negative! (see below).

After exiting the monochromator the electrons are accelerated to the crystal by lenses B1 and B2. B1 is split in a horizontal plane to deflect the beam vertically. Lack of horizontal deflection of the incident electrons is compensated for by translation and/or rotation of the sample. These lenses were based on the design of Froitzheim[2] and not optimized further. The hinged shield (which allows rotation of the spectrometer) is held at ground potential and therefore the crystal is housed in a field free region. The incident beam energy is determined by the potential difference between the center of the filament (cathode) and ground. However, the sample can be biased up to $\pm 5$ V above and below ground to compensate for work function changes upon gas adsorption. Typical beam currents at the sample are between 1 and 5 x $10^{-10}$ amps at an incident energy of 5 eV.

After scattering from the sample, the electrons are collected by lenses B3 and B4. In all of the experiments described below the angle of incidence was fixed at 70° to the surface normal and electrons were collected in the specular direction. The electron beam is retarded once

again and focused onto the entrance slit of the analyzer sector. The spectrometer is symmetric so that lenses B3 and B4 are identical to lenses B2 and B1, respectively. B1 through B4 and the hinged shield are fabricated from OFHC copper. The analyzer and monochromator are identical cylindrical sectors; thus the actual resolution of the spectrometer is $1/\sqrt{2}$ of the measured peak widths.[7]

After energy analysis, the electrons are detected by a channeltron electron multiplier (Galileo CEM 4028). Post acceleration of the exiting electrons into the cone of the channeltron was unnecessary and degraded the resolution slightly. The signal is then amplified (Ortec 109 PC Preamplifier), shaped (Ortec 471 Spectroscopy Amplifier, Ortec 550 Single Channel Analyzer) and counted (Ortec 449 Log/Lin Ratemeter) outside of the vacuum chamber. Spectra are scanned in an analog mode by linearly ramping the voltage on the analyzer slits with a variable speed motor driven potentiometer (Irwin Halstrup)(X axis) and plotting the output of the ratemeter (Y axis) on a recorder (Hewlett-Packard 7044A). Lenses B3 and B4 could also be scanned at variable rates to insure optimum electron focusing. Such scanning was found to be unnecessary under most operating conditions, however.

To reduce stray electron scattering throughout the spectrometer, the filament, all of the lenses and the channeltron are enclosed in copper shields.[7] The entire assemblage is held together with precision ground alumina rods and spacers thus insuring accurate alignment and electrical isolation. All surfaces exposed to the electron beam were coated with colloidal graphite (Aquadag) to further reduce electron reflection and to alleviate insulator charging problems. Resistive heaters (0.5 mm diameter tungsten wire) were installed in both the inner and

outer sectors of the monochromator and analyzer to outgas the graphite coating. These were run at 30-40 amps (~1000 K) while baking the vacuum system.

Voltages are supplied to each lens and sector through a precision voltage divider network controlled by a single 70 V power supply (Power Designs 1120S). Lenses B3, B4, the analyzer sector (inner and outer) and slits are biased by four separate floating power supplies (RO 105 and 106) so that they could be individually scanned. All potentiometers are Beckman 10 turn, 5 watt Helipots with 0.25% linearity (Model A). Difference potentials ($\Delta A1-\Delta A3$, $\Delta B1$, $\Delta B4$) are set using dual gang potentiometers. Ripple and noise were reduced below 2 mV peak-to-peak by placing simple RC low pass filters ($\tau \sim 0.1$ sec) on the output of each voltage divider. All connections from the power supplies to the vacuum chamber were made using shielded cables. Voltage connections inside the vacuum system were made with 0.25 mm diameter Advance wire. This copper-nickel alloy is relatively easy to spotweld, but retains no residual magnetic fields. OFHC copper wire was used for both the filament and heater leads. All wires inside the vacuum chamber were insulated using flexible borosilicate glass sleeving (Hygrade Thermoflex 1200).

Reduction of background magnetic fields was also important in the design of the spectrometer.[7,11] The fields due to the earth and to the ion pumps were reduced by placing a 1.5 mm thick, 29 cm diameter μmetal can inside the ultra-high vacuum chamber. The shield ran the entire length of the chamber and had small holes for access to each port. The top and bottom were capped to reduce field penetration. In addition, two layers of 0.1 mm thick silicon-iron foil were wrapped around the chamber (external) in the area of the spectrometer. The high saturation

index and relatively low permeability of this shielding material served to prevent the μmetal from saturating. Residual fields were reduced below 20 mGauss at the sample position. Three orthogonal 1 m square Helmholtz coils placed around the vacuum system were found to be of little additional use. The only source of magnetic fields inside the spectrometer was the filament leads. These were twisted to form a non-inductive winding and routed as far away from the sample as possible.

The electron filament, monochromator and lenses are rotatable so that possible angular effects could be studied. This also helped in the initial tuning of the system. Rotation was accomplished through the use of a linear motion feedthrough driving a rack and gear mounted on the axis of the spectrometer. Copper-beryllium bushings and 3 mm diameter sapphire ball bearings were used to reduce friction throughout. The spectrometer baseplate and rotation mechanism were constructed of type 304 stainless steel and thoroughly degaussed before use. As mentioned previously, the total scattering angle was fixed at 140° (70° angle of incidence) for all experiments. The sectors, lenses, rotation mechanism and all electrical feedthroughs were mounted on a single 200 mm OD Conflat flange. A photograph of the completed spectrometer is shown in Figure 3.

## B. The Tuning Procedure

Tuning up the high resolution ELS spectrometer for optimum performance is a straightforward albeit tedious task. To minimize discomfort, the following procedure has proved very effective. Before beginning this scheme, it is important that both the vacuum system and the spectrometer be well baked and that the sample be relatively clean and well ordered. First the current to the monochromator entrance slit must be

Figure 3. Photograph of the high resolution electron energy loss spectrometer shown schematically in Figure 1.

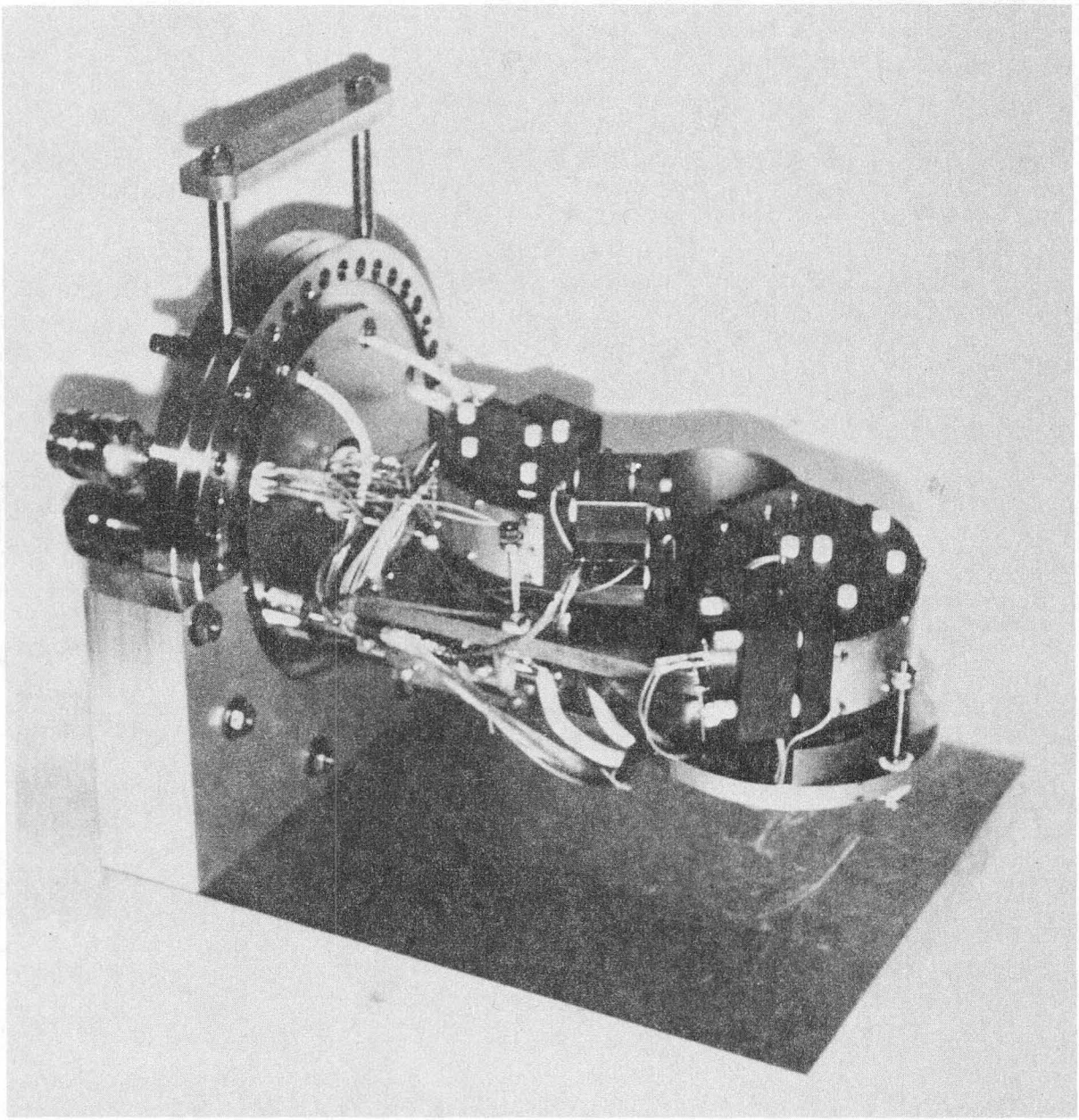

CBB 807-8612

optimized using the repeller and lenses A1 through A3. Current is measured using a Keithley 410 micro-microammeter (~25 μamps). Then the current that traverses the monochromator entrance slit and is collected at the outer half of the monochromator must be tuned for a maximum (~2 μamps). This usually requires an extensive readjustment of A1 and A3. Difference potentials on all lenses should be kept to a minimum. The repeller voltage must always be negative with respect to the cathode (filament center). Next, the sample is placed directly in front of the hinged shield (see Fig. 1) and the current to the crystal is optimized using principally B1 and B2 (~5 x $10^{-10}$ amps). The current at this point should not be extremely sensitive to the potentials placed on these two lenses, however, since both the crystal and the sample holder assembly act as electron collectors. The incident beam energy is also set at this time. It is important that the sample current go through a maximum as a function of filament current (~2.1 amps). This insures that the monochromator is functioning properly.

The crucial step at this stage is to position the crystal in the center of the spectrometer and rotate it to the proper angle so that lenses B3 and B4 can collect the scattered electrons. This is made easier by the center point on the axle of the monochromator rotation mechanism. Thus the lateral position (X and Y) of the sample can be accurately determined. The crystal can be positioned vertically (z) knowing the half-height of the hinged shield (20 mm). The rotation angle can be calculated fairly accurately by measuring the sample angle in the LEED position and knowing the relative orientation of the high resolution ELS spectrometer (-42°). At this point current to B3 should be easily measurable (1-5 x $10^{-10}$ amps). The current to the analyzer entrance slit can then be optimized using principally B1 through B4 and the crystal

bias (~1 x $10^{-10}$ amps). This will certainly cause a reduction in the current measured at the sample and may require extensive repositioning or biasing of the crystal (±1 V above or below ground). Once current is measured to the analyzer slit, the high voltage power supply (Power Designs HV-1544) on the channeltron electron multiplier can be turned on (+2500 V) and the entire system tuned for maximum signal (approximately 2 x $10^5$ counts per second in the elastic channel). Again, extensive repositioning, biasing and/or retuning may be required.

Once maximum signal is detected at the channeltron, the spectrometer is optimized for 1) maximum intensity in the inelastic scattering peaks and 2) minimum peak widths. Both of these are extremely sensitive to the voltages placed on lenses B1 to B4, to the sample position and to the crystal bias. Difference potentials (ΔB1 and ΔB4) are always kept to a minimum. The incident beam energy can also be important here due to rapid fluctuations in the sample reflectivity between 1 and 6 eV.[16,17] Optimization must occur in a cyclical fashion since the potential on any given lens or sector affects the tuning of all lenses and sectors. "Tuning down" the shoulders while maintaining signal in the peak maxima is the most effective method of minimizing peak widths and therefore improving resolution. This is not always accomplished by lowering ΔE on either the monochromator or analyzer since the signal decreases as well. Furthermore, as gases are adsorbed on the sample (and inadvertantly on the spectrometer itself), lenses B1 through B4 must be retuned to compensate for the work function changes. The crystal bias is extremely important in this respect. Typical values of the potentials placed on each lens and sector are listed in Table I. All voltages are with respect to the cathode (filament center) except where noted. These are only typical

Table I. Typical Potentials Applied to the High Resolution Electron Energy Loss Spectrometer (All voltages are with respect to the filament center unless otherwise noted).

Filament Current = 2.01 amps

Repeller = -0.261 V

| | |
|---|---|
| A1 Left = 3.659 | A1 Right = 3.679 |
| A2 Left = 46.02 | A2 Right = 41.26 |
| A3 Left = 0.665 | A3 Right = 0.677 |

Monochromator: Slit = -0.128

| | |
|---|---|
| Inner - Slit = 0.189 | Outer - Slit = -0.165 |

|Outer - Inner| = 0.355

| | |
|---|---|
| B1 Lower = 0.133 | B1 Upper = -0.010 |

B2 = 0.179

Beam (Incident Energy) = 4.786

Crystal Bias = 5.307

B3 = 1.062

| | |
|---|---|
| B4 Lower = 0.007 | B4 Upper = -0.050 |

Analyzer: Slit = -0.222

| | |
|---|---|
| Inner - Slit = 0.191 | Outer - Slit = -0.164 |

|Outer - Inner| = 0.356

Channeltron: Bias = 2500

Cage = -40

values and can vary tremendously depending on both the surface and the adsorbate under study. All potentials are measured with a Keithley 179 Digital Multimeter.

Due to the high gain of the preamplifier, the adjustment of the counting electronics is not critical. The spectroscopy amplifier is run at a gain of 5 to 10 and is primarily used for pulse shaping. A 0.5 sec time constant is essential for minimizing clipping at high count rates. The single channel analyzer is operated in the integral mode (as a discriminator) and is merely used to reduce the counting of stray electrons. The ratemeter is run with a 0.03 to 0.3 second time constant depending on the count rate, scan speed and signal stability. With these settings, the elastic scattering peak from a clean metal surface should contain between 1 and 2 x $10^5$ counts per second and have a full width at half maximum below 9 meV (70 $cm^{-1}$). Scattering into inelastic channels is between 10 and 1000 electrons per second depending on the oscillator strength of the excited vibrational mode. The ratemeter time constant on the more sensitive scales is generally increased to 3 to 10 seconds.

Following this tuning procedure can often lead to a "relative" signal maximum and not to the optimum operating conditions for the given crystal/adsorbate combination. Sometimes the potential on any given lens or sector must be arbitrarily changed and the remainder of the voltages retuned in order to reach the "absolute" signal maximum. Nevertheless, this section does provide a systematic procedure for tuning up the spectrometer which has proved to be very useful in performing the experiments described in Chapters IV through VIII.

## C. The Vacuum System

All experiments were carried out in a stainless steel ultrahigh vacuum (UHV) chamber built in two levels. A schematic diagram of the system is shown in Figure 4. The upper portion contained the standard single crystal surface analysis equipment: a four-grid retarding field energy analyzer (Varian) for low-energy electron diffraction and Auger electron spectroscopy (with a glancing incidence electron gun (Cliff-tronics)); a quadrupole mass spectrometer (UTI 100 C) for residual gas analysis, thermal desorption mass spectrometry and kinetic studies; a 2 kV argon ion sputtering gun (Physical Electronics Industries) for sample cleaning and a nude ionization gauge (Varian) for pressure measurement. For several studies a simple metal evaporation source and oscillating quartz crystal microbalance (Inficon XTM) were added to the upper level of the chamber as well. Their use is discussed in more detail in Chapter VII. Adsorbates entered the chamber through a variable leak valve connected to a stainless steel gas manifold. The manifold could be pumped by either two sorption pumps or by a liquid nitrogen trapped mechanical pump and had a base pressure below $5 \times 10^{-5}$ Torr.

After sample cleaning, characterization and gas dosing, the crystal was lowered into the high resolution electron energy loss spectrometer on the second level by an extended travel (250 mm) precision manipulator. This level also contains several extra ports in case an X-ray or ultraviolet source (for X-ray or ultraviolet photoelectron spectroscopy) is required in the future. The samples could be resistively heated to over 1500 K (approximately 5 V at 50 amps) or cooled to below 200 K with liquid nitrogen. As mentioned previously, the vacuum chamber was lined with layers of μmetal and silicon-iron shielding to reduce background

Figure 4. Schematic diagram of the complete vacuum system. Sample cleaning, characterization and gas dosing occur in the upper level, while the vibrational spectroscopy is performed in the lower level. The base pressure in the system is below $1 \times 10^{-10}$ Torr after a 36 hr bakeout at 450 K.

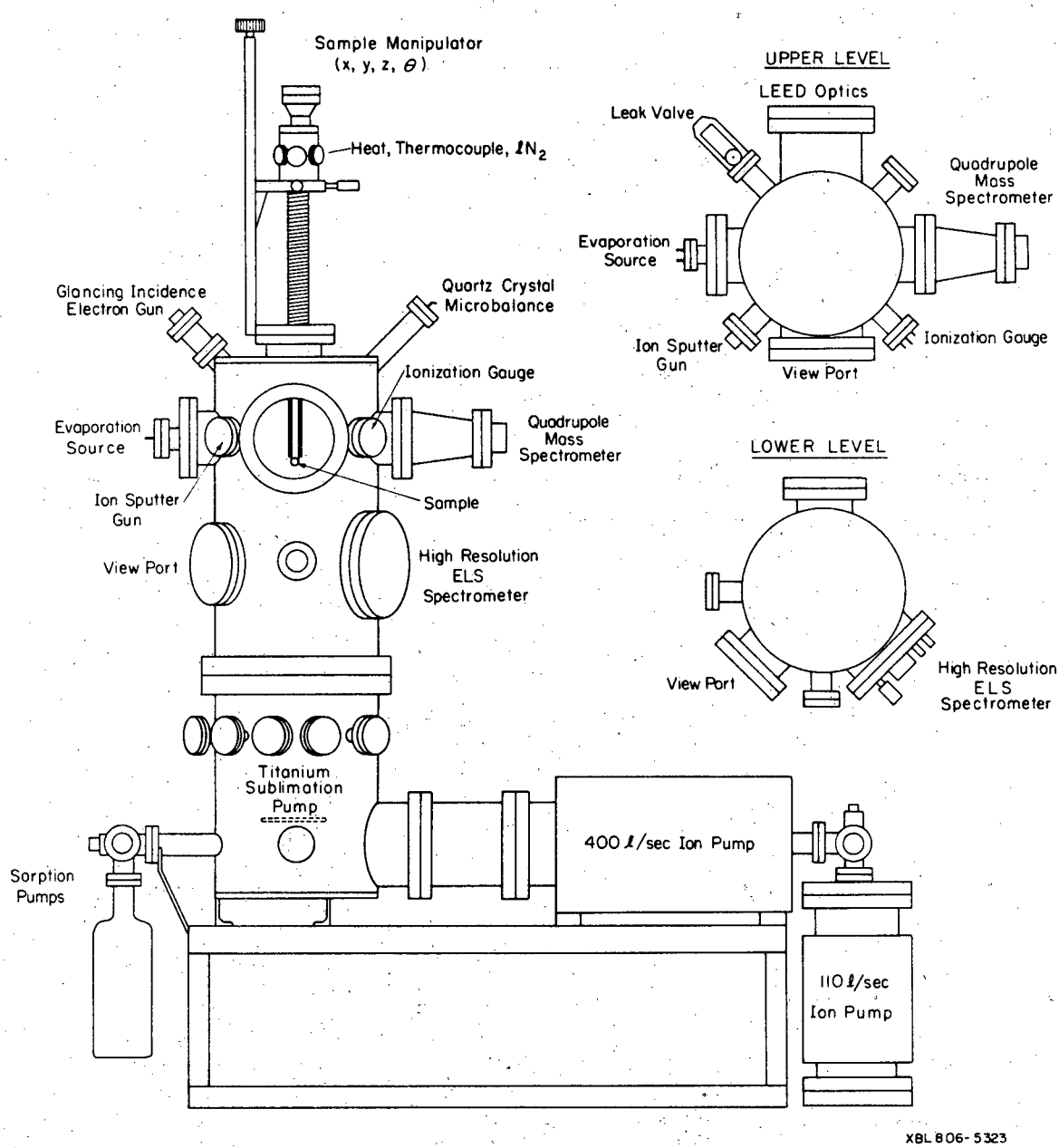
Sample Manipulator
(x, y, z, θ)
Heat, Thermocouple, ℓN2
Glancing Incidence
Electron Gun
Quartz Crystal
Microbalance
Ionization Gauge
Evaporation
Source
Quadrupole
Mass
Spectrometer
Ion Sputter
Gun
Sample
View Port
High Resolution
ELS
Spectrometer
Titanium
Sublimation
Pump
Sorption
Pumps
400 ℓ/sec Ion Pump
110 ℓ/sec
Ion Pump
UPPER LEVEL
LEED Optics
Leak Valve
Quadrupole
Mass
Spectrometer
Evaporation
Source
Ion Sputter
Gun
View Port
Ionization Gauge
LOWER LEVEL
View Port
High Resolution
ELS
Spectrometer
XBL 806-5323

magnetic fields. The upper and lower levels were also separated by μmetal. The base pressure in the system was maintained at $1 \times 10^{-10}$ Torr (after 36 hr, 450 K bakeout) with two sputter ion pumps (Varian 400 ℓ/sec and 110 ℓ/sec) and a water cooled titanium sublimation pump.

This combination of techniques allowed us to determine the structure of the adsorbed species while on the metal surface and after desorption into the gas phase. Furthermore, molecular rearrangements in the adsorbed overlayer as a function of both substrate temperature and background pressure could be studied.

The procedures for sample preparation, mounting and cleaning have been described in detail elsewhere.[18] Briefly, the rhodium single crystal rod (Materials Research Corp., MARZ Grade) was oriented to within ±½° using X-ray back reflection and 1 mm thick discs were cut by spark erosion. After mechanical polishing (final step: slurry of 0.05 μm $Al_2O_3$ in water), the samples were spot welded to etched tantalum foil and mounted inside the UHV chamber. A small jig and a helium-neon laser were used to insure accurate alignment of all samples. The rhodium crystals were cleaned by a combination of argon ion bombardment ($5 \times 10^{-5}$ Torr Ar, 30 ma emission current, 1000-2000 eV) followed by annealing in vacuum (~1100 K) and $O_2/H_2$ cycles ($5 \times 10^{-7}$ Torr, 1100 K) to remove carbon, sulfur and boron.[18]

Gas adsorption was studied at pressures between $5 \times 10^{-9}$ and $5 \times 10^{-5}$ Torr and at temperatures between 210 and 850 K. Temperatures were measured with a digital thermometer (Doric) and a chromel-alumel thermocouple spot welded to the top of the sample. Surface structures were observed both with increasing exposure and after the gas was pumped away. Neither gas exposures nor background pressures were corrected for ionization gauge sensitivity.

In the remainder of this thesis we will present several applications of high resolution electron energy loss spectroscopy to the characterization of molecules adsorbed on rhodium surfaces. It is clear from Chapter I that ELS is a very powerful technique for studying the vibrational spectra of chemisorbed molecules, however, no single surface sensitive probe alone can yield a complete picture of the structure, bonding and reactivity of adsorbed species.[19] Therefore we have designed a vacuum system which allows us to routinely perform a variety of complementary experiments on a single sample.

## References


1. H. Froitzheim, H. Ibach, and S. Lehwald, Rev. Sci. Instrum. 46, 1325 (1975).

2. H. Froitzheim, Diplomarbeit, Technischen Hochschule Aachen (1971).

3. G. Dalmai-Imelik, J. C. Bertolini, and J. Rousseau, Surface Sci. 63, 67 (1977).

4. C. Backx, B. Feuerbacher, B. Fitton, and R. F. Willis, Surface Sci. 63, 193 (1977).

5. G. E. Thomas and W. H. Weinberg, Rev. Sci. Instrum. 50, 497 (1979).

6. S. Andersson, Solid State Commun. 21, 75 (1977); Surface Sci. 79, 385 (1979).

7. D. Roy and J.-D. Carette, Electron Spectroscopy for Surface Analysis, H. Ibach, ed. (Springer-Verlag, Berlin, 1977) p. 13.

8. H. Ibach, "Proc. Conference on Vibrations in Adsorbed Overlayers" (Julich, Germany, 1978) p. 64 and references therein.

9. M. E. Rudd, Low Energy Electron Spectrometry, K. D. Sevier, ed. (John Wiley and Sons - Interscience, New York, 1972) p. 17.

10. D. Roy and J.-D. Carette, Appl. Phys. Lett. 16, 413 (1970); J. Appl. Phys. 42, 3601 (1971).

11. D. Roy, A. Delage, and J.-D. Carette, J. Phys. E. 8, 109 (1975).

12. A. L. Hughes and V. Rojansky, Phys. Rev. 34, 291 (1929).

13. H. Wollnik and H. Ewald, Nucl. Instr. Methods 36, 93 (1965).

14. H. Froitzheim and H. Ibach, Z. Physik 269, 17 (1974).

15. H. Ibach and D. Bruchmann, Phys. Rev. Lett. 41, 958 (1978).

16. A. Adnot and J.-D. Carette, Phys. Rev. Lett. 38, 1084 (1977).

17. B. A. Sexton and G. E. Mitchell, to be published.

18. D. G. Castner, Ph.D. Thesis, University of California, Berkeley (1979).

19. L. H. Dubois and G. A. Somorjai, ACS Symposium Series Vol. 000, A. T. Bell and M. L. Hair, eds. (American Chemical Society, Washington, D.C., 1980).

# Chapter IV. The Chemisorption of Carbon Monoxide on Rh(111)[1]

## A. Background

The bonding of carbon monoxide to transition metals is one of the most extensively studied chemisorption systems in surface science.[2,3] The interaction of CO with metal atoms or with clusters of metal atoms is also well studied by inorganic chemists.[4-6] As a result of these detailed investigations of CO, comparisons between surfaces and metal cluster carbonyls can now be made.[7,8] The bonding of carbon monoxide to rhodium is of special interest since this metal catalyzes the hydrogenation of CO in both heterogeneous and homogeneous media. The formation of small hydrocarbons from CO and $H_2$ over supported[9] and unsupported[10] rhodium surfaces is well-known. Furthermore, rhodium carbonyls catalyze the hydroformylation of olefins and produce ethylene glycol from mixtures of hydrogen and CO.[11] Because of the importance of this metal we have chosen to explore the vibrational spectrum of CO chemisorbed on a Rh(111) single crystal surface.

Much effort has gone into understanding the vibrational spectrum of carbon monoxide chemisorbed on rhodium.[12] More than 20 years ago Yang and Garland performed the first infrared studies using highly dispersed rhodium particles supported on an inert alumina substrate.[13] They provided convincing evidence for a species of the form $Rh(CO)_2$, a gem dicarbonyl, whose IR spectrum showed a doublet at 2095 and 2027 $cm^{-1}$. The presence of linear (~2060 $cm^{-1}$) and bridge bonded (1925 $cm^{-1}$) forms were also demonstrated. More recent investigations[12,14-18] agree extremely well with these early experiments except that the C-O vibration of the multiply coordinated species was found to lie near 1860 $cm^{-1}$ in most cases.

Supported rhodium cluster carbonyls of known molecular structure have also been studied and analogous stretching frequencies in the 1800 to 2100 $cm^{-1}$ region were reported.[19,20] Substrate adsorption below 1000 $cm^{-1}$ masked all Rh-CO vibrations. Both transmission and reflection IR studied employing evaporated rhodium films yield similar results.[12] Due to the high density of rhodium atoms, no species of the form $Rh(CO)_2$ were formed, however. This is expected to be the case on the (111) surface as well. Weak adsorptions between 400 and 575 $cm^{-1}$ were seen and are indicative of metal-adsorbate stretching and bending vibrations. Inelastic electron tunneling spectroscopic (IETS) measurements on alumina supported rhodium particles[21-23] add little new structural information except that peaks in the 400-600 $cm^{-1}$ region have been definitely assigned to Rh-CO bending and stretching modes. Ibach[24] has shown that high resolution electron energy loss spectroscopy and IR spectroscopy yield analogous information and therefore one would expect similar results from the present investigation. Selected vibrational frequencies for the chemisorption of carbon monoxide on rhodium are summarized in Table I.

The structure of CO adsorbed on rhodium surfaces has also been studied by low-energy electron diffraction. The first reported LEED experiments on the Rh(111)/CO system were carried out by Grant and Haas in 1970.[25] These results have only recently been expanded and systematized.[26,27] At room temperature CO forms a $(\sqrt{3}x\sqrt{3})R30°$ structure at exposures near 0.5 L (1 L=1 Langmuir = $10^{-6}$ Torr · sec = 1.33 x $10^{-4}$ Pascal·sec). At intermediate coverages a "split" (2x2) pattern is visible and can be explained by double diffraction from a hexagonal overlayer of molecular CO. The spot splitting decreases as the overlayer compresses into a closest packed configuration and finally a (2x2) LEED pattern is visible. Thermal desorption mass spectra yield only molecular CO

Table I. Selected Vibrational Frequencies for Carbon Monoxide on Rhodium[a]

| Surface | Technique | $\nu_{Rh-C}$ $\delta_{Rh-C=O}$ | Surface Sites: 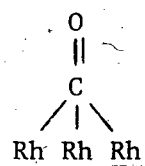 $\nu_{3\text{-fold}}$ | 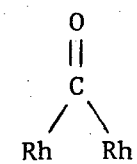 $\nu_{bridge}$ | 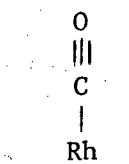 $\nu_{atop}$ | 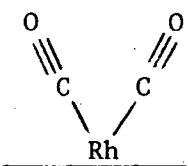 $\nu_{Rh-(CO)_2}$ |
|---|---|---|---|---|---|---|
| Rh(111)[b] | ELS | 420 | | 1870 | 2070 | |
| $Rh/Al_2O_3$[17] | IR | | | 1870 | 2070 | 2031,2101 |
| $Rh/SiO_2$[30] | IR | | | 1890-1900 | 2040-2065 | 1990-2020,2080 |
| evaporated Rh film[45] | Transmission IR | 400-575 | | 1852,1905 | 2055 | (2111) |
| $Rh/Al_2O_3$[23] | IETS | 413,465, 600 | | 1721[c] | 1942[c] | 1942[c] |
| $Rh_2(CO)_8$[32] | solution, IR | | | 1845,1861 | | 2061,2086 |
| $Rh_4(CO)_{12}$[33] | solid, IR | 393,423, 488 | | 1848 | | 2028-2105 |
| $Rh_6(CO)_{16}$[33] | solid, IR | 413,427, 513 | 1770 | | | 2016-2077 |

[a] all frequencies in $cm^{-1}$. b) this study.

[c] peaks shifted due to the geometry of the tunnel junction (see page 110 of text and Ref. 56).

desorbing from the surface ($E_d \simeq 31$ kcal/mole)[26-28] and show no evidence for CO dissociation under ultrahigh vacuum conditions.[28]

The effects of surface pretreatment on the chemisorption of CO on rhodium have also been considered previously. Early infrared experiments showed that hydrogen had little affect on the CO/rhodium vibrational spectrum.[13] More recent studies indicate a slight decrease in the gem dicarbonyl ($Rh(CO)_2$) species upon hydrogen exposure.[16,29] However, no evidence for changes in either the LEED patterns or the thermal desorption spectra of CO adsorbed on Rh(111) were found after exposing the surface to gaseous hydrogen at 300 K.[26] Infrared studies on $O_2$/CO co-adsorption show an increase in the concentration of the gem dicarbonyl species[13,14,16] and a decrease in the concentration of the bridge bonded species relative to the linear species.[13,16] Small shifts in the C-O stretching vibrations to higher frequencies have also been reported.[30] The formation of $CO_2$ at higher pressures and elevated temperatures has been seen as well.[10,13,31] Carbon pretreatment from the thermal decomposition of acetylene had a marked decreasing effect on the rate of methane formation from CO/$H_2$ mixtures over a polycrystalline rhodium foil.[10] Furthermore, CO thermal desorption spectra show a shift of 30 K to lower binding energy on these same pretreated surfaces.

In this study we have combined high resolution ELS with LEED and thermal desorption mass spectrometry to present a rather complete picture of CO chemisorption on the Rh(111) single crystal surface above 300 K. The vibrational spectra of carbon monoxide indicate two distinct binding sites (atop and bridged) whose relative populations and vibrational frequencies are a strong function of both substrate temperature and background pressure (coverage). TDS measurements show the bridge bonded CO

to have a lower binding energy to the surface than the species located in the atop site, and therefore this species can be selectively removed from the rhodium crystal. Surface pretreatment also had a marked effect on CO adsorption: oxygen and carbon both inhibited carbon monoxide chemisorption and weakened the metal-adsorbate bond strength. Hydrogen had no observable effects. Finally, by combining the present data with earlier IR[17] and IETS[23] studies a consistent set of force constants for the two types of chemisorbed carbon monoxide can be calculated.

## B. CO Chemisorption on Clean Rh(111)

The vibrational spectra of carbon monoxide chemisorbed on Rh(111) at 300 K as a function of gas dosage is shown in Figure 1. At very low exposures (less than 0.1 L) only one peak at 1990 $cm^{-1}$ is observed in the C≡O stretching region and no ordered LEED pattern is found. By comparison with the infrared spectra of relevant organorhodium compounds[32,33] and with matrix isolated metal carbonyls,[34] one can assign this loss to the carbon-oxygen stretching vibration of a linearly bonded species. This peak shifts to higher frequency as the coverage is increased. Possible causes for this include local field effects,[35,36] vibrational coupling,[36] dipole-dipole interactions[37-39] or simply a decrease in the total metal-carbon backbonding due to the increased number of adsorbate molecules.[40]

When a molecule is chemisorbed on a surface it will not only be influenced by the substrate, but by other neighboring adsorbate molecules as well. As the surface coverage increases, the average nearest neighbor spacing decreases and the magnitude of adsorbate-adsorbate repulsions and/or attractions increases. Calculations of these local field effects can only account for a 10 to 15 $cm^{-1}$ shift in the C≡O stretching

Figure 1. Vibrational spectra of CO chemisorbed on a clean Rh(111) surface at 300 K as a function of exposure. Note the shift in both the 480 and 1990 $cm^{-1}$ losses with increasing coverage.

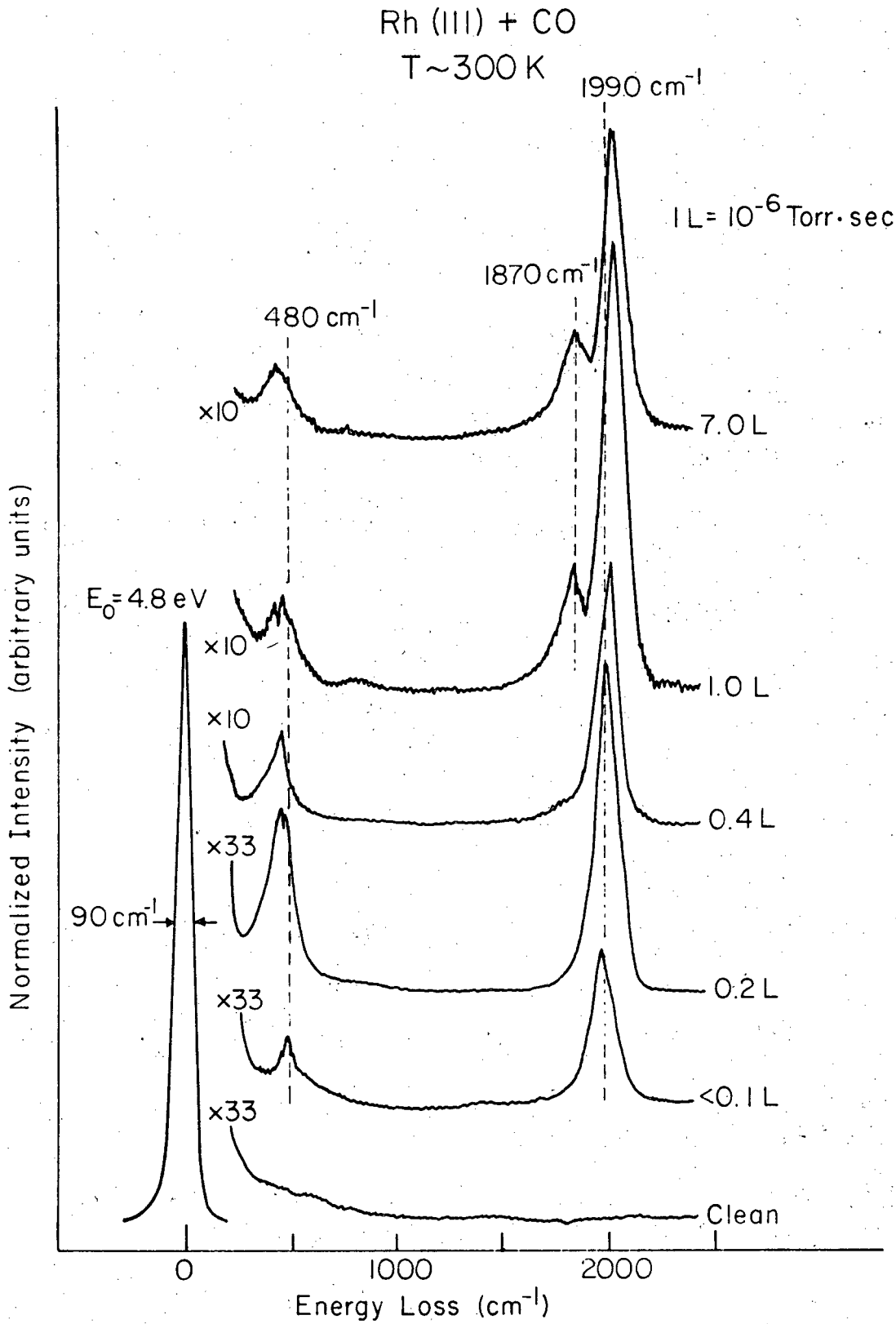
Rh (111) + CO
T~300 K
1990 cm⁻¹
1 L = 10⁻⁶ Torr·sec
1870 cm⁻¹
480 cm⁻¹
×10
7.0 L
E₀=4.8 eV
×10
1.0 L
×10
0.4 L
×33
90 cm⁻¹
0.2 L
×33
<0.1 L
×33
Clean
Normalized Intensity (arbitrary units)
0
1000
2000
Energy Loss (cm⁻¹)

XBL 793-5880

frequency, however.[36] Vibrational coupling between adjacent carbon monoxide molecules can also affect the CO vibrational spectrum. If one considers two carbon monoxide molecules (or ligands) bonded to a single metal atom, then coupling between vibrational modes of the same symmetry will certainly occur. However, this coupling will also be present (albeit not as strong) when CO's are bonded to neighboring metal atoms.[36] Such affects have been seen in the infrared spectrum of metal cluster carbonyls and can account for shifts up to 30 $cm^{-1}$, depending on the strength of the coupling constant.[36] Dipolar interactions can arise from a purely electrodynamic (or through space) coupling between one dipole and the oscillating electric field of another. Interactions with "image dipoles" must also be considered.[38,39,41] These forces are very long range, but again can only account for a 10 to 30 $cm^{-1}$ shift in the C≡O stretching frequency.[38,39] Finally, as the number of adsorbed molecules increases, the competition for the electrons of the surface atoms increases so that there is less charge available to put into each CO $2\pi^*$ antibonding orbital with the consequence that the carbon-oxygen bond becomes stronger and the C≡O stretching frequency increases. Currently one lacks a complete understanding of the changes of the forces involved and the individual effects of each perturbation cannot be completely decoupled. Recent infrared studies on single crystal platinum[42] and copper[43] surfaces have attempted to sort out these effects, but due to the extent of the shift here (see below), a combination of all of these mechanisms is most likely present.

A result of these effects is a decrease in the rhodium-carbon stretching frequency and possibly a weakening of the metal adsorbate bond. Figure 1 clearly shows a shift in the rhodium-carbon stretching vibration

for this linearly bonded species from 480 $cm^{-1}$ to lower frequency with increasing CO exposure. This is consistent with the weakening of the metal-adsorbate bond observed with increasing gas dosage in the CO thermal desorption spectra of Figure 2.[44] Previous studies have also shown a similar temperature drop in the TDS peak maximum with increasing carbon monoxide exposure.[26,27] No other vibrations corresponding to Rh-C≡O bending modes were observed in the specular direction and by invoking the normal dipole selection rule (see Chapter II) we conclude that the carbon-oxygen bond is oriented perpendicular to the surface.

At larger than 0.4 to 0.5 L CO exposures a small shoulder near 1870 $cm^{-1}$ appears (see Fig. 1). Again by comparison with relevant model compounds,[32-34] we can assign this peak to the carbon-oxygen stretch of a bridge bonded species. Unlike the loss near 2000 $cm^{-1}$, this peak grows at essentially constant frequency, never varying more than +5 $cm^{-1}$. By a CO exposure of 1.0 L the rhodium-carbon stretch has significantly broadened. The new low frequency shoulder appearing slightly above 400 $cm^{-1}$ corresponds to the metal-carbon stretch for the bridge bonded species. This weaker bond to the substrate for the new species can be correlated with the low temperature desorption peak appearing at high exposures in the thermal desorption spectra of Figure 2. Assuming first order desorption kinetics and a pre-exponential factor of $10^{13}$ $sec^{-1}$, the binding energy difference between these two sites is found to be approximately 4 kcal/mole. Again the bridge bonded species is oriented perpendicular to the surface since no bending or asymmetric stretching modes are observed in the specular direction.

Since Castner, et al.[26] found the (2x2) LEED pattern to room temperature to be stable only at relatively high gas pressures, we have explored

Figure 2. Thermal desorption spectra of CO from an initially clean Rh(111) surface.[44] The high temperature peak corresponds to the atop sites while the low temperature peak which grows in at larger CO exposures belongs to the bridge bonded species. The heating rate is 25 K/sec.

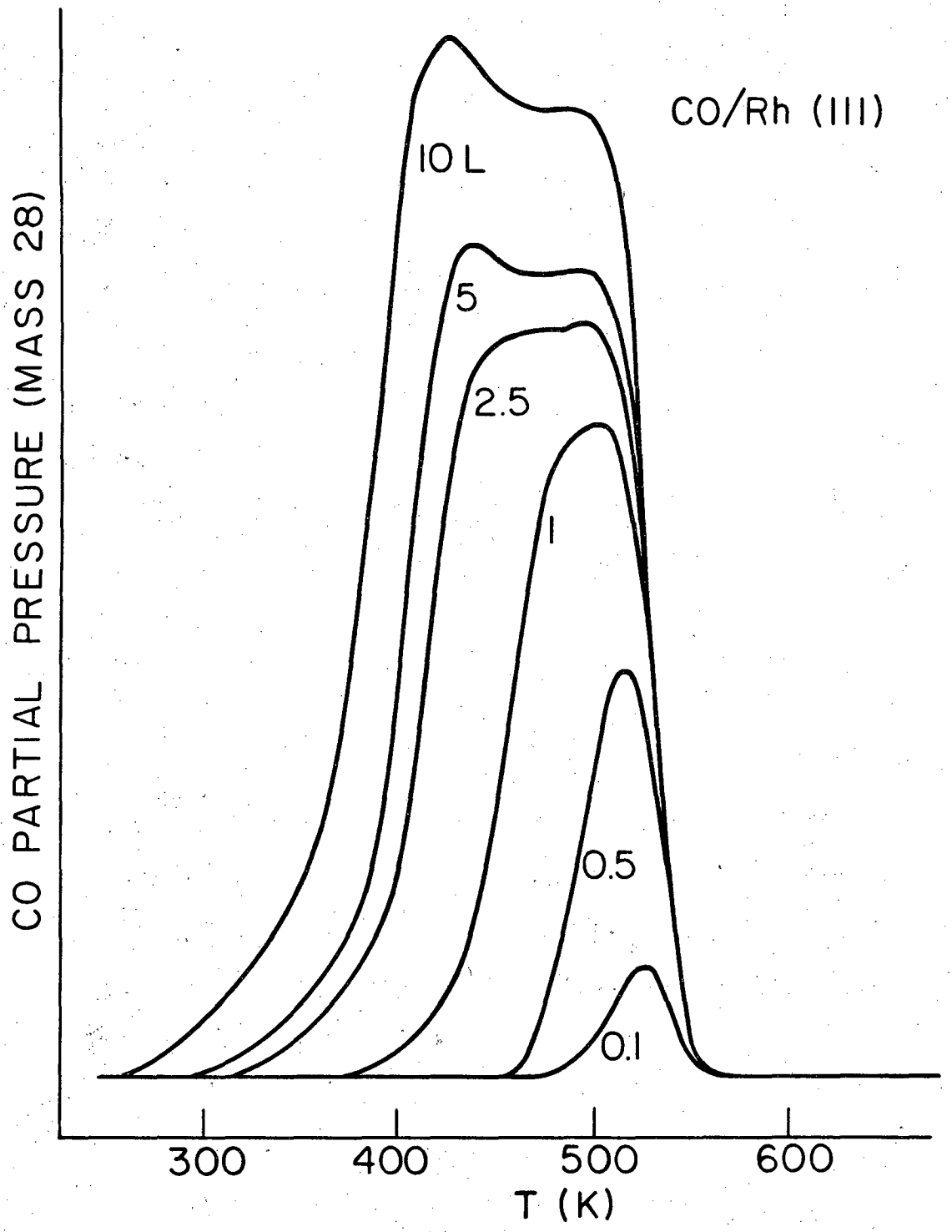


XBL 788-5563A

the vibrational spectrum of chemisorbed CO up to 1 x $10^{-5}$ Torr. This series of spectra is shown in Figure 3. Once again the carbon-oxygen stretch for the atop site continues to shift to higher frequency as a function of coverage and reaches a limiting value of 2060 to 2070 $cm^{-1}$. The rhodium-carbon stretch of the linear species simultaneously decreases to 420 $cm^{-1}$. The 1870 $cm^{-1}$ loss due to the bridge bonded species remains at a constant frequency with increasing coverage, however. The presence of gem dicarbonyl species cannot be ruled out here due to the limited resolution of ELS, but seem unlikely because of the high density of metal atoms on the (111) surface[12] that would lead to extreme crowding of CO molecules in the dicarbonyl configuration.

The high coverage values of the C≡O stretching frequencies measured here are in excellent agreement with most of the earlier infrared studies of carbon monoxide adsorption on both supported[12-20] and unsupported[12] rhodium samples. The small differences in the reported stretching frequencies may be due to dispersion and support effects. Representative infrared and ELS data for the CO-rhodium system are summarized in Table I.

The chemisorption of carbon monoxide on Rh(111) is completely reversible. As the background CO in Figure 3 is pumped away the carbon-oxygen stretching vibration for the bridge bonded species decreases in intensity and the metal-carbon and carbon-oxygen stretching vibrations for the atop site shift back into their original positions. The bridge bonded species can be selectively removed from the substrate by slowly heating the crystal to approximately 360 K in vacuum. This is shown in Figure 4a, where we have exposed the Rh(111) surface to an essentially infinite amount of CO (>1000 L) at 300 K and then evacuated the system. As the crystal is slowly heated, the 1870 $cm^{-1}$ peak, due to the more weakly bound bridged species, decreases first and the carbon-oxygen

Figure 3. Vibrational spectra of CO chemisorbed on Rh(111) at 300 K as a function of pressure.

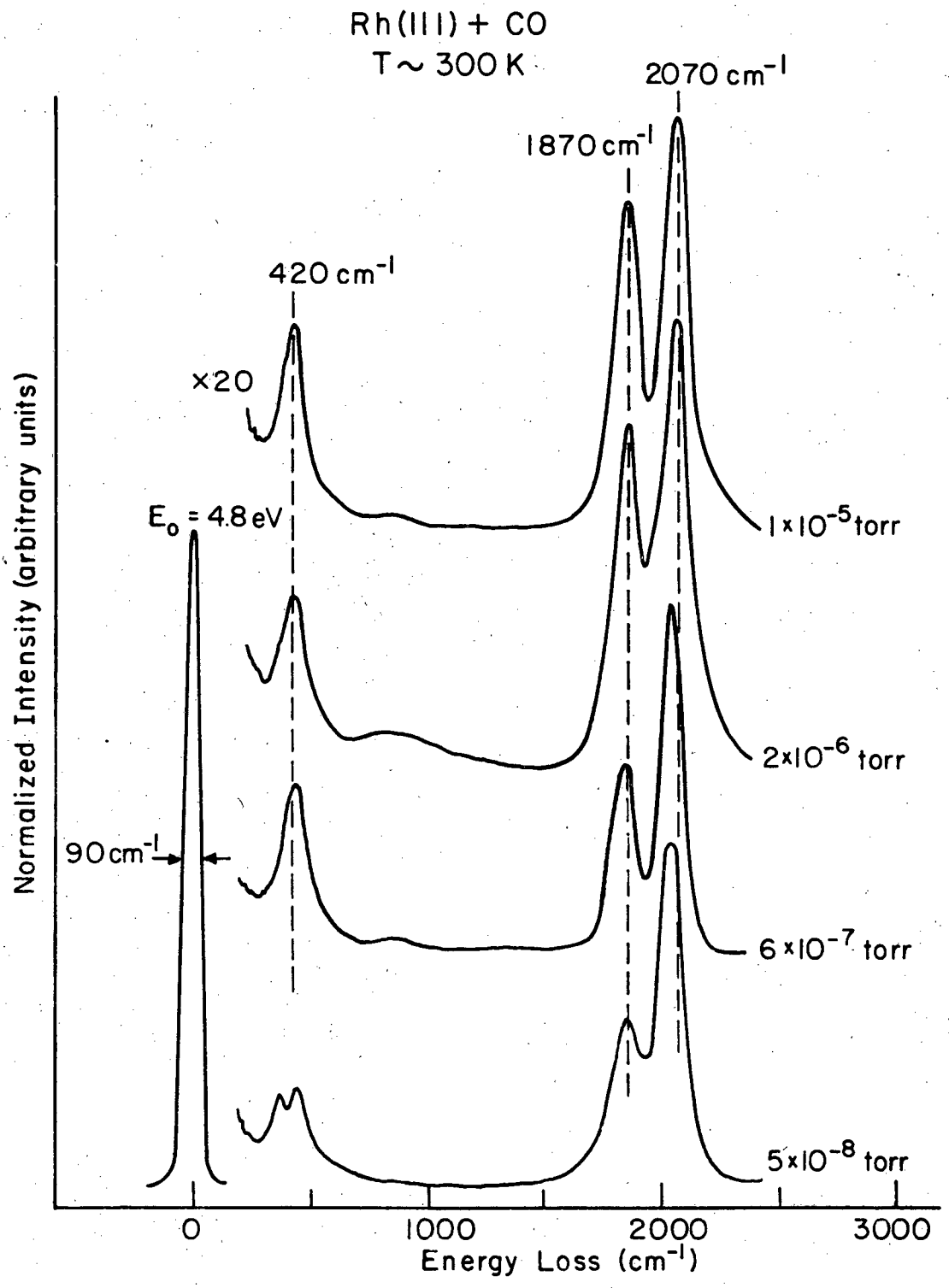
Rh(111) + CO
T ~ 300 K
2070 cm⁻¹
1870 cm⁻¹
420 cm⁻¹
×20
E₀ = 4.8 eV
90 cm⁻¹
1×10⁻⁵ torr
2×10⁻⁶ torr
6×10⁻⁷ torr
5×10⁻⁸ torr
Normalized Intensity (arbitrary units)
0
1000
2000
3000
Energy Loss (cm⁻¹)

XBL 793-5879

Figure 4. Temperature dependence of the CO on Rh(111) vibrational spectrum;

a. infinite exposure (>1000 L) to CO;

b. spectra run under $1 \times 10^{-5}$ Torr CO.

Note the desorption of the bridge bonded species first, in agreement with the TDS spectra of Figure 2.

Rh (III) + CO : Temperature Dependence

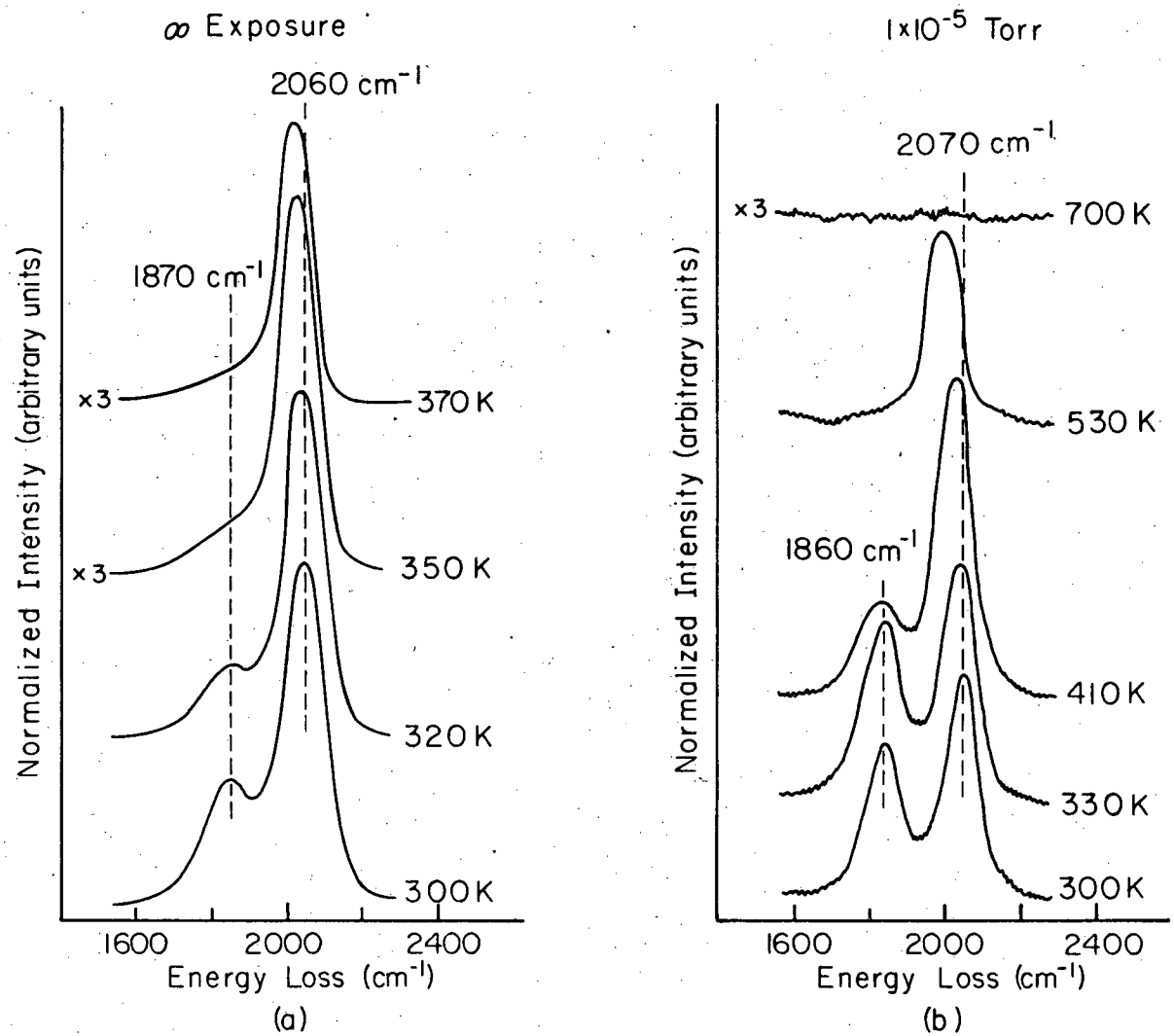


XBL 793-5882

stretch for the atop species shifts to lower frequency. This is entirely consistent with the thermal desorption spectra of Figure 2 which show a lower binding energy for bridge bonded carbon monoxide. The second series of spectra in Figure 4b were obtained in the presence of $1 \times 10^{-5}$ Torr of CO and at much higher temperatures. Once again the multiply coordinated species desorbs first. No CO decomposition was detected under any of the conditions employed in our experiments ($p \leq 1 \times 10^{-5}$ Torr CO, $T \leq 600$ K).[28]

The adsorption of CO on Rh(111) at 300 K produced a series of well ordered LEED patterns in excellent agreement with previous studies.[26,27] The $(\sqrt{3}x\sqrt{3})R30°$ LEED pattern observed at a 0.5 L CO exposure probably is due to an ordered array of CO molecules sitting in atop sites since the vibrational spectrum shows only a single peak in the carbon-oxygen stretching region at 2010 $cm^{-1}$ (see Fig. 5a). This has now been confirmed by a low-energy electron diffraction structure analysis.[46] At intermediate CO exposures we see a compression of this hexagonal overlayer until at pressures of $\sim 1 \times 10^{-6}$ Torr where a closest packed carbon monoxide overlayer has formed. This yields a (2x2) LEED pattern with two different CO species per unit cell and a surface coverage of 3/4. A real space model for this substrate-overlayer combination is shown in Figure 5b. The ratio of atop to bridge sites is two to one and is in reasonable agreement with the intensity ratio found in the vibrational spectrum. The relative populations of the two surface species could not be accurately measured from the thermal desorption spectra due to the asymmetric peak shapes. Relaxation processes occurring in the overlayer during the desorption process also complicate the determination of the coverages of the two types of CO species. Between these two limiting

Figure 5. Real space representations of CO chemisorbed on a Rh(111) surface:

a. $(\sqrt{3}x\sqrt{3})R30°$ overlayer structure visible at low exposures;

b. (2x2) structure seen at relatively high background pressures.

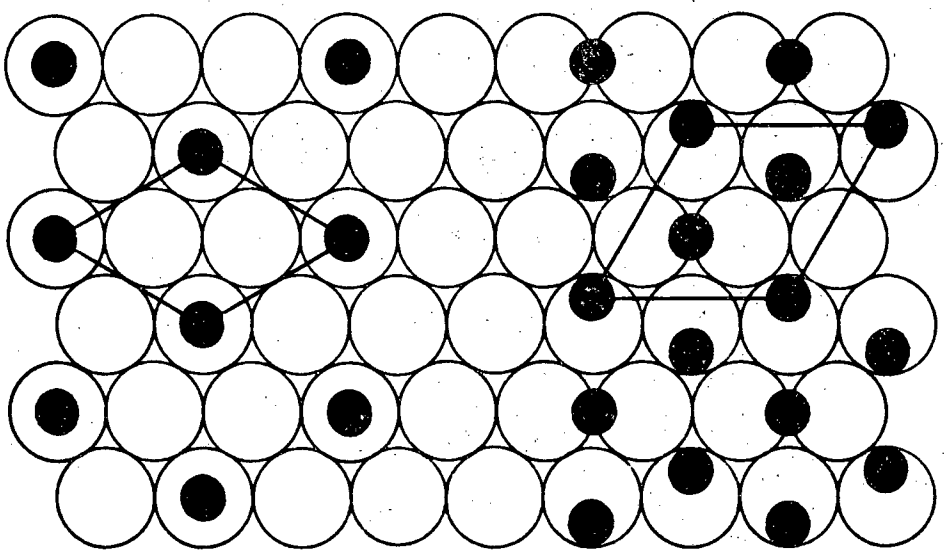

$(\sqrt{3} \times \sqrt{3})R30$ $\theta = 1/3$ a.

$(2 \times 2)$ $\theta = 3/4$ b.

XBL795-6248

coverages we see a continuous growth of all peaks and a shift in the loss above 2000 $cm^{-1}$, consistent with the compression of the carbon monoxide overlayer.

Pritchard[47] has shown that by slightly "relaxing" the overlayer structure, local site adsorption can be obtained without altering the diffraction pattern. Such effects may be taking place on Rh(111) and are consistent with the vibrational spectra. Further evidence for local site adsorption can be seen in Table I, where a comparison of the present results with earlier IR studies is shown. Linearly bonded carbon monoxide molecules have C≡O stretching frequencies between 2000 and 2100 $cm^{-1}$, regardless of the support or the dispersion. Similarly, bridge bonded species lie in the 1850-1900 $cm^{-1}$ region. Finally, the recent photoemission studies of Braun, et al. on the Rh(111)/CO chemisorption system show no evidence for adsorbate band formation.[48]

C. CO Chemisorption on Pretreated Rh(111)

Sexton and Somorjai showed that surface pretreatment had a marked effect on the rate of hydrocarbon formation from $H_2$/CO mixtures over polycrystalline rhodium foils:[10] oxidation enhanced the methanation rate while surface carbon inhibited product formation. We studied the effects of hydrogen, oxygen and carbon on the CO on Rh(111) vibrational spectra in the hope of understanding the effects of pre-adsorption. $H_2$ pre-adsorption or post-adsorption on Rh(111) at 300 K had no significant effect on either the CO vibrational spectra or on the CO thermal desorption spectrum (see Fig. 6b). Furthermore, no room temperature rhodium-hydrogen stretching vibrations are observed, even at $H_2$ exposures up to several thousand Langmuirs. Finally, no changes are seen after heating the crystal to 600 K in 1 x $10^{-5}$ Torr of a 3:1 $H_2$/CO mixture for 30

Figure 6. The effects of surface pretreatment on the thermal desorption spectrum of CO from Rh(111): a) clean surface; b) pretreated in hydrogen; c) pretreated in $O_2$; and d) pretreated with carbon. The heating rate is 15 K/sec.

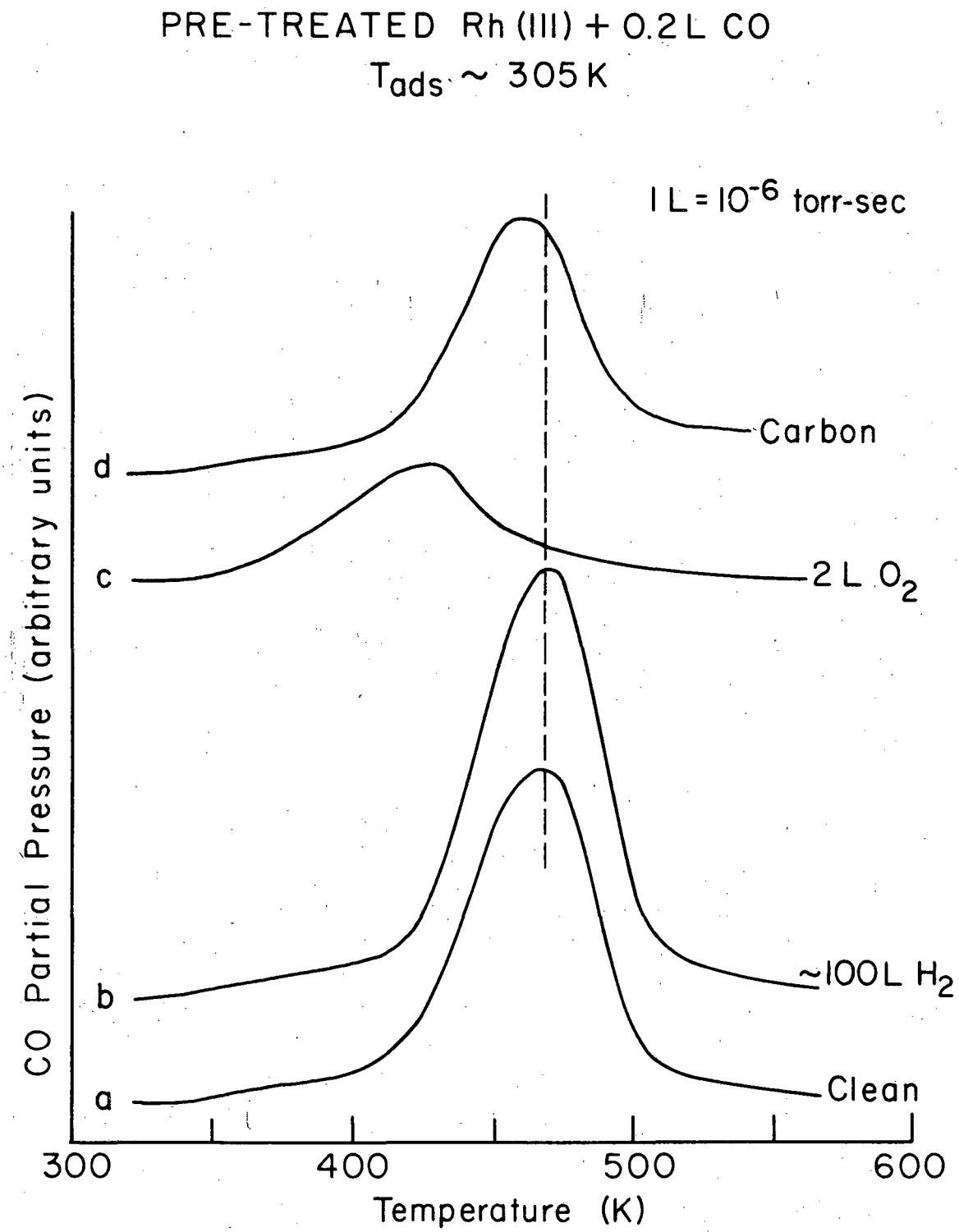
PRE-TREATED Rh (III) + 0.2 L CO
$T_{ads}$ ~ 305 K
1 L = $10^{-6}$ torr-sec
Carbon
2 L $O_2$
~100 L $H_2$
Clean
d
c
b
a
CO Partial Pressure (arbitrary units)
300
400
500
600
Temperature (K)

XBL795-6252

minutes.[49] Earlier LEED,[26] TDS[26] and IR[13,16,28] studies on a variety of rhodium surfaces also showed no effects at 300 K.

The effect of preadsorbed oxygen on the carbon monoxide vibrational spectrum is shown in Fig. 7. $O_2$ chemisorption on Rh(111) is dissociative at 300 K yielding a single metal-oxygen stretching vibration at 520 $cm^{-1}$ and a second order thermal desorption maximum.[26,31,50] This peak only remains as a shoulder on the more intense rhodium-carbon stretch as the CO coverage is increased. The formation of bridge bonded carbon monoxide is strongly inhibited in the presence of chemisorbed oxygen and the atop sites seem to saturate with CO by an exposure of only 1 L. It appears that pre-adsorbed oxygen blocks some of the surface sites so that CO cannot adsorb in many of the atop and bridge positions. Since oxygen is strongly electron withdrawing, the extent of rhodium-carbon backbonding has decreased and the C-O stretch has shifted approximately 50 $cm^{-1}$ to higher frequency. The strength of the metal adsorbate bond is determined by the electron density in both the $5\sigma$ and $2\pi^*$ molecular orbitals of carbon monoxide and should therefore decrease as well. Consistent with this is a decrease of at least 30 $cm^{-1}$ in the metal-carbon stretch and a lowering of the thermal desorption temperature by approximately 40 K (see Fig. 6c). The smaller thermal desorption peak area is also in agreement with fewer CO molecules on the surface in the presence of chemisorbed oxygen.

At CO pressures near $5 \times 10^{-7}$ Torr a small shoulder at 1860 $cm^{-1}$ appears and the bridge bonded species begins to form. By $5 \times 10^{-6}$ Torr of CO the Rh-O stretch is absent and bridge bonded carbon monoxide is definitely present. Furthermore, the metal-carbon and carbon-oxygen stretching vibrations have shifted into more "normal" positions ($\nu_{Rh-C}$ = 430 $cm^{-1}$, $\nu_{C=O}$ = 1860, 2070 $cm^{-1}$). Oxygen is soluble in bulk rhodium at

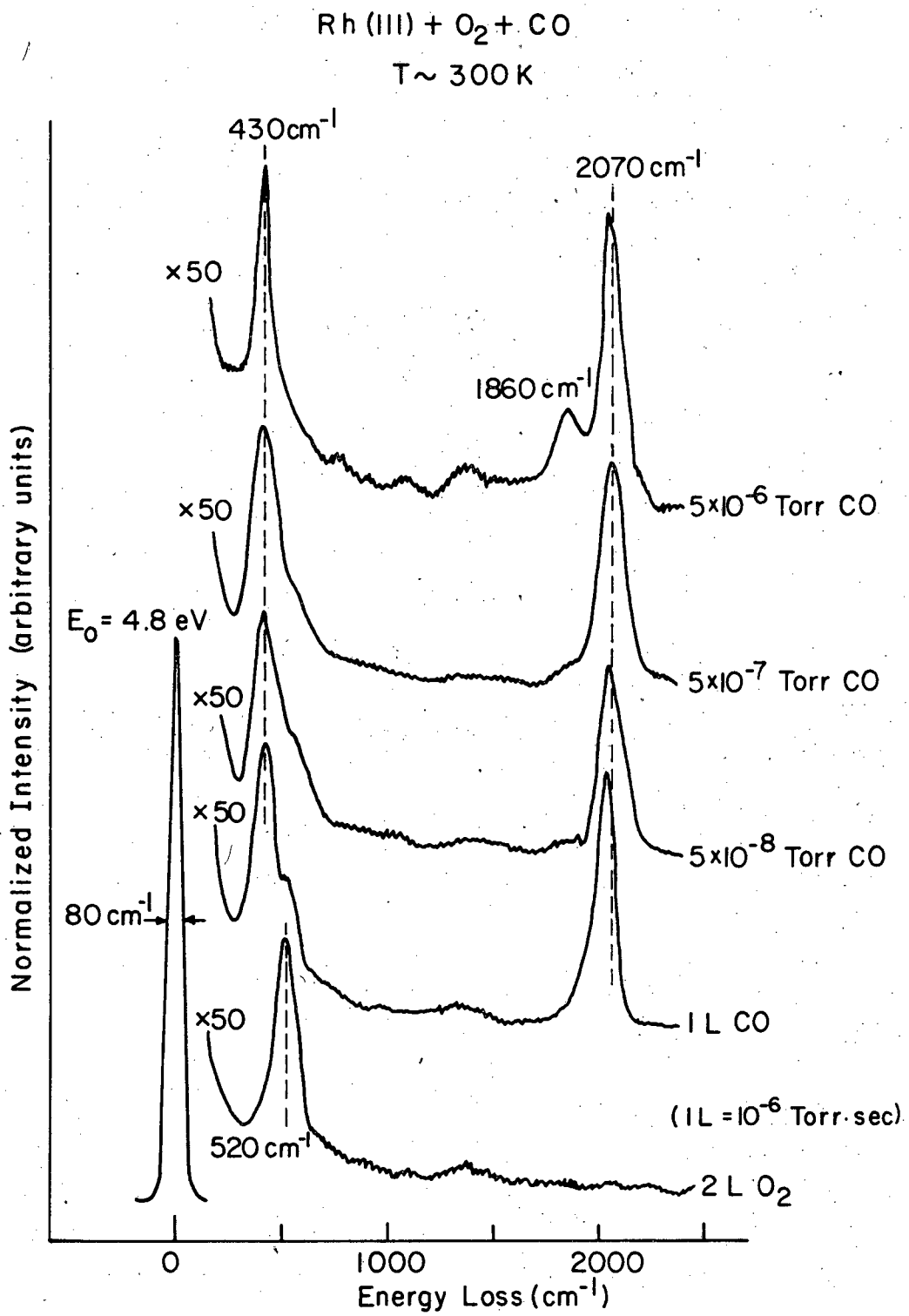
Rh (111) + O2 + CO
T ~ 300 K
430 cm-1
2070 cm-1
×50
1860 cm-1
5×10-6 Torr CO
×50
E0 = 4.8 eV
5×10-7 Torr CO
×50
×50
5×10-8 Torr CO
80 cm-1
×50
1 L CO
(1 L = 10-6 Torr·sec)
520 cm-1
2 L O2
Normalized Intensity (arbitrary units)
0
1000
2000
Energy Loss (cm-1)

XBL 793-5973

elevated temperatures and therefore may be residing beneath the surface.[26,31,50,51] Alternatively, the chemisorbed oxygen could slowly react with CO and desorb from the surface as $CO_2$.[26,31] No $CO_2$ was observed in the thermal desorption spectrum, however. This is not surprising since oxygen will diffuse into the bulk of the crystal rather quickly at these temperatures. Once the near surface region becomes oxygen rich, $CO_2$ will form in measurable quantities.[31]

These results are in qualitative agreement with earlier infrared studies:[13,16,30] shifts in the carbon-oxygen stretching vibration to higher frequency have been seen and the population of the linearly bonded species relative to the bridge bonded species has been reported to increase as well. Similar site changes and energy loss peak shifts have been observed in $CO/O_2$ co-adsorption studies on both Ni(100)[52] and Ru(001).[53] The post-adsorption of oxygen on a CO saturated surface showed no effects. This is consistent with the low pressure CO oxidation studies carried out over rhodium wires by Campbell and White.[31] Adsorbed carbon monoxide strongly inhibited oxygen adsorption and therefore decreased the reaction rate.

The Rh(111) surface was covered with carbon by decomposing $5 \times 10^{-7}$ Torr of either acetylene or ethylene at 1100 K for 10 minutes and subsequent flashing to 1200 K.[26] Pre-adsorbed carbon has a very strong inhibiting effect on carbon monoxide chemisorption as shown in Figure 8. This is the same effect it had on the methanation rate.[10] The low inelastic scattering intensity indicates relatively small CO coverages while the broad elastic peak and high background level are indicative of poor ordering. Consistent with this is a high background intensity in the LEED pattern and a decrease in the CO thermal desorption peak

Figure 8. The effects of preadsorbed carbon from the thermal decomposition of ethylene on the CO on Rh(111) vibrational spectrum.

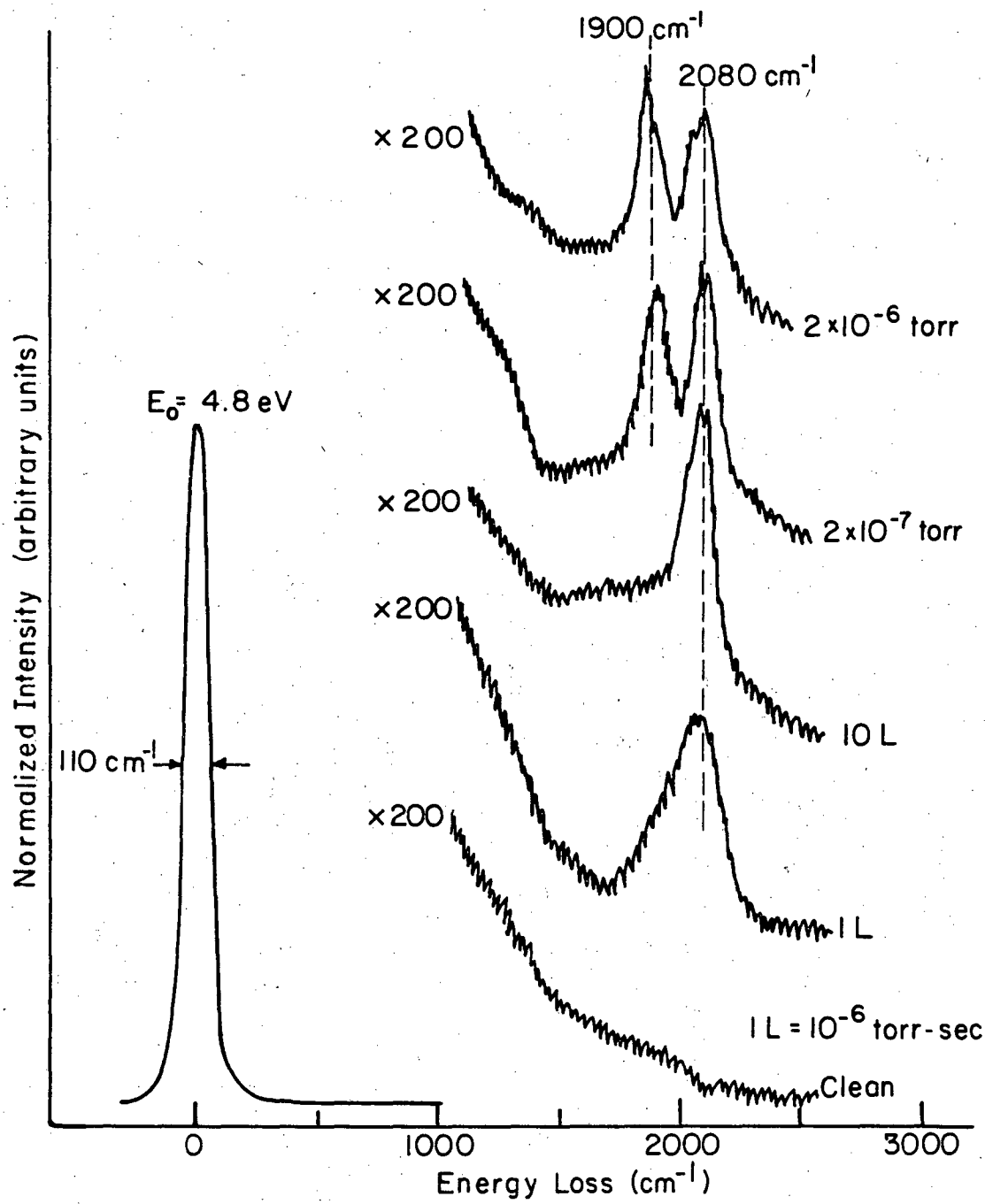
Rh(111) + C + CO
T ~ 300 K
1900 cm⁻¹
2080 cm⁻¹
×200
×200
×200
×200
×200
2×10⁻⁶ torr
2×10⁻⁷ torr
10 L
1 L
1 L = 10⁻⁶ torr-sec
Clean
E₀ = 4.8 eV
110 cm⁻¹
Normalized Intensity (arbitrary units)
0
1000
2000
3000
Energy Loss (cm⁻¹)

XBL795-6390

area (Fig. 6d). The carbon overlayer is covering most of the crystal face so that there are only a few sites open for CO chemisorption. The slightly more intense 1890 $cm^{-1}$ peak indicates that chemisorption of the linearly bound species is inhibited more than chemisorption of the bridge bonded species.

There is also an electronic interaction between the carbon overlayer and the adsorbed carbon monoxide molecules, since the vibrational peaks have shifted slightly and the thermal desorption temperature has dropped about 10 K (Fig. 6d). This altering of the metal-CO bond has also been observed in CO/hydrocarbon co-adsorption studies on other group VIII metals.[54,55]

## D. Vibrational Analysis of the CO/Rh System

Infrared spectroscopic studies on supported metal catalysts have an inherently high resolution, but are limited by support adsorption below 1000 $cm^{-1}$. Therefore metal-carbon stretching and bending vibrations are obscured. IR studies on either well characterized single crystal surfaces or evaporated films are limited, at present, to transitions with large dipole derivatives and therefore these same vibrations are not visible. Also, observation of modes parallel to the surface is prohibited by the normal dipole selection rule. High resolution ELS allows one to scan the entire infrared region of the spectrum with high sensitivity, but is hindered by relatively low resolution and again by the normal dipole selection rule. Inelastic electron tunneling spectroscopy has neither of these drawbacks. However, peaks in the vibrational spectrum are shifted due to the geometry of the tunnel junction. Here the presence of the upper lead electrode in the Al-$Al_2O_3$-Pb junction broadens and

shifts the vibrational frequencies due to an image dipole effect.[56] By combining the present ELS results at high CO coverage with earlier IR[17] and IETS[23] studies we can now calculate a consistent set of force constants for the Rh/CO system. For the species that gives rise to the losses at 420 and 2070 $cm^{-1}$ we assume a linear triatomic molecule of the form Rh-C≡O and take relevant bond lengths from $Rh_6(CO)_{16}$.[57] Using a valence force model (see Chapter I) one can easily obtain the force constants for the Rh-C and C≡O stretching vibrations as well as that for the Rh-C≡O bending modes.[58] The results of these calculations are shown in Table II. A comparison of the observed and calculated values for the $^{13}C$ labeled species is indicative of the accuracy of these calculations. We have only determined "effective" force constants here which depend not only on bond strengths,[59] but on image-dipole (electrodynamic[41]) forces as well.

Similar results can be obtained for bridge bonded carbon monoxide. Here we assume $C_{2V}$ symmetry for a species of the form 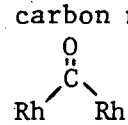 and to a first approximation neglect all bending modes. The results of these calculations are displayed in the second half of Table II. The agreement between the observed and calculated values for the isotopically labeled CO is not as good here due to the neglect of all interaction force constants (see Chapter I). Because of these assumptions, however, we can solve for the Rh-C-Rh bond angle and thus determine the rhodium-carbon bond length. This angle is calculated to be 88° and if we assume a Rh-Rh nearest neighbor distance of 2.69 Å,[60] we find a Rh-C bond length of 1.93 Å. This is in good agreement with both LEED studies for CO bridge bonded to Pd(100)[61] and with the X-ray structure of several organometallic rhodium clusters.[62] The agreement here is surprising in light of the simplicity of the calculations.

Table II. CO on Rhodium, Vibrational Analysis

| Species | Mode | $^{12}CO$ (observed) | Force Constants | | $^{13}CO$ (observed) | $^{13}CO$ (calculated) |
|---|---|---|---|---|---|---|
| linear | $\nu_{Rh-CO}$ [a] | 420 | $K_{Rh-C}$ | 2.40 md/Å | – [d] | 415 |
| O ‖ C \| Rh | $\delta_{Rh-C\equiv O}$ [b] | 469 | $K_{\beta}$ | 0.607 md Å/rad$^2$ | 454 | 455 |
| | $\nu_{C\equiv O}$ [c] | 2070 | $K_{C\equiv O}$ | 16.5 md/Å | 2024 | 2021 |
| bridged | $\nu_{Rh_2>O}$ [a] (symmetric) | 420 | $K_{Rh_2>C}$ | 2.38 md/Å | – [d] | 414 |
| O ‖ C / \ Rh Rh | $\nu_{Rh_2>CO}$ [b] (asymmetric) | 605 | | | 589 | 584 |
| | $\nu_{C=O}$ [c] | 1870 | $K_{C=O}$ | 13.3 md/Å | 1832 | 1826 |

[a] by ELS, this study

[b] by IETS[23]

[c] by IR[17]

[d] not a resolvable shift by ELS

E. Correlation Between Surface Structure and C≡O Vibrational Frequency

The accepted picture of carbon monoxide bonding to metals is by electron transfer from the 5σ orbital of CO to the metallic d orbitals and by backbonding of the metallic electrons into the empty 2π* orbital of the adsorbate.[12] This scheme has been used by both surface scientists and inorganic chemists to explain the infrared spectra of chemisorbed carbon monoxide and of metal carbonyls. Since the electron density in the CO antibonding orbital is increased, the carbon-oxygen stretching frequency should decrease below the gas phase value of 2143 $cm^{-1}$. Furthermore, as the CO is bound to an increasing number of metal atoms this frequency should drop even further as shown in the IR spectra of model organometallic compounds of known molecular structure.[12]

It is generally assumed that species with C≡O stretching frequencies above 2000 $cm^{-1}$ correspond to linearly bonded CO, frequencies between about 1850 and 2000 $cm^{-1}$ belong to bridge bonded species and those below approximately 1850 $cm^{-1}$ are for face bridging or three-fold coordination.[12] Although, the validity of this rule has not been well tested on single crystal surfaces, some preliminary data to support these divisions has been obtained (see Table III). This correlation of the structure of carbon monoxide (determined by low-energy electron diffraction) with the C≡O stretching frequency (from both IR and high resolution ELS studies) is very limited at present. Clearly more work needs to be done before any simple interpretation of carbon-oxygen vibrational frequencies can be used to infer the structure of chemisorbed CO. One must also recall that the presence of other either electron donating or withdrawing substituents on the surface can alter the CO electron density and will certainly shift the observed stretching frequencies.[54,55]

Table III. Correlation of Structure and Vibrational Frequency for CO Chemisorbed on Transition Metal Surfaces

| Surface | Overlayer Structure | Position from LEED | Vibrational Frequency ($cm^{-1}$) |
|---|---|---|---|
| Ni(100) | c(2x2) | atop[63,64] | 2069[65] |
| Cu(100) | c(2x2) | atop[64] | 2079[43,66], 2089[67], 2097[68] |
| Rh(111) | $(\sqrt{3}x\sqrt{3})R30°$ | atop[46,69] | 2020[1] |
| Pd(100) | c(4x2)R45° | bridge[61] | 1949[70], 1903[61] |

Finally, LEED, TDS and UPS studies on the interaction of carbon monoxide with the hexagonally closest packed faces of the group VIII metals show numerous similarities. This is not true of the vibrational spectroscopic data. These results are summarized in Table IV. CO almost always forms a $(\sqrt{3}x\sqrt{3})R30°$ surface structure at low coverages.[26,27,71-79] This LEED pattern compresses through a number of intermediate steps into a hexagonal closest packed overlayer of carbon monoxide molecules. This is the case despite varying electronic configurations and different metal-metal distances.[60] The metal-adsorbate bond energies derived from TDS measurements vary by only ±3 kcal/mole on the surfaces where no CO decomposition is detected.[26-28, 71, 73,74, 76, 78-80] Furthermore, the binding energy difference between the 4σ and 5σ carbon monoxide molecular orbitals, Δ(4σ-5σ), varies by only ±0.3 eV.[48,77,81-85] The vibrational spectra show tremendous differences, however. Both nickel[88] and palladium[70] form multiply coordinated carbonyl species at low CO exposures and the atop species are only seen at high coverage. The CO chemisorption behavior on Rh(111)[1] and Pt(111)[89-91] are the opposite: here the atop sites populate first and predominate at low CO exposures. Bridge bonded species begin to form at intermediate coverages. Ruthenium is totally different: only a single carbon-oxygen stretching vibration is present at all coverages.[53,86,87] The reasons for these differences in the nature of CO bonding to the various transition metal surfaces will have to be explored further in the future.

## F. Summary

By combining the present ELS and TDS studies with previous LEED experiments[26,27] we can now present a fairly complete picture of CO

Table IV. Chemisorption of CO on the Group VIII Metals

| Surface | Nearest neighbor distance (Å)[60] | LEED | $E_d$ (kcal/mole) | $\Delta(4\sigma-5\sigma)$ | Vibrational Spectra ($cm^{-1}$) $\nu_{M=C}$ | $\nu_{C\equiv O}$ |
|---|---|---|---|---|---|---|
| Fe(111) | 2.48 | (1x1) (71)[71]<br>decomposed | 24[71] | 3.2[81] | | |
| Ru(0001) | 2.65 | $(\sqrt{3}x\sqrt{3})R30°$[72,73]<br>$(2\sqrt{3}x2\sqrt{3})R30°$<br>$(5\sqrt{3}x5\sqrt{3})R30°$ | 28[73] | 3.1[82] | 445 | 1984[53,86,87]<br>2080,2061 |
| Co(0001) | 2.50 | $(\sqrt{3}x\sqrt{3})R30°$[74]<br>hexagonal | 25[74] | | | |
| Rh(111) | 2.69 | $(\sqrt{3}x\sqrt{3})R30°$[26,27]<br>split (2x2)<br>(2x2) | 31[26-28] | 3.2[48] | 480<br>420 | 1990<br>2070 1870[1] |
| Ir(111) | 2.71 | $(\sqrt{3}x\sqrt{3})R30°$[75]<br>$(2\sqrt{3}x2\sqrt{3})R30°$<br>split $(2\sqrt{3}x2\sqrt{3})$ | 29.5[80] | 2.7[83] | | |
| Ni(111) | 2.49 | $(\sqrt{3}x\sqrt{3})R30°$[76,77]<br>c(4x2)<br>$(\sqrt{7}x\sqrt{7})R19.2°$ | 26[76] | 2.8[77] | 400 | 1810<br>1910 2050[88] |
| Pd(111) | 2.75 | $(\sqrt{3}x\sqrt{3})R30°$[78]<br>c(4x2)<br>split (2x2)<br>(2x2) | 30.1[78] | 3.3[84] | | 1823<br>1946 2092[70] |
| Pt(111) | 2.77 | $(\sqrt{3}x\sqrt{3})R30°$[79]<br>c(4x2)<br>hexagonal | 28[79] | 3.0[85] | 476<br>380 | 2089<br>1856[89-91]<br>1872 |

chemisorption on Rh(111). At very low exposures a single species is present on the surface located in an atop site ($\nu_{Rh-CO}$ = 480 $cm^{-1}$, $\nu_{C\equiv O}$ = 1990 $cm^{-1}$). As the coverage increases, the bonding to the surface becomes weaker ($\nu_{Rh-C}$ decreases, $\nu_{C\equiv O}$ increases, TDS peak maximum shifts to lower temperatures).[26-28] This process continues until an approximately 0.5 L exposure where a $(\sqrt{3}x\sqrt{3})R30°$ LEED pattern is seen and all of the adsorbed CO molecules are linearly bounded to individual rhodium atoms (Fig. 5a). Above this coverage a second C≡O stretching vibration corresponding to a bridge bonded species is observed ($\nu_{Rh-CO} \simeq 400$ $cm^{-1}$, $\nu_{C=O}$ = 1870 $cm^{-1}$). A "split" (2x2) LEED pattern is seen indicating a loosely packed hexagonal overlayer of adsorbate molecules. This overlayer structure compresses upon further CO exposure. Throughout this intermediate coverage regime there is a mixed layer of atop and bridge bonded CO species and we see a continuous growth of all ELS peaks and a shift in the loss above 2000 $cm^{-1}$. Two peaks are also visible in the TDS spectra with the bridge bonded carbon monoxide having an approximately 4 kcal/mole lower binding energy to the surface than the species located in the atop site. Finally, by a background pressure of approximately $1 \times 10^{-6}$ Torr CO at 300 K, a (2x2) LEED pattern forms whose unit cell consists of three carbon monoxide molecules--two atop and one bridged (Fig. 5b), in reasonable agreement with the two-to-one peak intensity ratio found in the ELS spectra (Fig. 3). The high coverage values of the C≡O stretching frequencies for the two types of chemisorbed carbon monoxide ($\nu_{bridge}$ = 1870 $cm^{-1}$, $\nu_{atop}$ = 2070 $cm^{-1}$) also agree with previous infrared studies (see Table I).

The pre-adsorption of hydrogen had no effect on CO chemisorption on Rh(111) as evidenced by both TDS and high resolution ELS. Oxygen and carbon blocked many sites for CO chemisorption and weakened the metal-adsorbate interaction ($\nu_{Rh-C}$ decreases, $\nu_{C\equiv O}$ increases, TDS peak maximum shifts to lower temperature).

## References


1. L. H. Dubois and G. A. Somorjai, Surface Sci. 91, 514 (1980).

2. R. R. Ford, Adv. Catalysis, 51, 21 (1970).

3. A. M. Bradshaw, Surface Sci. 80, 215 (1979).

4. R. B. King, Prog. Inorg. Chem. 15, 287 (1972).

5. P. Chini, G. Longini and V. G. Albano, Adv. Organomet. Chem. 14, 285 (1976).

6. G. A. Ozin, Acc. Chem. Res. 10, 21 (1977).

7. E. L. Muetterties, Bull. Soc. Chim. Belg. 84, 959 (1975); 85, 451 (1976).

8. E. L. Muetterties, T. N. Rhodin, E. Band, C. F. Brucker, and W. R. Pretzer, Chem. Rev. 79, 91 (1979).

9. M. M. Bhasin, W. J. Bartley, P. C. Ellgen, and T. P. Wilson, J. Catal. 54, 120 (1978).

10. B. A. Sexton and G. A. Somorjai, J. Catal. 46, 167 (1977).

11. R. L. Pruett, Ann. N.Y. Acad. Sci. 295, 239 (1977).

12. See N. Sheppard and T. T. Nguyen in Advances in Infrared and Raman Spectroscopy Vol. 5, R. J. H. Clark and R. E. Hester, eds. (Heyden and Son, London, 1978) p. 67 and references therein.

13. A. C. Yang and C. W. Garland, J. Phys. Chem. 61, 1504 (1957).

14. H. Arai and H. Tominga, J. Catal. 43, 131 (1976).

15. H. C. Yao and W. G. Rothschild, J. Chem. Phys. 68, 4774 (1978).

16. M. Primet, J. C. S. Faraday I 74, 2570 (1978).

17. J. T. Yates, Jr., T. M. Duncan, S. D. Worley, and R. W. Vaughn, J. Chem. Phys. 70, 1219 (1979).

18. D. J. C. Yates, L. L. Murrell, and E. B. Prestridge, J. Catal. 57, 41 (1979).

19. G. C. Smith, T. P. Chojnacki, S. R. Drasgupta, K. Iwatata, and W. L. Watters, Inorg. Chem. 14, 1419 (1975).

20. H. Conrad, G. Ertl, H. Knözing, J. Küppers, and E. E. Latta, Chem. Phys. Lett. 42, 115 (1976).

21. P. K. Hansma, W. C. Kaska, and R. M. Laine, J. Am. Chem. Soc. 98, 6064 (1976).

22. J. Klein, A. Leger, S. de Cheveigne, C. Guinet, M. Belin, and D. Defourneau, Surface Sci. 82, L288 (1979).

23. R. M. Kroeker, W. C. Kaska, and P. K. Hansma, J. Catal. 57, 72 (1979); 61, 87 (1980).

24. H. Ibach, Surface Sci. 66, 56 (1977).

25. J. T. Grant and T. W. Haas, Surface Sci. 21, 76 (1970).

26. D. G. Castner, B. A. Sexton, and G. A. Somorjai, Surface Sci. 71, 519 (1978).

27. P. A. Thiel, E. D. Williams, J. T. Yates, Jr., and W. H. Weinberg, Surface Sci. 84, 54 (1979).

28. J. T. Yates, Jr., E. D. Williams, and W. H. Weinberg, Surface Sci. 91, 562 (1980).

29. J. T. Yates, Jr., S. D. Worley, T. M. Duncan, and R. W. Vaughn, J. Chem. Phys. 70, 1225 (1979).

30. C. R. Guerra and J. H. Schulman, Surface Sci. 7, 229 (1967).

31. C. T. Campbell and J. M. White, J. Catal. 46, 167 (1977).

32. R. Whyman, J. C. S. Chem. Comm., 1194 (1970).

33. W. P. Griffith and A. J. Wickam, J. Chem. Soc. A, 834 (1969).

34. L. A. Hanlan and G. A. Ozin, J. Am. Chem. Soc. 96, 6324 (1974).

35. J. G. Roth and M. J. Dignam, Can. J. Chem. 54, 1388 (1976).

36. M. Moskovits and J. W. Hulse, Surface Sci. 78, 397 (1978).

37. R. M. Hammaker, S. A. Francis, and R. P. Eischens, Spectrochim. Acta 21, 1295 (1965).

38. G. D. Mahan and A. A. Lucas, J. Chem. Phys. 68, 1344 (1978).

39. M. Scheffler, Surface Sci. 81, 562 (1979).

40. G. Blyholder, J. Phys. Chem. 68, 2772 (1964).

41. S. Efrima and H. Metiu, Surface Sci. 92, 433 (1980).

42. A. Crossley and D. A. King, Surface Sci. 68, 528 (1977).

43. P. Hollins and J. Pritchard, Surface Sci. 89, 486 (1979).

44. D. G. Castner, Ph.D. Thesis, University of California, Berkeley, 1979.

45. C. W. Garland, R. C. Lord, and P. F. Troiano, J. Phys. Chem. 71, 343 (1967).

46. M. A. Van Hove, L. H. Dubois, R. J. Koestner, and G. A. Somorjai, Proc. 8th Intern. Vacuum Congress (Cannes, 1980), in press.

47. J. Pritchard, Surface Sci. 79, 231 (1979).

48. W. Braun, M. Neumann, M. Iwan and E. E. Koch, Solid State Commun. 27, 155 (1978).

49. The Rh(111) surface is catalytically active for Fischer-Tropsch synthesis but at pressures above 1 atmosphere (D. G. Castner, R. L. Blackadar, and G. A. Somorjai, J. Catal., in press).

50. P. A. Thiel, J. T. Yates, Jr., and W. H. Weinberg, Surface Sci. 82, 22 (1979).

51. D. G. Castner and G. A. Somorjai, Appl. Surface Sci., in press.

52. S. Anderson, Solid State Commun. 24, 183 (1977).

53. G. E. Thomas and W. H. Weinberg, J. Chem. Phys. 70, 954 (1979).

54. H. Ibach and G. A. Somorjai, Appl. Surface Sci. 3, 293 (1979).

55. J. Wojtczak, R. Queau, and R. Poilblanc, J. Catal. 37, 391 (1975).

56. J. R. Kirtley and P. K. Hansma, Phys. Rev. B12, 531 (1975).

57. E. R. Corey, L. F. Dahl, and W. Beck, J. Am. Chem. Soc. 85, 1202 (1963).

58. G. Herzberg, Molecular Spectra and Molecular Structure II; Infrared and Raman Spectra of Polyatomic Molecules (Van Nostrand, Princeton, N.J., 1945).

59. J. W. Gadzuk, Phys. Rev. B19, 5355 (1979).

60. C. Kittel, Introduction to Solid State Physics (John Wiley and Sons, New York, 1976) p. 32.

61. R. J. Behm, K. Christmann, G. Ertl, M. A. Van Hove, P. A. Thiel, and W. H. Weinberg, Surface Sci. 88, L59 (1979).

62. O. S. Mills and E. F. Paulus, J. C. S. Chem. Comm., 815 (1966).

63. M. Passler, A. Ignatiev, F. Jona, D. W. Jepsen, and P. M. Marcus, Phys. Rev. Lett. 43, 360 (1977).

64. S. Andersson and J. B. Pendry, Phys. Rev. Lett. 43, 363 (1977).

65. S. Andersson, Solid State Commun. 21, 75 (1977).

66. K. Horn and J. Pritchard, Surface Sci. 55, 701 (1976).

67. B. A. Sexton, Chem. Phys. Lett. 63, 451 (1979).

68. S. Andersson, Surface Sci. 89, 477 (1979).

69. M. A. Van Hove, R. J. Koestner, and G. A. Somorjai, submitted to Surface Sci.

70. A. M. Bradshaw and F. M. Hoffman, Surface Sci. 72, 513 (1978).

71. K. Yoshida and G. A. Somorjai, Surface Sci. 75, 46 (1978).

72. E. D. Williams and W. H. Weinberg, Surface Sci. 82, 93 (1979).

73. T. E. Madey and D. Menzel, Japan J. Appl. Phys. Supp. 2, Part 2, 229 (1974).

74. M. E. Bridge, C. M. Comrie, and R. M. Lambert, Surface Sci. 67, 393 (1977).

75. J. Kuppers and A. Plagge, J. Vac. Sci. Technol. 13, 259 (1976).

76. K. Christmann, O. Schober, and G. Ertl, J. Chem. Phys. 60, 4719 (1974).

77. H. Conrad, G. Ertl, J. Kuppers, and E. E. Latta, Surface Sci. 57, 475 (1976).

78. H. Conrad, G. Ertl, J. Koch, and E. E. Latta, Surface Sci. 43, 462 (1974).

79. G. Ertl, M. Neumann, and K. M. Streitt, Surface Sci. 64, 393 (1977).

80. B. E. Nieuwenhuys, D. I. Hagen, G. Rovida, and G. A. Somorjai, Surface Sci. 59, 155 (1976).

81. H. M. Textor, I. D. Gay, and R. Mason, Proc. Roy. Soc. London, Ser A. 356, 37 (1977).

82. J. C. Fuggle, T. E. Madey, M. Steinkilberg, and D. Menzel, Phys. Lett. 51A, 163 (1975); Surface Sci. 52, 521 (1975).

83. P. A. Zhdan, G. K. Boreskov, A. I. Baronin, W. F. Egelhoff, Jr., and W. H. Weinberg, Chem. Phys. Lett. 44, 528 (1976).

84. D. R. Lloyd, C. M. Quinn, and N. V. Richardson, Solid State Commun. 20, 409 (1976).

85. Y. Iwasawa, R. Mason, M. Textor, and G. A. Somorjai, Chem. Phys. Lett. 44, 468 (1976).

86. G. E. Thomas and W. H. Weinberg, J. Chem. Phys. 70, 1437 (1979).

87. H. Pfnur, D. Menzel, F. M. Hoffmann, A. Ortega, and A. M. Bradshaw, Surface Sci. 93, 431 (1980).

88. W. Erley, H. Wagner, and H. Ibach, Surface Sci. 80, 612 (1979).

89. H. Froitzheim, H. Hopster, H. Ibach, and S. Lehwald, Appl. Phys. 13, 147 (1977).

90. H. Hopster and H. Ibach, Surface Sci. 77, 109 (1978).

91. A. M. Baro and H. Ibach, J. Chem. Phys. 71, 4812 (1979).

# CHAPTER V. The Dissociative Chemisorption of Carbon Dioxide on Rhodium Surfaces[1]

## A. Background

There is much uncertainty in the literature concerning the nature of carbon dioxide chemisorption on rhodium surfaces. Recent results from our laboratory which show the dissociation of $CO_{2(g)}$ to $CO_{ads}$[†] and $O_{ads}$ on several single crystal[2,3] and polycrystalline samples[4] do not agree with those of others indicating the absence of chemisorption for carbon dioxide.[5-8] In order to obtain additional proof of $CO_2$ dissociation on rhodium surfaces we have applied high resolution electron energy loss spectroscopy and thermal desorption mass spectrometry to a study of $^{12}CO_2$ and $^{13}CO_2$ chemisorption on the Rh(111) single crystal surface. The combination of these two techniques allows one to determine the nature of the adsorbed species while on the metal surface and after desorption into the gas phase. We present convincing evidence for the dissociative chemisorption of carbon dioxide to $CO_{ads}$ and $O_{ads}$ at 300 K. The difficulty in detecting $CO_2$ dissociation upon adsorption is due to the low sticking probability of the molecule on rhodium[2-8] and to the rapid back reaction $CO_{ads} + O_{ads} \rightarrow CO_{2(g)}$ at elevated temperatures in the presence of excess chemisorbed oxygen.[2,3,7,8]

Early infrared studies employing alumina supported rhodium samples showed no evidence for $CO_2$ chemisorption--either molecular or dissociative.[5] Similarly, volumetric uptake measurements on evaporated rhodium films indicate that very little $CO_2$ chemisorption is taking place.[6]

---

[†] ads denotes an adsorbed species.

Simple calculations of heats of adsorption for dissociatively chemisorbed $CO_2$ yield values between 10 and 29 kcal/mole, implying only weak chemisorption, if any.[6,9] Kinetic studies on polycrystalline rhodium wires by Campbell and White also show no $CO_2$ adsorption at 330 K.[7] A small CO peak was observed in the thermal desorption spectrum, but it was attributed to chemisorption from the ambient. More recently, Primet found no evidence for carbon dioxide chemisorption on zeolite supported rhodium catalysts at 300 K using infrared spectroscopy.[8] Samples on an alumina support under identical conditions, however, showed bands at 1860 and 2025 $cm^{-1}$. This was interpreted in terms of a very low coverage of carbon monoxide derived from dissociatively chemisorbed $CO_2$. Finally, he found that preadsorbed oxygen inhibited the dissociation of carbon dioxide at 300 K.

Low energy electron diffraction studies on rhodium single crystal surfaces provided the first evidence for $CO_2$ chemisorption. Grant and Haas observed a "rather complex" diffraction pattern after exposing an initially clean Rh(111) surface to 60 L of $CO_2$.[10] Castner, Sexton and Somorjai showed that CO and $CO_2$ gave an identical series of LEED patterns and thermal desorption spectra on both the (111) and (100) rhodium surfaces.[2] The only difference noted between the two adsorbates was that $CO_2$ required an approximately five-fold higher exposure to achieve the same surface structures. They interpreted these findings in terms of carbon dioxide dissociation into adsorbed CO and oxygen. Further studies on stepped rhodium surfaces are in full agreement with this interpretation.[3] Recent catalytic experiments on rhodium foils indicate that $CO_2$ does indeed dissociatively chemisorb and is extremely reactive toward hydrogen.[4]

## B. Experimental Results

To clarify the nature of carbon dioxide adsorption on rhodium we have studied the chemisorption of both $^{12}CO_2$ and $^{13}CO_2$ (Merck Isotopes, 90.5% purity) on the (111) single crystal surface of rhodium by high resolution electron energy loss spectroscopy and thermal desorption mass spectrometry. Figure 1 shows a series of high resolution ELS spectra of $^{12}CO_2$ chemisorbed on Rh(111) at 300 K as a function of gas exposure and background pressure. The vibrational spectra are almost identical to those shown in Chapter IV, Figures 1 and 3. The only major difference (in agreement with previous studies[2,3]) is that an approximately ten-fold higher exposure of carbon dioxide is required to form the same surface species. This clearly indicates the dissociative chemisorption of carbon dioxide. For the case of molecular $CO_2$ adsorption one would expect several extra peaks in the 800-1600 $cm^{-1}$ region. Such stretching vibrations have been seen for two distinct types of carbon dioxide bonding in rhodium - $CO_2$ coordination complexes,[11] but are clearly not visible here, even at high scale expansions. One can assign all of the observed losses by comparison with several rhodium carbonyls,[12,13] with matrix isolation experiments,[14] and with previous infrared studies on supported rhodium catalysts;[5,8,15] 430 $cm^{-1}$: $\nu_{Rh-C}$, 1870 $cm^{-1}$: $\nu_{C=O}$ (multiply coordinated site) and 2060 $cm^{-1}$: $\nu_{C\equiv O}$ (atop site). The details of these assignments are presented in Chapter IV and Reference 16.

The lower portion of Figure 2 shows a comparison between the high resolution ELS spectra of $^{12}CO$ and $^{12}CO_2$ chemisorbed on Rh(111) at 5 x $10^{-7}$ Torr background pressure and 300 K. The position of the carbon-oxygen stretch at 2060 $cm^{-1}$ is a strong function of coverage (see Chapter IV) and is therefore not well suited for isotopic studies. The peak at

Figure 1. High resolution ELS spectra of $^{12}CO_2$ chemisorbed on Rh(111) at 300 K as a function of gas exposure and background pressure. Note the similarity between these spectra and those shown in Figures 1 and 3 of Chapter IV.

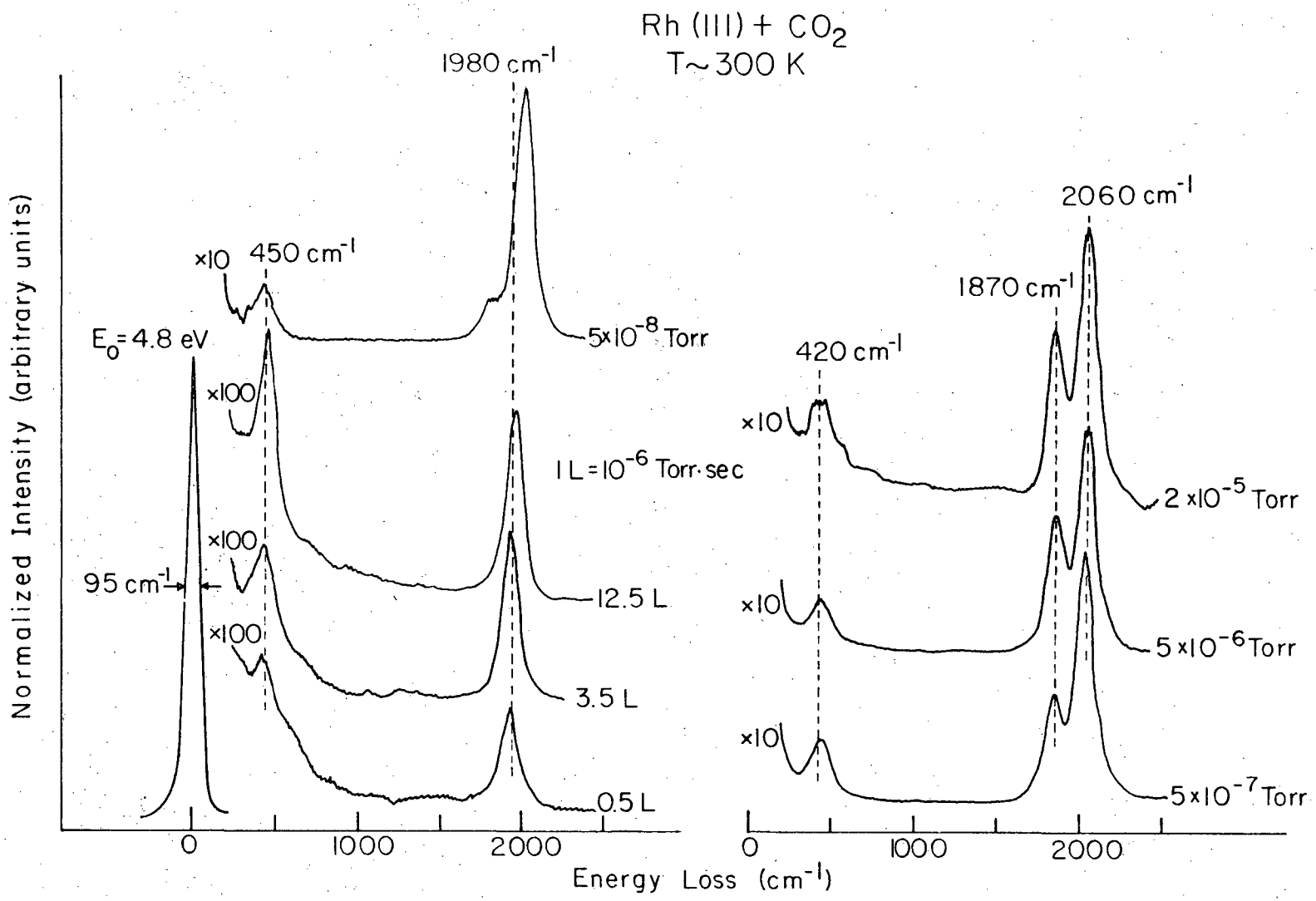
Rh (111) + $CO_2$
T~300 K
1980 cm$^{-1}$
2060 cm$^{-1}$
1870 cm$^{-1}$
450 cm$^{-1}$
420 cm$^{-1}$
$E_0$=4.8 eV
95 cm$^{-1}$
×10
×100
1 L=10$^{-6}$ Torr·sec
5×10$^{-8}$ Torr
12.5 L
3.5 L
0.5 L
2 ×10$^{-5}$ Torr
5 ×10$^{-6}$ Torr
5×10$^{-7}$ Torr
Normalized Intensity (arbitrary units)
0
1000
2000
Energy Loss (cm$^{-1}$)

XBL 793-5881

Figure 2. High resolution ELS spectra of chemisorbed $^{12}CO$, $^{12}CO_2$ and $^{13}CO_2$ on Rh(111) at 300 K under approximately 5 x $10^{-7}$ Torr background pressure. Note the absence of extra peaks for carbon dioxide chemisorption. The frequency shifts are summarized in Table I.

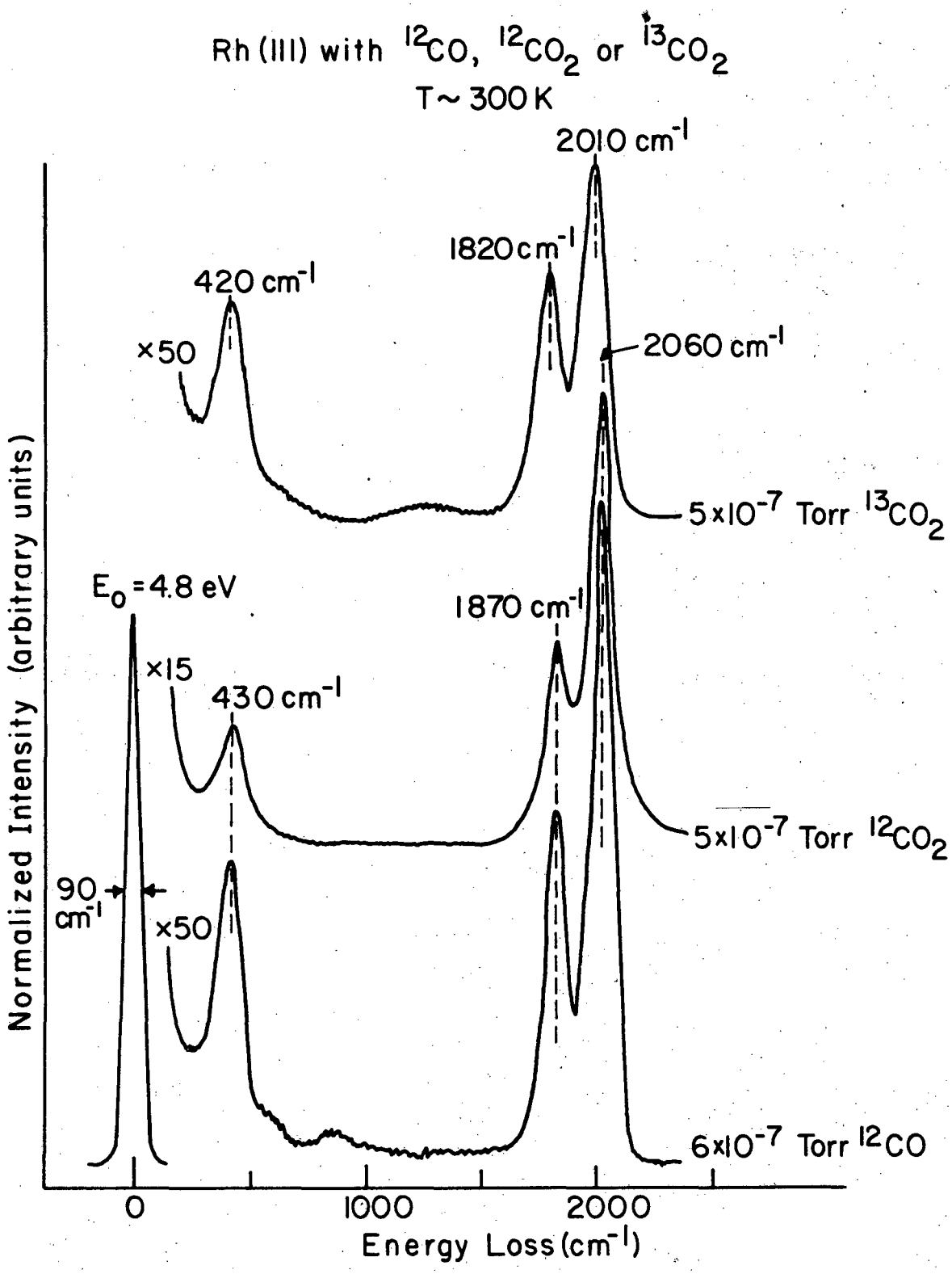
Rh (III) with $^{12}CO$, $^{12}CO_2$ or $^{13}CO_2$
T ~ 300 K
2010 cm$^{-1}$
1820 cm$^{-1}$
420 cm$^{-1}$
×50
2060 cm$^{-1}$
5×10$^{-7}$ Torr $^{13}CO_2$
$E_0$ = 4.8 eV
1870 cm$^{-1}$
×15
430 cm$^{-1}$
5×10$^{-7}$ Torr $^{12}CO_2$
90 cm$^{-1}$
×50
6×10$^{-7}$ Torr $^{12}CO$
Normalized Intensity (arbitrary units)
0
1000
2000
Energy Loss (cm$^{-1}$)

XBL 793-5974

1870 $cm^{-1}$ grows in at constant frequency, however, and is ideal for labeling experiments. Relatively high pressures of $^{12}CO$, $^{12}CO_2$ and $^{13}CO_2$ were applied in order to insure adequate population of this site. It is clear from the $^{13}CO_2$ chemisorption spectrum in the top of Figure 2 that $^{13}CO_2$ dissociatively chemisorbs on Rh(111) and forms $^{13}CO_{ads}$. This result eliminates the possibility that $CO_{ads}$ is produced by the chemisorption of background CO in the vacuum system. Gas chromatographic analysis of $^{12}CO_2$ and $^{13}CO_2$ showed CO impurities below 12 parts per million in both cases. The calculated shifts of the vibrational frequencies presented in Table I agree quite well with the predicted values, despite the limited resolution of ELS. They are also in excellent agreement with the shifts observed in the recent infrared results of Yates, et al., for $^{12}CO$ and $^{13}CO$ chemisorbed on alumina supported rhodium particles.[15] Several researchers have shown that adsorbed oxygen has only a small effect on the C≡O stretching vibration[5,8,16,17] and therefore one would not expect large shifts here. Further studies have shown that the weak Rh-O stretch from adsorbed oxygen at 520 $cm^{-1}$ is probably hidden beneath the $\nu_{Rh-C}$ peak (see Chapter IV and Reference 16). Oxygen is soluble in bulk rhodium at elevated temperatures and therefore may be residing beneath the surface.[2,3,18,19] Evidence for the mobility of oxygen in rhodium at temperatures below 300 K has also been reported recently.[18]

The TDS spectra of chemisorbed CO and $CO_2$ are also quite similar (see Fig. 3) in agreement with previous studies.[2,3] $^{13}CO_2$ yields only $^{13}CO$, as expected. Again, an approximately five- to ten-fold higher exposure is required for the adsorption of carbon dioxide. No molecular $CO_2$ (either m/e = 44 or 45) was observed desorbing from the surface and

Table I. Isotopic Frequency Shifts for $CO_2$ Chemisorption on Rhodium[a]

| Mode | Observed on Rh(111)[b] | | Calculated[c] | Observed on Supported Rhodium[15] | |
|---|---|---|---|---|---|
| | $^{12}CO_2$ | $^{13}CO_2$ | $^{13}CO$ | $^{12}CO$ | $^{13}CO$ |
| $\nu_{Rh-C}$ | 430 | 420 | 423 | -- | -- |
| $\nu_{C=O}$(multiply coordinated) | 1870 | 1820 | 1828 | 1870 | 1832 |
| $\nu_{C\equiv O}$(atop) | 2060 | 2010 | 2014 | 2070 | 2024 |

[a] All frequencies in $cm^{-1}$.

[b] Observed values are reproducible to $\pm 7$ $cm^{-1}$.

[c] $\nu^* = (\frac{\mu}{\mu^*})^{\frac{1}{2}} \nu$, where $\mu$ is the reduced mass for the vibrational mode of interest and * refers to the labeled species.

Figure 3. Thermal desorption spectra for $^{12}CO$, $^{12}CO_2$ and $^{13}CO_2$ chemisorbed on Rh(111). The heating rate was approximately 20 K/sec. CO (m/e = 28 or 29) was the only species detected desorbing from the surface.

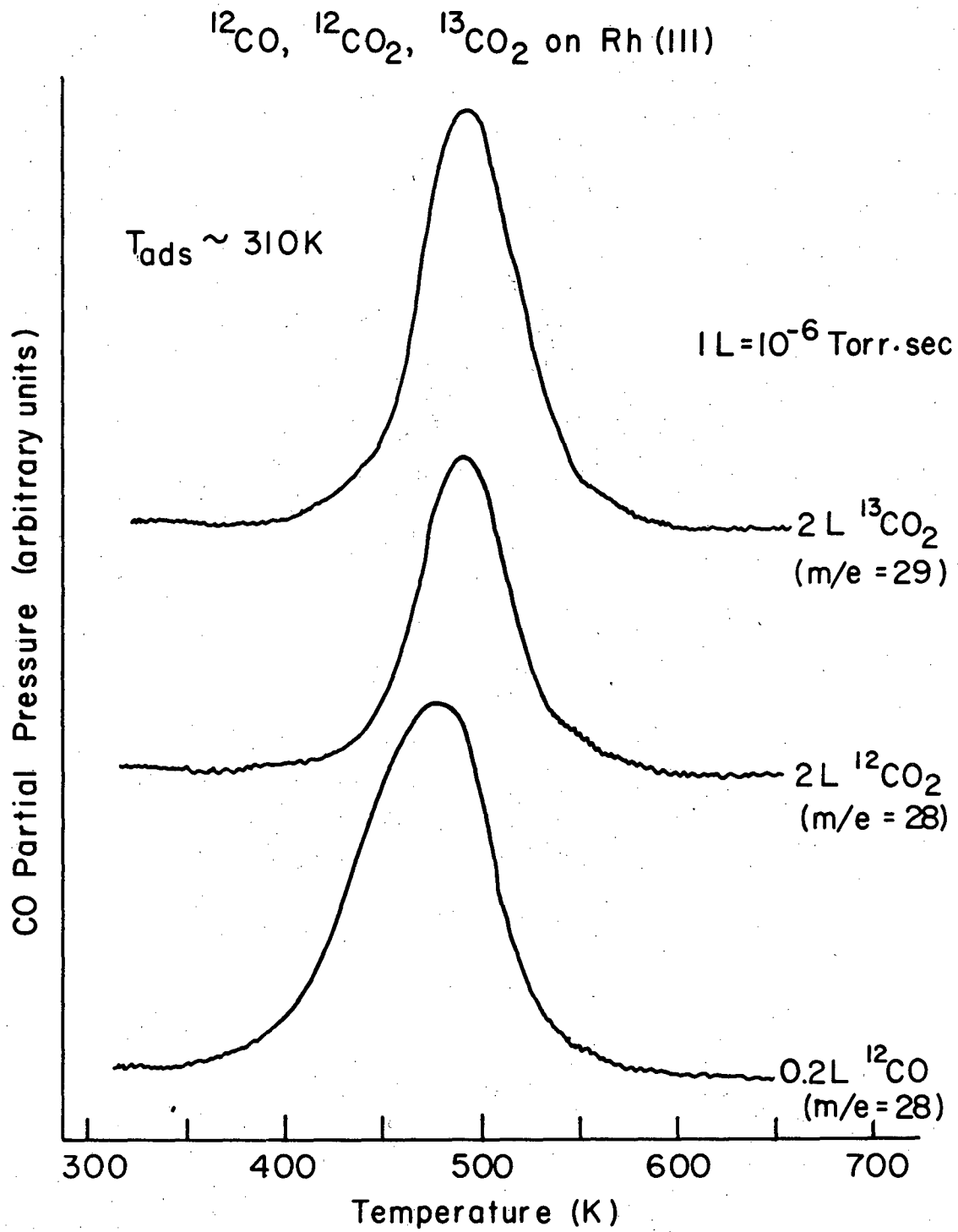
$^{12}CO$, $^{12}CO_2$, $^{13}CO_2$ on Rh (111)
$T_{ads} \sim 310K$
1 L = $10^{-6}$ Torr·sec
2 L $^{13}CO_2$
(m/e = 29)
2 L $^{12}CO_2$
(m/e = 28)
0.2 L $^{12}CO$
(m/e = 28)
CO Partial Pressure (arbitrary units)
300
400
500
600
700
Temperature (K)

XBL793-5972

this is consistent with the solubility of oxygen in bulk rhodium samples.[2,3,18,19] These labeling studies provide clear evidence that background adsorption is not causing the observed LEED, ELS or TDS features.

## C. Discussion

The question still remains: Why was it difficult to detect the dissociative chemisorption of carbon dioxide on rhodium in other experiments? It appears that relatively high gas exposures are necessary to detect any chemisorption due to the low sticking probability of $CO_2$. Also, CO readily reacts with, and is easily removed by, excess chemisorbed oxygen, even at 320 K.[2,3,7,8] Thus, if the rhodium surface is partially oxygen covered, the low sticking probability and the high rate of the association reaction, $CO_{ads} + O_{ads} \rightarrow CO_{2(g)}$, will yield the apparent result that $CO_2$ does not adsorb.

Finally, the dissociation of carbon dioxide ($CO_{2(g)} \rightarrow CO_{ads} + O_{ads}$) can only occur if the heat of adsorption of oxygen ($\Delta H_{ads}(O_2)$) on rhodium is quite large. Consider the following scheme:

| | |
|---|---|
| $CO_{2(g)} \rightarrow C_{(s)} + O_{2(g)}$ | $\Delta H = 94.05$ kcal/mole[20] |
| $C_{(s)} + \frac{1}{2}O_{2(g)} \rightarrow CO_{(g)}$ | $-26.42$[20] |
| $CO_{(g)} \rightarrow CO_{ads}$ | $-31$[2,3,7,16,21] |
| $\frac{1}{2}O_{2(g)} \rightarrow O_{ads}$ | $\frac{1}{2}\Delta H_{ads}(O_2)$ |
| $CO_2(g) \rightarrow CO_{ads} + O_{ads}$ | $\Delta H = 36.6 - \frac{1}{2}\Delta H_{ads}(O_2)$ kcal/mole |

Thus, thermodynamics requires the oxygen heat of adsorption to be $\gtrsim 73$ kcal/mole in order for carbon dioxide to dissociatively chemisorb. $\Delta H_{ads}(O_2)$ is a strong function of the surface oxygen coverage,

however.[2,3,7,18,19] This is clearly shown in Figure 4. According to the work of Thiel et al., 40% of a monolayer of oxygen must be present on the Rh(111) surface before any $O_2$ desorption (m/e = 32) is measured with a mass spectrometer.[18] Using this as the zero of oxygen coverage yields a value for $\Delta H_{ads}(O_2)$ of only 57 kcal/mole. Extrapolation to the true zero oxygen coverage yields a value of 117 kcal/mole (see Fig. 4). We expect the heat of adsorption of oxygen in our experiments to lie somewhere in between these two limiting values. Experiments on evaporated rhodium films yield values as high as 120 kcal/mole,[22] however. As the near surface region of the sample becomes saturated with oxygen, $\Delta H_{ads}(O_2)$ will decrease and carbon dioxide will no longer dissociate into $CO_{ads}$ and $O_{ads}$. It is clear that $CO_2$ chemisorption will only occur when the surface oxygen concentration is quite low. Thus, the ability of oxygen to penetrate the rhodium lattice may be partly responsible for the observed dissociative chemisorption of carbon dioxide on rhodium surfaces.

### D. "Surface Oxide" Formation on Rh(111)

Castner and Somorjai were able to identify four distinct states in the interaction of oxygen with rhodium surfaces: chemisorbed oxygen atoms, dissolution of oxygen into the rhodium lattice, formation of an unreactive surface oxide ("strongly bound oxygen") and epitaxial growth of $Rh_2O_3$.[19] The non-reactive surface oxide and dissolved oxygen probably have the most catalytic importance.[19] However, all of these different forms can inhibit carbon dioxide chemisorption by lowering $\Delta H_{ads}(O_2)$. Figure 5 shows a comparison between the high resolution ELS spectra of oxygen chemisorbed on Rh(111) at 300 K (lower trace) and after heating

Figure 4. The heat of adsorption of oxygen on Rh(111) is a strong function of the surface oxygen concentration (as determined by Auger electron spectroscopy).[18] Extrapolation to zero coverage yields values between 57 and 117 kcal/mole, depending on the method used. The experimental data is from Reference 18.

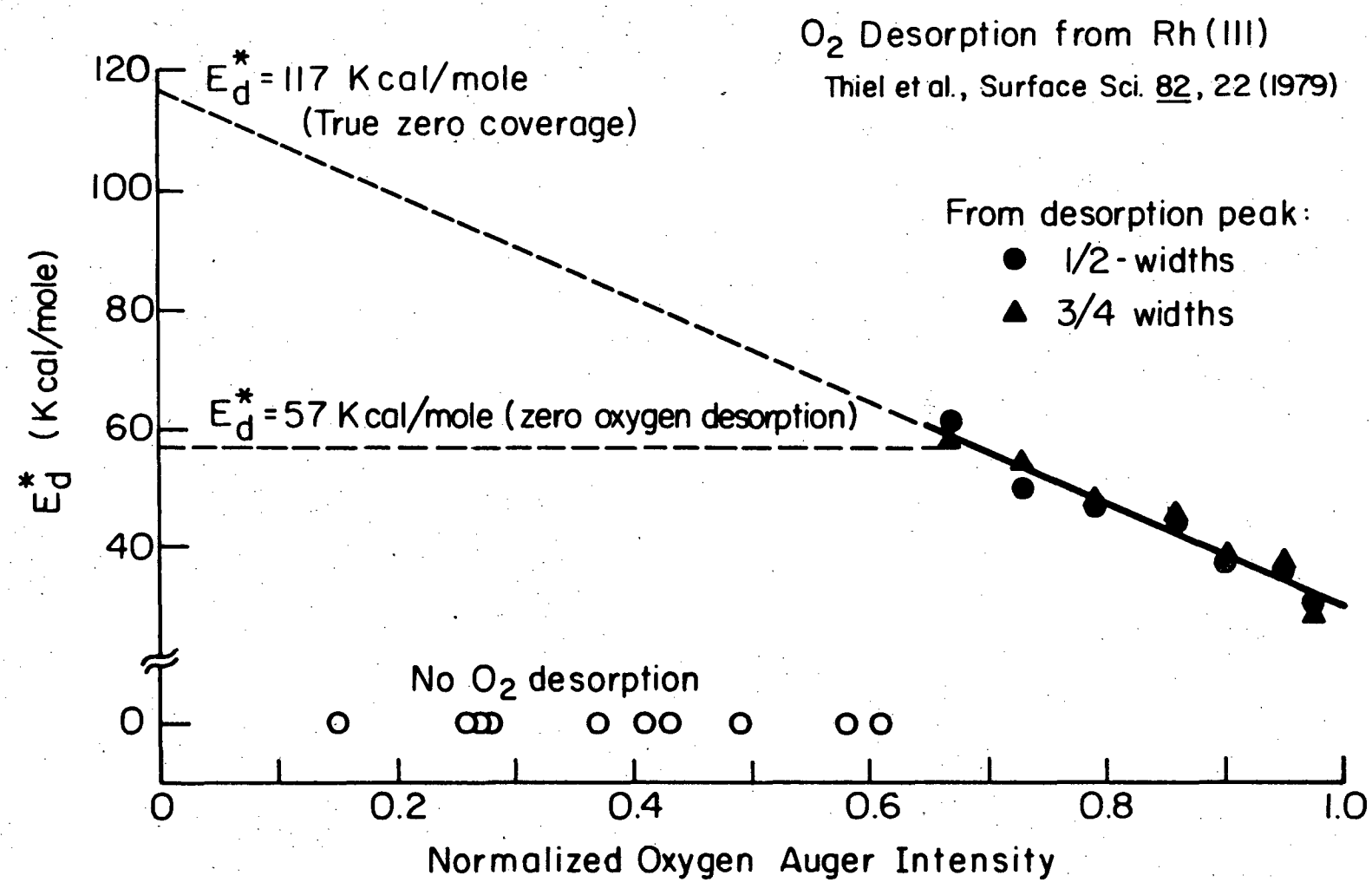
$O_2$ Desorption from Rh (III)
Thiel et al., Surface Sci. 82, 22 (1979)
$E_d^* = 117$ Kcal/mole
(True zero coverage)
$E_d^* = 57$ Kcal/mole (zero oxygen desorption)
From desorption peak:
1/2-widths
3/4 widths
No $O_2$ desorption
$E_d^*$ (Kcal/mole)
120
100
80
60
40
0
0
0.2
0.4
0.6
0.8
1.0
Normalized Oxygen Auger Intensity

XBL806-5317

the sample in 5 x $10^{-7}$ Torr of $O_2$ at 1100 K for 10 minutes (upper trace). The 520 $cm^{-1}$ peak visible in both spectra is due to the dissociative chemisorption of oxygen[16] and similar bands have now been seen on other faces of rhodium.[23] LEED structural analyses of $O_2$ chemisorption on Ni(111) indicate that oxygen always resides in a three-fold hollow site and is dissociatively adsorbed.[24] This should be the case on the (111) faces of other group VIII metals[25] and is consistent with the relatively low value of the rhodium-oxygen stretching frequency measured here. Comparable bands have been seen on both Ni(111) ($\nu_{Ni-O}$ = 580 $cm^{-1}$)[26] and Ru(001) ($\nu_{Ru-O}$ = 516-596 $cm^{-1}$).[27] $O_2$ TDS spectra from Rh(111) display second order desorption kinetics, in agreement with the dissociative adsorption of oxygen.[3,18] The ELS spectra indicate that this peak grows in at constant frequency with increasing gas exposure. Furthermore, both its position and width are independent of surface order (as determined by observation of the LEED pattern).

The conditions to observe the 1410 $cm^{-1}$ peak (Fig. 5, upper trace) are similar to those used by Castner and Somorjai to form the unreactive surface oxide,[19] however, the character of this mode is not well-known. This peak is 400 $cm^{-1}$ above typical M-O stretching frequencies in diatomic,[28] polyatomic[29-31] and bulk[31] metal oxides. This band is quite close to the gas phase stretching frequency of dioxygen (1555 $cm^{-1}$),[31] but is significantly higher than the characteristic O-O stretching vibrations in $O_2$-transition metal coordination complexes.[31] Furthermore, one would not expect such a species to be stable on the rhodium surface at these temperatures. Associatively adsorbed $O_2$ has been seen on Pt(111), but only at temperatures below 150 K.[32] The activation energy for dissociation of the O=O bond is only 7 kcal/mole on this surface. Backx has

Figure 5. The lower trace shows the high resolution ELS spectra of oxygen chemisorbed on Rh(111) at 300 K and the upper trace shows the same surface after heating the sample to 1100 K in $5 \times 10^{-7}$ Torr of $O_2$ for 10 min. The broad band centered near 800 $cm^{-1}$ may be caused by stray electron reflection from the outer half of the analyzer (see Chapter III and Reference 39).

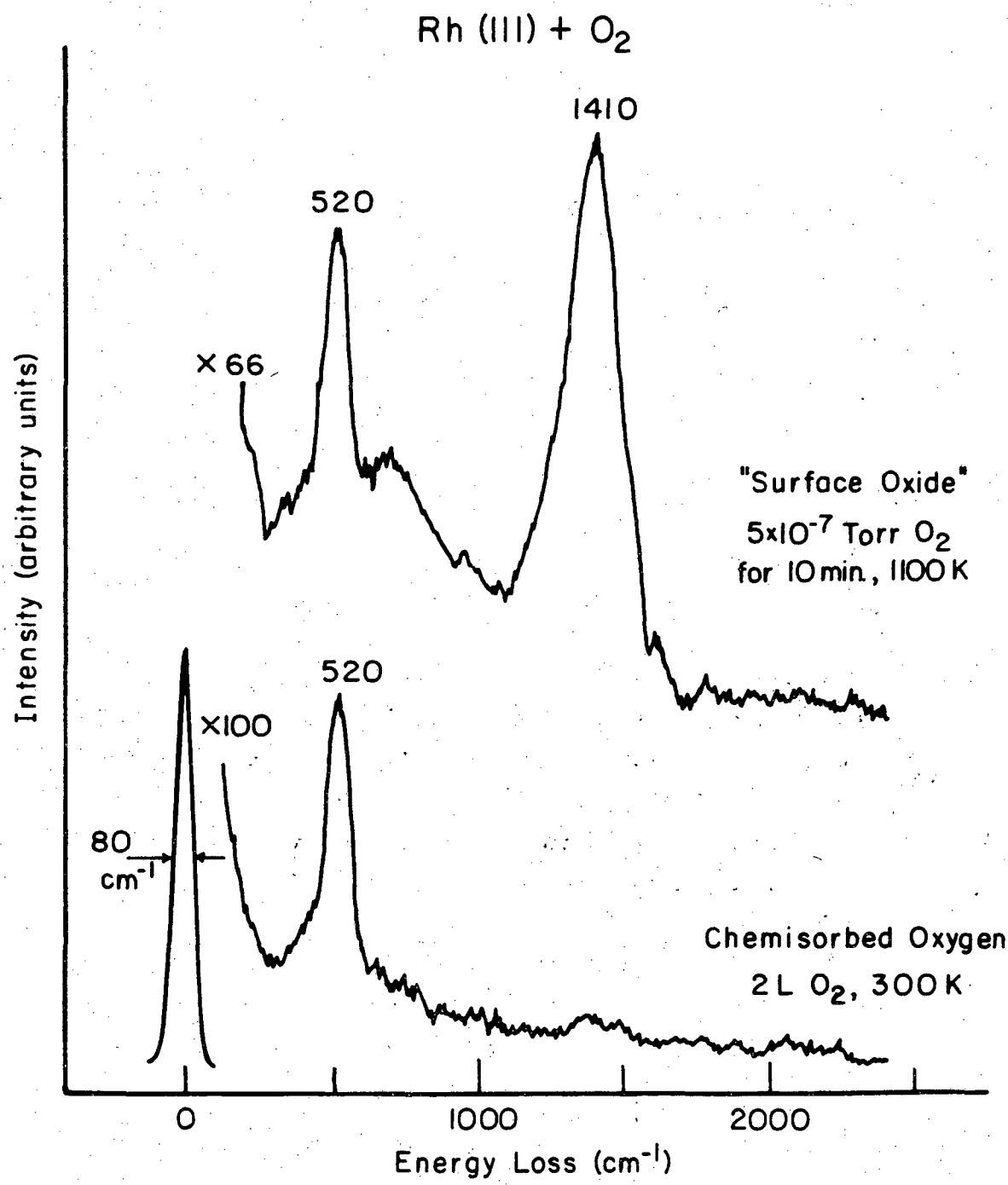
Rh (111) + O2
1410
520
X 66
"Surface Oxide"
5x10-7 Torr O2
for 10 min., 1100 K
520
X100
80
cm-1
Chemisorbed Oxygen
2 L O2, 300 K
Intensity (arbitrary units)
0
1000
2000
Energy Loss (cm-1)

XBL 806-5318

seen a similar broad, intense peak near 1500 $cm^{-1}$ on platinum after a comparable oxygen treatment.[33] Platinum is also known to form an unreactive surface oxide and this phase is important in catalysis as well.[34,35] Recent low energy helium ion scattering experiments from pretreated Pt(111) have shown this oxygen to be residing below the top layer of metal atoms.[36] This may be the case on Rh(111) as well. Metal cluster analogs for this type of bonding (polyoxo anions) have been known for many years now.[37] Octahedrally coordinated oxygen atoms have been particularly well studied, although this structure is generally associated with the early transition metals.[37] However, both infrared and Raman spectra show no bands above approximately 1000 $cm^{-1}$ for this type of species.[29,30] There is one report of a metal-oxygen stretching vibration at 1337 $cm^{-1}$ in several vanadyl porphine complexes,[38] but more recent publications have brought this assignment into question.[29] The character of this mode still remains in doubt. The small peak near 800 $cm^{-1}$ may be caused by stray electron scattering from the outer half of the analyzer sector (see Chapter III and Ref. 39).

A similar peak near 1430 $cm^{-1}$ has also been seen during several $CO_2$ chemisorption and/or pretreatment experiments although this feature could not be reproduced at will. In all cases this peak was quite broad and its intensity varied tremendously depending on the oxidation conditions. Once formed, however, this mode was quite stable and required high temperature annealing (>1100 K) in vacuum to remove. Further exploration of the nature of this unreactive surface oxide and particularly its effect on chemisorption and catalysis over the group VIII metals should prove to be very interesting.

## References


1. L. H. Dubois and G. A. Somorjai, Surface Sci. 88, L13 (1979).

2. D. G. Castner, B. A. Sexton, and G. A. Somorjai, Surface Sci. 71, 519 (1978).

3. D. G. Castner and G. A. Somorjai, Surface Sci. 83, 60 (1979).

4. B. A. Sexton and G. A. Somorjai, J. Catal. 46, 167 (1977).

5. A. C. Yang and C. W. Garland, J. Phys. Chem. 61, 1504 (1957).

6. A. C. Collins and B. M. W. Trapnell, Trans. Faraday Soc. 53, 1476 (1957).

7. C. T. Campbell and J. M. White, J. Catal. 54, 289 (1978).

8. M. Primet, J. C. S. Faraday I 74, 2570 (1978).

9. D. Brennan and D. O. Hayward, Philos, Trans. Roy. Soc. (London) Ser. A, 258, 375 (1965).

10. J. T. Grant and T. W. Haas, Surface Sci. 21, 76 (1970).

11. See M. Aresta and C. F. Nobile, Inorg. Chim. Acta 24, L49 (1977) and references therein.

12. R. Whyman, J. C. S. Chem. Comm., 1194 (1970).

13. W. P. Griffith and A. J. Wickam. J. Chem. Soc. A, 834 (1969).

14. L. A. Hanlan and G. A. Ozin, J. Am. Chem. Soc. 96, 6324 (1974).

15. See, for example, J. T. Yates, Jr., T. M. Duncan, S. D. Worley, and R. W. Vaughan, J. Chem. Phys. 70, 1219 (1979).

16. L. H. Dubois and G. A. Somorjai, Surface Sci. 91, 514 (1980).

17. C. R. Guerra and J. H. Schulman, Surface Sci. 7, 229 (1967).

18. P. A. Thiel, J. T. Yates, Jr., and W. H. Weinberg, Surface Sci. 82, 22 (1979).

19. D. G. Castner and G. A. Somorjai, Appl. Surface Sci., in press.

20. G. N. Lewis and M. Randall, Thermodynamics, revised by K. S. Pitzer and L. Brewer, 2nd Ed (Mc Graw Hill Book Company, New York, 1961) p. 682.

21. P. A. Thiel, E. D. Williams, J. T. Yates, Jr., and W. H. Weinberg, Surface Sci. 84, 54 (1979).

22. D. Brenan, D. O. Hayward, and B. M. W. Trapnell, Proc. Roy. Soc. London, Ser. A 256, 81 (1960).

23. L. H. Dubois, P. K. Hansma, and G. A. Somorjai, J. Catal., in press.

24. P. M. Marcus, J. E. Demuth, and D. W. Jepson, Surface Sci. 53, 501 (1975).

25. G. A. Somorjai and M. A. Van Hove, Structure and Bonding 38, 1 (1979).

26. H. Ibach and D. Bruchmann, Phys. Rev. Lett. 44, 36 (1980).

27. G. E. Thomas and W. H. Weinberg, J. Chem. Phys. 70, 954 (1979).

28. K. P. Huber and G. Herzberg, Molecular Spectra and Molecular Structure IV. Constants of Diatomic Molecules (Van Nostrand Publishing Company, New York, 1979).

29. C. G. Barraclough, J. Lewis and R. S. Nyholm, J. Chem. Soc., 3552 (1959).

30. R. S. Tobias, Can. J. Chem. 43, 1222 (1965).

31. K. Nakamoto, Infrared and Raman Spectra of Inorganic and Coordination Compounds, 3rd Ed. (John Wiley and Sons, Inc., New York, 1978).

32. J. L. Gland, Surface Sci. 93, 487 (1980).

33. C. Backx, private communication.

34. C. E. Smith, J. P. Biberian, and G. A. Somorjai, J. Catal. 57, 426 (1979).

35. S. M. Davis and G. A. Somorjai, Surface Sci. 91, 73 (1980).

36. H. Niehus and G. Comsa, Surface Sci. 93, L147 (1980).

37. D. L. Kepert, Comprehensive Inorganic Chemistry Vol. 4, J. C. Bailar, H. J. Emeleus, R. Nyholm, and A. F. Trotman-Dickinson eds. (Pergamon Press, Oxford, 1973) p. 607.

38. K. Ueno and A. E. Martell, J. Phys. Chem. 60, 934 (1956).

39. H. Froitzheim, H. Ibach, and S. Lehwald, Rev. Sci. Instrum. 46, 1325 (1975).

# CHAPTER VI. Evidence for an Oxygen Intermediate in the Catalytic Reduction of NO by CO on Rhodium Surfaces[1]

## A. Introduction

The desire for clean air has stimulated both legislation and research on the reduction of nitrogen oxides ($NO_x$) in fossil fuel combustion exhaust. Recent interest has focused on the catalytic reduction of NO to $N_2$ by carbon monoxide in automobile exhaust. A promising catalyst for this reaction is rhodium.[2,3] The mechanism of nitric oxide reduction over Rh has been illuminated in several recent publications. Campbell and White used thermal desorption mass spectrometry (TDS), surface titration and steady-state reaction kinetics to study the chemisorption and reactivity of nitric oxide on a polycrystalline rhodium wire at temperatures between 330 and 950 K and at pressures below $2 \times 10^{-8}$ Torr.[4] They concluded that the mechanism must involve NO dissociation and a subsequent reaction of CO with the atomic oxygen intermediates remaining on the surface. No direct evidence for this surface oxygen species was presented, however.

Unland,[5] Arai and Tominaga[6] and more recently Solymosi and Sárkány[7] applied infrared spectroscopy to a study of NO and CO chemisorption on alumina supported rhodium particles. In addition to observing stretching vibrations for numerous molecular NO and CO species between 300 and 670 K and at pressures up to 150 Torr, they found an absorption band which they associated with a surface isocyanate (NCO) complex. There now is evidence for a migration of this isocyanate species from the rhodium particles to the support.[7,8] Finally, Iizuka and Lunsford studied the reduction of nitric oxide by carbon monoxide to form $N_2O$ and $CO_2$ over rhodium-Y zeolites.[9] They proposed a $[Rh^{I}(CO)_2NO]^+$ complex as a reaction intermediate based on infrared spectroscopic evidence. The spectral range of

all of these studies did not extend to the region below 1000 $cm^{-1}$ where vibrations from surface N and O atoms from dissociated nitric oxide would be expected. Thus these studies neither supported nor contradicted the previous evidence for the presence of a surface oxygen intermediate.

An adsorbed oxygen species from NO dissociation has been observed on the surface of other transition metals. Thomas and Weinberg and Lehwald et al. reported such a species on both the Ru(001)[10] and Ni(111)[11] single crystal surfaces using high resolution electron energy loss spectroscopy (ELS). Zhdan et al. observed a similar species on the Ir(111) surface with both X-ray and ultraviolet photoelectron spectroscopy.[12,13] These authors argue convincingly for a surface oxygen intermediate in the reduction of NO by CO over iridium catalysts.

In this chapter we report on studies of the molecular chemisorption and subsequent dissociation of nitric oxide on a Rh(331) single crystal surface. Here we combine high resolution ELS and Auger electron spectroscopy (AES) to determine the structure and chemical composition of the adsorbed species with TDS and kinetic studies to monitor the reaction products after desorption into the gas phase. These new high resolution ELS and AES measurements on a single crystal rhodium surface complement the previous studies[2-7,9] to present a complete picture of a mechanism involving a surface oxygen intermediate under our reaction conditions.

## B. The Molecular Chemisorption of NO on Rh(331)

The lowest trace of Figure 1 shows the high resolution ELS spectrum from the adsorption of 1 L of NO on the initially clean Rh(331) single crystal surface at 300 K. Using the stepped surface notation of Lang, et al.[14] this crystal plane can be viewed as a Rh(S)-[3(111) x (111)] surface. The three atom wide (111) terraces are uniformly spaced by

Figure 1. Nitric oxide molecularly adsorbs on the Rh(331) single crystal surface at 300 K as shown by the presence of N=O stretching vibrations (1704, 1815 $cm^{-1}$) in the bottom high resolution ELS spectrum. This species dissociates by 450 K as indicated by the absence of the N=O stretching vibrations in the middle spectrum. The 520 $cm^{-1}$ peak in this spectrum is similar to that obtained from the adsorption of $O_2$ gas at 300 K (top spectrum).

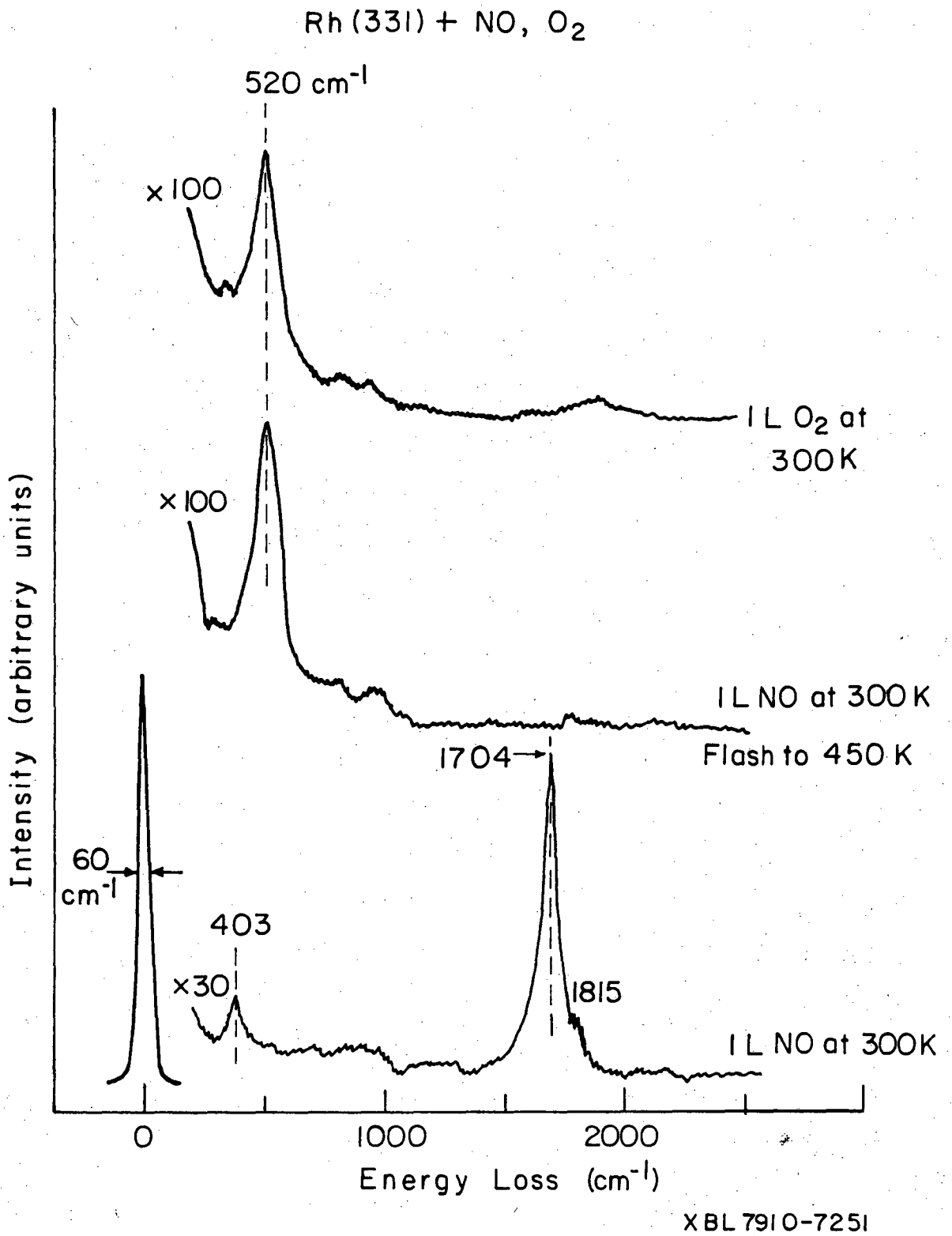
Rh (331) + NO, O2
520 cm-1
x100
1 L O2 at 300K
x100
1 L NO at 300K
Flash to 450 K
1704
60 cm-1
403
x30
1815
1 L NO at 300K
Intensity (arbitrary units)
0
1000
2000
Energy Loss (cm-1)
XBL 7910-7251

monatomic height steps also of (111) orientation. A real space drawing of this surface is presented in Reference 15. The strong band above 1700 $cm^{-1}$ is typical of a N=O stretching vibration for molecularly adsorbed nitric oxide.[16] By comparison with the infrared spectra of model nitrosyl compounds of known molecular structure, we can assign the 1704 $cm^{-1}$ loss to a terminally bonded NO species.[20-22] The Rh-N=O bond is most likely bent,[18,20-22] but the exact angle cannot be determined here. Using a similar analysis, the small shoulder at 1815 $cm^{-1}$ can be assigned to a linear nitrosyl species. The weak band at 403 $cm^{-1}$ is characteristic of a metal-nitrogen bending mode for an associatively adsorbed species.[17,18] This is in agreement with the observation of a bent nitrosyl. The normal dipole selection rule (see Chapter II) would not allow the observation of such a mode if the adsorbate was bonded perpendicular to the surface. The metal-nitrogen stretching vibration from such a species is expected to be 100-200 $cm^{-1}$ lower in frequency.[18,23] The results of detailed infrared studies on numerous nitrosyl compounds have been reviewed recently by Pirug, et al.[18] They conclude that the experimental data on both the halogen nitrosyls and transition metal nitrosyls provide evidence for well separated M-N=O bending and stretching frequencies with the latter always lower than the former.

Based on the coordination chemistry of metal nitrosyls, one can postulate a large number of nitric oxide bonding geometries on rhodium surfaces. These include linear, bent and bridge bonded NO, as well as formation of $NO^+$ and $NO^-$ species.[20,23,24] Infrared studies have identified a variety of these species on alumina supported rhodium catalysts.[5-7] Characteristic N=O stretching frequencies have been tabulated by Arai and Tominaga.[6] We have now observed the formation of at least five different

NO species on the Rh(111) surface using high resolution ELS.[19] Each species is stable on the surface over a small temperature and coverage range. Because of the "relative simplicity" of the NO vibrational spectrum on the (331) plane of rhodium we have decided to pursue our catalytic studies on this surface. The reasons for the differences in the nature of NO bonding to the various crystal faces of rhodium is a promising area for future research.

The conclusions of this chapter do not, however, hinge on a detailed assignment of the observed energy loss peaks. The point we wish to make here is that nitric oxide molecularly chemisorbs on the Rh(331) surface at 300 K.

Both the relative intensities and the positions of the energy loss peaks in the lower trace of Figure 1 were found to be essentially independent of gas exposure (from 0.1 to 10 L). The integrated intensity of the ELS peaks does increase with increasing gas dosage, however. Absolute nitric oxide coverages were not determined.

## C. The Dissociation of NO on Rh(331)

As the rhodium substrate is heated above 450 K the molecular NO vibrational bands in the lower trace of Figure 1 disappear and a single peak near 520 $cm^{-1}$ appears (Fig. 1, middle trace). The disappearance of the high frequency mode and the simultaneous appearance of the 520 $cm^{-1}$ band clearly indicates the dissociation of nitric oxide. Furthermore, at least one of the dissociation products must remain on the surface. The upper trace in Figure 1 shows the vibrational spectrum from the adsorption of 1 L of $O_2$ on the Rh(331) surface at room temperature. A single band at 520 $cm^{-1}$ due to dissociatively chemisorbed oxygen[15] is

visible. This suggests that the 520 $cm^{-1}$ band produced from NO dissociation is due to surface oxygen. The absence of a second peak is not necessarily evidence for nitrogen desorption since it is thought that the M-N stretch from dissociated NO should be weak.[10,11] This peak could be hidden beneath the relatively intense rhodium-oxygen stretch.[11]

We could not detect either the molecular or the dissociative chemisorption of dinitrogen on the Rh(331) single crystal surface at 300 K at $N_2$ exposures up to $10^4$ L. Mimeault and Hansen found that dinitrogen could adsorb on a polycrystalline rhodium wire upon activation with a hot tungsten filament.[25] This has also been reported recently by Campbell and White.[4] Due to the long distance (~15 cm) and the relatively low temperature of our thoriated-iridium mass spectrometer and ion gauge filaments, we were unable to detect any activated nitrogen adsorption, even at $N_2$ exposures greater than $10^4$ L. Thus we could not measure the atomic nitrogen vibrational spectrum. However, the absence of surface nitrogen in the middle vibrational spectrum of Figure 1 can be confirmed by thermal desorption mass spectrometry and by Auger electron spectroscopy.

Figure 2 displays TDS spectra for $N_2$ and $O_2$ desorption from the Rh(331) single crystal after exposing the surface to 1 L of NO. Note that if NO is adsorbed at room temperature the nitrogen desorbs as $N_2$ (m/e = 28) below 500 K (Fig. 2b) while the oxygen desorbs as $O_2$ (m/e = 32) (Fig. 2a) only at much higher temperatures. Figure 2a also shows that $O_2$ desorption is similar whether the rhodium surface is exposed to gaseous nitric oxide or to oxygen. The NO (m/e = 30) TDS spectrum showed only one peak near 460 K. $N_2O$ (m/e = 44) desorption from this surface has also been reported.[15] Similar thermal desorption results have been obtained previously both by Campbell and White on polycrystalline rhodium

Figure 2. a) $O_2$ desorption (m/e = 32) from the adsorption of 1 L of either $O_2$ (lower trace) or NO (upper trace) on the Rh(331) single crystal surface at 300 K. (b) $N_2$ desorption (m/e = 28) from the adsorption of 1 L of NO at either 300 K (lower trace) or 700 K (upper trace). The small peak at 325 K is presumably due to nitrogen desorption from the crystal support wires. The heating rate was 40 K/sec.

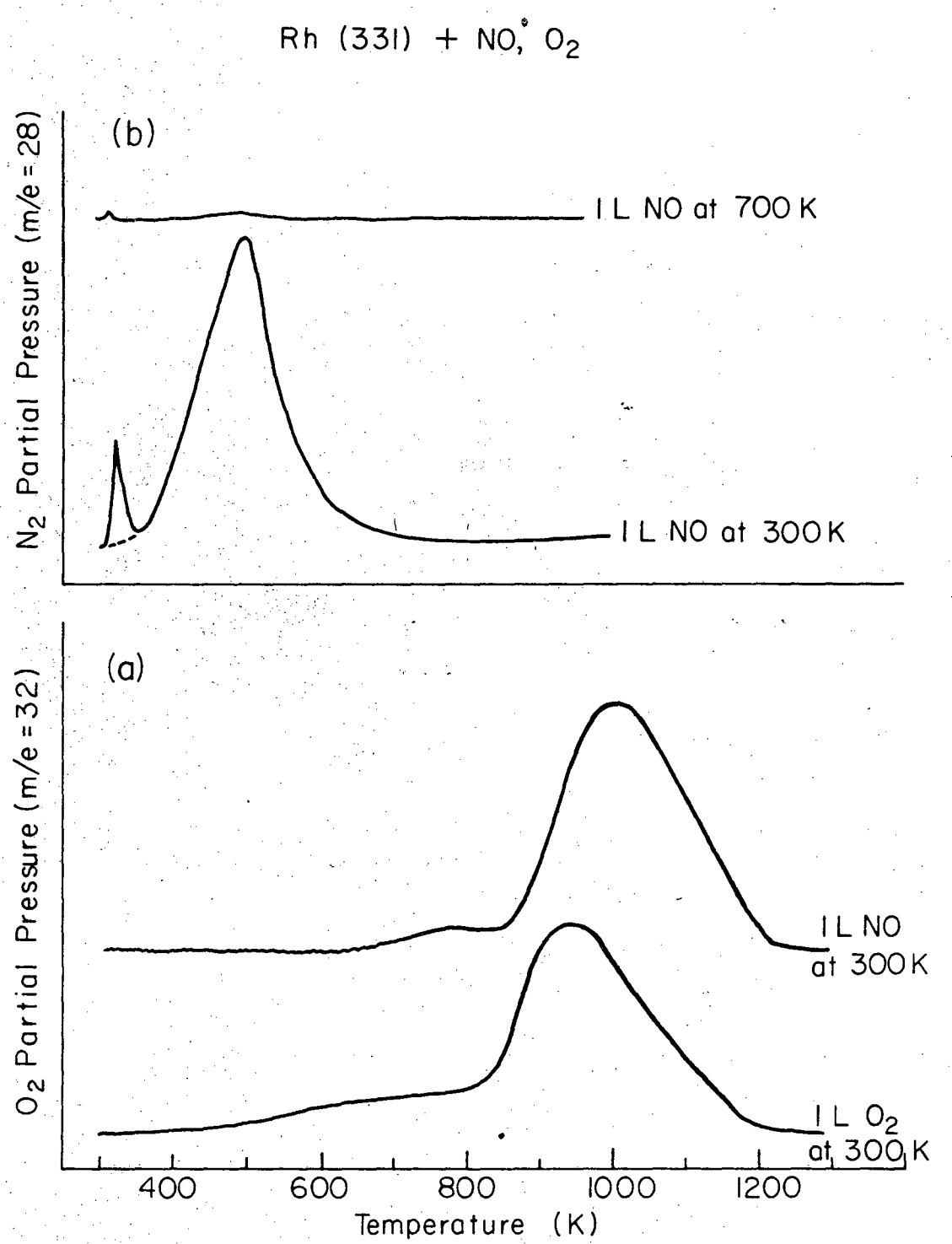


XBL 7910-7252

wire[4] and by Castner and Somorjai on stepped rhodium single crystal surfaces[15] during NO chemisorption studies. Finally, note that if NO is adsorbed on the rhodium surface at 700 K (a typical reaction temperature for an automobile catalytic converter) and the crystal cooled to 300 K; subsequent flashing yields negligible nitrogen desorption from the surface (Fig. 2b). This is consistent with the relatively low temperature found for $N_2$ desorption from adsorbed NO.

The absence of surface nitrogen is also confirmed by Auger electron spectroscopy (see Fig. 3). The chemisorption of 1 L of NO on the Rh(331) single crystal surface at 300 K (lower trace) results in both nitrogen and oxygen present on the surface.[26] This is consistent with the molecular chemisorption of nitric oxide indicated by the vibrational spectra in Figure 1. Chemisorption of 1 L of NO at 700 K results in only oxygen present on the surface (upper trace). Both the TDS and AES results lead us to conclude that the peak at 520 $cm^{-1}$ in the middle trace of Figure 1 is due solely to adsorbed oxygen.

Thus at a typical operating temperature for a catalytic converter (700 K) the adsorption of NO results in the liberation of $N_2$ gas and in the formation of a stable surface oxygen species. Vibrational spectra recorded after flashing the crystal to successively higher temperatures indicate that the metal-oxygen stretch is visible until above 850 K.

### D. The Chemisorption of CO on Rh(331)

Much effort has gone into understanding the vibrational spectrum of carbon monoxide chemisorbed on rhodium. A review of previous work is presented in Chapter IV and will not be repeated here. The lowest trace of Figure 4 shows the high resolution ELS spectrum from the adsorption of

Figure 3. The Auger spectrum of NO chemisorbed on the initially clean Rh(331) single crystal surface shows both nitrogen and oxygen peaks when adsorbed at 300 K, but only oxygen transitions when adsorbed at 700 K. The fine structure between the primary peaks is irreproducible and presumably due to noise.

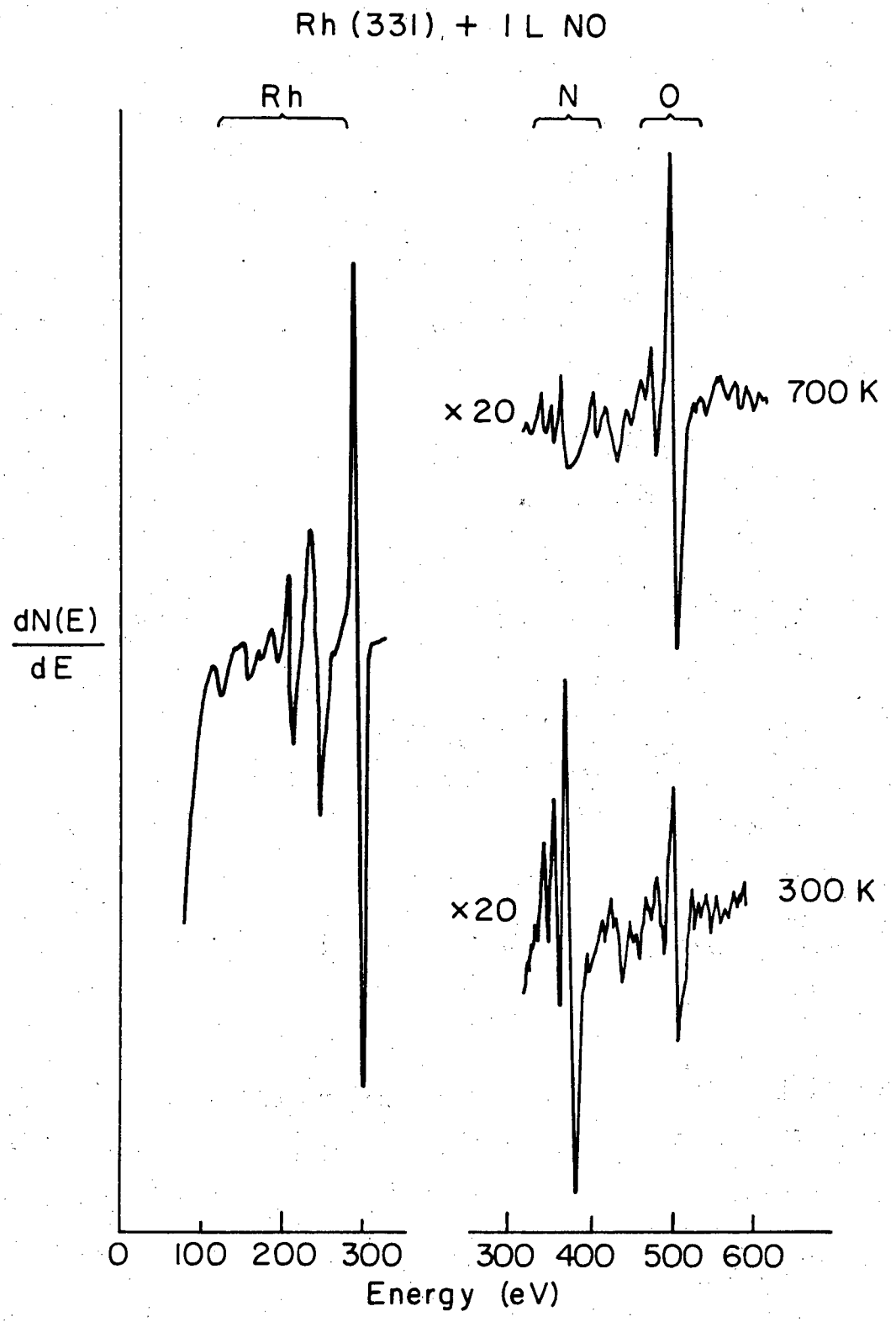


XBL 7910-7253

0.1 L of CO on the initially clean Rh(331) single crystal surface at 300 K. Only two losses at 430 and 2060 $cm^{-1}$ are visible. The broad peak (dashed line) centered near 800 $cm^{-1}$ is most likely due to electron reflection from the outer half of the analyzer. The causes of this peak are discussed in detail by Froitzheim, et al.[27] By comparison with the infrared spectra of model organometallic compounds of known molecular structure we can assign the 2060 $cm^{-1}$ loss to the carbon-oxygen stretching vibration of a linearly bonded CO species.[28,29] The 430 $cm^{-1}$ loss is the rhodium-carbon stretching and/or bending vibration for this species.[30,31] ELS spectra of CO chemisorbed on the (111) plane of rhodium also show the presence of linearly bonded carbonyl species.[28] Molecular CO desorbs from both of these surfaces with first order kinetics and with an activation energy of 31 kcal/mole.[15,28,32] This activation energy decreases with increasing coverage on both surfaces as well.[15,28,32] Therefore, we conclude that at low CO exposures carbon monoxide is molecularly adsorbed on the Rh(331) single crystal surface and is linearly bonded to a single rhodium atom on the (111) terraces.

The middle trace of Figure 4 shows that by a 0.2 L CO exposure a third energy loss peak at 1930 $cm^{-1}$ is observed. A detailed assignment of this mode is difficult at present. Linearly bonded rhodium carbonyls (Rh-CO) have C≡O stretching frequencies near 2060 $cm^{-1}$ while bridge bonded species ($Rh_2$>CO) have C=O stretching frequencies at 1870 $cm^{-1}$.[28,29] However, both Pearce[29] and Yang and Garland[33] observed a similar mode (1925 $cm^{-1}$) in the infrared spectra of CO chemisorbed on either silica or alumina supported rhodium particles. These authors found that the intensity of the mode decreased as the sample reduction temperature increased and the particle sizes became larger.[29,33] Both groups assigned this peak to a bridge bonded species. Pearce suggested that sintering removes

Figure 4. Carbon monoxide molecularly adsorbs on the Rh(331) single crystal surface at 300 K. At a 0.1 L exposure (lower trace) CO is linearly bonded to single rhodium atoms on the (111) terraces ($\nu_{C\equiv O}$ = 2060 $cm^{-1}$). The 430 $cm^{-1}$ loss is the Rh-CO stretching and/or bending vibration for this species. The broad band centered near 800 $cm^{-1}$ (dashed line) may be caused by electron reflection from the outer half of the analyzer (see text).[27] Above a 0.2 L CO exposure (middle trace) carbon monoxide molecules bonded to rhodium step atoms are formed ($\nu_{C\equiv O}$ = 1930 $cm^{-1}$). The room temperature spectra do not change up to a 20 L CO exposure (upper trace).

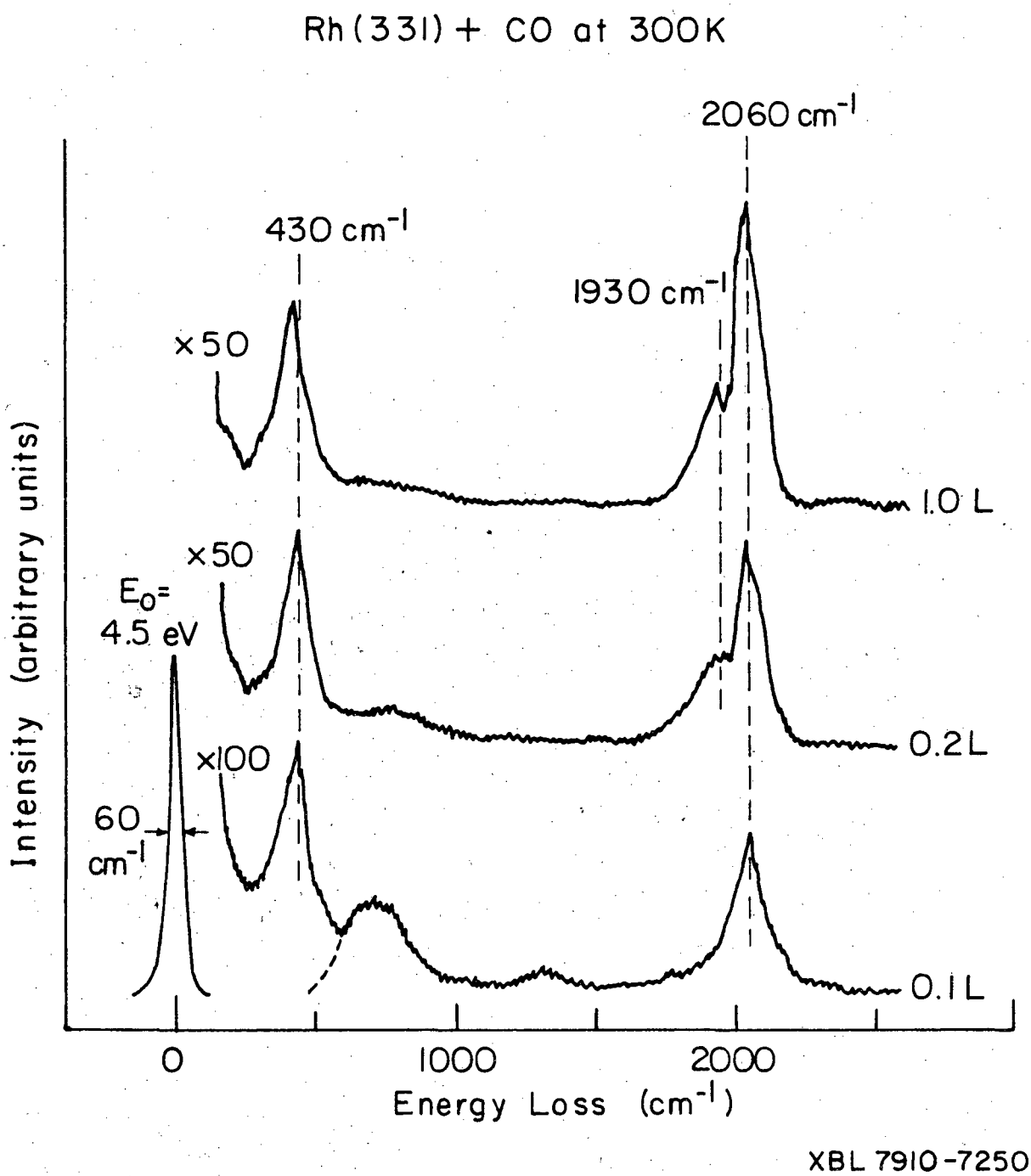
Rh(331) + CO at 300K
2060 cm⁻¹
430 cm⁻¹
1930 cm⁻¹
×50
×50
×100
E₀=
4.5 eV
60
cm⁻¹
1.0 L
0.2L
0.1L
Intensity (arbitrary units)
0
1000
2000
Energy Loss (cm⁻¹)
XBL 7910-7250

the high-index planes on which this bridged species adsorbs.[29] In agreement with this, we have only observed the 1930 $cm^{-1}$ mode on the stepped Rh(331) surface and not on the flat Rh(111) surface.[28] This species may be located along the step edges or at least be associated with the step atoms. The results of recent low-energy electron diffraction (LEED), thermal desorption mass spectrometry and Auger electron spectroscopy studies also lead us to this conclusion.[15]

Castner and Somorjai showed that the chemisorption of carbon monoxide on the Rh(331) surface formed a series of well-ordered LEED patterns at 300 K.[15] A hexagonal overlayer of carbon monoxide molecules is seen at all coverages. A proposed mechanism for the transformation between ordered structures is by compression of the hexagonal layer parallel to the step edge.[15] This would require that the ratio of occupied terrace sites to occupied step sites remain approximately constant over the entire coverage range. This is precisely what we see in the vibrational spectra: the intensity ratio of the 2060 $cm^{-1}$ loss to the 1930 $cm^{-1}$ loss does not significantly change with increasing CO exposure (up to at least 20 L of CO (Fig. 4, top)). Furthermore, this intensity ratio (~2.5:1) is in reasonable agreement with the ratio of the number of exposed rhodium terrace atoms to step atoms (~2.3:1).

Recent TDS and AES studies indicate that carbon monoxide can dissociate on both stepped single crystal ((331), (755))[15,34] and polycrystalline[35] rhodium samples, but not on the Rh(111) surface[28,32,36] at elevated temperatures under ultrahigh vacuum conditions. Recall that we only see the 1930 $cm^{-1}$ mode on the stepped Rh(331) surface and not on the flat Rh(111) surface. This peak completely disappears upon flashing a CO saturated surface to 450 K in vacuum. This is well below the temperature for carbon monoxide desorption from the low index terraces of the

crystal.[15,28,32] (The TDS peak maximum occurs at ~550 K, depending on initial surface coverage and heating rate.) Erley, et al. have shown that low frequency C≡O stretching vibrations on nickel surfaces can be associated with the chemisorption of carbon monoxide at step sites.[37] These species also can be dissociated by heating the sample to 430 K in cacuum. All of these studies are consistent with the assignment of the 1930 $cm^{-1}$ mode to the C≡O stretching vibration of a carbon monoxide molecule chemisorbed along or near the step edge.

Again, the conclusions of this chapter do not hinge on a detailed assignment of the observed energy loss peaks since high resolution ELS and TDS studies indicate that neither the linear nor the 'step' CO species is present on the surface at 700 K under ultrahigh vacuum conditions. The important point here is that carbon monoxide molecularly chemisorbs on the Rh(331) single crystal surface at 300 K. Step sites may play an important role in the catalytic chemistry of rhodium surfaces at elevated temperatures however.[34]

## E. The Interaction of CO with Molecular NO

The coadsorption of NO and CO on the Rh(331) surface at 300 K yield vibrational spectra that are essentially the sum of Figures 1 and 4. The frequencies of the N=O and C≡O stretching vibrations are shifted downward slightly when compared to the values measured in Figures 1 and 4. Small peak shifts have also been seen in the ELS spectra of NO and CO coadsorbed on the (001) face of ruthenium.[38] No energy loss peaks corresponding to new surface species are observed. Specifically, the characteristic stretching vibrations of surface NCO and Rh(CO)(NO) are not seen.[5-7] Such species are reported to form on supported rhodium

catalysts, but only at elevated temperatures and pressures.[5-7] High resolution ELS studies indicate that the sequential adsorption of NO and CO (either NO followed by CO or the reverse) at 300 K did not yield any new surface species either. It is interesting to note that the NO saturated Rh(331) surface inhibited all CO adsorption while the bent nitrosyl species could still find a few open sites on the CO saturated surface. This bent NO species could also form on an oxygen pretreated rhodium surface. Reference 4 contains an extensive discussion of TDS and low pressure kinetic studies on the NO + CO system.

## F. The Reaction of CO with Dissociated NO

Carbon monoxide readily reacts with the oxygen remaining on the surface after NO dissociation. Figure 5 shows what happens to the Rh-O stretching vibration as CO is added to either dissociatively chemisorbed $O_2$ (a) or NO (b) at 700 K. Note that in both cases the intensity of the 520 $cm^{-1}$ loss is measurably decreased by a 1 L CO exposure and has disappeared into the noise by a 5 L CO exposure. Surface oxygen produced during $O_2$ chemisorption is more easily removed than surface oxygen formed as a result of the dissociation of NO. This is a reproducible effect that will be discussed in more detail below.

We carried out a kinetic study to determine which gases are produced when CO reacts with surface oxygen. In Figure 6 the rhodium substrate was first heated to 700 K and then dosed with either 1 L of $O_2$ (lower trace) or NO (upper trace) to produce a surface oxygen species. The reaction products were monitored with a mass spectrometer located approximately 15 cm from the crystal as $4 \times 10^{-8}$ Torr of CO was admitted to the vacuum chamber at t=0. As one might expect, carbon dioxide (m/e = 44) was the primary product. $CO_2$ was produced until the CO exposure was of order

Figure 5. The 520 $cm^{-1}$ peak in the high resolution ELS spectra of either $O_2$ (a) or NO (b) adsorbed on the Rh(331) single crystal surface at 700 K decreases rapidly upon exposure to gas phase carbon monoxide.

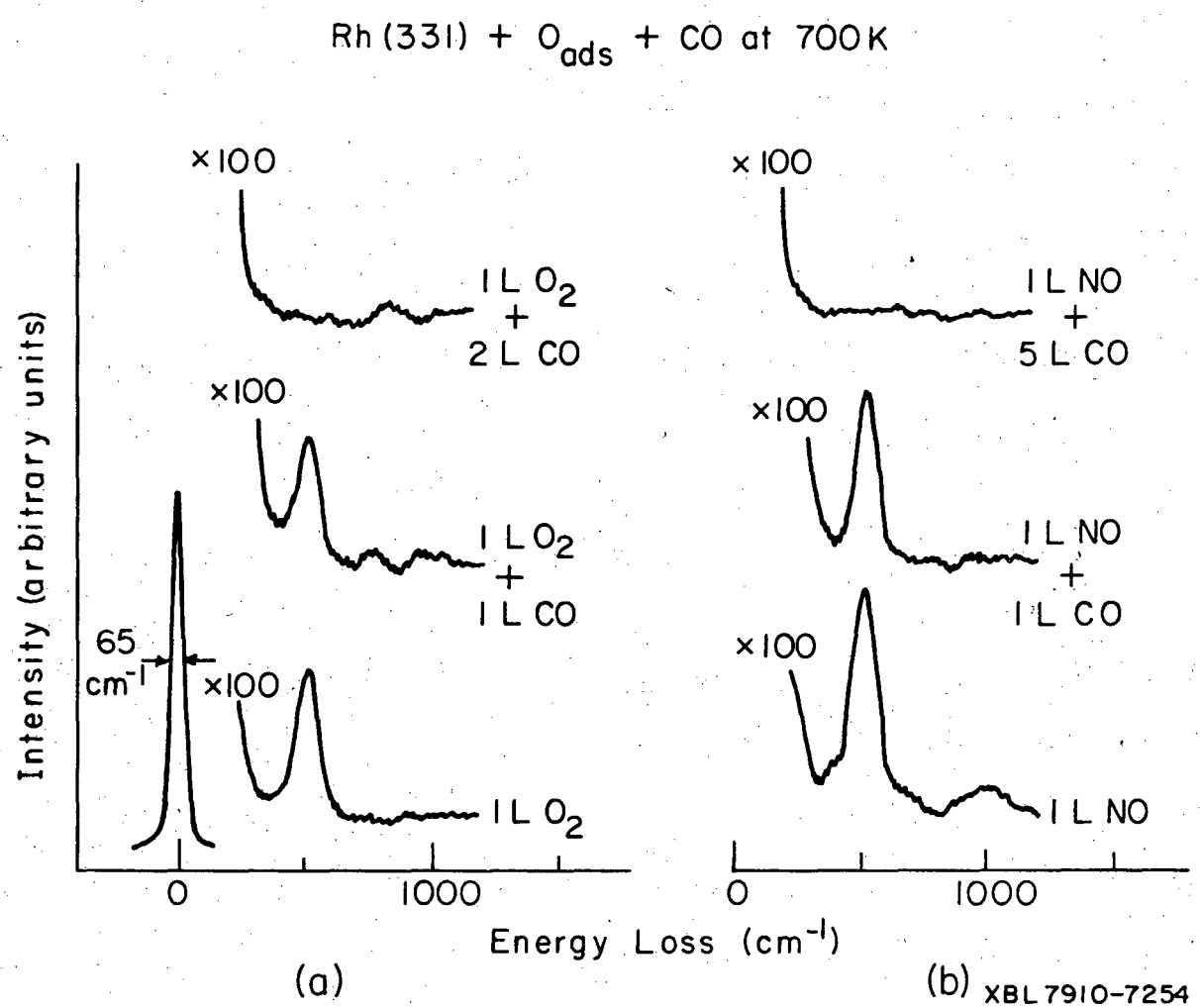
Rh (331) + $O_{ads}$ + CO at 700K
×100
1 L $O_2$
+
2 L CO
×100
1 L $O_2$
+
1 L CO
65
$cm^{-1}$
×100
1 L $O_2$
×100
1 L NO
+
5 L CO
×100
1 L NO
+
1 L CO
×100
1 L NO
Intensity (arbitrary units)
0
1000
0
1000
Energy Loss ($cm^{-1}$)
(a)
(b)
XBL 7910-7254

5 L (2 min. at 4 x $10^{-8}$ Torr). This observation correlates with the high resolution electron energy loss results of Figure 5 which showed that the surface oxygen disappeared by a 5 L CO exposure.

There is evidence that CO reacts with adsorbed oxygen directly from the gas phase (an Eley-Rideal mechanism) as well as after being adsorbed on the surface (a Langmuir-Hinshelwood mechanism) . Campbell, et al. studied the reaction between adsorbed oxygen and carbon monoxide over polycrystalline rhodium wires.[39,40] They concluded that the formation of carbon dioxide proceeded by both Langmuir-Hinshelwood and Eley-Rideal kinetics, depending on substrate temperature and gas pressure. They also found both mechanisms to be operative in their recent investigation of the catalytic reduction of NO by CO over polycrystalline rhodium wires.[4]

The dashed lines in Figure 6 represent the background reactivity of both the rhodium single crystal surface and the mass spectrometer filaments without predosing the sample with either $O_2$ or NO. The initial spike in all of these traces is caused by reactions taking place on either the edges of the rhodium crystal or on the sample support wires. Due to our resistive heating methods both of these areas are warmer than the front surface of the crystal.

## G. The Reaction Mechanism

From the above we conclude that under our experimental conditions the reaction of NO and CO to form $N_2$ and $CO_2$ proceeds by the following two consecutive steps:

$$(1) \quad 2NO_{(g)} \rightarrow N_{2(g)} + 2O_{(ads)}$$

$$(2) \quad 2O_{(ads)} + 2CO \rightarrow 2CO_{2(g)}.$$

Figure 6. Gaseous $CO_2$ production on the Rh(331) surface at 700 K after predosing the crystal with 1 L of either $O_2$ (lower trace) or NO (upper trace). $4 \times 10^{-8}$ Torr of CO is admitted to the vacuum chamber at $t = 0$ and $CO_2$ production is monitored by mass spectroscopy (m/e = 44). The dotted curves show the background $CO_2$ liberation if the surface was not pre-exposed to either NO or $O_2$ before CO admission.

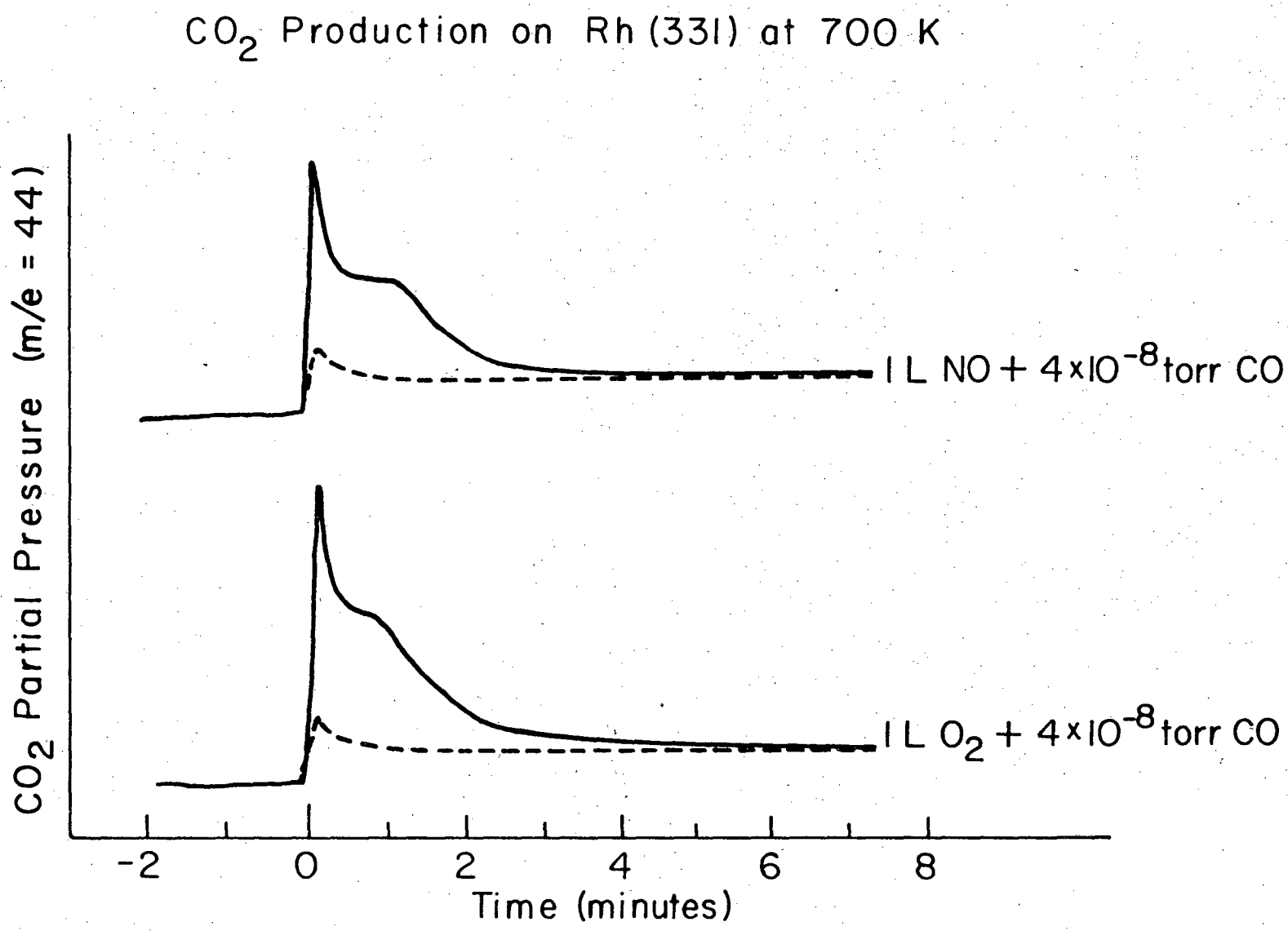


XBL 7910-7255

In the present study we have sequentially reacted nitric oxide and carbon monoxide over the Rh(331) surface to form gaseous dinitrogen and carbon dioxide. This reaction can be run continuously by heating our rhodium crystal to 700 K in $5 \times 10^{-7}$ Torr of a 1:1 NO:CO mixture. Unfortunately, due to the rapid reaction of these gases on the mass spectrometer filaments, we could not perform meaningful kinetic studies with the present apparatus.

An interesting feature of the data is that surface oxygen from NO desorbs at a slightly higher temperature (Fig. 2a, Refs. 4 and 15) than the surface oxygen from dissociated NO. The 60 K shift in the $O_2$ peak temperature cannot be accounted for by different surface oxygen concentrations since the integrated areas of the two desorption peaks in Figure 2a agree to within 5%. Surface oxygen from NO also reacts somewhat less readily with CO (Figs. 5 and 6) than the surface oxygen from dissociated $O_2$. Though we do not understand these effects, they are consistent with recent kinetic studies on supported rhodium catalysts under simulated reaction conditions.[2] Specifically, the rate of conversion of NO to $N_2$ and $CO_2$ by the reaction with CO is less than the rate of conversion of $O_2$ to $CO_2$ by CO under identical experimental conditions.[2] In contrast, on iridium, the rate of reaction of NO with CO is higher than that of $O_2$.[2] Further research into the mechanism of this reaction selectivity might be both scientifically interesting and technologically important.

## H. Summary

The following evidence for a surface oxygen intermediate in the reaction $2NO_{(g)} + 2CO_{(g)} \rightarrow N_{2(g)} + CO_{2(g)}$ was presented:

a) NO dissociates on the Rh(331) single crystal surface below 450 K, well below typical catalytic converter reaction temperatures of 600-800 K (Fig. 1).

b) The nitrogen from dissociated NO desorbs as $N_2$ below 500 K (Fig. 2).

c) The oxygen from dissociated NO is stable on the surface at typical reaction temperatures in vacuum (Figs. 2, 3 and 5).

d) The oxygen from dissociated NO is readily removed by CO under our experimental conditions (Fig. 5).

e) The reaction of CO with the surface oxygen produces gaseous $CO_2$ (Fig. 6).

The reaction mechanism may now be expressed as $2NO_{(g)} \rightarrow N_{2(g)} + 2O_{(ads)}$ and $2O_{(ads)} + 2CO \rightarrow 2CO_{2(g)}$. Key to this mechanism is the identification of the 520 $cm^{-1}$ peak as surface oxygen in the high resolution electron energy loss spectrum resulting from the dissociation of adsorbed NO (Fig. 1, middle trace; Figs.5 and 6). This identification is supported by:

a) The presence of a similar 520 $cm^{-1}$ peak from the adsorption of $O_2$ (Fig. 1).

b) Thermal desorption traces indicating that nitrogen from dissociated NO desorbs at a temperature below temperatures at which this peak is stable (Fig. 2).

c) AES results showing only oxygen and the clean rhodium surface features when the 520 $cm^{-1}$ peak is present (Fig. 3) and

d) Kinetic studies indicating that the 520 $cm^{-1}$ peak from dissociated NO was removed with similar (but not identical) kinetics to that from adsorbed $O_2$ (Figs. 5 and 6).

Although there can be little doubt that this reaction mechanism operates in high vacuum, it is not clear that it is the predominant mechanism on rhodium catalysts under automobile exhaust operating conditions. Furthermore, we cannot rule out a number of the possible mechanisms proposed by other authors. However, recent studies on $Pt/SiO_2$ catalysts under high pressure reducing conditions found kinetics and produce selectivities in good agreement with a mechanism based upon the dissociation of NO as the rate limiting step.[8]

## References


1. L. H. Dubois, P. K. Hansma, and G. A. Somorjai, J. Catal., in press.

2. K. C. Taylor and J. C. Schlatter, J. Catal. 63, 53 (1980).

3. L. L. Hegedus, J. C. Summers, J. C. Schlatter, and K. Baron, J. Catal. 56, 321 (1979).

4. C. T. Campbell and J. M. White, Appl. Surface Sci. 1, 347 (1978).

5. M. L. Unland, J. Catal. 31, 459 (1973); J. Phys. Chem. 79, 610 (1975).

6. H. Arai and H. Tominaga, J. Catal. 43, 131 (1976).

7. F. Solymosi and J. Sárkány, Appl. Surface Sci. 3, 68 (1979).

8. D. Lorimer and A. T. Bell, J. Catal. 59, 233 (1979).

9. T. Iizuka and J. H. Lunsford, J. Molec. Catal., in press.

10. G. E. Thomas and W. H. Weinberg, Phys. Rev. Lett. 41, 118 (1978).

11. S. Lehwald, J. T. Yates, Jr., and H. Ibach, Proc. 8$^{th}$ Intern. Vacuum Congress (Cannes, 1980), in press.

12. P. A. Zhdan, G. K. Boreskov, W. F. Egelhoff, Jr., and W. H. Weinberg, J. Catal. 45, 281 (1976).

13. P. A. Zhdan, G. K. Boreskov, A. I. Boronin, A. P. Schepelin, W. F. Egelhoff, Jr., and W. H. Weinberg, Appl. Surface Sci. 1, 25 (1977).

14. B. Lang, R. W. Joyner, and G. A. Somorjai, Surface Sci. 30, 454 (1972).

15. D. G. Castner and G. A. Somorjai, Surface Sci. 83, 60 (1979).

16. Vibrational spectra of associatively adsorbed NO have been recorded on the Pt(111),[17] Pt(100),[18] Ni(111),[11,19] Ru(001),[10] single crystal surfaces.

17. H. Ibach and S. Lehwald, Surface Sci. 76, 1 (1976).

18. G. Pirug, H. P. Bonzel, H. Hopster, and H. Ibach, J. Chem. Phys. 71, 593 (1979).

19. L. H. Dubois and P. K. Hansma, unpublished observations.

20. F. A. Cotton and G. Wilkinson, Advanced Inorganic Chemistry, 3$^{rd}$ Ed. (John Wiley and Sons, Inc., New York, 1972).

21. K. Nakamoto, Infrared and Raman Spectra of Inorganic and Coordination Compounds, 3rd Ed. (John Wiley and Sons, Inc., New York, 1978).

22. C.-C. Su and J. W. Faller, J. Organomet. Chem. 84, 53 (1975).

23. E. Miki, K. Mizumachi, T. Ishimori, and H. Okuno, Bull. Chem. Soc. Japan 47, 656 (1974).

24. R. Eisenberg and C. D. Meyer, Acc. Chem. Res. 8, 26 (1975).

25. V. J. Mimeault and R. S. Hansen, J. Phys. Chem. 70, 3001 (1966).

26. Handbook of Auger Electron Spectroscopy, 2nd Ed (Physical Electronics Industries, Eden Prairie, MN, 1978).

27. H. Froitzheim, H. Ibach, and S. Lehwald, Rev. Sci. Instrum. 46, 1325 (1975).

28. L. H. Dubois and G. A. Somorjai, Surface Sci. 91, 514 (1980).

29. N. Sheppard and T. T. Nguyen, in Advances in Infrared and Raman Spectroscopy Vol. 5, R. J. H. Clark and R. E. Hester, eds. (Heyden and Son, Ltd., London, 1978) p. 67.

30. R. M. Kroeker, W. C. Kaska, and P. K. Hansma, J. Catal. 57, 72 (1979); J. Catal. 61, 87 (1980).

31. L. H. Dubois, P. K. Hansma, and G. A. Somorjai, Appl. Surface Sci., in press.

32. P. A. Thiel, E. D. Williams, J. T. Yates, Jr., and W. H. Weinberg, Surface Sci. 84, 54 (1979).

33. A. C. Yang and C. W. Garland, J. Chem. Phys. 61, 1504 (1957).

34. D. G. Castner, L. H. Dubois, B. A. Sexton, and G. A. Somorjai, submitted to Surface Sci.

35. B. A. Sexton and G. A. Somorjai, J. Catal. 46, 167 (1977).

36. J. T. Yates, Jr., E. D. Williams, and W. H. Weinberg, Surface Sci. 91, 562 (1980).

37. W. Erley, H. Ibach, S. Lehwald, and H. Wagner, Surface Sci. 83, 585 (1979).

38. P. A. Thiel, W. H. Weinberg, and J. T. Yates, Jr., J. Chem. Phys. 71, 1643 (1979).

39. C. T. Campbell and J. M. White, J. Catal. 54, 289 (1978).

40. C. T. Campbell, S.-K. Shi, and J. M. White, Appl. Surface Sci. 2, 382 (1979).

# CHAPTER VII. The Application of High Resolution Electron Energy Loss Spectroscopy to the Study of Model Supported Metal Catalysts[1]

## A. Introduction

The characterization of molecules adsorbed on supported metal catalysts is of key importance for gaining a fundamental understanding of the mechanisms of catalysis. Vibrational spectroscopy has been, and will continue to be, one of the most important tools for this characterization.[2] To date, infrared spectroscopy has been the most widely used technique.[3,4] Its key advantage is that it can be applied to real catalysts under conditions similar to those used in the chemical technology with very high resolution (<1 $cm^{-1}$). However, due to light adsorption by the oxide support below ~1200 $cm^{-1}$ low frequency vibrational modes, which are essential in structural determination, are completely masked.[5-7] More recently, Raman spectroscopy[8] and inelastic electron tunneling spectroscopy have been used to obtain the vibrational spectra of molecules adsorbed on model supported catalysts.[9-11] These spectroscopic techniques can extend the spectral range over which a catalyst can be studied, but both present problems of their own including fluorescence and sample heating in the case of Raman spectroscopy[8] and uncertainty due to the top metal electrode in the case of tunneling spectroscopy.[12] Nevertheless, the problem of characterizing adsorbed molecules on surfaces is sufficiently complex that any vibrational spectroscopy that can yield new information or information from a different perspective will be useful. In this sense these spectroscopies complement one another.

In this chapter we report the first application of high resolution electron energy loss spectroscopy to the study of molecules adsorbed on model supported metal catalysts. Most ELS experiments to date have

employed well-characterized single crystal substrates under ultrahigh vacuum conditions.[13] High resolution ELS has been successful in these studies due to its broad spectral range (400-4000 $cm^{-1}$) and high surface sensitivity (0.001 monolayer for strong scatterers[13]).

We have now extended our previous ELS experiments on single crystal rhodium surfaces[14,15] to include studies of the chemisorption of carbon monoxide on model rhodium on alumina catalysts. Good quality vibrational spectra were obtained from CO adsorbed on small rhodium particles vapor deposited on an oxidized aluminum substrate. We employed the same catalyst preparation procedure that proved successful in inelastic electron tunneling investigations.[10] The ELS results can be favorably compared with the vibrational spectra of adsorbed carbon monoxide obtained by infrared[16-18] and inelastic electron tunneling[10] spectroscopy on similar rhodium on alumina model catalysts.

## B. Sample Preparation

Figure 1 shows a cross sectional view of our model supported metal catalysts. They were formed by:

1. evaporating from 200 to 2000 Å average thickness of Al from an aluminum wire on a stranded tungsten filament onto a clean metal substrate in the upper level of the vacuum chamber (see Chapter III, Fig. 4). The metal deposition rate was approximately 10 Å/sec. In our studies a Pt(111) single crystal was used as the metal substrate, although the results should be independent of the substrate material. The evaporated aluminum layer is polycrystalline with grain sizes on the order of microns.[9] Metal deposition was monitored using an oscillating quartz crystal microbalance.

Figure 1. Cross-sectional view of the model supported metal catalyst. If a small quantity of rhodium is evaporated onto oxidized aluminum it agglomerates into small particles. For an average thickness of 4 Å the rhodium particles are 20 to 30 Å in diameter.[10] The oxidized aluminum substrate is 10 to 15 Å thick and is similar to γ-alumina.[19,20]

Model Supported Rhodium Catalyst

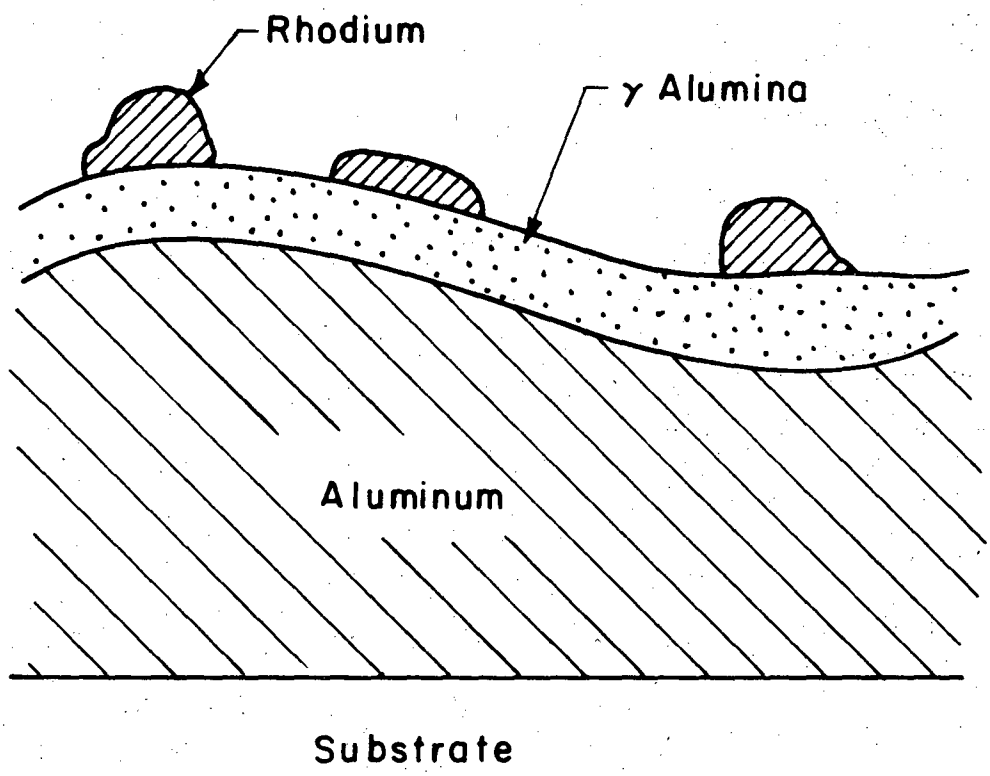


XBL 802-4730

2. oxidizing this aluminum in oxygen or air at exposures ranging from 1000 L to greater than $10^6$ L at temperatures between 300 and 480 K. Aluminum oxidized in this manner has been shown to resemble γ-alumina in both its physical and catalytic properties.[19,20] The oxide layer is typically 10 Å thick;[21,22] and its morphology is not known.

3. evaporating from 1 to 20 Å average thickness of Rh from a rhodium wire wrapped around a stranded tungsten filament in $1 \times 10^{-5}$ Torr of CO. The metal deposition rate was approximately 0.25 Å/sec. Rhodium evaporated in this manner has been shown to agglomerate into small, highly dispersed particles on the alumina support.[10] Kroeker, et al. using the same type of rhodium sources, source to substrate distances and oxidized aluminum substrates found with transmission electron microscopy that typical Rh particle diameters were 20-30 Å for a 4 Å average thickness.[10] These particles are similar in both size and distribution to those formed from the reduction of transition metal salts on alumina to prepare commercial catalysts.

After fabrication, the sample was lowered into the high resolution electron energy loss spectrometer. The incident energy was fixed at approximately 5 eV. The elastic scattering peak had a full width at half maximum (FWHM) between 80 and 100 $cm^{-1}$ and a maximum intensity of $1 \times 10^4$ counts per second. Preparing samples by first evaporating rhodium in vacuum and then exposing the dispersed metal particles to carbon monoxide caused a decline in both the scattering intensity and in the resolution of the vibrational spectra. Similar observations have been reported using inelastic electron tunneling spectroscopy;[23] however, the reasons for these findings are not understood at present.

## C. Experimental Results

Figure 2 shows Auger spectra of the oxidized aluminum used as a substrate for our model supported metal catalysts (upper trace), the substrate plus evaporated rhodium particles (middle trace), and a single crystal surface of rhodium (lower trace). Note in the Auger spectrum of the oxidized aluminum substrate that there are only peaks corresponding to the aluminum in an oxidized state and to oxygen.[24] This Auger spectrum is independent of oxidation conditions over the range studied. After the evaporation of the rhodium particles in $1 \times 10^{-5}$ Torr of carbon monoxide the characteristic rhodium Auger peaks can be clearly seen.[25] All peaks in the spectrum can be accounted for as due to oxidized aluminum, to rhodium metal or to carbon monoxide adsorbed on the metal surface. In particular, there are no observable peaks due to the possible evaporation of tungsten from the filament sources (100-200 eV).[26] We also studied the evaporation of iron and platinum from tungsten filaments and find no trace of tungsten in the deposited particles.

The lower trace in Figure 3 is the high resolution electron energy loss spectrum of the oxidized aluminum substrates. The most prominent feature in this spectrum can be assigned to the aluminum oxide phonons. It is a broad band centered just below 900 $cm^{-1}$ and asymmetric to lower energies. This relatively intense alumina phonon band is similar in both position and shape to the peak found by inelastic electron tunneling spectroscopy.[6,20] It is independent of the oxidation conditions over the range studied. A relatively broad, weak band between 3500 and 3600 $cm^{-1}$ corresponding to the O-H stretching mode of surface hydroxyl groups is generally seen in both the infrared[3] and inelastic electron tunneling spectra[19,20] of $\gamma$-alumina. Due to the rather low intensity of this band

Figure 2. The top trace shows the Auger electron spectrum of the oxidized aluminum support material. Only aluminum in an oxidized state and oxygen peaks are present.[24] The middle trace shows the spectrum after 4 Å average thickness of rhodium has been evaporated in the presence of $1 \times 10^{-5}$ Torr of carbon monoxide. Both the oxygen and aluminum peaks from the support material are attenuated and there are new peaks due to rhodium and carbon. The bottom trace shows the Auger electron spectrum from a clean single crystal surface of rhodium.

Auger Electron Spectra of Model Catalysts

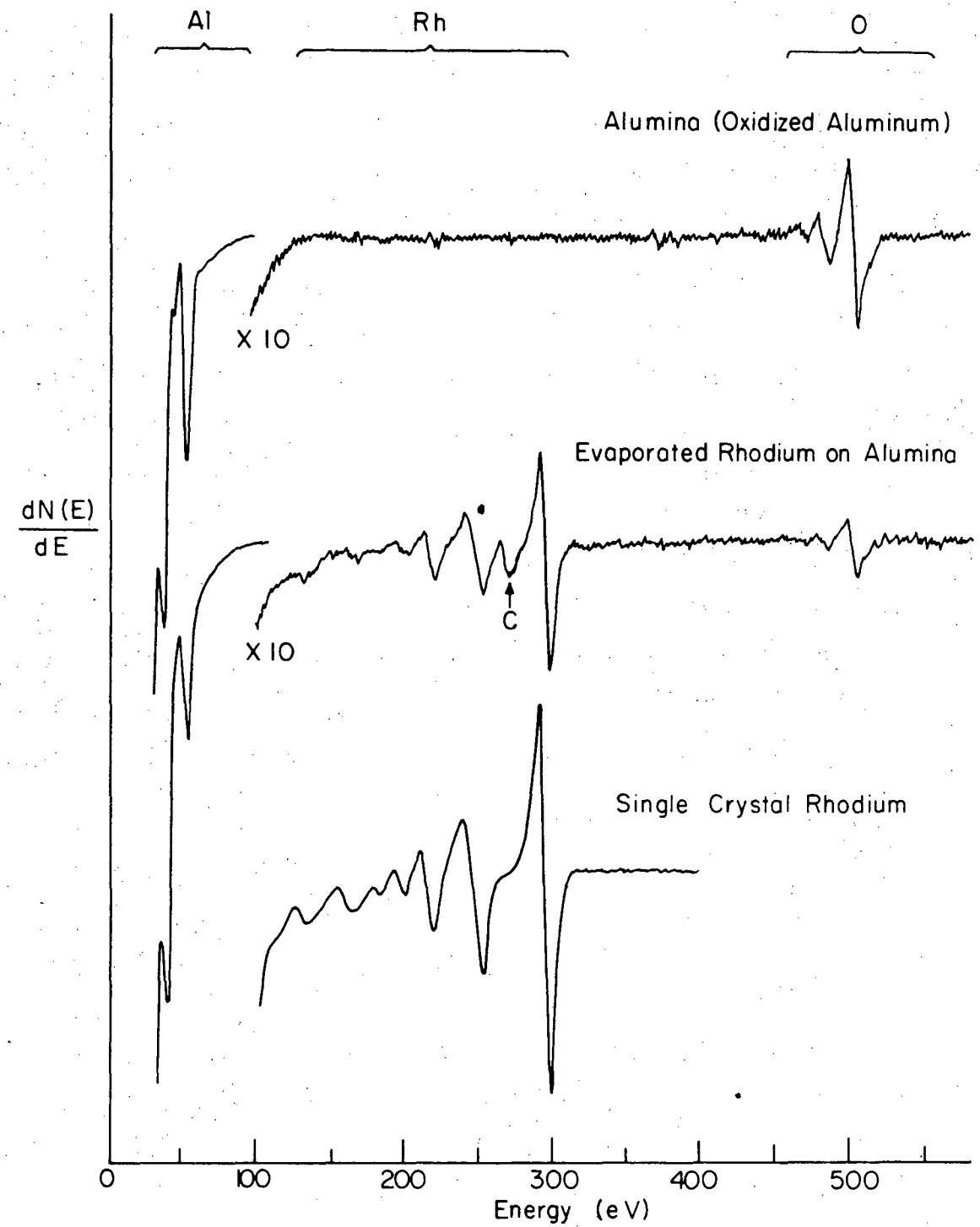


XBL 802-4731

Figure 3. The high resolution ELS spectrum for the aluminum oxide support is shown in the lowest trace. The broad band, asymmetric to lower wavenumbers and centered around 860 $cm^{-1}$ is the aluminum oxide phonon band.[10,20] The upper two traces show the ELS spectra for two different amounts of rhodium evaporated onto the alumina support in $1 \times 10^{-5}$ Torr of CO (4 Å and 20 Å average Rh thicknesses). The assignment of the observed losses is discussed in the next section.

Vibrational Spectra of Model Catalysts

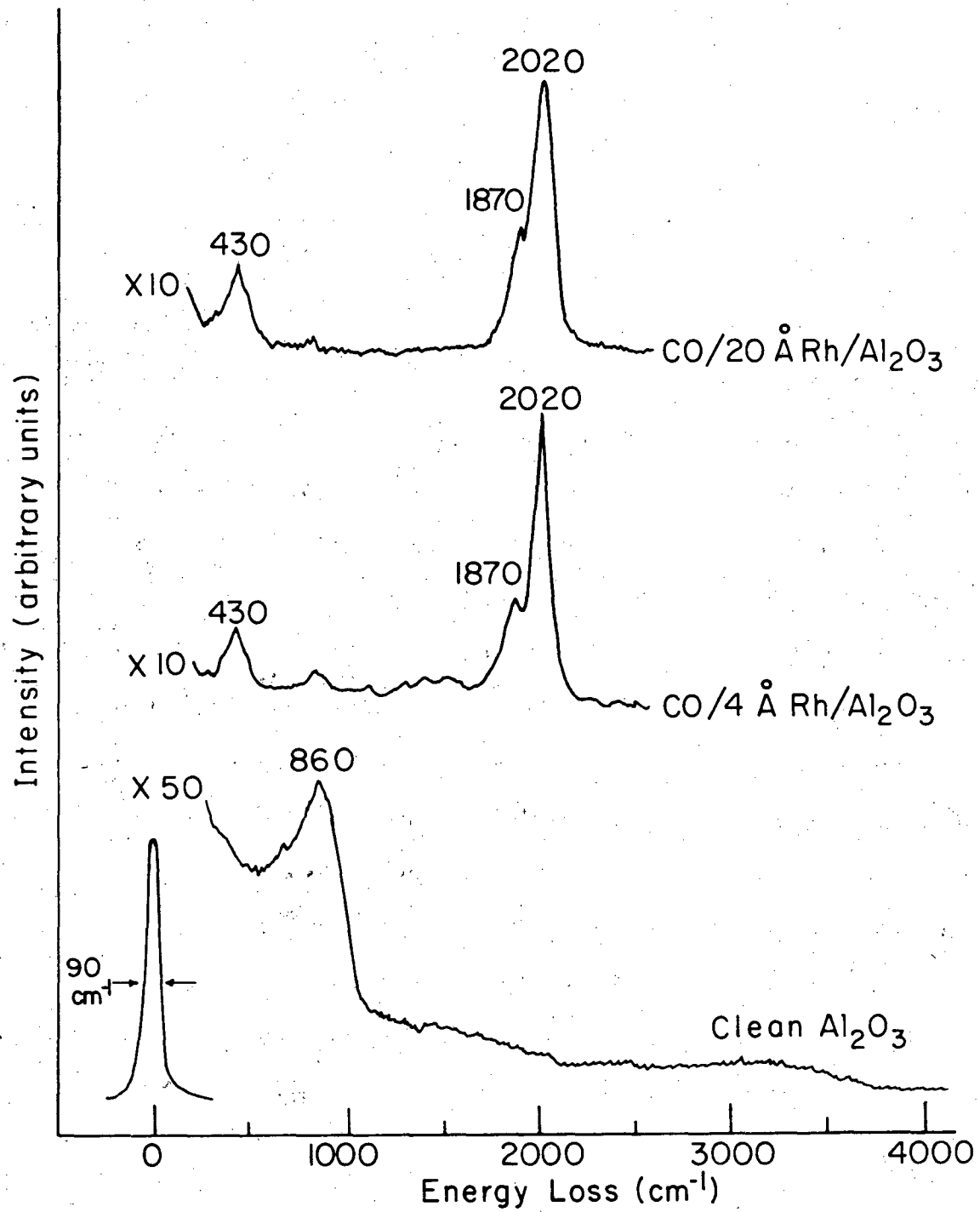


XBL802-4732

and to the decreased sensitivity of our spectrometer at these relatively high energies, this mode is not resolved here. The broad, weak feature centered above 3000 $cm^{-1}$ is not reproducible and may possibly be due to hydrocarbon impurities.

The middle and upper traces of Figure 3 show the vibrational spectra of CO chemisorbed on the highly dispersed rhodium particles supported on the oxidized aluminum. We carried out experiments on 1, 2, 4, 5 and 20 Å average thicknesses of evaporated rhodium. Representative spectra for carbon monoxide chemisorbed on 4 and 20 Å average rhodium thicknesses are shown here. These spectra have a smaller expansion scale than the alumina spectrum (x10 as compared to x50) and this represents a relatively large ratio of inelastic electron scattering to elastic electron scattering. Furthermore, the rhodium is covering a significant portion of the exposed alumina surface. By a 4 Å average thickness of evaporated rhodium (middle trace) the intensity of the aluminum oxide phonon band has decreased by a factor of approximately 2 (note scale change). By a 20 Å average thickness of rhodium (upper trace) this mode has completely disappeared. The prominent low frequency band centered above 400 $cm^{-1}$ is typical of Rh-CO stretching and bending modes[10,14,15,27,28] while the two losses near 2000 $cm^{-1}$ are characteristic of C≡O stretching vibrations.[10,14-18,27,28] In the next section we will discuss the interpretation of these spectra by comparison with infrared[16-18] and inelastic electron tunneling[10] results on similar model systems.

As can be seen from Figure 3, the results are not particularly sensitive to rhodium coverage over the range studies (1-20 Å average thickness), neither are they sensitive to additional CO exposure. Spectra run with CO partial pressures as high as $1 \times 10^{-5}$ Torr show no substantial differences. However, the relative intensities of the two high frequency C≡O

stretching modes can be significantly altered by heating the sample above 530 K in vacuum. After exposing this surface to >1000 L of CO only a single carbon-oxygen stretching vibration is observed at 2010 $cm^{-1}$. The 1870 $cm^{-1}$ mode is now only a shoulder and not well resolved here. This is clearly shown in the middle trace of Figure 4. Spectra run with 1 x $10^{-5}$ Torr of CO in the background also show no significant intensity in the 1870 $cm^{-1}$ mode (Fig. 4, upper trace). The shift in the C≡O stretching vibration is within the reproducibility of our measurements ($\pm$10 $cm^{-1}$).

## D. Discussion

Figures 3 and 4 clearly show that we are now able to obtain high resolution electron energy loss spectra from carbon monoxide adsorbed on model rhodium on alumina catalysts. One might anticipate charging of the aluminum oxide and diffuse scattering due to the rough surface. We find that charging does not present a problem because the oxidized aluminum layer is thin enough (10-15 Å) to allow relatively low impedance electron tunneling. In particular, under similar oxidation conditions we expect an Al-$Al_2O_3$-Pb tunnel junction to have a barrier impedance of much less than 100 ohms for a 1 $cm^2$ sample.[10] The incident beam current in our spectrometer is less than $10^{-9}$ amps (see Chapter III); thus the potential across the oxide is expected to be less than $10^{-7}$ volts.

We could not calculate in advance the effect of the diffuse surface scattering, although the aluminum grains are in the micron size range and the rhodium particles are 20-30 Å in diameter. Experimentally we find that though both the elastic and inelastic peaks are broader in their angular distribution when compared to scattering from a clean

Figure 4. Vibrational spectra of CO chemisorbed on a 4 Å average thickness of rhodium as a function of temperature. The lower trace was run after formation of the model catalyst. The middle trace was taken after flashing the sample to 530 K in vacuum and then adding > 1000 L of CO at 300 K. The upper trace was run in $1 \times 10^{-5}$ Torr of CO also at 300 K.

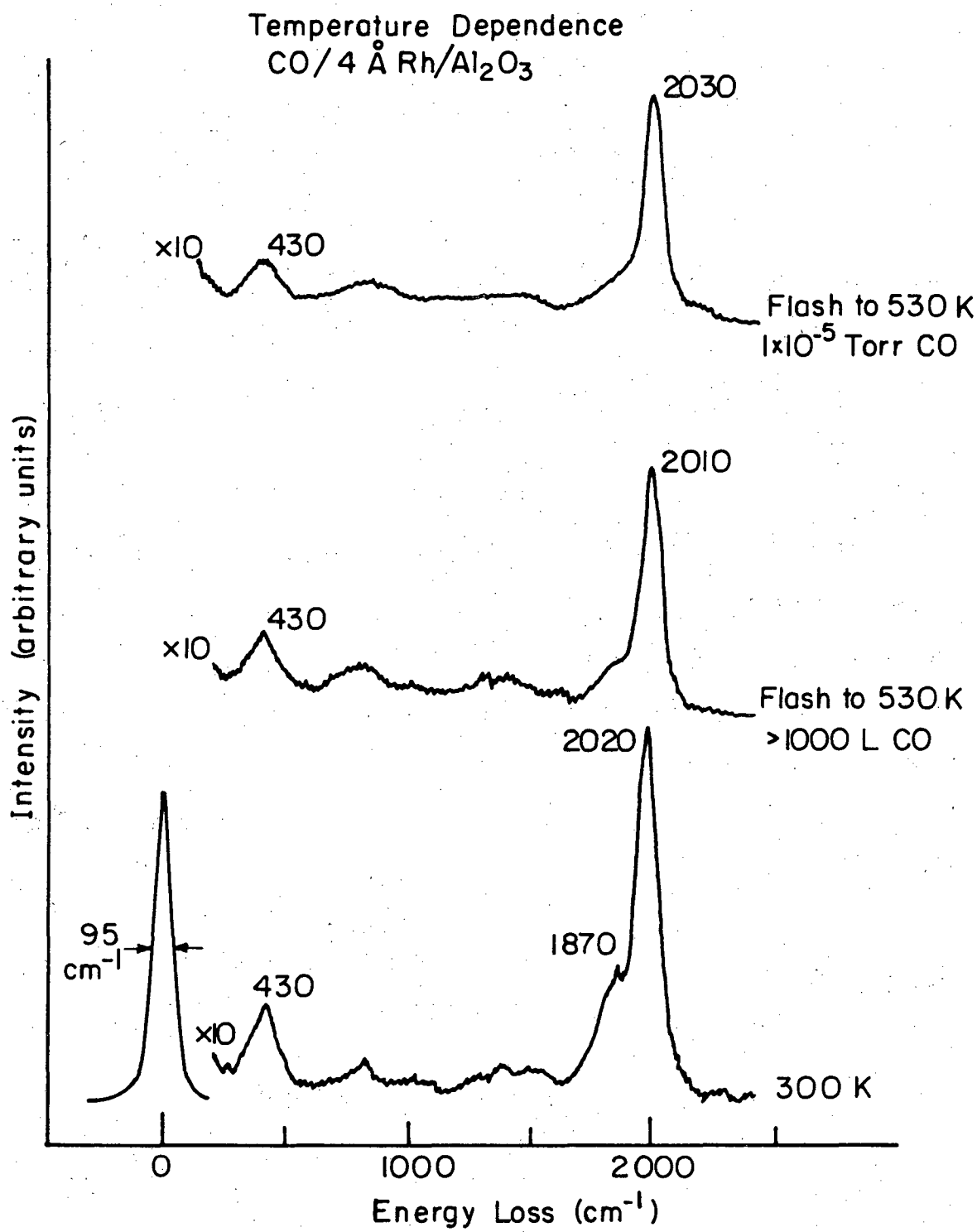
Temperature Dependence
CO/4 Å Rh/Al2O3
2030
x10
430
Flash to 530 K
1x10-5 Torr CO
2010
x10
430
Flash to 530 K
>1000 L CO
2020
95
cm-1
1870
430
x10
300 K
Intensity (arbitrary units)
0
1000
2000
Energy Loss (cm-1)

XBL803-4861

Rh(111) surface,[14] the intensity loss is not severe enough to prevent the measurements. We find that the elastic peak intensity ($I_o$) is down by roughly an order of magnitude; the inelastic peak intensity ($I_1$) is down by less than an order of magnitude. The reasons for the relatively large ratio of inelastic electron scattering to elastic electron scattering ($I_1/I_o$) are not understood at present. Approximate values for the dynamic effective charge (dipole derivative) of the C≡O stretching vibrations can be obtained from both inelastic electron tunneling and infrared spectroscopy. Measurements on similar rhodium on alumina model catalysts range from 11 to 18 Debye/Å.[10] These are 3 to 6 times higher than the value for gas phase CO (3.1 Debye/Å[29]) and imply that a relatively large ratio of inelastic to elastic electron scattering should be observed in our experiments. They are also far higher than the value that can be derived from the chemisorption of carbon monoxide on a flat Rh(111) single crystal surface (~7 Debye/Å).[14,30] Furthermore, Ibach[30] has shown that due to the non-zero collection angle of the spectrometer this intensity ratio ($I_1/I_o$) can be a function of surface disorder. In particular, $I_1/I_o$ increases with increasing surface disorder and therefore care must be taken in the analysis of peak intensities.

Finally, we see no evidence for significant peak broadening and loss of resolution due to local charging. However, with this sample configuration both the elastic and inelastic scattering peaks are approximately 10 $cm^{-1}$ broader (FWHM) when compared to scattering from either a CO covered Rh(111)[14] or Rh(331)[15] single crystal surface.

Figure 5 compares the electron energy loss spectra of the current work to previously obtained inelastic electron tunneling[10] and infrared spectra[17] of CO on rhodium supported on alumina. Some of the advantages and disadvantages of the various techniques are clear in this figure.

Figure 5. Vibrational spectra taken by three different techniques for carbon monoxide adsorbed on rhodium particles supported on alumina. The infrared spectra (upper traces) are from the work of Yates, et al.[17] The high resolution of IR spectroscopy is evident. The inelastic electron tunneling spectrum (lower trace), taken from the work of Kroeker, et al.,[10] shows the downshift in the CO stretching vibrations that are characteristic of tunneling spectroscopy and the relatively strong low frequency modes. The electron energy loss spectrum of the present work (middle trace) approximates the low frequency (400 - 1000 $cm^{-1}$) tunneling spectrum and the high frequency (1000 - 2500 $cm^{-1}$) infrared spectra.

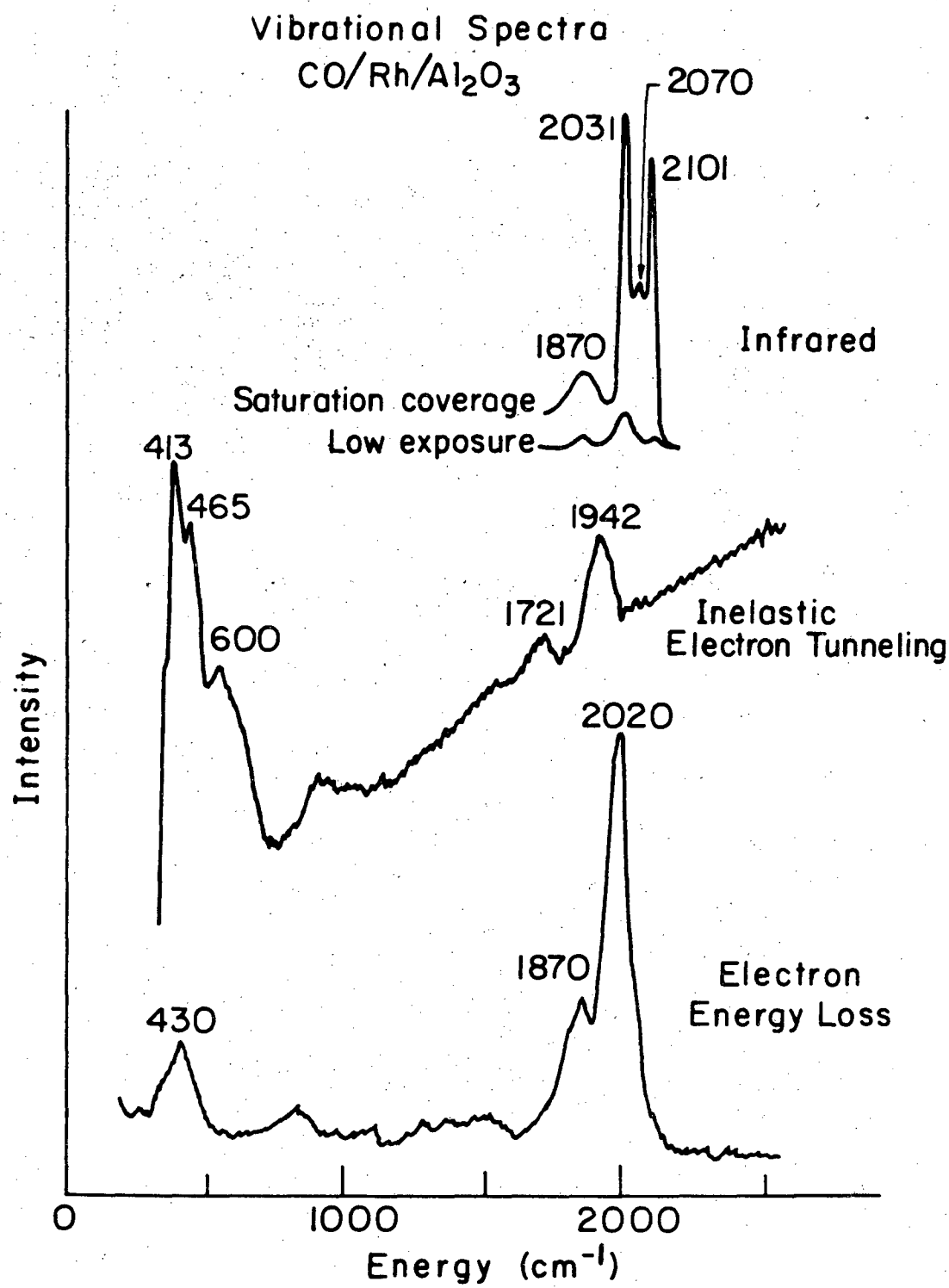
Vibrational Spectra
CO/Rh/Al2O3
2070
2031
2101
1870
Infrared
Saturation coverage
Low exposure
413
465
600
1942
1721
Inelastic
Electron Tunneling
2020
1870
430
Electron
Energy Loss
Intensity
0
1000
2000
Energy (cm-1)

XBL802-4733

Infrared spectroscopy has the best resolution but the spectrum does not extend to the low frequency region. Tunneling spectroscopy has reasonable resolution in the low frequency region, but there are questions about the effects of the top metal electrode that are not fully answered in the existing literature. In particular, how much should the low frequency modes be perturbed by the presence of the top metal electrode? Although there are estimates based on the observed mode shifts in other systems,[12] there have been no direct measurements on this type of system.

Previous researchers have identified three different types of carbon monoxide molecules adsorbed on alumina supported rhodium catalysts (see Fig. 5).[16-18] These include a bridge bonded species, $Rh_2 > CO$ ($\nu_{C=O} \approx 1870\ cm^{-1}$), a terminally bonded species, Rh-CO ($\nu_{C\equiv O} \approx 2020$ to $2070\ cm^{-1}$, depending on coverage and catalyst preparation) and a gem dicarbonyl species, $Rh-(CO)_2$ ($\nu_{C\equiv O\ symmetric} \approx 2031\ cm^{-1}$, $\nu_{C\equiv O\ asymmetric} \approx 2101\ cm^{-1}$). Similarly, we can assign the $1870\ cm^{-1}$ loss in the ELS spectrum of Figure 5 to a bridge bonded carbonyl. The $2020\ cm^{-1}$ mode most likely belongs to a linearly bonded CO species. The infrared spectrum taken at low CO exposures near the top of Figure 5 is similar to the high resolution ELS spectra that we observe. Linearly bonded carbon monoxide molecules dominate the C≡O stretching region, but some gem dicarbonyl species are also present. The presence of $Rh-(CO)_2$ species cannot be ruled out on our model supported catalysts since the observed loss at $\sim 2020\ cm^{-1}$ is quite broad ($\sim 100\ cm^{-1}$ full width at half maximum and $>200\ cm^{-1}$ wide at the base of the peak). Furthermore, such species are seen with inelastic electron tunneling[10] on model rhodium on alumina catalysts prepared in similar manner (Fig. 5, middle). Although the symmetric and asymmetric C≡O stretching vibrations of this species cannot be resolved here,

analysis of the low frequency modes indicates the presence of two distinct forms of linearly bonded carbon monoxide.[10] The infrared spectrum labeled "saturation coverage" was taken under 50 Torr of CO[17] and at these pressures one would expect the gem dicarbonyl surface species to be abundant.

A comparison between the inelastic electron tunneling and electron energy loss spectra in Figure 5 indicate that the ELS results are similar to the tunneling results in the low frequency region (400-1000 $cm^{-1}$). The low frequency modes observed with high resolution electron energy loss spectroscopy for the chemisorption of carbon monoxide on single crystal metal surfaces have been traditionally assigned as metal-CO stretching vibrations on the basis of the normal dipole selection rule (see Chapter IIF). This selection rule, which has been proposed for infrared spectroscopy as well as for high resolution ELS, suggests that only vibrations with a component of the oscillating dipole moment normal to the surface can be excited. Thus if the carbon monoxide is oriented perpendicular to a plane metal surface, the incident electrons will only couple to the metal-CO and carbon-oxygen stretching modes. Isotopic substitution studies,[10] however, have shown that the two most intense low frequency modes in the tunneling spectrum of model rhodium on alumina catalysts (413 and 465 $cm^{-1}$) are bending modes. Thus one wonders if the low frequency vibrations observed in this spectrum with high resolution ELS are bending or stretching modes. More studies are clearly needed to resolve this question.

Analysis of the low frequency vibrational modes by comparison with the infrared and Raman spectra of model rhodium cluster carbonyls of known molecular structure is rather difficult at present. To our knowledge,

no normal coordinate calculations have been carried out on these compounds. Although numerous vibrational modes between 393 and 513 $cm^{-1}$ have been observed in $Rh_4(CO)_{12}$ and $Rh_6(CO)_{16}$,[31] no simple comparison with our results can be made. Recent studies have shown that care must be taken in making the direct analogy between metal cluster carbonyls and adsorbed CO.[32]

The only way we found to significantly alter the intensity ratio of the two C≡O stretching modes was to heat the rhodium sample above 530 K in vacuum and then to re-expose the surface to carbon monoxide (Fig. 4). The vibrational spectra indicate that there is negligible CO remaining on the surface above 500 K. Carbon monoxide may decompose on both stepped single crystal[33,34] and polycrystalline[35] rhodium samples at this temperature. Residual carbon and/or oxygen from this dissociated CO may be blocking some of the surface sites and inhibiting further CO adsorption. This is not the case for CO adsorbed on the (111) face of rhodium. Here the chemisorption of carbon monoxide is completely reversible and no CO bond breaking is observed.[13,36] The decrease in the intensity of the 1870 $cm^{-1}$ mode could also be due to a redistribution (sintering) of the rhodium sample upon heating. Consistent with this is a decrease in the total integrated intensity of all of the observed ELS peaks. Even with $1 \times 10^{-5}$ Torr of CO above the catalyst sample, no significant intensity is seen in the 1870 $cm^{-1}$ mode (Fig. 4, upper trace).

## E. Summary

1. High resolution electron energy loss spectroscopy can be used to study the vibrational spectra of molecules adsorbed on model supported metal catalysts. This technique works well in spite of the surface

disorder and roughness. The elastic intensity is lowered by about one order of magnitude from its intensity on single crystal substrates; the inelastic peak intensity is decreased by less than an order of magnitude. The angular distribution of all peaks is broader.

2. ELS spectra of oxidized aluminum (a model system for $\gamma$-alumina) are similar to those found by inelastic electron tunneling. They show a relatively intense alumina phonon band that is broad, asymmetric to lower energies and centered around 860 $cm^{-1}$.

3. High resolution electron energy loss spectroscopy, inelastic electron tunneling spectroscopy and infrared spectroscopy are complementary techniques for studying the vibrational spectra of molecules adsorbed on model supported metal catalysts. The low frequency ELS spectrum (400-1000 $cm^{-1}$) is similar to the tunneling spectrum; the high frequency electron energy loss spectrum (1000-2500 $cm^{-1}$) is similar to the infrared spectrum.

## References


1. L. H. Dubois, P. K. Hansma, and G. A. Somorjai, Appl. Surface Sci., in press.

2. Surface Science of Catalysis: Vibrational Spectroscopies Applied to the Characterization of Adsorbed Species on Catalysts. ACS Symposium series, Vol. 000, A. T. Bell and M. L. Hair, eds., (American Chemical Society, Washington, D.C., 1980).

3. L. H. Little, Infrared Spectra of Adsorbed Species (Academic Press, London, 1966).

4. M. L. Hair, Infrared Spectroscopy of Surface Chemistry (Dekker, New York, 1967).

5. W. H. Weinberg, Ann. Rev. Phys. Chem. 29, 115 (1978).

6. P. K. Hansma, Phys. Rep. 30, 145 (1977).

7. J. Kirtley and P. K. Hansma, Acc. Chem. Res. 11, 440 (1978).

8. W. Krasser and A. Renouprez, Proc. Conference on Vibrations in Adsorbed Overlayers (Julich, Germany, 1978) p. 175.

9. H. E. Evans, W. M. Bowser, and W. H. Weinberg, Surface Sci. 85, L497 (1979).

10. R. M. Kroeker, W. C. Kaska, and P. K. Hansma, J. Catal. 57, 72 (1979); J. Catal. 61, 87 (1980).

11. H. E. Evans and W. H. Weinberg, J. Am. Chem. Soc. 102, 872 (1980).

12. J. Kirtley and P. K. Hansma, Phys. Rev. B13, 2910 (1976).

13. H. Ibach, Proc. Conference on Vibrations in Adsorbed Overlayers (Julich, Germany, 1978) p. 64.

14. L. H. Dubois and G. A. Somorjai, Surface Sci. 91, 514 (1980).

15. L. H. Dubois, P. K. Hansma, and G. A. Somorjai, J. Catal., in press.

16. A. C. Yang and C. W. Garland, J. Phys. Chem. 61, 1504 (1957).

17. J. T. Yates, Jr., T. M. Duncan, S. D. Worley, and R. W. Vaughn, J. Chem. Phys. 70, 1219 (1979).

18. D. J. C. Yates, L. L. Murrell, and E. B. Prestridge, J. Catal. 57, 41 (1979(.

19. P. K. Hansma, D. A. Hickson, and J. A. Schwarz, J. Catal. 48, 234 (1977).

20. W. M. Bowser and W. H. Weinberg, Surface Sci. 64, 377 (1977).

21. M. F. Muldoon, R. A. Dragoset, and R. V. Coleman, Phys. Rev. B20, 416 (1979).

22. D. G. Walmsley, R. B. Floyd, and W. E. Timms, Solid State Commun. 22, 497 (1977).

23. R. M. Kroeker and P. K. Hansma, to be published.

24. Handbook of Auger Electron Spectroscopy, 2nd Ed. (Physical Electronics Industries, Eden Prairie, MN, 1978) p. 47.

25. Ibid., p. 137.

26. Ibid., p. 213.

27. N. Sheppard and T. T. Nguyen, Advances in Infrared and Raman Spectroscopy, Vol. 5, R. J. H. Clark and R. E. Hester, eds. (Heyden, London, 1978) p. 67, and references therein.

28. N. V. Richardson and A. M. Bradshaw, Surface Sci. 88, 255 (1979).

29. R. A. Toth, R. H. Hunt, and E. K. Plyer, J. Mol. Spectr. 33, 85 (1969).

30. H. Ibach, Surface Sci. 66, 56 (1977).

31. W. P. Griffith and A. J. Wickham, J. Chem. Soc. A, 834 (1969).

32. R. M. Kroeker, P. K. Hansma and W. C. Kaska, J. Chem. Phys. 72, 4845 (1980).

33. D. G. Castner and G. A. Somorjai, Surface Sci. 83, 60 (1979).

34. D. G. Castner, L. H. Dubois, B. A. Sexton, and G. A. Somorjai, submitted to Surface Science.

35. B. A. Sexton and G. A. Somorjai, J. Catal. 46, 167 (1977).

36. J. T. Yates, Jr., P. A. Thiel, and W. H. Weinberg, Surface Sci. 91, 562 (1980).

# CHAPTER VIII. The Chemisorption of Acetylene and Ethylene on Rh(111)[1]

## A. Introduction

The chemisorption of simple hydrocarbons and subsequent surface reactions on well-characterized transition metal surfaces has become a topic of considerable interest in surface science. The aim of such studies is to provide fundamental information on the initial stages of hydrocarbon catalysis and to establish a framework for the interpretation of results on more complex catalysts. Determination of the molecular structure of adsorbed monolayers on metal surfaces is now possible by a variety of complementary techniques. Recently a combination of low-energy electron diffraction intensity analysis and high resolution electron energy loss spectroscopy has been used to determine the structure of ethylene ($C_2H_4$) chemisorbed on Pt(111) at 300 K.[2] High resolution ELS is a particularly valuable technique for probing hydrocarbon interactions with metal surfaces because of both its sensitivity to hydrogen and its broad spectral range (which includes M-C stretching vibrations, C-C stretching vibrations and C-H stretching and bending vibrations). Furthermore, ordered adsorbate overlayers are not needed to obtain intense ELS spectra (see Chapter I and VII). A dynamical LEED structure analysis provides bond lengths, bond angles and the position of the adsorbate on the surface if the overlayer is ordered. It is not very effective, however, in determining the location of hydrogen atoms - an important question in hydrocarbon surface chemistry. Changes in bonding with coverage and temperature can only be studied by LEED if the adsorbate layer remains well ordered.

We report here the results of a detailed investigation of the chemisorption and reactivity of $C_2H_2$ and $C_2H_4$ on the Rh(111) single crystal surface. In the present study we have extended previous LEED and thermal desorption mass spectrometry[3] investigations to lower temperatures ($T \sim 210$ K) and have complemented these results with data obtained by high resolution ELS and Auger electron spectroscopy. This combination of techniques allows us to determine the structure of these hydrocarbons on the surface and follow their molecular rearrangements as a function of temperature between 210 and 470 K. We have also studied the vibrational spectra of chemisorbed $C_2D_2$ and $C_2D_4$ and the reactions of these molecules with hydrogen. Finally, the bonding of acetylene and ethylene on Rh(111) is compared to data previously obtained on the (111) single crystal faces of both platinum and nickel.

B. LEED Studies of Acetylene and Ethylene Adsorption on Rh(111)

Exposing the clean Rh(111) surface (Fig. 1a) between 230 and 250 K to $C_2H_4$ results in the appearance of sharp half order diffraction spots in the LEED pattern (Fig. 1b) from a (2x2) surface structure. If the crystal temperature is below ~230 K, ethylene adsorption is disordered and the only change observed in the LEED pattern is an increased background intensity. This disordered hydrocarbon layer can be transformed into an ordered (2x2) surface structure by heating the crystal to between 230 and 250 K. Acetylene adsorption on the Rh(111) surface between 210 and 250 K also produces a (2x2) surface structure. The new diffraction spots from the ordered (2x2) hydrocarbon structures are sensitive to surface coverage. Although the spots are visible after a 1 L gas exposure, they do not become sharp and intense until 1.5 L and then immediately begin disordering above 1.5 L. A 15 sec exposure of $1 \times 10^{-7}$ Torr

Figure 1. LEED patterns from surface structures produced by either $C_2H_2$ or $C_2H_4$ adsorption on Rh(111). (a) clean Rh(111) at 92.5 eV, (b) Rh(111)-(2x2) from $C_2H_4$ chemisorption at 74 eV and (c) Rh(111)-c(4x2)-$C_2H_2$ + H at 67.5 eV.

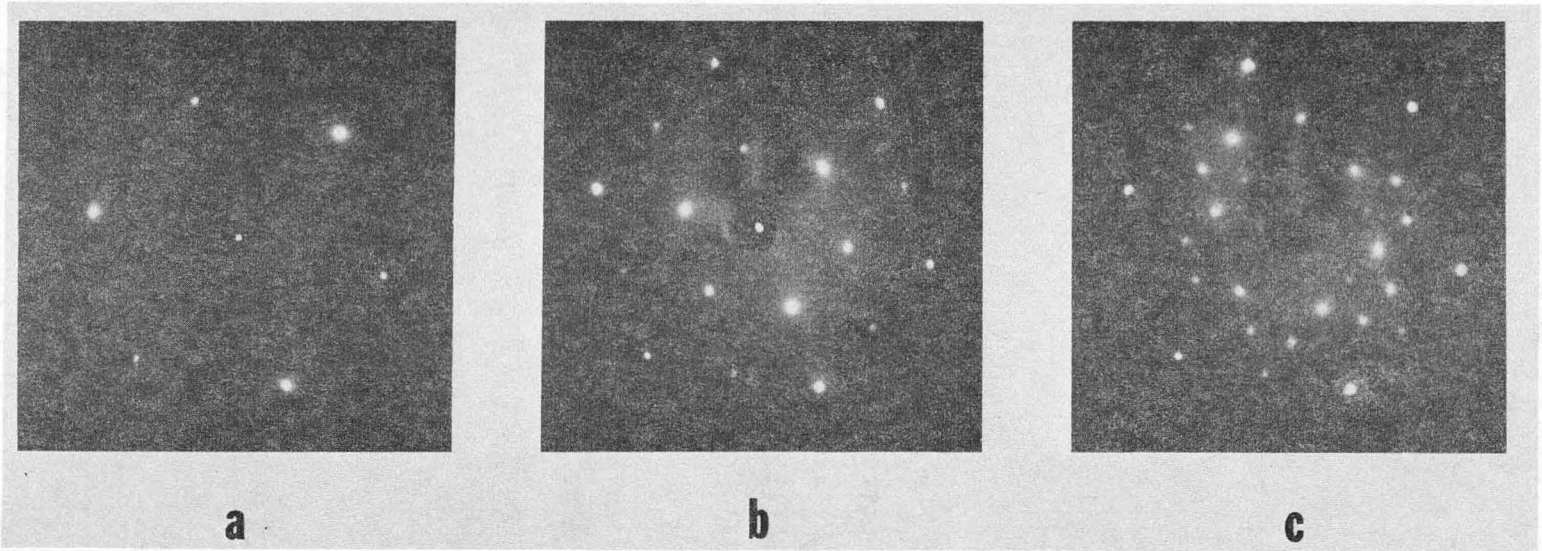


XBB 788-10161

$C_2H_4$ or a 150 sec exposure of 1 x $10^{-8}$ Torr $C_2H_2$ produce optimum (2x2) surface structures.

A diffraction pattern corresponding to a c(4x2) surface structure (Fig. 1c) can be generated from the (2x2) surface structure without additional hydrocarbon exposure. For adsorbed $C_2H_4$ the transformation occurs in vacuum by slowly warming the crystal to 300 K over the course of several hours. Rapid heating results in the formation of a disordered c(4x2) structure (broad, diffuse diffraction features and some streaking). For adsorbed $C_2H_2$ even this slow warm-up results in a disordered overlayer. To form a well ordered c(4x2) structure from adsorbed acetylene the crystal must be annealed for ~4 minutes at 273 K in 1 x $10^{-8}$ Torr of $H_2$ with the mass spectrometer filaments on. These filaments are located approximately 5 cm from the crystal and provide the surface with a good source of atomic hydrogen.[4] Castner et al.[2] previously observed the c(4x2) surface structures from the chemisorption of either acetylene or ethylene on Rh(111) near room temperature. The reported diffraction patterns were neither as sharp nor as intense as that shown in Fig. 1c, however. The (2x2) hydrocarbon surface structures have not been seen previously.

In the transformation from the (2x2) to the c(4x2) structures the orientation and shape of the unit cell change,[5] but the areas of the primitive unit cells of these two structures are the same (25 $Å^2$ on Rh(111)). Thus, no variation in the surface coverage occurs. Furthermore, AES shows that the carbon coverage from the (2x2) structures produced during $C_2H_2$ and $C_2H_4$ chemisorption are the same and remain constant during the conversion to the c(4x2) structures. Thus, changes in binding site and adsorbate geometry are probably taking place without any change

in the adsorbate coverage. Determination of the overlayer structure by LEED requires the analysis of the intensity vs incident energy (I-V) beam profiles. We have not undertaken such calculations in the present study. The transformation from the (2x2) to the c(4x2) surface structures is irreversible; once the c(4x2) structure forms, the crystal can be cooled to 210 K with no visible changes in the diffraction pattern. The c(4x2) structures can only be altered by heating the crystal above 420 K which causes the surface to irreversibly disorder.

C. High Resolution ELS Studies of Acetylene Adsorption on Rh(111)

The vibrational spectrum of the (2x2) hydrocarbon surface structure formed from the chemisorption of $C_2H_2$ on Rh(111) between 210 and 270 K is shown in the lower trace of Figure 2. The peak positions and their relative intensities[6] are listed in Table I. Although some of the peaks are not readily visible in this figure, their positions and intensities are obtained from the analysis of at least six spectra. A complete analysis of the low frequency region in this spectrum is hampered by a spurious background peak near 800 $cm^{-1}$. This apparent loss, first observed by Froitzheim et al,[8] may be caused by electron reflection from the outer half of the analyzer (see Chapter III). The dashed lines in Figures 2, 3, 4, and 9 indicate the approximate location and magnitude of this peak. As a result of this experimental artifact, both the position and intensity of all loss features between 650 and 900 $cm^{-1}$ are rather uncertain. Isotopic substitution is of some help in assigning the observed vibrational frequencies to normal modes of the adsorbed species. The ELS spectrum of the (2x2) $C_2D_2$ surface structure is shown in the middle trace of Figure 2.

Figure 2. High resolution ELS spectra of chemisorbed acetylene on Rh(111). (2x2)-$C_2H_2$ (lower trace), (2x2)-$C_2D_2$ (middle trace) and c(4x2)-$C_2H_2$ + H (upper trace). The vibrational frequencies are listed in Table I (lower and middle traces) and II (upper trace). The broad peak (dashed line) centered near 800 $cm^{-1}$ may be caused by stray electron reflection inside the spectrometer (see text).

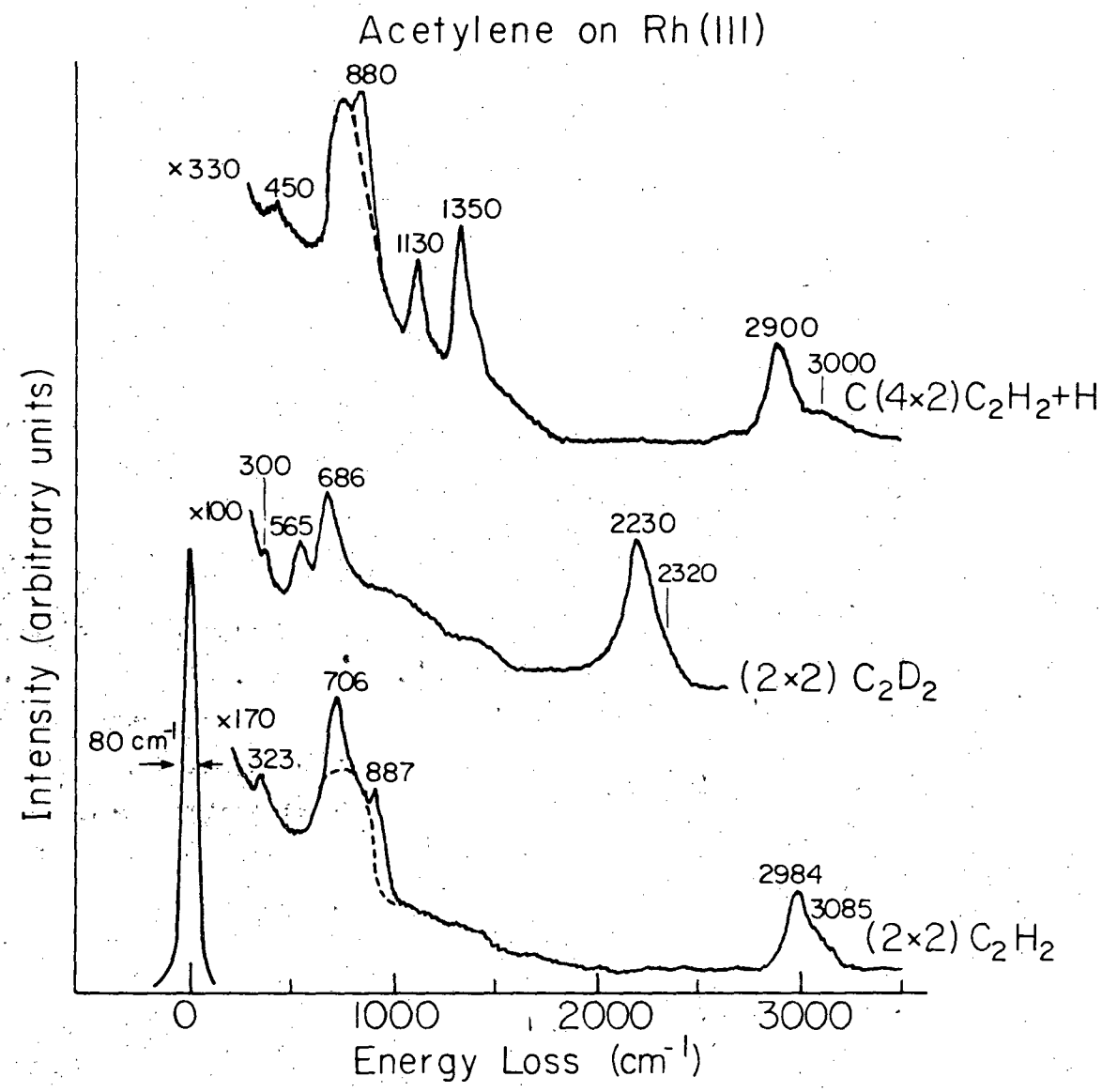
Acetylene on Rh(III)
880
×330
450
1350
1130
2900
3000
C(4×2)C2H2+H
300
686
×100
565
2230
2320
(2×2) C2D2
706
×170
80 cm-1
323
887
2984
3085
(2×2) C2H2
Intensity (arbitrary units)
0
1000
2000
3000
Energy Loss (cm-1)

XBL798-6968

Table I. Vibrational Modes for the Metastable (2x2)-$C_2H_2$ ($C_2D_2$) Species Observed on Rh(111) at T < 270 K

(all frequencies in $cm^{-1}$)

| $C_2H_2$ ($C_2D_2$) on Rh(111) | | $C_2H_2Co(CO)_6$ ($C_2D_2Co(CO)_6$)[10,11] | | Assignment |
|---|---|---|---|---|
| Observed Frequencies | $\nu_{C-H}/\nu_{C-D}$ | Observed Frequencies | $\nu_{C-H}/\nu_{C-D}$ | |
| 3085 (~2320) w | 1.33 | 3116 (2359) m | 1.32 | C-H (C-D) stretch |
| 2984 (2230) m | 1.34 | 3086 (2297) m | 1.34 | |
| a | | 1403 (1346) s | 1.04 | C-C stretch |
| 887 (686) m | 1.29 | 894 (751) s | 1.19 | C-H (C-D) bend |
| 706 (565) m | 1.25 | 768 (602) s | 1.28 | |
| 323 (~300) w | 1.08 | 605 (561) w | 1.08 | M-C stretch |
| | | 551 (520) m | 1.06 | |

[a] Small, broad peak in the 1300-1400 $cm^{-1}$ region is observed in several spectra.

Intensity: s = strong; m = medium; w = weak

The vibrational spectra of the (2x2) acetylene overlayer in Figure 2 does not change up to 270 K in vacuum. Furthermore, the positions and relative intensities of the observed energy loss peaks are independent of the acetylene exposure (from >0.2 L to <50 L) and, more importantly, are independent of surface order (as determined by observation of the LEED pattern). Thus, using high resolution ELS we conclude that the bonding of the adsorbed molecules do not change upon disordering.

The frequencies of the carbon-hydrogen (carbon-deuterium) stretching vibrations can be used to characterize the state of hybridization of the adsorbed species. Acetylene, $C_2H_2$ ($C_2D_2$),[9] is sp hybridized in the gas phase and has C-H (C-D) stretching vibrations between 3289 and 3374 (2439 and 2701) $cm^{-1}$; ethylene, $C_2H_4$ ($C_2D_4$),[9] is $sp^2$ hybridized and has C-H (C-D) stretching vibrations between 2989 and 3106 (2200 and 2345) $cm^{-1}$; while ethane, $C_2H_6$ ($C_2D_6$),[9] is $sp^3$ hybridized and has C-H (C-D) stretching vibrations between 2896 and 2985 (2083 and 2235) $cm^{-1}$. Thus, the losses at 2980 (2230) and 3085 (~2320) $cm^{-1}$ in Figure 2 and Table I correspond to the C-H (C-D) stretching vibrations of a molecule near $sp^2$ hybridization. This indicates that the C≡C-H (C≡C-D) bond in adsorbed acetylene is no longer linear.

Assignment of the remaining energy loss peaks by comparison to the infrared spectra of model organometallic compounds of known molecular structure is quite difficult at present. Most metal-acetylene complexes are synthesized from substituted acetylenes (usually methyl- or phenyl-acetylenes) and their vibrational spectra bear little resemblance to what one would expect from chemisorbed acetylene. Furthermore, we know of only one acetylene-transition metal compound, $C_2H_2Co_2(CO)_6$, which has been extensively studied by both infrared spectroscopy and X-ray

crystallography.[10,11] The IR absorption bands for this molecule are listed in Table I. These vibrational frequencies are considerably different from those observed for chemisorbed $C_2H_2$ due to the differences in both bonding and geometry. Nevertheless, a comparison of the ratios of $\nu_{C-H}/\nu_{C-D}$ will help us to accurately assign the vibrational modes of acetylene chemisorbed on Rh(111) (see Table I). A similar analysis has been successfully used in the past.[12,13] Our vibrational mode assignments are summarized in Table I. The low frequency mode at 323 $cm^{-1}$ does not shift significantly upon deuteration (~20 $cm^{-1}$) and most likely corresponds to the entire molecule vibrating against the surface. The two largest peaks in the spectrum at 706 and 887 $cm^{-1}$ shift by almost 200 $cm^{-1}$ ($\nu_{C-H}/\nu_{C-D}$ = 1.29 and 1.25, respectively) when $C_2D_2$ is chemisorbed and can be assigned to C-H (C-D) bending modes (see Table I). We assume the adsorbate is oriented with its carbon-carbon axis approximately parallel to the surface since only small, broad peaks (1300 - 1400 $cm^{-1}$) are seen in the C-C stretching region. Observation of such a mode in the specular direction is prohibited by the normal dipole selection rule if the C≡C bond is parallel to the surface (see Chapter II).

Bond lengths, bond angles and the position of adsorbed $C_2H_2$ on the surface cannot be accurately determined without a complete dynamical LEED intensity analysis. Nevertheless, the high resolution ELS results indicate that acetylene chemisorbs on Rh(111) below 270 K with its C≡C axis oriented approximately parallel to the surface. The molecule is near $sp^2$ hybridization and therefore the C≡C-H bond angle is no longer linear. A similar $C_2H_2$ geometry is seen in numerous organometallic cluster compounds.[14,15]

Both LEED and ELS indicate that the (2x2) acetylene overlayer is stable on the surface in vacuum between 210 and 270 K. The addition of

$H_2$ to adsorbed $C_2H_2$ below ~260 K causes no changes in the observed ELS spectra, although this surface species is still quite reactive. The addition of $H_2$ to chemisorbed $C_2D_2$ below 260 K results in a complex vibrational spectrum with peaks in both the C-H and C-D stretching and bending regions. Although the deuterium and hydrogen readily exchange, no change in the adsorbate geometry is detected by high resolution ELS. The vibrational spectra of adsorbed acetylene only begin to change when the crystal is heated above 270 K in vacuum. The (2x2) $C_2H_2$ surface structure also disorders at this temperature.

The vibrational spectrum from the c(4x2) acetylene overlayer is shown in the upper trace of Figure 2. This spectrum can either be obtained by warming the (2x2) acetylene overlayer to ~270 K in the presence of $1 \times 10^{-8}$ Torr of hydrogen or by chemisorbing $C_2H_2$ on Rh(111) above 300 K. Hydrogen addition to the surface species above 270 K is necessary to obtain good quality, intense ELS spectra, however. Hydrogen addition was also required to complete this conversion in the LEED studies. This species is stable on the surface up to ~420 K. The structure of this hydrocarbon overlayer will be discussed in the next section.

D. High Resolution ELS Studies of Ethylene Adsorption on Rh(111)

The vibrational spectra from the (2x2) and c(4x2) ethylene surface structures are shown in Figure 3. The ELS spectrum in the lower trace of Figure 3 is obtained by chemisorbing $C_2H_4$ on the crystal below 270 K. The middle trace in Figure 3 can either be observed by slowly warming the (2x2) overlayer structure (lower trace) to room temperature or by simply adsorbing ethylene on the Rh(111) surface above 290 K. The

Figure 3. High resolution ELS spectra of chemisorbed ethylene on Rh(111). (2x2) from $C_2H_4$ chemisorption (lower trace), c(4x2) from $C_2H_4$ chemisorption (middle trace) and (2x2) from $C_2D_4$ chemisorption (upper trace). The vibrational frequencies are listed in Table II.

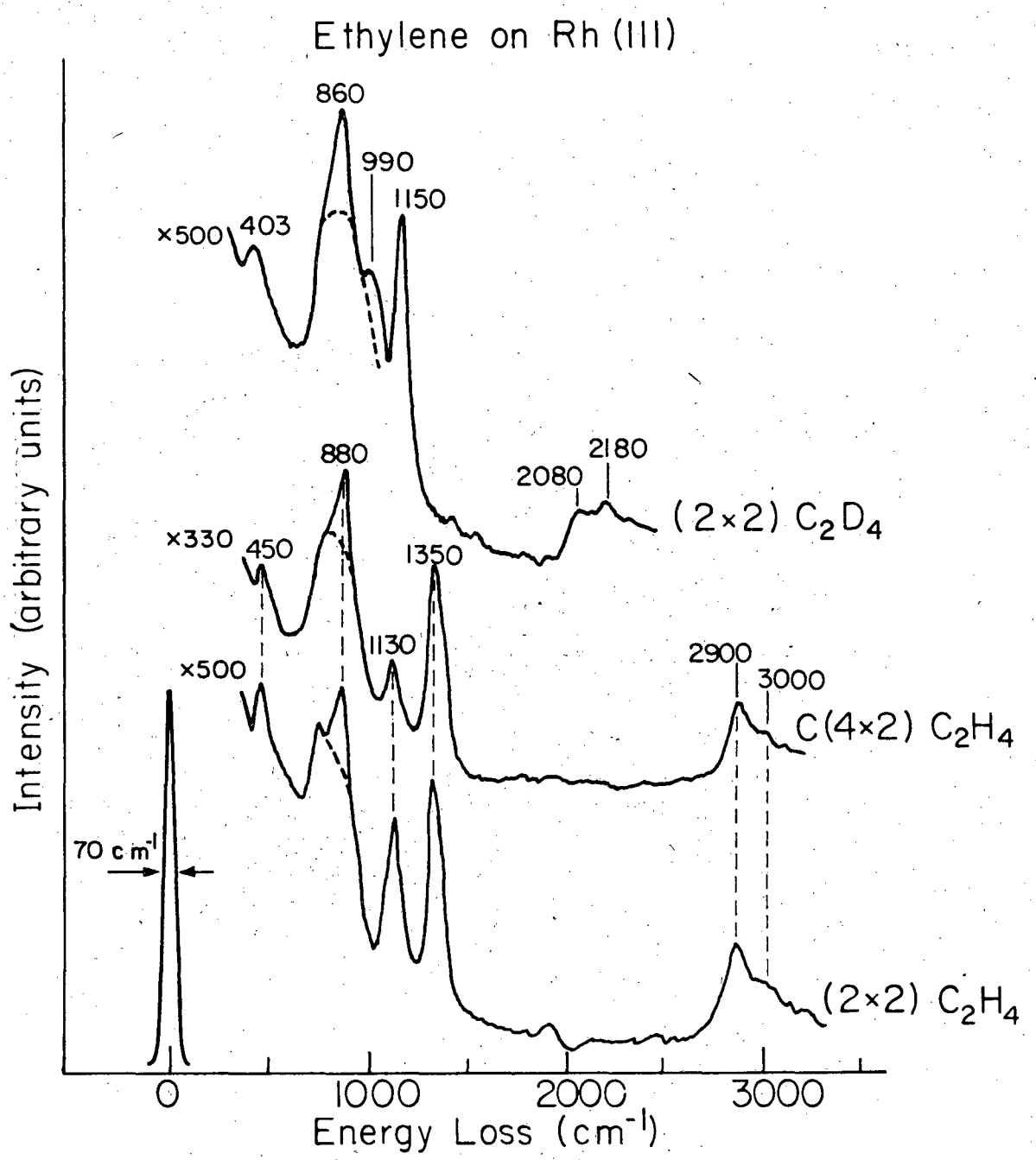
Ethylene on Rh (111)
860
990
1150
×500
403
880
2180
2080
(2×2) $C_2D_4$
×330
450
1350
1130
2900
3000
×500
C(4×2) $C_2H_4$
70 cm$^{-1}$
(2×2) $C_2H_4$
Intensity (arbitrary units)
0
1000
2000
3000
Energy Loss (cm$^{-1}$)

XBL798-6969

measured peak positions are listed in Table II. Small peaks in the 1800 to 2100 $cm^{-1}$ region are due to background CO adsorption.[16] The assignment of the peak positions and their relative intensities are obtained from the analysis of at least six spectra. Once again, the observed vibrational frequencies are independent of surface order and hydrocarbon exposure (>0.2 to <50 L). Note that these ELS spectra are almost identical to the vibrational spectrum from the stable c(4x2) acetylene overlayer shown in the upper trace of Figure 2. The hydrocarbon species derived from ethylene chemisorption is also stable on the surface up to ~420 K. Degradation of both the c(4x2) LEED pattern and of the vibrational spectrum occur at this temperature.

The ELS spectrum resulting from the chemisorption of either $C_2H_4$ or $C_2H_2$ and $H_2$ on Pt(111)[4,12] above room temperature are quite similar (see Fig. 4) and their stretching frequencies are listed in Table II. The vibrational spectrum from the chemisorption of $C_2D_4$ on either Rh(111) (Fig. 3c upper trace and Table II) or Pt(111)[4] (Table II) are also quite similar. Although the chemisorption of ethylene on Pt(111) has been studied by numerous techniques,[2,4,12,17] there is still debate over the precise geometry of the stable surface species. We simply point out that the stable hydrocarbon overlayer formed from the chemisorption of either ethylene or acetylene and hydrogen on both Pt(111) and Rh(111) yield identical vibrational spectra. A more complete discussion of the similarities between the chemisorption of ethylene on Rh(111) and Pt(111) will be presented in Section F.

It is interesting to note that the geometry of the adsorbed ethylene species on Rh(111) remains the same (as indicated by the ELS spectra) while the overlayer structure changes from a (2x2) to a c(4x2). This chemisorbed hydrocarbon should be an excellent candidate for a LEED

Table II. Vibrational Modes for the Stable Species Observed on Rh(111) and Pt(111) Upon Adsorption of Either $C_2H_4$ or $C_2H_2$ and H above 300 K

(all frequencies in $cm^{-1}$)

| Chemisorption of $C_2H_4$ or $C_2H_2$+H | | Chemisorption of $C_2D_4$ | |
|---|---|---|---|
| Rh(111) | Pt(111)[4,12] | Rh(111) | Pt(111)[4,12] |
| ~3000 w | 3025 - 3105 w | 2180 w | broad unresolved band |
| ~2900 w | 2900 - 2940 m | 2080 m | |
| shoulder | 1420 m | 1150 s | 1150 s |
| 1350 s | 1350 - 1360 s | 990 | 1010 w |
| 1130 s | 1130 s | 860 m | 850 w |
| 880 m | 900 m | 403 w | 430 m |
| 450 w | 435 m | | |

Intensity: s = strong

m = medium

w = weak

Figure 4. Comparison of the vibrational spectra for ethylene chemisorbed on a Pt(111) (lower trace)[4] and Rh(111) (upper trace). A discussion of the similarities between acetylene and ethylene chemisorption on Rh(111) and Pt(111) is presented in Section F.

Ethylene Chemisorption on Rh and Pt

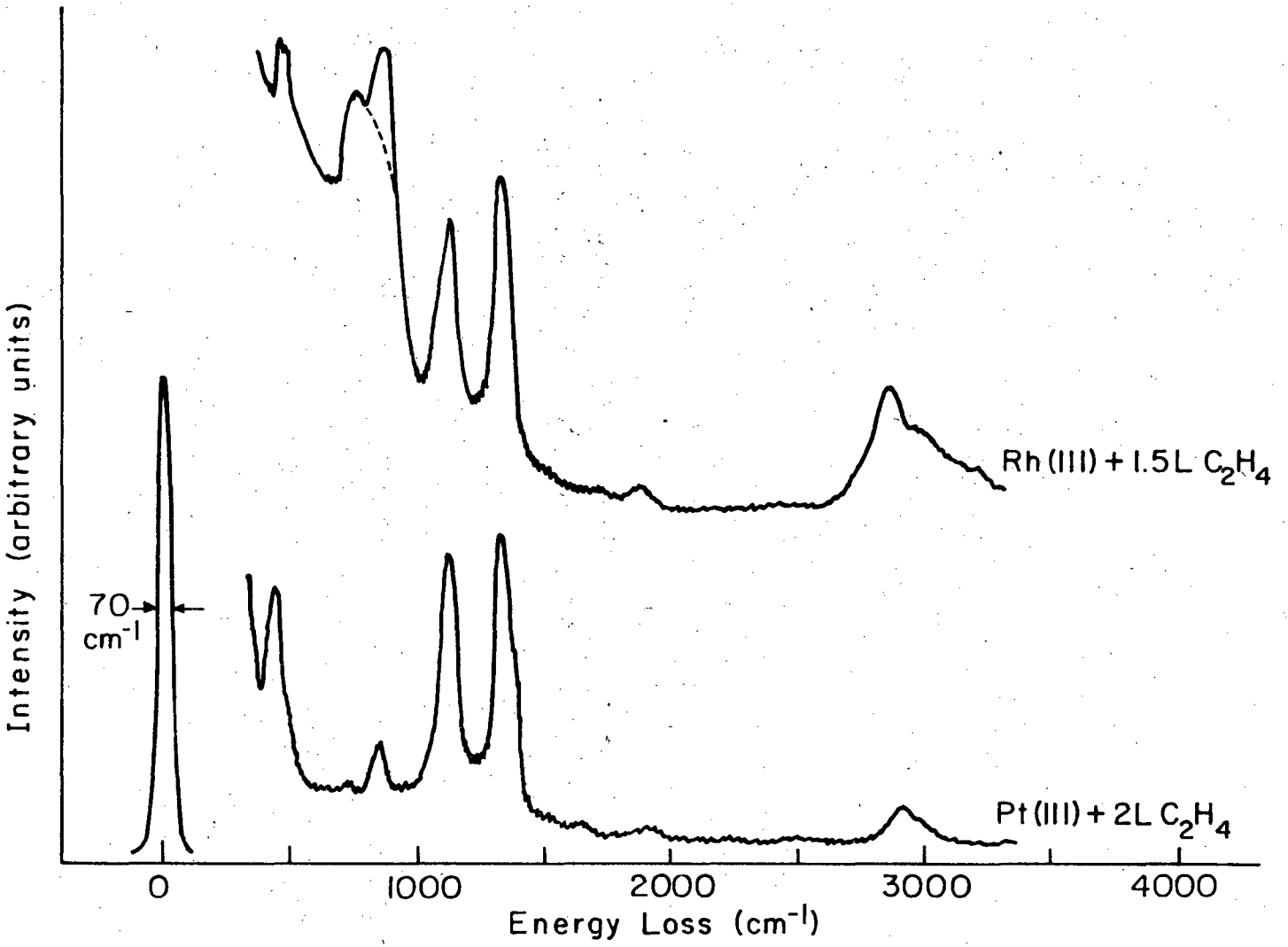


XBL 7911-7290

structural analysis since the I-V beam profiles should change while the molecular geometry does not. The order-order transformation observed by LEED is irreversible at the low pressures employed in our experiments, and again no intermediate species are observed. Although this conversion is not affected by the presence of hydrogen, H-D exchange will occur in the hydrocarbon overlayer when $H_2$ is added to chemisorbed $C_2D_4$. No change in the adsorbate geometry is detected by high resolution ELS.

E. TDS Studies of Acetylene and Ethylene Adsorption on Rh(111)

Castner et al.[3,18] have previously shown that both $C_2H_2$ and $C_2H_4$ decompose on the Rh(111) single crystal surface upon heating to yield gas phase molecular hydrogen and surface carbon. The $H_2$ thermal desorption traces from the room temperature adsorption of these hydrocarbons have one major peak near 500 K followed by continuous hydrogen evolution up to approximately 750 K. The position of this desorption maximum was found to be independent of gas exposure.[18]

Hydrogen desorption spectra from the ordered hydrocarbon overlayers chemisorbed on Rh(111) are shown in Figure 5. Traces 5a and 5d are from the (2x2) structures formed at 240 K from the adsorption of 1.5 L of acetylene and ethylene, respectively. Spectra 5b and 5c are from the c(4x2) surface structures formed from the metastable (2x2) $C_2H_2$ and $C_2H_4$ structures, respectively. After forming the c(4x2) structures, the crystal is cooled to 240 K before initiating the desorption experiments. Molecular $C_2H_2$ and $C_2H_4$ desorption near 375 K is also observed.[18] The amount of hydrocarbon that is detected desorbing is less than 1% of the amount of hydrogen desorbed indicating that most of the adsorbed hydrocarbons decompose on the surface upon heating. The hydrogen desorption

Figure 5. Hydrogen desorption from (a) (2x2) and (b) c(4x2) overlayer structures formed during $C_2H_2$ adsorption on Rh(111) and from (c) c(4x2) and (d) (2x2) structures from $C_2H_4$ adsorption on Rh(111). After forming the c(4x2) surface structures, the crystal was cooled to 240 K before initiating the desorption experiments. The heating rate is 40 K/sec.

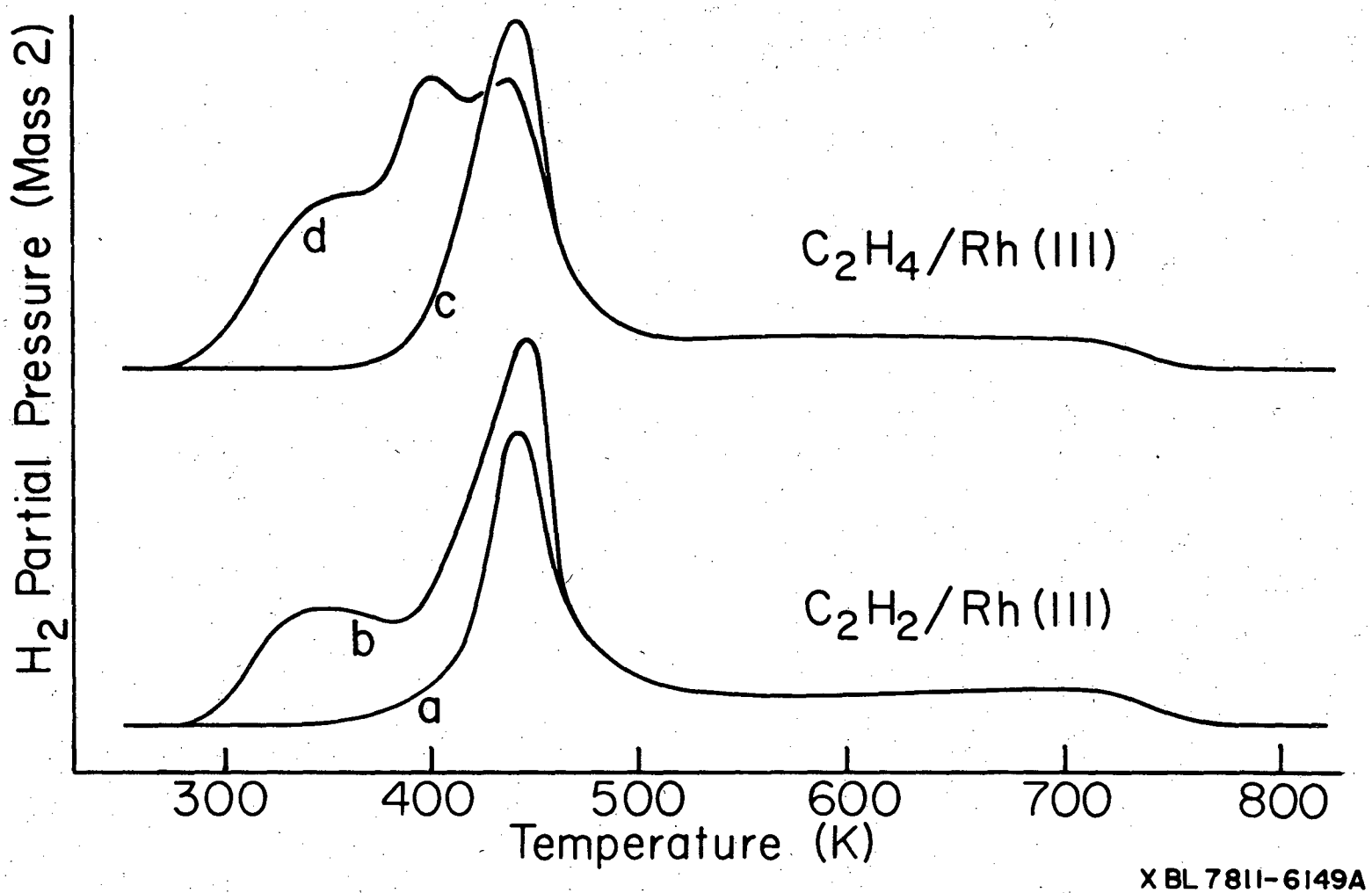
$H_2$ Partial Pressure (Mass 2)
d
c
$C_2H_4$/Rh (III)
b
a
$C_2H_2$/Rh (III)
300
400
500
600
700
800
Temperature (K)
XBL 7811-6149A

spectrum from the c(4x2) ethylene species (Fig. 5c) has a single desorption peak at 440 K followed by continuous hydrogen evolution until 750 K. This suggests that the desorption peak at 440 K in Figure 5d is from the stable hydrocarbon species which can be formed as the crystal is heated during the TDS experiments. The desorption peak at 350 K in Figure 5d is due to chemisorbed hydrogen on the Rh(111) surface. This desorption peak has been observed from hydrogen adsorption on clean Rh(111)[2,18,19] and after annealing the Rh(111)-(2x2)-$C_2H_2$ structure in hydrogen (Fig. 5b). A similar peak is seen in $H_2$ TDS spectra from ethylene chemisorbed on Pt(111) at 320 K.[17] The origin of the desorption peak at 395 K in Figure 5d remains in question. Possible assignments include an unstable low temperature ethylene species or a transient intermediate hydrocarbon fragment present during the conversion of the metastable adsorbate to the stable surface phase.

Desorption traces b and c in Figure 5 from the c(4x2) hydrocarbon surface structures are identical above ~400 K. The low temperature peak in 5b is from the hydrogen added in order to form a well ordered c(4x2) overlayer structure. This is in agreement with both the LEED and ELS results. ELS spectra taken before and after heating the crystal to 350 K show no major differences. Finally, the amount of $H_2$ desorbed from the surface in 5c is significantly less than the amount desorbed in 5d, indicating that the stable ethylene phase on Rh(111) is partially dehydrogenated.

If we increase the sensitivity of the mass spectrometer and study the high temperature $H_2$ desorption tail (above 450 K), we find two peaks at 560 and 640 K. This is shown in the lower trace of Figure 6. The positions of the peak maxima are independent of gas exposure and can be

Figure 6. The expanded scale above 450 K (x5) in the $H_2$ desorption spectrum from 0.25 L of $C_2H_4$ on Rh(111) at 220 K indicates the presence of a "tightly bonded" hydrogen species (lower trace). The relative intensity of this species can be increased by either dosing the surface at 225 K and flashing to 470 K (middle trace) or by dosing the surface at 470 K (upper trace). The heating rate is 40 K/sec.

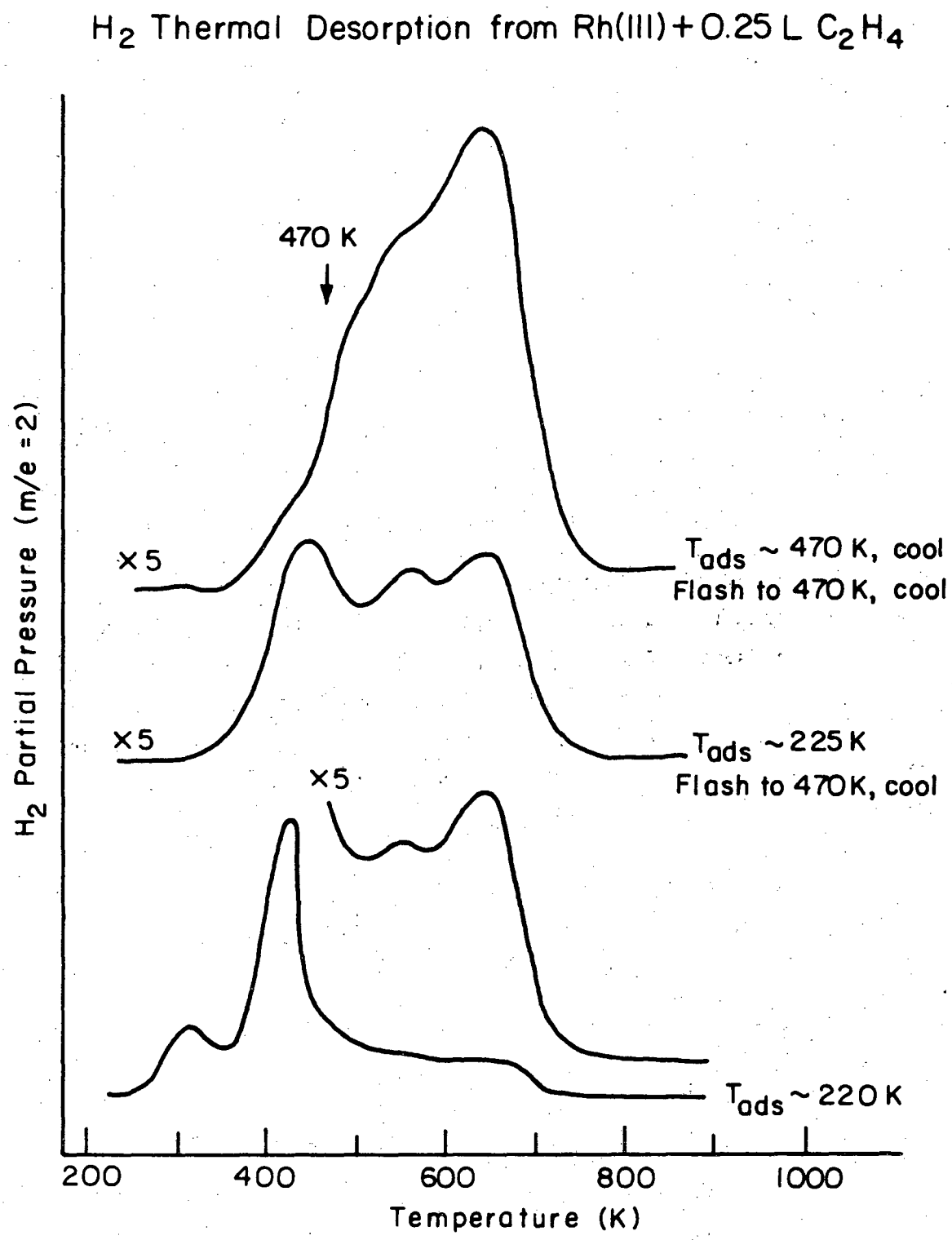
H2 Thermal Desorption from Rh(III) + 0.25 L C2H4
470 K
×5
×5
×5
Tads ~ 470 K, cool
Flash to 470 K, cool
Tads ~ 225 K
Flash to 470 K, cool
Tads ~ 220 K
H2 Partial Pressure (m/e = 2)
200
400
600
800
1000
Temperature (K)

XBL 806-5319

seen from the chemisorption of either acetylene or ethylene on this surface. Although the majority of the hydrogen has desorbed below 450 K, it is clear from these desorption traces that hydrogen strongly bonded to either the surface or to the adsorbate exists. The relative intensity of these two peaks can be enhanced by either adsorbing the ethylene at 225 K and then flashing the surface to 470 K to remove most of the hydrogen (middle trace) or by adsorbing the ethylene at 470 K, cooling and then flashing again to 470 K to remove any excess hydrogen adsorbed during the cooling process (upper trace). In Section H we will show that this hydrogen is from the decomposition of CH species formed on Rh(111) during the heating process. Such species have been postulated as important surface intermediates under high pressure catalytic conditions.[20,21]

F. Correlations with $C_2H_2$ and $C_2H_4$ Chemisorption on Pt(111)

One of the few transition metal-hydrocarbon chemisorption systems studied by several complimentary surface analysis techniques is the adsorption of acetylene and ethylene on the platinum (111) surface. These systems have been most recently studied by ultraviolet photoelectron spectroscopy (UPS),[17,22,23] low-energy electron diffraction,[2,24,25] high resolution electron energy loss spectroscopy[4,12] and thermal desorption spectroscopy.[17] The authors have all reported the presence of at least two binding states and conversion from one state to the other as a function of temperature. However, the bonding and the nature of the adsorbed species is not completely characterized. Below room temperature $C_2H_2$ and $C_2H_4$ associatively adsorb on Pt(111) with their C-C bond oriented approximately parallel to the surface.[4,12,25] Both

molecules form (2x2) surface structures[24] and are significantly rehybridized.[4,12,25] These species are only metastable and can be transformed into a single stable phase by gently heating the crystal.[4,12,24,25] Addition of hydrogen and heating to ~350 K are necessary for acetylene to complete this conversion.[4] Although the stable species remains in a (2x2) surface structure, the LEED intensity vs incident energy beam profiles change significantly.[24,25] This transformation has also been detected by UPS[17,24,25] and by high resolution ELS,[4,12] but there is still disagreement as to the geometry of the stable surface state. Proposed structures include ethylidyne ($\equiv C-CH_3$)[2], a vinyl species ($>CH-CH_2-$) and ethylidene ($>CH-CH_3$).[4,12] These are shown schematically in Figure 7. Finally, the partial dehydrogenation of the surface ethylene species during the metastable to stable transition was observed by a combination of TDS and UPS.[17]

The chemisorption behavior of these two simple hydrocarbons on Rh(111) and Pt(111) are summarized in Table III. The similarities are quite striking. The rhodium substrate appears to be more reactive, however, since the conversion to the stable state occurs at a lower temperature. This can be correlated with the relative positions of these two metals in the periodic table; in general the bonding of small molecules to transition metal surfaces becomes stronger as one moves to the left in the periodic table.[26] By analogy with Pt(111) one might expect a weakly parallel bonded ethylene phase to form on Rh(111) at low temperatures. Such a species is not detected under our experimental conditions.

Table III. Summary of LEED, ELS and TDS Data for the Chemisorption of $C_2H_2$ and $C_2H_4$ on Rh(111) and Pt(111)

| | Rh(111) | | Pt(111) | |
|---|---|---|---|---|
| | $C_2H_2$ | $C_2H_4$ | $C_2H_2$ | $C_2H_4$ |
| Metastable Species: | | | | |
| LEED | (2x2) | (2x2) | (2x2)[24] | |
| ELS | parallel bonded (~$sp^2$) | $C_2H_n$[a] | parallel[4,12,25] bonded (~$sp^2$) | parallel[4,12] bonded (~$sp^3$) |
| Conversion to Stable Species:[b] | | | | |
| Temperature | ~270 K | ~270 K | ~350 K[4,12,24,25] | ~300 K[4,12] |
| Addition of hydrogen? | yes | no | yes[4] | no[4] |
| Stable Species: | | | | |
| LEED | c(4x2) | c(4x2) | (2x2)[24] | (2x2)[25] |
| ELS | $C_2H_n$[a] | $C_2H_n$[a] | $C_2H_n$[a] | $C_2H_n$[a] |
| Partial dehydrogenation (TDS) | no | yes | no[17] | yes[17] |
| Decomposition temperature | 420 K | 420 K | 450 K[24,25] | 450 K[24,25] |

[a] Vibrational spectrum previously assigned as ethylidyne ($\equiv$C-$CH_3$),[2] ethylidene (>CH-$CH_3$)[4,12] and a vinyl species (>CH-$CH_2$-),[17] see text.

[b] Conditions for complete conversion.

## G. The Chemisorption of Ethylene on Pt(111): Evidence for Ethylidyne Formation

LEED,[2] high resolution ELS,[2,4] UPS[27] and TDS[17] studies indicate that the stable species formed from the chemisorption of either $C_2H_4$ or $C_2H_2$ + H on Pt(111) is ethylidyne ($\equiv C-CH_3$). It is interesting that this species has only recently been proposed to form on metal surfaces[2] in spite of the large number of classical studies of ethylene and acetylene chemisorption on metal catalysts. Nevertheless, these species have been known to organometallic chemists for a number of years.[28-32] We have found that both the LEED structure and the vibrational modes of the surface species compare very favorably with related organometallic compounds containing co-ordinated ethylidyne.[2] This is clearly shown in the following summary of previous results:

LEED: The structures shown in Figure 7 have been reported for organometallic compounds and served as the focal point of our LEED analysis. Distorted acetylene (Figure 7a), the ethylidyne group (Fig. 7b), vinylidene (Fig. 7c) and a vinyl species (Fig. 7d) have been observed in the reaction of ethylene with certain trinuclear organometallic compounds. Acetylene can be bonded in a variety of ways depending on the metal and the geometry of the cluster involved.[33,34] Ethylidyne is located in a triangular site with its C-C axis perpendicular to the surface. X-ray crystallographic studies of related clusters indicate three equal metal-carbon bond lengths of approximately 2 Å.[29,32] Vinylidene is also symmetrically placed in a threefold site with the lower carbon atom located 1.2 Å above the center of the metal triangle. The X-ray crystal structure shows the hydrocarbon fragment tilted approximately 45° to the surface normal.[30] The structures of the vinyl species[31]

Figure 7. Models for the stable chemisorption state discussed in the text: (a) distorted acetylene, (b) ethylidyne, (c) vinylidene, (d) the vinyl species and (e) ethylidene.

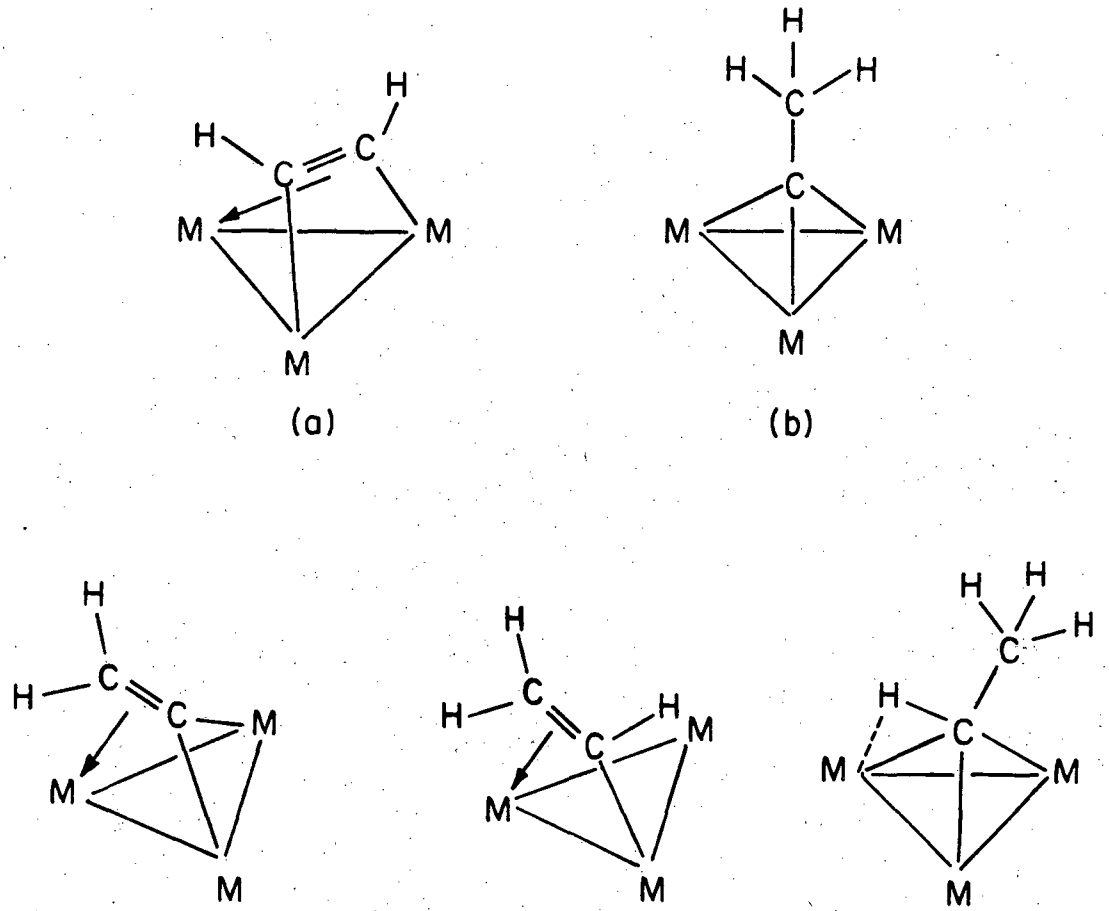


XBL 786-5141

and of ethylidene[35] are not known and have only been postulated on the basis of $^1$H NMR results. Both steric and bond angle considerations require a considerable ($\gtrsim 20°$) tilt of the C-C axis from the surface normal for the latter species. Ibach has proposed a similar tilt angle for ethylidene by analyzing the intensity of certain vibrational modes.[4] Note that these are only model structures and we varied both their C-C and C-Pt distances as well as the bond angle and site geometry in our model calculations.[2]

An extensive LEED intensity analysis of the most stable surface structure favors a hydrocarbon species coordinated to a threefold Pt surface site with structural parameters characteristic of the ethylidyne group, i.e., a C-C bond length of 1.50 Å ± 0.05 Å, three equivalent Pt-C bond lengths of 2.00 Å ± 0.05 Å with the C-C axis normal to the surface within an estimated uncertainty of ~15°.[2] The geometry of this species is shown in Figure 8. Further support for this model comes from comparison to X-ray structure determinations for the organometallic compounds $CH_3CCo_3(CO)_9$[29] and $CH_3CRu_3(CO)_9H_3$,[32] as shown in Table IV. There is a remarkable agreement between the bond lengths (±0.05 Å after correcting for metal-metal bond lengths) and bond angles for the Pt(111) surface ethylidyne complex and those found in the trinuclear metal cluster compounds.

The question arises as to whether or not other model structures could provide better or equally good agreement with experiment. Since LEED is very insensitive to the additional hydrogen atom in ethylidene or to the loss of a hydrogen atom in vinylidene, probable differences in C-C axis orientation must be considered. If we tilt the C-C axis away from the surface normal while maintaining the C-$Pt_3$ nature of the

Figure 8. Optimum structure for the ethylidyne species observed on the Pt(111) surface indicated by the LEED analysis. The C-C and Pt-C bond lengths have uncertainties of $\pm 0.05$ Å. The hydrogen atoms were not located in the LEED analysis.

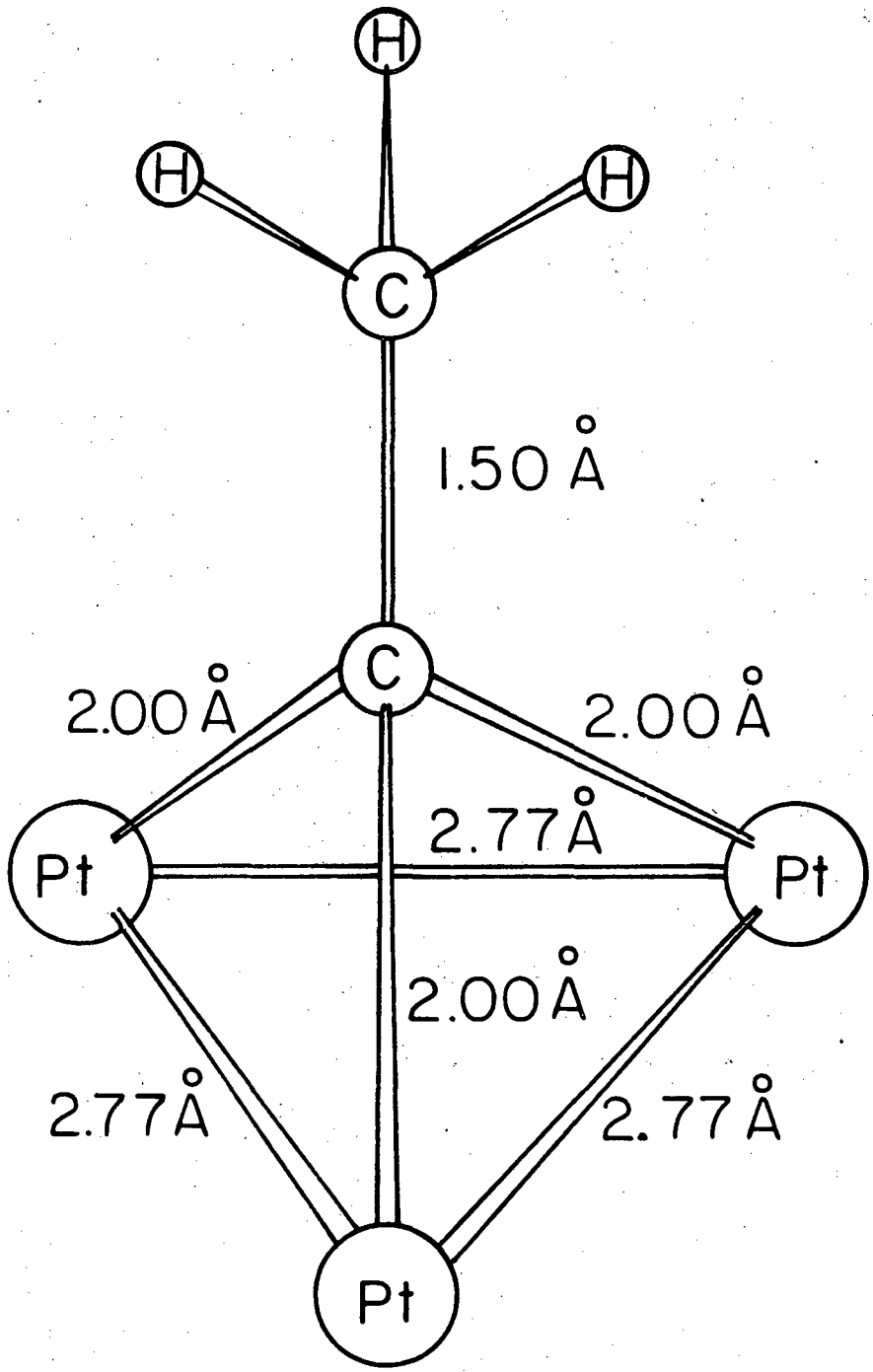


XBL 7712-6591

Table IV. Structural Comparison Between Pt(111) Surface and Organometallic Clusters

| Compound | C-C (Å) | C-M (Å) | M-M (Å) | <M-C-M° |
|---|---|---|---|---|
| Pt(111) - Ethylidyne Surface Complex[2] | 1.5 | 2.0 | 2.77 | 88 |
| $CH_3CCo_3(CO)_9$[29] | 1.53 | 1.90 | 2.47 | 81 |
| $CH_3CRu_3(CO)_9H_3$[32] | 1.51 | 2.08 | 2.84 | 86 |

molecule-surface bond, then such a class of species would include vinylidene ($\Theta_{tilt}$ = 45°, C=C=1.34 Å),[30] the vinyl species ($\Theta_{tilt}$ = 55°, C=C=1.34-1.54 Å)[31] and ethylidene ($\Theta_{tilt}$ = 25°, C-C=1.54 Å).[35] Our results show that only the ethylidyne geometry with $\Theta_{tilt}$ = 0° and C-C=1.50 Å gives satisfactory agreement with experiment.[2]

We should emphasize here that the LEED analysis cannot distinguish between ≥C-$CH_3$ and >CH-$CH_3$ if each species is oriented normal to the surface at a threefold hollow site, since the difference due to hydrogen scattering would be negligible. However, we suggest that such a configuration is unlikely for ethylidene since the lone H atom would have Pt-H ~ 1.6 Å - 1.8 Å for the optimum geometry given by LEED. This would imply a strong Pt-H interaction (which is inconsistent with the ELS analysis (see below)) and it is improbable that such an arrangement would be stable on the surface.

ELS: During the past two years several groups have offered an interpretation of the high resolution electron energy loss spectra of the stable species formed when either $C_2H_2$ or $C_2H_4$ is chemisorbed on Pt(111). These data, originally published by Ibach et al.,[4,12] have led researchers to consider the following three models: ethylidene (>CH-$CH_3$),[4,12] ethylidyne (≥C-$CH_3$)[2] and a vinyl species (>CH-$CH_2$-).[17] At first glance it is not obvious that acetylene and ethylene should yield identical vibrational spectra when adsorbed on Pt(111) since either $C_2H_2$ needs to gain hydrogen or $C_2H_4$ must lose hydrogen. However, Ibach conclusively showed that in order for acetylene to make a transition from the metastable to the stable state, hydrogen atoms must be present.[4] Ethylene rapidly undergoes this transition at room temperature.[4]

Currently the best method for analyzing vibrational spectra of adsorbed species is by comparison with model compounds. The model proposed by Ibach for ethylidene is $Cl_2CH-CH_3$.[4] We have recently compared the ELS spectra of the surface complex with the infrared spectra of both $Co_3(C-CH_3)(CO)_9$ and $Br_3C-CH_3$.[2] Demuth has chosen $Sn_2(CH=CH_2)_6$ as a model for the vinyl species.[17]

Table V shows a comparison of the observed vibrational frequencies of the various suggested surface species with those of the model compounds. It is clear that the ethylidyne species shows the best agreement. Not only do the number of vibrational modes match, but their frequencies are quite close as well. Problems occur with the other two models: for the case of ethylidene, at least one mode (methyl rock) is missing. More importantly, for a species oriented at an angle of $\lesssim 20°$ to the surface normal[4] there should be a strong interaction between the lone hydrogen and the nearest platinum atom (see Fig. 7e). Such a weakening of the C-H bond has been clearly seen for $C_2H_4$ chemisorbed on Ni(111),[39] but is not visible here. Finally, Kroeker et al. have studied the formation of ethylidene from the reaction of CO and $H_2$ over alumina supported rhodium particles using inelastic electron tunneling spectroscopy.[40] Their vibrational assignments were based on the analysis of isotope shift data and they agree extremely well with those of the model compounds ($CH_3-CHCl_2$, $CH_3-CHBr_2$). They are in very poor agreement with the assignments of Ibach et al.,[4,12] however.

Demuth's assignments for the vinyl species also contain numerous problems.[17] He assigns the 900 $cm^{-1}$ peak to a C=C double bond stretch, but this is far too low in energy for this type of vibration (typical values are between 1500 and 1700 $cm^{-1}$).[9] Also, a C-H stretch at 2900-

Table V. Vibrational Assignments for "Stable Species" on the Pt(111) Surface

(all vibrational frequencies are in $cm^{-1}$)

| Surface Species[4,12] | $CH_3CHCl_2$[36] | Ethylidene[4] | $CH_3CCo_3(CO)_9$[28] | $CH_3$-$CBr_3$[37] | Ethylidyne[2] | $Sn_2(CHCH_2)_6$[38] | Vinyl Species[17] |
|---|---|---|---|---|---|---|---|
| 3025-3105 w | 3015 m | CH stretch | 2924 m | 2993 m | $CH_3$ stretch (a) | 3040 s | $CH_2$ stretch (a) |
| --- | 3001 w | $CH_3$ stretch (a) | | | | | |
| 2900-2940 m | 2946 m | $CH_3$ stretch (s) | 2882 m | 2938 m | $CH_3$ stretch (s) | 2980,2940 vs | CH,$CH_2$ stretch (s) |
| 1420 m | 1446 m | $CH_3$ deform (a) | 1420 m | 1432 m | $CH_3$ deform (a) | 1390 vs | $CH_2$ scissors |
| 1350-1360 s | 1381 m | $CH_3$ deform (s) | 1359 m | 1373 m | $CH_3$ deform (s) | 1245 vs | CH deform |
| 1130 s | 1280 m | CH bend | 1161 m | 1064 s | $CH_3$ rock | 998,945 vs | $CH_2$ rock, wag |
| --- | 1091 w | $CH_3$ rock | | | | | |
| 900 m | 982 m | C-C stretch | 1006 s | 1045 m | C-C stretch | 1582 | C-C stretch |
| 435 m | 650 m | C-Pt stretch | 650-600 var | 408 m | C-Pt stretch | 520,480 vs | C-Pt stretch |

Intensity: vs = very strong, s = strong, m = medium, w = weak, var = variable (a) = asymmetric, (s) = symmetric

3000 $cm^{-1}$ is not representative of an olefinic species.[9] Furthermore, the CH deformation and the $CH_2$ rock (and/or wag) are over 100 $cm^{-1}$ below the expected values, based on his choice of model compounds. Again, more modes should be observed in the vibrational spectrum of the vinyl species.

By invoking the dipole selection rule Ibach recently stated that the ethylidyne surface species should have only one $CH_3$ bending mode of $A_1$ symmetry and therefore is not consistent with the vibrational spectrum.[41] The methyl rocking (1130 $cm^{-1}$), the antisymmetric methyl deformation (1420 $cm^{-1}$) and the antisymmetric methyl stretching (3025-3105 $cm^{-1}$) modes are all of E symmetry. There have been several reports, however, indicating that the dipole selection rule does not rigorously hold and vibrational modes parallel to the surface have been seen. These are discussed in detail in Chapter II. These apparent breakdowns in the normal dipole selection rule also imply that more modes should be visible for both the ethylidene and the vinyl species.

Further evidence for the ethylidyne group comes from a study of the deuterated species. This is shown in Table VI. Again, the agreement between the observed vibrational frequencies and those found in the model compounds is quite good. A question that should be answered is why the ELS spectrum of the stable species shows two intense features while that for the deuterated species displays only one. The answer comes from vibrational mode mixing. The extent of this mode mixing can only be determined from a normal coordinate analysis. Such analyses have been carried out for the model compounds,[36,37] and they do show extensive mode mixing upon deuteration. Therefore this phenomenon should also be present on the surface.

Table VI. Vibrational Assignments for the Denterated "Stable Species" on the Pt(111) Surface*

(all vibrational frequencies are in $cm^{-1}$)

| Surface Species[4,12] | $CD_3$-$CDCl_2$[36] | Ethylidene ($d_4$)[4] | $CD_3$-$CBr_3$[37] | Ethylidyne ($d_3$)[2] |
|---|---|---|---|---|
| broad | 2165 w | CD stretch | | |
| unresolved | 2248 m | $CD_3$ stretch (a) | 2241 | $CD_3$ stretch (a) |
| band | 2125 w | $CD_3$ stretch (s) | 2116 | $CD_3$ stretch (s) |
| not resolved | 1047 m | $CD_3$ deform (a) | 953 w | C-C stretch |
| 1010 w | 1014 m | $CD_3$ deform (s) | 1038 w | $CD_3$ deform (a) |
| 850 w | 775 m | CD bend | 883 m | $CD_3$ rock |
| --- | 932 | $CD_3$ rock | | |
| 1150 s | 1151 s | CC stretch | 1110 w | $CD_3$ deform (s) |
| 430 m | 600 m | C-Pt stretch | 388 s | C-Pt stretch |

* An assignment for the deuterated vinyl species was not presented in Ref. 17.

Intensity: s = strong, m = medium, w = weak

Definitive interpretation of high resolution ELS spectra is quite difficult at this time since the theory is not well-established. Originally, long-range dipole interactions between the incident electrons and the vibrating adsorbate molecules were thought to account for all of the observed modes. Recent results have indicated that possible negative ion resonances and/or short-range interactions are present (see Chapter II).

UPS: Demuth has tried to rule out the presence of a surface $\geqslant C-CH_3$ species on the basis of his UPS results.[17] Unfortunately early calculations did not include any reasonable models for the ethylidyne species and more recent calculations on the energy levels of $Li_3C-CH_3$ did not converge.[17] However, the self-consistent extended Hückel calculations of Baetzhold[27] fit the HeI UPS data of Lo et al.[23] for the chemisorption of acetylene on Pt(111) quite well. Furthermore, the recent molecular orbital calculations of Gavezzotti and Simonetta indicate that the $\geqslant C-CH_3$ species should have a platinum-carbon binding energy of over 80 kcal/mole.[42] Calculated bond lengths are also in agreement with the LEED results of Kesmodel et al.[2] Finally, calculations of the metal-carbon stretching frequency (400-450 $cm^{-1}$) for this species is in excellent agreement with experiment[43] (see Table V). This is not the case for either ethylidene or for the vinyl species.[43]

TDS: Demuth used a combination of TDS and UPS to clearly show that the stable species formed from the chemisorption of $C_2H_4$ on the Pt(111) surface must be partially dehydrogenated.[17] He concluded that the stoichiometry of this species is $C_2H_3$ and therefore the presence of ethylidene ($C_2H_4$) can be effectively ruled out.[17]

Analogies with Organometallic Chemistry: A natural extension of the discussion of two (a metastable (parallel bonded) and a stable) surface species is the development of a mechanism for their conversion. Here again a study of related organometallic compounds is of some use and is also in agreement with the formation of a surface ethylidyne group. Acetylene reacts with $H_2Os_3(CO)_{10}$ (I)[44] under very mild conditions to give $HOs_3(CHCH_2)(CO)_{10}$ (II)[31] and upon heating yields $H_2Os_3(C{=}CH_2)(CO)_9$ (III)[31]. We have recently proposed vinylidene ($>C{=}CH_2$) as an intermediate in the formation of ethylidyne.[2] This species has also been proposed by Demuth on the basis of some UPS and ELS results.[17] Ethylene reacts with $Os_3(CO)_{12}$ to give the identical compound.[30] Furthermore (II) has been proposed as a very short lived intermediate for this transformation as well.[31] Finally, the more stable ethylidyne complex, $H_3Os_3(C{-}CH_3)(CO)_9$ (IV), can be formed by bubbling $H_2$ through a refluxing n-heptane solution of (III) for 24 hours.[30] This is analogous to the surface phase transformation undergone by $C_2H_2$ upon heating and the addition of hydrogen. The surface mechanism can then be written as follows:

$$CH{\equiv}CH \xrightarrow{Pt(111)} (HC{=}CH)^* \rightarrow {}^*C{=}CH_2 \xrightarrow[\text{or}\ H^*]{H} {}^*C{-}CH_3$$

$$H_2C{=}CH_2 \xrightarrow{Pt(111)} (H_2C{=}CH_2)^* \rightarrow {}^*CH{=}CH_2{+}H^* \rightarrow {}^*C{=}CH_2{+}2H^* \rightarrow {}^*C{-}CH_3{+}H^*$$

* indicates an adsorbed species. This is only one possible reaction scheme and the lifetimes of the intermediates are not known, but it does seem likely that vinylidene is an intermediate in the formation of ethylidyne on Pt(111) since it must be present in the cluster analogs. Strongly bound olefinic species such as $Os_3(HC{=}CH)(CO)_{10}$ cannot be hydrogenated to (IV) nor can they be converted to (III).[45]

The structural parameters of the surface ethylidyne species and several trinuclear organometallic compounds[29,32] are also quite similar. This was clearly shown in Table IV. Furthermore, the infrared data of $Co_3(C\text{-}CH_3)(CO)_9$[28] and the high resolution ELS spectra of the proposed ethylidyne surface species agree remarkably well. Finally, it has been shown that the metal triangle in $Co_3(C\text{-}CH_3)(CO)_9$ is electron withdrawing with respect to the apical substituent[46] and this is precisely what is seen on the surface: upon adsorption of either acetylene or ethylene, the work function of Pt(111) decreases by 1.5 eV.[47] A delocalized carbyne type bonding between the lower carbon atom and the three cobalt atoms has been proposed for the cluster analog.[46] This is consistent with the short metal-carbon bond distance measured here.

In summary, we have found consistent evidence from LEED, high resolution ELS and thermal desorption mass spectrometry to indicate the formation of a stable ethylidyne species on the Pt(111) surface. A structure with the C-C axis approximately normal to the surface and a C-C bond length of 1.50 Å ± 0.05 Å has been determined by the LEED intensity analysis.[2] This is characteristic of a carbon-carbon single bond and is consistent with a C-C stretching vibration at 900 $cm^{-1}$[9] found in the ELS spectrum of the stable species. The presence of methyl stretching (2900-3100 $cm^{-1}$), deformation (1360, 1420 $cm^{-1}$) and rocking (1130 $cm^{-1}$) modes confirms the existence of a saturated carbon species. The TDS experiments of Demuth[17] indicating a surface stoichiometry of $C_2H_3$ clearly rule out the presence of additional hydrogen. The LEED analysis further shows a rather short Pt-C bond length of 2.00 Å ± 0.05 Å, suggestive of strong carbyne type bonding. Both the LEED structure and the vibrational spectra of the surface species compare very favorably with related organometallic compounds containing coordinated ethylidyne.

## H. Correlations with $C_2H_2$ and $C_2H_4$ Chemisorption on Ni(111): Evidence for Surface CH Species

The chemisorption of acetylene and ethylene on Ni(111) is quite different from that on either Rh(111) or Pt(111). Both molecules are associatively adsorbed at low temperatures,[7,13,39,48-50] but upon heating, the C-C bond of chemisorbed $C_2H_2$ is broken.[48] The remaining CH fragments undergo either carbon-hydrogen bond cleavage to leave carbon atoms on the surface or self-hydrogenation to form $CH_2$ species.[48] Alternatively, at high gas exposures acetylene can cyclotrimerize on the Ni(111) surface to form chemisorbed benzene.[49] Upon heating, chemisorbed ethylene first dehydrogenates to adsorbed acetylene[7,49,50] and then can undergo a similar C-C and C-H bond breaking sequence.

The stable ethylene or acetylene plus hydrogen overlayer on Rh(111) can also be decomposed to surface CH (CD) species above ~420 K. The LEED pattern disorders at this temperature as well. The high resolution ELS spectra of these two hydrocarbon fragments are shown in Figure 9. Based on the discussion in Section C, the band observed at 3025 (2260) $cm^{-1}$ is clearly the C-H (C-D) stretching vibration ($\nu_{CH\ (CD)}$).[9] Furthermore, we can assign the mode observed at 770 (545) $cm^{-1}$ to a C-H (C-D) bending mode ($\delta_{CH\ (CD)}$) on the basis of its isotope shift: observed, $\delta_{CH}/\delta_{CD} = 1.41$; predicted, $\delta_{CH}/\delta_{CD} = 1.36$. This ratio should be approximately 1.04 for a rhodium-carbon stretching vibration of a surface CH (CD) species. No other modes are observed. We can easily rule out the possibility of surface CCH or $CCH_2$ species on Rh(111) as these would both show an intense C-C stretching vibration between 1400 and 2100 $cm^{-1}$.[9] Similarly, surface $CH_2$ fragments should display the characteristic $CH_2$ scissor mode near 1400 $cm^{-1}$.[9] Finally, surface CD species formed from

Figure 9. Surface CH (CD) species can be formed on Rh(111) by heating chemisorbed $C_2H_2$ (lower trace) or $C_2D_4$ (upper trace) to 450 K in vacuum. The peak assignments are discussed in the text.

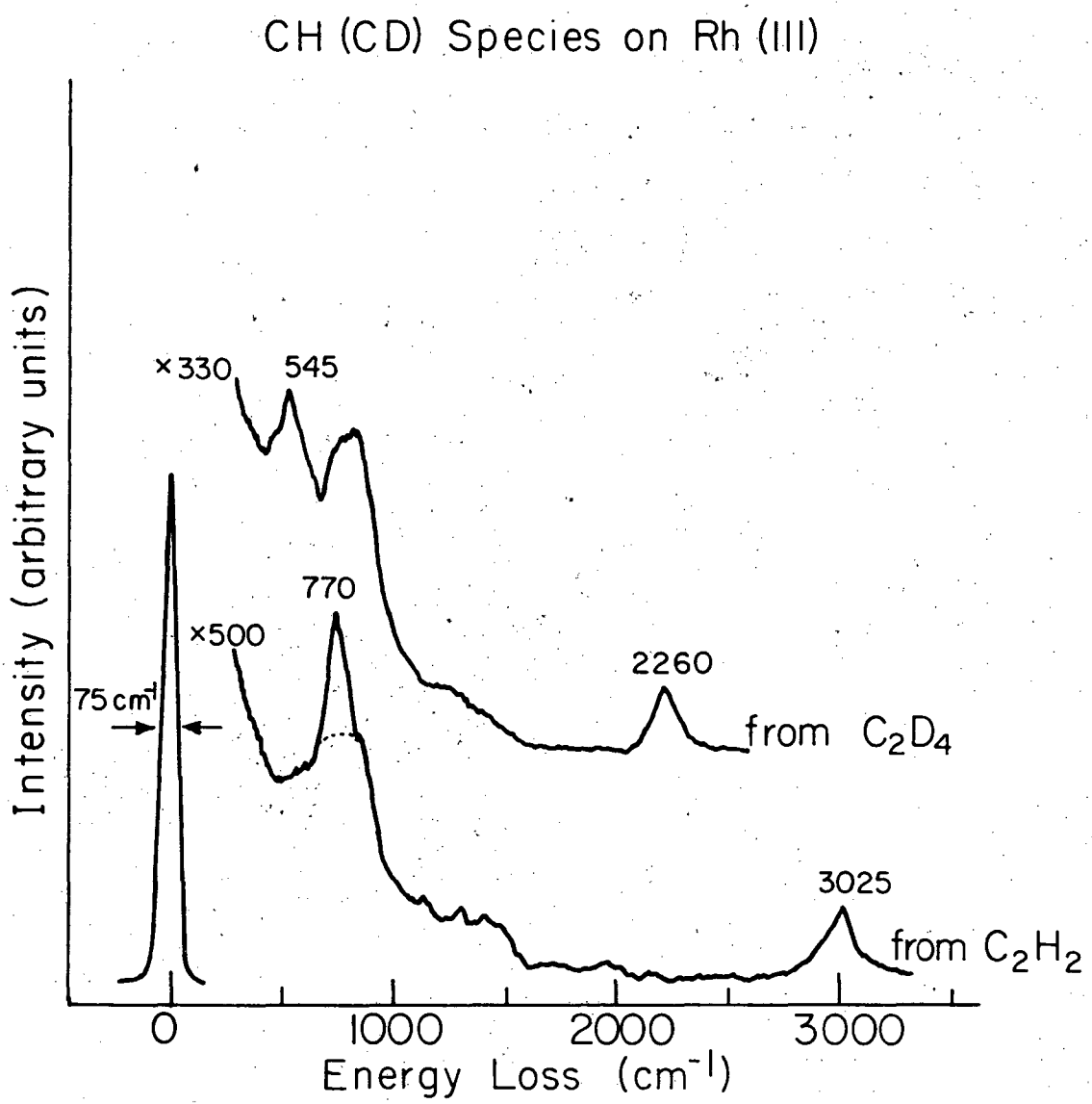
CH (CD) Species on Rh (III)
Intensity (arbitrary units)
×330
545
770
×500
75 cm⁻¹
2260
from C2D4
3025
from C2H2
0
1000
2000
3000
Energy Loss (cm⁻¹)

XBL 798-6970

the chemisorption of either $C_2D_2$ or $C_2D_4$ on Rh(111) readily exchange hydrogen under high vacuum conditions (<1 x $10^{-7}$ Torr $H_2$) at 300 K.

The CH (CD) stretching and bending modes are observed at 2980 (2160) $cm^{-1}$ and 790 (550) $cm^{-1}$, respectively on Ni(111).[48] These assignments were based on isotope shift data ($\nu_{CH}/\nu_{CD}$ = 1.38; $\delta_{CH}/\delta_{CD}$ = 1.44) and correspond quite well to the modes observed in $CHCl_3$ (a reasonable model compound.). Demuth and Ibach use their high resolution ELS results to conclude that the carbon atom bonds to three nickel atoms and the C-H moiety is skewed to the surface.[48] The exact angle is dependent on the state of hybridization of the observed species. A weak interaction between the hydrogen atom and the surface was postulated. The observation of the CH (CD) bending modes of a tilted species is in keeping with the normal dipole selection rule (see Chapter II). A similar geometry has been observed for a CH species bonded to a trinuclear osmium cluster ($H_3Os_3(CO)_9(CH)$).[51] No complete vibrational spectra were reported, however. Based on the similarity of the vibrational spectra we conclude that the geometry of the CH species detected on Rh(111) should be quite similar to that observed on Ni(111).

Unfortunately high temperature studies on the chemisorption of either $C_2H_2$ or $C_2H_4$ on Pt(111) have not been reported. Extension of these studies to Pd(111) would also be quite interesting.

## I. Summary

These investigations lead to the following conclusions:

1. The chemisorption of acetylene and ethylene on Rh(111) yields a series of ordered structures:

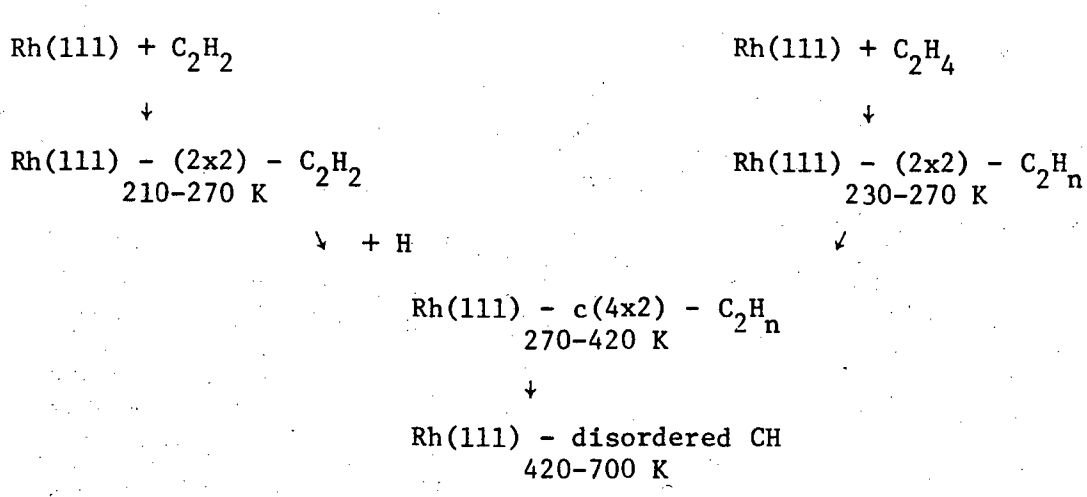


where $C_2H_n$ stands for the stable hydrocarbon species with undetermined hydrogen content. These order-order transformations are irreversible.

2. Below 270 K acetylene chemisorbs on Rh(111) with its C≡C bond oriented parallel to the surface forming an approximately $sp^2$ hybridized species.

3. Adsorption of $C_2H_2$ + H or $C_2H_4$ above 300 K on Rh(111) produces the same stable species. TDS studies show this species to have a stoichiometry of $C_2H_n$, where n is less than 4. Adsorption of $C_2H_2$ + H or $C_2H_4$ on Pt(111) above 350 K leads to a similar, and most likely identical, species. This species has now been identified as ethylidyne (≡C-$CH_3$).

4. The geometry of the adsorbed ethylene species on Rh(111), as determined by ELS, does not change during the conversion from the metastable to the stable species although the overlayer structure changes from a (2x2) to a c(4x2).

5. The addition of $H_2$ to chemisorbed $C_2D_2$ or $C_2D_4$ results in H-D exchange, but no change in the adsorbate geometry is detected by ELS.

6. The stable ethylene or acetylene plus hydrogen overlayer on Rh(111) can be decomposed to surface CH (CD) species above ~420 K.

## References


1. L. H. Dubois, D. G. Castner, and G. A. Somorjai, J. Chem. Phys. 72, 5234 (1980).

2. L. L. Kesmodel, L. H. Dubois, and G. A. Somorjai, Chem. Phys. Lett. 56, 267 (1978); J. Chem. Phys. 70, 2180 (1979).

3. D. G. Castner, B. A. Sexton, and G. A. Somorjai, Surface Sci. 71, 519 (1978).

4. H. Ibach and S. Lehwald, J. Vac. Sci. Technol. 15, 407 (1978).

5. On the (111) crystal face of an fcc metal the (2x2) unit cell is a rhombohedron while the c(4x2) primitive unit cell is a rectangle.

6. The loss intensities are a strong function of the incident electron energy and only average values are reported here. This could be due to resonance or short-range scattering as discussed by Lehwald and Ibach for the case of acetylene chemisorption on Ni(111).[7]

7. S. Lehwald and H. Ibach, to be published.

8. H. Froitzheim, H. Ibach and S. Lehwald, Rev. Sci. Instrum. 46, 1325 (1975).

9. See for example, T. Shimanouchi, Tables of Molecular Vibrational Frequencies, Consolidated Vol. 1, U. S. Dept. of Commerce publication NSRDS-NBS 39.

10. Y. Iwashita, F. Tamura, and A. Nakamura, Inorg. Chem. 8, 79 (1969).

11. Y. Iwashita, Inorg. Chem. 9, 1178 (1970).

12. H. Ibach, H. Hopster, and B. Sexton, Appl. Phys. 14, 21 (1977); Appl. Surface Sci. 1, 1 (1977).

13. J. E. Demuth and H. Ibach, Surface Sci. 85, 365 (1979).

14. E. L. Muetterties, Bull. Soc. Chim. Belg. 85, 451 (1977).

15. E. L. Muetterties, T. N. Rhodin, Elliot Band, C. F. Brucker, and W. R. Pretzer, Chem. Rev. 79, 91 (1979).

16. L. H. Dubois and G. A. Somorjai, Surface Sci. 91, 514 (1980).

17. J. E. Demuth, Surface Sci. 80, 367 (1979); 93, L82 (1980).

18. D. G. Castner, Ph.D. Thesis, University of California, Berkeley, 1979.

19. J. T. Yates, Jr., P. A. Thiel, and W. H. Weinberg, Surface Sci. 84, 427 (1979).

20. T. Hattori and R. L. Burwell, J. Phys. Chem. 83, 241 (1979).

21. S. M. Davis and G. A. Somorjai, to be published.

22. J. E. Demuth, Chem. Phys. Lett. 45, 12 (1977); IBM J. Res. Develop. 22, 265 (1978).

23. W. J. Lo, Y. W. Chung, L. L. Kesmodel, P. C. Stair, and G. A. Somorjai, Solid State Commun. 22, 335 (1977).

24. P. C. Stair and G. A. Somorjai, Chem. Phys. Lett. 41, 391 (1976); J. Chem. Phys. 66, 2036 (1976).

25. L. L. Kesmodel, R. C. Baetzold, and G. A. Somorjai, Surf. Sci. 66, 299 (1977).

26. I. Toyoshima and G. A. Somorjai, Catal. Rev. Sci. Eng. 19, 105 (1979).

27. R. Baetzhold, Chem. Phys. 38, 313 (1979).

28. W. T. Dent, L. A. Duncanson, R. G. Guy, H. W. B. Reed, and B. L. Shaw, Proc. Chem. Soc. 169 (1961).

29. P. W. Sutton and L. F. Dahl, J. Am. Chem. Soc. 89, 261 (1967).

30. A. J. Deeming and M. Underhill, J. C. S. Chem. Comm., 277 (1973); J. C. S. Dalton, 1415 (1974).

31. A. J. Deeming, S. Hasso, and M. Underhill, J. C. S. Dalton, 1614 (1975).

32. G. M. Sheldrick and Y. P. Yesinowski, J. C. S. Dalton, 813 (1975).

33. R. Mason and K. M. Thomas, Annals N.Y. Acad. Sci. 239, 225 (1974).

34. C. G. Pierpont, Inorg. Chem. 16, 636 (1977).

35. C. R. Eady, B. F. G. Johnson, and J. Lewis, J. C. S. Dalton, 477 (1977).

36. J. R. Durig, A. E. Sloan, and J. D. Witt, J. Phys. Chem. 76, 3591 (1972).

37. T. R. Stengle and R. C. Taylor, J. Mol. Spectrosc. 34, 33 (1970).

38. F. G. Glockling, M. A. Lyle, and S. R. Stobart, J. C. S. Dalton, 2537 (1974).

39. J. E. Demuth, H. Ibach, and S. Lehwald, Phys. Rev. Lett. 40, 1044 (1978).

40. R. M. Kroeker, W. C. Kaska, and P. K. Hansma, J. Catal. 61, 87 (1980).

41. H. Ibach, Proc. Conference on Vibrations in Adsorbed Layers (Julich, Germany, June, 1978) p. 64.

42. A. Gavezzotti and M. Simonetta, to be published.

43. M. Simonetta, private communication.

44. Simple hydrocarbons are generally added to unsaturated hydridocarbonyl clusters (such as (I)) since these reactions can be run under milder conditions.

45. M. A. Andrews and H. D. Kaesz, J. Am. Chem. Soc. 99, 6763 (1977).

46. D. C. Miller and T. B. Brill, Inorg. Chem. 17, 240 (1978).

47. J. L. Gland and G. A. Somorjai, Adv. Coll. and Inter. Sci. 5, 205 (1976).

48. J. E. Demuth and H. Ibach, Surface Sci. 78, L238 (1978).

49. J. C. Bertolini, J. Massardier, and G. Dalmai-Imelik, J. C. S. Faraday I 74, 1920 (1978).

50. J. C. Bertolini and J. Rousseau, Surface Sci. 83, 531 (1979).

51. R. B. Calvert and J. R. Shapley, J. Am. Chem. Soc. 99, 5225 (1977).

This report was done with support from the Department of Energy. Any conclusions or opinions expressed in this report represent solely those of the author(s) and not necessarily those of The Regents of the University of California, the Lawrence Berkeley Laboratory or the Department of Energy.

Reference to a company or product name does not imply approval or recommendation of the product by the University of California or the U.S. Department of Energy to the exclusion of others that may be suitable.

*TECHNICAL INFORMATION DEPARTMENT*
*LAWRENCE BERKELEY LABORATORY*
*UNIVERSITY OF CALIFORNIA*
*BERKELEY, CALIFORNIA 94720*